

Alma Mater Studiorum – Università di Bologna

DOTTORATO DI RICERCA IN

Meccanica e Scienze Avanzate dell'Ingegneria

Ciclo XXXI

**Settore Concorsuale: 09/C2**

**Settore Scientifico Disciplinare: ING-IND/10**

ALMABEST: A NEW WHOLE BUILDING ENERGY SIMULATION  
SIMULINK-BASED TOOL FOR NZEB DESIGN

**Presentata da:** Jean Pierre Campana

**Coordinatore Dottorato**

Prof. Marco Carricato

**Supervisore**

Prof. Gian Luca Morini

**Esame finale anno 2019**









---

# ABSTRACT

---

In this Thesis the new tool ALMABEST for the dynamic energy simulation of the whole building coupled to HVAC systems is presented. This tool, developed in the Matlab environment, consists of two libraries, ALMABuild and ALMAHVAC, dedicated to the building and HVAC system modelling respectively; this Thesis is focused in particular on ALMABuild.

A large number of software for the analysis of dynamic behaviour of buildings have been proposed and are now available for the designers. For this reason, the reader can have some doubt about the need of a new software for dynamic energy building simulations.

One of the main goals of this Thesis is to demonstrate that ALMABEST presents complementary features with respect to the commercial codes available in the market, which can greatly help the user in the design of new NZEB. In fact, the main features required for the NZEB design (ability to perform multi-objective optimizations, detailed comfort assessments and accurate evaluation of the energy performance of buildings and HVAC systems also in presence of active occupants) are aspects that the codes available on the market only partially are able to manage.

In the first part of this Thesis, the description of ALMABuild, which consists of a Simulink library and a set of Graphical User Interfaces (GUIs), is presented. In particular, the models implemented in the main ALMABuild blocks are explained and the procedure for the creation of the building model by using a series of GUIs is illustrated. It is emphasized how the use of these GUIs allows to overcome the drawback of other Simulink-based tools in terms of introduction of building data and of implementation of the model in the Simulink desktop. The benchmark of ALMABuild has been performed following the BESTEST procedure, adopted for the validation of the main *whole building software* available in the market. Results of analytical and empirical tests have confirmed the validity of the models implemented in ALMABuild. The same result has been confirmed by the comparative tests made by using a series of reference software under a set of univocally defined cases. The results highlight how the comparison suggested by the BESTES procedure need to be continuously updated by varying the list of the reference software used for comparisons in order to obtain a more updated benchmark and be able to take correctly into account the natural evolution of the building modelling.

In the second part of this work, applications of the ALMABEST tool are illustrated with the aim to highlight the main features of this tool. In particular,

the detailed evaluation of the spatial distribution of radiative, indoor air and operative temperature obtained by means of ALMABEST has been used in order to compare six different emitters (from radiators to radiant floors) with the aim to put in evidence how the indoor local comfort conditions are influenced by the emitters. Furthermore, the impact of the temperature sensor position in a room on the local indoor comfort conditions and on the dynamic response of the emitters has been analysed.

The coupling of the Matlab Optimization Toolbox with ALMABuild is illustrated by means of a series of single and multi-objective optimizations in which the total annual energy demand is minimized by modifying a series of specific building parameters, like thermal insulation thickness and the total clear area. Results remark the significant improvements of the building energy performance that can be obtained by using this design approach, with energy savings up to 65% with respect to a reference building configuration. The limited number of simulations required by the optimization algorithm to find the optimal solution, even for a large number of possible configurations underlines how these optimization algorithms can be nowadays used during the design of a NZEB with limited computational costs.

Finally, the impact of occupant interactions with the building elements, in particular windows, on comfort and heating energy consumptions is analysed. The effects of the occupant behaviour on the optimal building parameters configuration able to maximize comfort conditions and minimize the energy demand are investigated by means of multi-objective optimizations. A robustness parameter is introduced in order to individuate the main configurations which tend to minimize the role of the occupant on the indoor comfort conditions and on the energy demand (occupant-free configuration). Results emphasize how the presence of occupants and their active behaviour cannot be ignored if an accurate and realistic evaluation of the building performance have to be obtained.

---

# CONTENTS

---

<b>ABSTRACT</b> .....	<b>I</b>
<b>CONTENTS</b> .....	<b>III</b>
<b>LIST OF FIGURES</b> .....	<b>VII</b>
<b>LIST OF TABLES</b> .....	<b>XIII</b>
<b>NOMENCLATURE</b> .....	<b>I</b>
<b>1 CONTEXT AND OBJECTIVE</b> .....	<b>1</b>
1.1 GENERAL CONTEXT.....	2
1.2 NZEB DESIGN.....	3
1.3 DYNAMIC ENERGY SIMULATIONS.....	4
1.4 DYNAMIC ENERGY SIMULATION TOOLS.....	6
1.5 TIME STEP DISCRETIZATION.....	8
1.6 DESCRIPTION OF THE MAIN WBES TOOLS.....	10
1.6.1 <i>ESP-r</i> .....	11
1.6.2 <i>EnergyPlus</i> .....	11
1.6.3 <i>TRNSYS</i> .....	13
1.6.4 <i>Limitations and comparison of the main WBES</i> .....	14
1.7 MATLAB/SIMULINK BUILDING PERFORMANCES SIMULATION LIBRARIES.....	16
1.7.1 <i>IBPT</i> .....	17
1.7.2 <i>CARNOT</i> .....	18
1.7.3 <i>HAMBASE</i> .....	19
1.7.4 <i>SIMBAD</i> .....	20
1.8 CONSTRAINTS OF MATLAB/SIMULINK LIBRARIES.....	21
1.9 THESIS OUTLINE.....	21
<b>2 ALMABUILD DESCRIPTION</b> .....	<b>25</b>
2.1 SIMULINK ENVIRONMENT AND ALMABEST LIBRARY.....	26
2.2 DEVELOPMENT OF THE BUILDING MODEL.....	29
2.3 BUS SIGNALS USED IN ALMABUILD.....	31
2.4 BUILDING MODEL IN ALMABUILD.....	32
2.5 WEATHER DATA.....	34
2.5.1 <i>Weather Data Reader block</i> .....	35
2.5.2 <i>Solar Data block</i> .....	36
2.5.3 <i>Solar Radiation Calculator and Solar Radiation Reader block</i> .....	37
2.6 OPAQUE ENVELOPE ELEMENTS IN ALMABUILD.....	39
2.6.1 <i>Modelling of envelope elements in ALMABuild</i> .....	40
2.6.2 <i>Building Massive Element block</i> .....	42
2.7 WINDOWS IN ALMABUILD.....	47
2.7.1 <i>Building Clear Component block</i> .....	49
2.7.2 <i>Distribution of the incoming solar radiation</i> .....	51
2.8 SHADINGS.....	54
2.8.1 <i>Shading model</i> .....	55
2.9 DEFINITION OF THERMAL ZONES.....	57
2.9.1 <i>Building Thermal Balance block</i> .....	58
2.9.2 <i>BTB simple model</i> .....	59

2.10	IMPLEMENTATION OF THE BUILDING MODEL.....	63
2.11	CONCLUSIONS.....	63
<b>3</b>	<b>ALMABUILD VALIDATION.....</b>	<b>65</b>
3.1	THE BESTEST PROCEDURE.....	66
3.2	ANALYTICAL VERIFICATIONS.....	67
3.3	EMPIRICAL VALIDATION.....	69
3.4	COMPARATIVE TESTS.....	71
3.4.1	<i>Validation of the solar contributions on the external surfaces.....</i>	<i>75</i>
3.4.2	<i>Validation of the optical model for clear component.....</i>	<i>77</i>
3.4.3	<i>Validation of the shading model.....</i>	<i>78</i>
3.4.4	<i>Thermal zone balance validation in free-float temperature conditions.....</i>	<i>79</i>
3.4.5	<i>Thermal zone balance validation in presence of an ideal HVAC system.....</i>	<i>82</i>
3.5	COMPARISON WITH OTHER REFERENCES.....	87
3.6	CONCLUSIONS.....	94
<b>4</b>	<b>EVALUATION OF THE 3D TEMPERATURE FIELD OF A ZONE.....</b>	<b>97</b>
4.1	GUIs FOR DETAILED THERMAL ZONE MODELS.....	98
4.2	DETAILED BTB BLOCKS.....	99
4.2.1	<i>Radiative model.....</i>	<i>100</i>
4.2.2	<i>Convective model.....</i>	<i>103</i>
4.2.3	<i>Fully detailed model.....</i>	<i>109</i>
4.3	NUMERICAL PERFORMANCES OF BUILDINGS MODELS.....	109
4.4	VERIFICATION OF THE VIEW FACTOR CALCULATION PROCEDURE.....	111
4.5	APPLICATION OF THE RADIATIVE MODEL: A CASE STUDY.....	112
4.5.1	<i>The reference thermal zone.....</i>	<i>113</i>
4.5.2	<i>Heat emitter characteristics.....</i>	<i>115</i>
4.5.3	<i>Heating system control.....</i>	<i>115</i>
4.5.4	<i>Inputs for the indoor thermal comfort analysis.....</i>	<i>116</i>
4.5.5	<i>Discussion of the results.....</i>	<i>116</i>
4.6	APPLICATION OF THE FULLY DETAILED MODEL: A CASE STUDY.....	127
4.6.1	<i>Case study description.....</i>	<i>127</i>
4.6.2	<i>Constant water inlet temperature control strategy.....</i>	<i>129</i>
4.6.3	<i>Use of weather compensation.....</i>	<i>138</i>
4.6.4	<i>Fast restart strategy.....</i>	<i>143</i>
4.7	CONCLUSIONS.....	146
<b>5</b>	<b>OPTIMIZATIONS IN BUILDING DESIGN.....</b>	<b>149</b>
5.1	INTRODUCTION.....	150
5.2	CASE STUDY 1.....	153
5.3	CASE STUDY 2.....	157
5.4	CASE STUDY 3.....	159
5.5	CASE STUDY 4.....	160
5.6	MULTI-OBJECTIVE OPTIMIZATION CASE STUDY.....	162
5.6.1	<i>Analysis of the sensitivity of the objective functions to different building configurations.....</i>	<i>163</i>
5.6.2	<i>Results of the multi-objective optimization.....</i>	<i>166</i>
5.7	CONCLUSIONS.....	167
<b>6</b>	<b>OCCUPANT BEHAVIOUR.....</b>	<b>169</b>
6.1	INTRODUCTION.....	170
6.2	OCCUPANT BEHAVIOUR MODEL.....	173
6.3	REFERENCE BUILDING.....	174
6.4	CASE STUDY.....	175
6.4.1	<i>Input data.....</i>	<i>176</i>
6.4.2	<i>Results ignoring the occupant behaviour.....</i>	<i>177</i>

6.4.3	<i>Results considering the occupant behaviour</i>	183
6.4.4	<i>Comparison of results</i>	189
6.4.5	<i>Implications of the occupant behaviour on energy consumptions and indoor comfort conditions sensitivity to design parameters</i>	190
6.4.6	<i>Multi-objective optimizations</i>	194
6.5	USER-FREE SOLUTIONS	200
6.6	CONCLUSIONS	203
<b>CLOSURE</b>		<b>205</b>
<b>REFERENCE</b>		<b>207</b>
<b>APPENDIX A</b>		<b>A-1</b>
<b>APPENDIX B</b>		<b>B-1</b>
<b>APPENDIX C</b>		<b>C-1</b>
<b>APPENDIX D</b>		<b>D-1</b>



---

# List of Figures

---

Figure 1.1 Fraction of energy sources in the residential sector in Europe, in 2016 (from [5]).	3
Figure 1.2. Example of elements composing a building-HVAC system, characterised by different time constants.	8
Figure 2.1. Simulink library.	26
Figure 2.2. Example of a simple model implemented in Simulink.	27
Figure 2.3. ALMABEST hierarchical levels.	28
Figure 2.4. Plant of a two-stage building.	29
Figure 2.5. Simulink model of the two-stage building developed by means of ALMABEST.	30
Figure 2.6. ALMABuild library main level.	32
Figure 2.7. Example of models that compose a <i>Thermal zone</i> block.	33
Figure 2.8. ALMABuild main interface.	34
Figure 2.9. Exploded of the <i>Weather Data</i> block of the ALMABuild library.	34
Figure 2.10. Exploded of the <i>Climatic Data</i> block for a building characterised by three orientations (East, West, South).	35
Figure 2.11. <i>Weather Data Reader</i> block.	36
Figure 2.12. <i>Solar Data</i> block.	36
Figure 2.13. <i>Solar Radiation Calculator</i> model.	38
Figure 2.14. Structure GUI used for the definition of main characteristics of massive elements.	39
Figure 2.15. Blocks composing the <i>Building Components</i> blockset.	42
Figure 2.16. Equivalent 3R4C network associated to an opaque envelope building.	43
Figure 2.17 Floor on ground RC network.	45
Figure 2.18. Equivalent RC network related to an opaque element with an active layer ( <i>l<sub>active</sub></i> ).	45
Figure 2.19. BME block of an external wall.	46
Figure 2.20. Window GUI, for the definition of characteristics of clear envelope elements.	48
Figure 2.21. BCC block for a double pane window.	51
Figure 2.22. Connections of a BCC block to <i>Direct</i> and <i>Diffuse distribution</i> blocks.	52

Figure 2.23. Graphical representation of a building with a horizontal shading device (in grey), obtained by the ALMABuild shading GUI. ....	54
Figure 2.24. Thermal zone properties GUI. ....	57
Figure 2.25. GUI for the insertion of the thermal zone geometry for simple model. ....	58
Figure 2.26. Convective star node. ....	60
Figure 2.27. Radiative exchange between three surfaces, delta (a) and star (b) network. ....	61
Figure 2.28. BTB blocks for the evaluation, by means of the simple model, of the temperature of the zone (left block) and of the ideal power for fixed thermal zone conditions (right block). ....	62
Figure 3.1. BESTEST validation scheme. ....	67
Figure 3.2. (a), (b) and (c): Experimental set-up. (1) is the heat flow meter that, together with the Pt1000 RTD sensors (2) and (3), composes the Optivelox Thermozig, (4) and (5) are outdoor and indoor air temperature sensor and (6) is the data acquisition system. ....	70
Figure 3.3. Hourly profile for the incident solar radiation over the wall (a) and of internal heat gains (b) used for the evaluation of the internal wall surface temperature with ALMABuild. ....	70
Figure 3.4. Comparison between the empirical data and the numerical result obtained using ALMABuild in terms of internal surface temperature of the wall. ....	71
Figure 3.5. The reference building geometry indicated by BESTEST for software verification. ....	74
Figure 3.6. Horizontal shading device for cases 610 and 910 (a); vertical and horizontal shading devices for cases 630 and 930. ....	74
Figure 3.7. Hourly incident solar radiation during a clear (higher profile) and cloudy (lower profile) day for: South (a) and West (b) orientation. ....	76
Figure 3.8. Trend of hourly free-floating internal air temperature for Case 600FF (a) and Case 900FF (b): comparison with the BESTEST limits. ....	81
Figure 3.9. Trend of hourly free-floating internal air temperature for case 650FF (a) and case 950FF (b): comparison with the BESTEST limits. ....	82
Figure 3.10. Comparison of the annual energy demand [MWh] predicted by EnergyPlus, the Standard EN 52016 and ALMABuild for lightweight BESTEST buildings. ....	89
Figure 3.11. Comparison of the annual energy demand [MWh] predicted by EnergyPlus, the Standard EN 52016 and ALMABuild for heavyweight BESTEST buildings. ....	90
Figure 3.12. Comparison of the annual power peak [kW] predicted by EnergyPlus, the Standard EN 52016 and ALMABuild for lightweight BESTEST buildings. ....	91
Figure 3.13. Comparison of the annual power peak [kW] predicted by EnergyPlus, the Standard EN 52016 and ALMABuild for heavyweight BESTEST buildings. ....	92
Figure 4.1. <i>Thermal zone properties</i> GUI for the data insertion for the BTB block <i>radiative model</i> . ....	98
Figure 4.2. GUI for the definition of the temperature sensor position and of the spatial discretization, for the radiative model (a) and graphical representation of the inserted data (b). The sensor is represented as the green cube in (b), whilst the grid points are in grey. ....	99



Figure 4.3. BTB block for detailed radiative model.....	101
Figure 4.4. Temperature map sub-system. Inputs are the temperature of the inner surfaces of the zone in addition to the temperature zone bus, whereas the outputs are the map of mean radiant and operative temperature distribution within the zone.....	102
Figure 4.5. Building Massive Element block for thermal zone described by the radiative model. ....	103
Figure 4.6. Layers between two cells: vertical (a) and horizontal (b). ....	105
Figure 4.7. Pressure difference ( $\Delta P$ ) between cell $i$ and cell $j$ in a vertical layer, if only buoyance forces are considered. The neutral point is located where $\Delta P$ is zero.....	106
Figure 4.8. BTB block for detailed convective model. ....	108
Figure 4.9. Customized Air Temperature Map block.....	108
Figure 4.10. BTB block for <i>fully detailed model</i> .....	109
Figure 4.11. Reference room for the validation of the MATLAB routine for view factors calculation. ....	111
Figure 4.12. (a) Plan of the room with indication of the position of the sensor; (b) Position and size of window and radiator for case A; (c) Position and size of window and radiator for case B and C. ....	114
Figure 4.13. Vertical profile of the operative temperature at the centre of the room for the coldest day of the year when the heaters reach their maximum surface temperature. ....	119
Figure 4.14. Room operative temperature distribution ( $^{\circ}\text{C}$ ) in the coldest day of the year when the heaters reach their maximum surface temperature, at three levels above the floor (0.1 m, 0.9 m and 1.7 m) in case of low thermal insulation (Case A). ....	121
Figure 4.15. Operative temperature of the room measured in the coldest winter day by the room sensor in presence of different emitters and envelope thermal insulations. ....	122
Figure 4.16. Characteristic time $\Delta t_{on}$ (a) and $\Delta t_{off}$ (b) for different emitters and for different building thermal insulation, by considering the control system dead band of 19-20.5 $^{\circ}\text{C}$ .....	123
Figure 4.17. $t_{comf}$ for emitters (1), (2) and (3), considering both low and high insulated buildings. ....	125
Figure 4.18. $t_{comf}$ for emitters (4), (5) and (6), considering both low and high insulated building. ....	126
Figure 4.19. Plant view of offices. Comfort zone is evidenced in blue, whilst A, B and C refer to the position of the temperature sensor.....	127
Figure 4.20. Room discretization in air cells, plant view (a) and height discretization (b). ....	128
Figure 4.21. Cumulative distribution of the operative temperature of the comfort zone. ....	130
Figure 4.22. Operative temperature distribution at 1 m height from the floor, when the indoor temperature reaches the upper value of the control band (20.5 $^{\circ}\text{C}$ ). a, b, c refers to the sensor position, highlighted with the red point. The red rectangle represents the comfort area. ....	131
Figure 4.23. Comparison between the operative temperature of the sensor and in the comfort zone, for two typical days of the year. The sensor is in position A (a), B (b) and C (c).....	132
Figure 4.24. Cumulative distribution of the number of daily on-off cycles of the radiator. ....	133

Figure 4.25. Cumulative distribution of the mean operative temperature of the comfort zone, sensor in position A. ....	134
Figure 4.26. Comparison of the cumulative distribution of the mean operative temperature in the comfort zone, for sensors in position C, with different settings, and Case B.....	136
Figure 4.27. Cumulative distribution of the mean operative temperature in the comfort zone, for cases R2, for different thermostat sensor position (A, B and C).....	136
Figure 4.28 Comparison between cumulative mean operative temperature for case B, with inlet water temperature of 80 °C (red solid line) and 60 °C (blue dotted line).....	137
Figure 4.29. Weather compensation curves for Case R1 and R2. ....	139
Figure 4.30. Cumulative distribution of the mean operative temperature of the comfort zone. ....	139
Figure 4.31. Cumulative distribution of the number of daily on-off cycles of the heating system adopting the weather compensation. ....	141
Figure 4.32. Cumulative distribution of the mean operative temperature of the comfort zone in cases R2 adopting the weather compensation, for different sensor position. ....	142
Figure 4.33. Cumulative distribution of the mean operative temperature in the comfort zone, for fast restart cases.....	144
Figure 5.1. Example of Pareto Frontier. In red is highlighted the Pareto frontier, composed by points B and C, whilst A represent a dominated solution.....	152
Figure 5.2. Geometry of the reference building. ....	154
Figure 5.3. Total annual energy demand [MWh] as a function of the insulation thickness of the external walls and roof and of the total clear area. ....	155
Figure 5.4. Ratio between the total energy consumptions and the total energy consumptions for the reference case, as a function of non-dimensional insulation thickness and clear area. The red point indicates the reference case. ....	157
Figure 5.5. Total, heating and cooling annual energy demand as a function of the overhang length.....	158
Figure 5.6. Annual heating (a) and cooling (b) energy demand [MWh], as a function of insulation thickness and overhang length. ....	159
Figure 5.7. Total annual energy demand as a function of insulation thickness of opaque envelope elements and overhang length. The dotted line is the local minimum curve. ....	160
Figure 5.8. Total energy demand [MWh] as a function of insulation thickness and overhang length for total clear area of 8 (a), 10 (b), 12 (c) and 14 (d) m <sup>2</sup> .....	161
Figure 5.9. Local minimum curve: the optimal overhang length is expressed as a function of the total clear area, considering the maximum insulation thickness. ....	162
Figure 5.10. Heating energy demand and mean annual PPD for buildings with windows in both East and West walls (total clear area of 9 m <sup>2</sup> ) considering different insulation levels, both in the external and internal layers. The filled markers refer to solutions that compose the Pareto frontier.....	164
Figure 5.11. Heating energy demand and mean annual PPD for buildings characterised by total clear area of 8 m <sup>2</sup> , considering different insulation thicknesses (on the external side of the elements) and various windows exposition. Filled markers concern solution of the Pareto frontier. ....	165

Figure 5.12. Indoor operative temperature for a typical winter (a) or summer (b) day, for buildings with two window expositions: East-West (blue solid line) or South (red dashed line). .....	166
Figure 5.13. Pareto frontier for the optimization of mean annual PPD and of heating energy demand. Results concern buildings composed by windows on the South wall; filled markers refer to internal insulation of opaque elements. ....	167
Figure 6.1. Air change rate (ACH) as a function of the absolute temperature difference between indoor and outdoor.....	175
Figure 6.2. Annual comfort time ( $t_{comf}$ ) for different insulation thickness, shadings and windows for cases with set point temperature equal to 21 °C, neglecting the occupant behaviour. (a) refers to window $D1$ , (b) to window $D2$ , (c) to window $D3$ and (d) to $T1$ . ....	179
Figure 6.3. Overheating ( <i>hot</i> ) and undercooling ( <i>cold</i> ) times for the optimal (highest comfort time) configuration for each window typology. ....	180
Figure 6.4 Annual comfort time for different insulation thickness, shadings and windows for cases with set point temperature equal to 23 °C, neglecting the occupant behaviour. (a) refers to window $D1$ , (b) to window $D2$ , (c) to window $D3$ and (d) to $T1$ . ....	181
Figure 6.5. Overheating time ( $t_{hot}$ ) for window $D2$ , as a function of insulation thickness and shadings, indoor set-point temperature of 23 °C.....	182
Figure 6.6. Relative standard deviation for comfort time (a) and heating energy consumptions (b), for each building configuration, due to the stochastic user behaviour model. ....	184
Figure 6.7. Annual comfort time ( $t_{comf}$ ) for different insulation thickness, shadings and windows in cases with set point temperature equal to 21 °C, considering the occupant behaviour. (a) refers to window $D1$ , (b) to window $D2$ , (c) to window $D3$ and (d) to $T1$ . ....	186
Figure 6.8. Overheating ( <i>hot</i> ) and undercooling ( <i>cold</i> ) times for the optimal (highest comfort time) configuration for each window typology, considering occupant behaviour. ....	187
Figure 6.9. Annual comfort time ( $t_{comf}$ ) for different insulation thickness, shadings and windows in cases with set point temperature equal to 23 °C, considering the occupant behaviour. (a) refers to window $D1$ , (b) to window $D2$ , (c) to window $D3$ and (d) to $T1$ . ....	187
Figure 6.10. Overheating time ( $t_{hot}$ ) for buildings characterised by window $D1$ , shading $Sh_2$ and set-point of 21 °C as a function of insulation thickness, both considering and neglecting the occupant behaviour. ....	189
Figure 6.11. Comfort time sensitivity to insulation ( $S_{comf,i}$ ) considering (blue bars) or neglecting (green bars) the occupant behaviour, for different shadings and windows: (a), (b), (c) and (d) refer to window $D1$ , $D2$ , $D3$ and $T1$ , respectively. ....	191
Figure 6.12. Comfort time sensitivity to shadings ( $S_{comf,sh}$ ) considering (blue bars) or neglecting (green bars) the occupant behaviour, for different insulations and window: (a), (b), (c) and (d) refer to window $D1$ , $D2$ , $D3$ and $T1$ , respectively. ....	192
Figure 6.13. Comparison of $S_{E,i}$ for different shadings and windows: (a), (b), (c), (d) refers to windows $D1$ , $D2$ , $D3$ and $T1$ , respectively.....	193
Figure 6.14. Sensitivity of energy demand on shadings $S_{E,sh}$ , both considering (blue bars) and neglecting (green bars) the occupant behaviour, for different insulations and windows $D1$ (a), $D2$ (b), $D3$ (c) and $T1$ (d). ....	194

Figure 6.15. Pareto frontiers of multi-objective optimizations for different window typologies, referring to buildings with set point of 21 °C. (a) refers to buildings composed by window *D1*, (b) to buildings with windows *D2*, (c) to cases with window *D3* and (d) to window *T1* cases..... 196

Figure 6.16. Pareto frontiers of multi-objective optimizations for different windows typology, referring to buildings with thermostat set point equals to 23 °C. (a) refers to buildings composed by window *D1*, (b) to buildings with windows *D2*, (c) to cases with window *D3* and (d) to window *T1* cases. .... 198

Figure 6.17. Pareto frontiers of multi-objective optimizations referring to buildings with thermostat set point equals to 21 °C (a) and 23 °C (b)..... 199

Figure 6.18. Sensitivity to the occupant behaviour of optimal building configurations for each window typology..... 202

Figure 6.19. Maximum number of window openings for specific window and shading configurations. .... 202

---

# List of Tables

---

Table 1-1. Main features of ESP-r, EnergyPlus and TRNSYS. ....	14
Table 1-2. Main features of Simulink toolboxes for building performance simulation. ....	21
Table 2-1. ALMABuild bus signals. ....	31
Table 2-2. Optical window properties. ....	48
Table 2-3. Gas gap properties ....	48
Table 2-4. Glass properties. ....	49
Table 2-5. Frame properties. ....	49
Table 3-1. Wall stratigraphy for the room considered in the ALMABuild analytical verification. ....	68
Table 3-2. Comparison between analytical [103] and numerical values of the indoor air temperature (in °C) obtained with ALMABuild. ....	68
Table 3-3. Stratigraphy of the measured wall. ....	69
Table 3-4. List of the qualification cases analysed during the comparative tests. ....	73
Table 3-5. Annual incident solar radiation [kWh/(m <sup>2</sup> year)] on the external walls of the building of Figure 3.5 obtained by using the reference software and ALMABuild. ....	75
Table 3-6. Annual solar radiation [kWh/(m <sup>2</sup> year)] transmitted by the reference windows, and its mean annual transmissivity coefficient. ....	77
Table 3-7. Annual solar radiation [kWh/(m <sup>2</sup> year)] transmitted by the reference shaded windows, and the mean annual shading factor. ....	79
Table 3-8. Annual internal air temperature values (°C) obtained for free-float (FF) BESTEST cases compared with the minimum and maximum threshold values indicated by BESTEST. ....	80
Table 3-9. Annual Heating Load (MWh) obtained for non-free-float lightweight BESTEST cases compared with the minimum and maximum threshold values indicated by BESTEST. ....	83
Table 3-10. Annual Cooling Load (MWh) obtained for non-free-float lightweight BESTEST cases compared with the minimum and maximum threshold values indicated by BESTEST. ....	83
Table 3-11. Annual Heating Load (MWh) obtained for non-free-float heavyweight BESTEST cases compared with the minimum and maximum threshold values indicated by BESTEST. ....	84
Table 3-12. Annual Cooling Load (MWh) obtained for non-free-float heavyweight BESTEST cases compared with the minimum and maximum threshold values indicated by BESTEST. ....	84
Table 3-13. Annual Heating Peak (kW) obtained for non-free-float lightweight BESTEST cases compared with the minimum and maximum threshold values indicated by BESTEST. ....	85

Table 3-14. Annual Cooling Peak (kW) obtained for non-free-float lightweight BESTEST cases compared with the minimum and maximum threshold values indicated by BESTEST. ....	85
Table 3-15. Annual Heating Peak (kW) obtained for non-free-float heavyweight BESTEST cases compared with the minimum and maximum threshold values indicated by BESTEST. ....	86
Table 3-16. Annual Cooling Peak (kW) obtained for non-free-float heavyweight BESTEST cases compared with the minimum and maximum threshold values indicated by BESTEST. ....	86
Table 3-17. Annual heating and cooling load [MWh] and peak [kW] for back zone of Case 960, compared with the minimum and maximum threshold values indicated by BESTEST. ....	87
Table 3-18. Discrepancy [%] between the maximum and minimum BESTEST threshold values for all the qualification tests. Highest and lowest discrepancies are evidenced in bold.....	88
Table 3-19. Specific heat capacity of massive envelope elements, according to EN 52016 [62]. ....	93
Table 3-20. Classification of elements by mass distribution, according to EN 52016 [62].....	93
Table 3-21. Distribution of the element capacity to the RC network node, according to EN 52016. ....	93
Table 3-22. List of validation tests performed and ALMABuild blocks (recalling the section in which are described) involved for each test.....	94
Table 4-1. Computing runtime for annual dynamic simulations of buildings in free-float conditions, adopting different kind of models. Simulations are performed with a desktop computer with a quad-core 3.40 GHz processor and 8 GB of RAM. The multizone building is composed by four thermal zones. ....	110
Table 4-2. View factors obtained with TRISCO, COMSOL and ALMABuild for the reference room, referring to surface labelled in Figure 4.11. ....	112
Table 4-3. Thermo-physical properties of the main envelope elements. ....	114
Table 4-4: List of radiant and convective heat emitters considered in numerical simulations. $n_{ej}$ is the number of element composing the radiator. ....	115
Table 4-5. Radiative power share for the different heaters. ....	117
Table 4-6. Convective ( $T_a$ ) and mean radiant temperature ( $T_{rad}$ ) when the room sensor measures an operative temperature of 20.5 °C, during the coldest day of the year, as a function of the adopted heat emitters with a low building thermal insulation level (case A).....	117
Table 4-7. Inner surface temperature (°C) distribution in the room when the emitters reach their maximum surface temperature ( $T_{em,max}$ ) during the coldest day of the year as a function of the thermal insulation level (A or B) and of the adopted emitter. ....	118
Table 4-8. Maximum specific emitted thermal power as a function of emitter and of thermal insulation level. ....	123
Table 4-9. U-values of building elements. ....	128
Table 4-10. Comfort and overheating time ( $t_{comf}$ and $t_{hot}$ ) in the comfort zone for different position of the sensor. ....	130
Table 4-11. Control system dynamics and energy demand with different sensor position (A, B, C). ....	133
Table 4-12. Comfort and overheating time ( $t_{comf}$ and $t_{hot}$ ) in the comfort zone, with sensor in position A. ....	135

Table 4-13. Comfort parameters for cases with radiator water inlet temperature of 60 °C.....	137
Table 4-14. Control parameters for cases with radiator water inlet temperature of 60 °C, and comparison ( $\Delta$ ) with case R1. ....	138
Table 4-15. Comfort and overheating time ( $t_{comf}$ and $t_{hot}$ ) in comfort zone adopting the weather compensation. ....	140
Table 4-16. Control parameters for cases with weather compensation. ....	140
Table 4-17. Comfort parameters for cases R2 with weather compensation, for different sensor position, and comparison ( $\Delta$ ) with results obtained for radiator R1. ....	142
Table 4-18. Control parameters for cases R2, for different sensor position, and comparison ( $\Delta$ ) with cases R1, considering the weather compensation. ....	143
Table 4-19. Comfort and overheating time for fast restart cases, and comparison to cases without fast restart strategy, Case R2. ....	144
Table 4-20. Control parameters for fast restart cases, sensor in different positions, and comparison to cases without the adoption of the fast restart strategy, Case R2.....	145
Table 5-1. Thermal transmittance values of the envelope elements in the reference case.....	154
Table 5-2. Main characteristics of a radiator element. ....	163
Table 5-3. Constant parameters for the evaluation of indoor comfort conditions. ....	163
Table 6-1. Main characteristics of a radiator element. ....	174
Table 6-2. Thermal transmittance of external opaque envelope elements for different thermal insulation thicknesses. ....	176
Table 6-3. Characteristics of the analysed windows. ....	176
Table 6-4. Shading factor for different overhang geometries. ....	177
Table 6-5. Annual heating energy consumptions [MWh/y], for cases with set-point temperature equal to 21 °C, for different shadings, insulation thicknesses and windows. For each window, minimum energy demand is highlighted on bold. ....	177
Table 6-6. Heating energy demand [MWh/y], for cases with high set-point, varying shadings, insulation and windows, neglecting the occupant behaviour. For each window, minimum energy demand is highlighted on bold. ....	183
Table 6-7. Heating energy consumptions [MWh/y], for cases with set-point temperature equal to 21 °C, for different shadings, insulation thickness and windows, considering the occupant behaviour. For each window, minimum energy demand is highlighted on bold. ....	185
Table 6-8. Heating energy consumptions [MWh/y], for cases with set-point temperature equal to 23 °C, for different shadings, insulation thickness and windows, considering the occupant behaviour. For each window, minimum energy demand is highlighted on bold. ....	188
Table A-6-9. List of tools from the BEST directory [14]. ....	A-2
Table B- 1. Components of the Weather Data bus. ....	B-1

Table B- 2. Component of the Sun bus .....	B-2
Table B- 3. Components of the Power Bus.....	B-3
Table B- 4. Components of the Ventilation bus.....	B-3
Table C- 1. List of blocks of the Climatic Data blockset.....	C-2
Table C- 2. List of Building Massive Element blocks, for thermal zone described by means of the <i>simple model</i> .....	C-3
Table C- 3. List of Building Massive Element blocks adopted if the <i>radiative model</i> is used for the description of the thermal zone, for non-active envelope elements.....	C-6
Table C- 4. List of Active Building Massive Element blocks.....	C-11
Table C- 5. List of blocks composing the Building Clear Component subsystem.....	C-16
Table C- 6. List of Building Thermal Balance blocks, for both temperature and ideal power evaluations. .	C-19
Table C- 7. Additional blocks used for the description of a thermal zone.....	C-22



---

# Nomenclature

---

## Roman letters

A	Area
AM	Relative optical air mass
c	Specific heat capacity
C	Total heat capacity
Cd	Discharge coefficient
cp	Specific heat capacity
d	Wall layer thickness
D	Radiosity
E	Energy
F	View factor
Fr	View factor between external component and sky
g	Gravitational acceleration
h	Heat transfer coefficient
H	Solar radiation
l	Wall layer
m	Mass flow
N	Nodes of RC models
nl	Number of wall layers
Nu	Nusselt number
P	Pressure
PPD	Predicted Percentage of dissatisfied
Prob	Probability
Q	Power
Ra	Rayleigh number
S	Sensitivity
SF	Mean annual shading factor
SG	Solar gain
SH	Shading factor
t	Time
T	Temperature
U	Thermal transmittance
Wop	Number of window openings
x	Position on a layer
Z	Height

## Greek letters

$\alpha$	Solar absorbance
$\beta$	Slope of a surface
$\gamma$	Azimuth angle of a surface
$\delta$	Solar declination
$\Delta$	sky's brightness
$\epsilon$	sky's clearness
$\epsilon_s$	Surface emissivity
$\zeta$	Sensitivity of an objective function vector
$\theta$	Angle of incident of solar radiation
$\lambda$	Thermal conductivity
$\mu$	Mean values
$\xi$	Albedo
$\rho$	Density
$\sigma$	Standard deviation
$\sigma_0$	Stefan-Boltzmann constant
$\tau_s$	Solar transmissivity
$\tau_c$	Time constant of the <i>i</i> -th element
$\Phi$	Latitude of a location
$\varphi_{\text{sky}}$	Radiative thermal flux with the sky per unit area
$\Psi$	Sola elevation angle
$\omega$	Solar hour angle

## Subscripts

a	air
b	direct component of incident solar radiation
bh	beam radiance component on horizontal plane
C	referred to the position in which the first quarter of the total thermal capacity of a wall is reached
Cd	conduction
comf	comfort
conv	convection
d	diffuse component of incident solar radiation
dh	diffuse radiance component on horizontal plane
disc	discomfort
e	external condition
em	emitter
et	extraterrestrial
fl	floor

g	ground
hot	Occupant comfort state <i>hot</i>
is	referred to the insulation layer
m	mean value
off	related to time periods in which the heating system is off
on	related to time periods in which the heating system is on
op	operative temperature
opaque	opaque envelope element
rad	radiative heat transfer
refl	reflected radiance component
rmo	running mean outdoor
roof	roof
se	external surface
sg	solar gain
sh	shaded
si	inner surface
sky	long-wave radiative heat transfer with the sky
sol	related to solar radiation
unsh	unshaded
w	window
wall	wall



# Context and Objective

---

## Abstract

In this *Chapter*, the main motivations of this work are presented. Firstly, the concept of dynamic energy simulation is introduced and the main features of tools for dynamic energy simulations of buildings and HVAC systems required by NZEB designers are described. Analysing three of the most popular *Whole Building Energy Simulation (WBES)* software available in the market, i.e. TRNSYS, ESP-r and EnergyPlus, the main features and limitations of these tools are evidenced.

Then, the features of Matlab/Simulink as framework for developing new WBES tools are discussed with the aim to demonstrate that the Matlab framework can overcome the limitations of many available WBES tools. In particular, the possibility to use all the Matlab toolboxes for solving problems concerning different issues (e.g. optimizations, CFD...) in a single computational environment, avoiding the need of coupling different software packages as well as the possibility to adopt a variable time step discretization for simulations are some of the most attractive features of Matlab for the development of new WBES tools. Therefore, the existing libraries based on Matlab/Simulink for building energy performance simulation are examined, emphasizing the main drawbacks that limited their diffusion up to now.

Finally, the outline of the Thesis, focused on the development of a new Matlab tool for the dynamic energy simulation of buildings and HVAC systems, is presented.

---

## 1.1 General context

In the last century, the economic growth and the improvement of living conditions have been accompanied by the explosion of the world energy demand, mainly characterised by the exploitation of fossil fuels like carbon, oil and natural gas. However, the exploitation of fossil fuels has two important drawbacks: the finiteness of the available resources and the negative impact on the environment (pollution and climate change).

For these reasons, in the last two decades, a series of International Agreements, like the Kyoto Protocol [1] and the Paris Agreement [2], have been concluded with the aim to limit the rise of the global temperature up to 1.5°C - 2°C, reducing the primary energy demand and encouraging the exploitation of clean and Renewable Energy Sources (RES). In Europe, the so called 20-20-20 targets reveal the great effort of the European Union (EU) to reduce the negative environmental effects due to fossil fuel exploitation. In fact, by means of the 20-20-20 targets, reported in the Directive 2009/29/EC [3], the EU imposed a 20% reduction of the GreenHouse Gas (GHG) emissions and of the energy consumptions with respect to the values measured in 1990 and a 20% of the RES share on the final energy consumption, by 2020. More restrictive targets have been established by EU for the following years, with the aim to move toward a competitive low carbon economy in 2050 [4]: in this scenario, mid-term targets have been imposed to be achieved by 2030 in the 2030 Climate and Energy Policy Framework [5]: 40% reduction of GHG emissions, compared to 1990 level, the increase of the energy efficiency at least of 27% and the RES share up to 27%.

Residential and service sectors can play an important role for the reduction of energy consumptions and GHG emissions, since they are responsible of about 34% of the global energy consumption [6]. Focusing on Europe, in 2016 the final energy consumption of the residential and service sectors has been of 434 MToe, corresponding to 40% of the total energy consumptions [7]. In Figure 1.1, it is possible to appreciate that around half of the energy used by the residential sector is provided by fossil fuels and only 16% comes from RES [7].

From these data, it is clear that important measures have to be taken, in order to achieve the European targets in the next years. In fact, in the last ten years, EU published a series of Directives, for encouraging the adoption of RES systems, enhancing the building energy efficiency and reducing the use of fossil fuels, for both new and current buildings. The European Directive 2010/31/EU [8], known as the Energy Performance of Building Directive (EPBD), contains the definitions of minimum level of energy performance for building and heating, cooling and ventilation (HVAC) systems for both new and current buildings, according to the “cost optimal approach”. Moreover, EPBD 2010 imposes to the Member States (MS) the transition toward the Nearly Zero Energy Building (NZEB) for new

buildings within 2020. In 2012 EU issued the Energy Efficiency Directive (EED) [9] that imposes a renovation rate of at least 3% for the building stock of central governments of MS, since the current renovation rate in Europe is close to only 1% [10], whilst it has been recognized that around 97% of the European building stock has to be renovate in order to achieve a decarbonised building stock by 2050 [11].

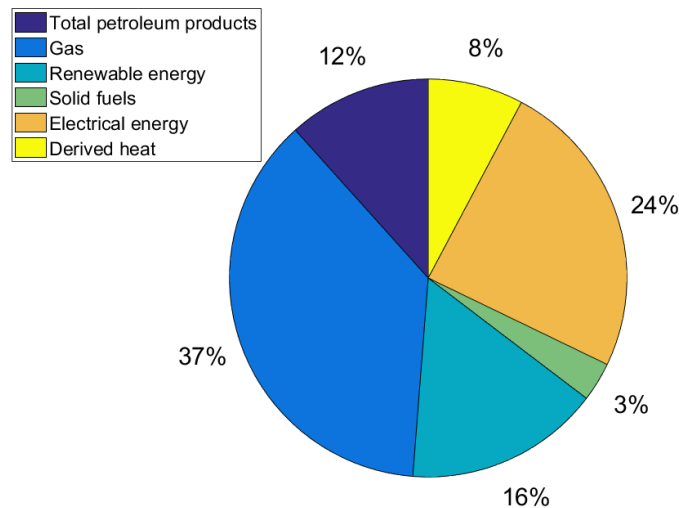


Figure 1.1 Fraction of energy sources in the residential sector in Europe, in 2016 (from [5]).

## 1.2 NZEB design

Even if there isn't a unique, harmonised concept of NZEB across the MS, EPBD 2010 defines NZEB as buildings characterised by a very high energy performance, in which the very low energy needs are mainly covered by RES. These goals cannot be achieved using classical design strategies, based on a quasi-stationary calculation approach, by means of which energy consumption assessments are obtained considering monthly mean conditions. In fact, NZEB can be designed only by means of a detailed evaluation of the effect of shadings, of the different thermal inertia of building elements, of the internal gain profile and the occupant behaviour (e.g. windows operation, thermostat set-point control) on the energy needs of a building. In addition, the designers must be able to characterise properly RES systems, whose performance strongly depends on variable external conditions (i.e. heat pumps performances depend on the external air temperature and humidity, photovoltaic systems or thermal solar collectors by the incident solar radiation and so on). Besides, the adoption of multi-sources heat generators able to use different energy sources, introduces the problem of the automatic selection of the generation system that, in a specific moment, is able to guarantee the highest performance or the minimum costs or

the highest exploitation of RES, according to different control strategies. In all these cases, a quasi-stationary calculation approach becomes inadequate for the prediction of global energy needs of NZEB.

For these reasons, during the last decade more and more designers are moving from a quasi-stationary approach to a dynamic one for the energy modelling of buildings. Actually, dynamic simulations can be used for the evaluation of passive behaviour of a building, predicting the hourly profile of the internal temperature in free-running conditions (with no HVAC system in operation), as an example.

The design phase of a NZEB requires also a detailed comfort assessment; in fact, energy savings should not lead to a reduction of indoor comfort conditions. On the contrary, optimal design solutions have to be found in order to save energy improving, at the same time, indoor comfort conditions, as it can be done by eliminating overheating/undercooling periods during the year.

It is clear how NZEB design requires the research of a trade-off between energy savings, indoor comfort conditions and economical convenience, that leads the designer to the optimisation of two or more conflicting goals. Multi-objective optimisation can help the designer to comply with these goals, giving the important feedbacks about the selection of envelope elements and HVAC components.

### 1.3 Dynamic Energy Simulations

The building dynamic energy simulation is an advanced calculation tool based on specific numerical models by means of which detailed information about the thermo-energetic behaviour of the whole building-HVAC system can be obtained. Dynamic simulations are able to give to the designer an accurate reconstruction of the time variation of thermal loads obtained by using adequate time steps, thanks to the introduction of a large amount of input data:

- geometrical information, from orientations and area of each envelope component for the simplest model to the coordinates that define each building component in a three-dimensional cartesian space, required in detailed models in which the internal radiative heat transfer is evaluated by means of view factors;
- thermophysical properties (i.e. thermal conductivity, density, specific heat capacity, water vapour permeability...) of each layer of massive envelope element like walls, roofs and floors;
- windows properties: optical and radiative glass properties, thermophysical data for the gas contained in windows cavity and for the frame;



- thermal zone user profiles: occupancy, internal gains, ventilation profiles, indoor temperature set-up schedule;
- performance maps of each HVAC component (look up tables);
- weather data, like external temperature, vapour pressure, external humidity ratio, wind velocity and direction, solar radiation collected with hourly or sub-hourly frequency.

Contrary to dynamic simulations, models based on a quasi-stationary approach require less input data: as an example, external conditions are described by monthly mean values, whilst for envelope elements only the thermal conductivity is considered among the thermophysical properties. The typology and the number of input data required by quasi-stationary models are described in several National Standard, like the UNI TS 11300 in Italy, where standard profiles for ventilation and internal heat gains can be found.

On the contrary, for the dynamic approach, up to date there is the lack of a Standard which defines the minimum input data required and where some standard schedule for the main user profile can be found (in Italy there is only a draft for a new Standard focused on the base assumptions for building dynamic energy performance simulations [12]). Moreover, it has to be remarked that all the input data required by models based on quasi-stationary approach can be got from technical data sheet, whilst for dynamic models this does not happen. A common example of this lack of information is represented by the window: for its description several dynamic models require information about the angular dependencies of the optical properties, but in common data sheet only aggregate or mean values are reported, that are enough for quasi-stationary models. This lack of standardization of the input data needed by dynamic models leads to two important drawbacks:

- Uncertainty of the building description, due to the lack of information;
- Variability of the input data required by different dynamic models.

In quasi-stationary simulations, internal conditions (i.e. air temperature) in quasi-stationary simulations are constant input data and from these input data monthly energy consumption and energy losses through the building are estimated. On the other hand, in dynamic simulations internal conditions are not input data, but they are calculated as response to the external and internal (due to HVAC, presence of people, internal gains...) loads; the evaluation of internal conditions is possible thanks to the adoption of short time steps and a correct evaluation of the thermal inertia of the massive building elements in the energy balance equations. In addition, it has to be remarked that in dynamic simulations several physical phenomena (i.e. conductive, convective and radiative heat transfer, mass transfer...) are taken into account together.

As for input data, dynamic simulations are characterised by a huge number of outputs by means of which the dynamic behaviour of the simulated building-HVAC system is described. The main outputs of a dynamic simulation are:

- Air temperature of the thermal zone;
- Surface temperature of each envelope component;
- Thermal fluxes of each envelope component;
- Occupant thermal comfort indexes (i.e. Predicted Mean Vote and Predicted Percentage of Dissatisfied [13]);
- Instantaneous values of solar shadings;
- Thermal power released by the HVAC system to the thermal zone.

Due to important simplifications which characterise quasi-stationary simulations, this approach is typically used for the estimation of the energy consumption of a building considering fixed conditions, with the aim to obtain a building energy performance certificate. On the contrary, dynamic simulations are used for voluntary certifications, like LEED (Leadership in Energy and Environmental Design) certificate developed by the U.S. Green Building Council, which considers all the aspect of a building (e.g. economic issues, water consumption, indoor air quality, energy consumption and GHG emissions) and it is used for ranking energy and water efficient, healthy, environmentally-friendly cost saving buildings. Moreover, dynamic simulations are adopted each time it is required to analyse the behaviour of the building-HVAC system in particular conditions or for making energetic diagnosis or in the design of high energy performant buildings or refurbishments.

### 1.4 Dynamic Energy Simulation Tools

In section 1.2, the three main characteristics of the NZEB design have been highlighted:

- Adoption of a dynamic approach instead of the quasi-stationary one for the analysis of the energy performances;
- Detailed comfort assessment;
- Multi-objective optimisation issues (comfort, cost, energy savings).

In order to help the designer to comply with these new goals, a great number of tools has been developed in the last years. In the Building Energy Simulation Tools (BEST) directory, previously managed by the Department of Energy of the United States and now under the control of the International Building Simulation Association (IBPSA), a list of 181 software tools can be found [14]. The BEST's directory enumerates tools related to the building energy performance assessment; as reported in *Appendix A*, where the tools collected in BEST's directory are listed (except the training and support service tools), these tools have different capabilities. Not all these tools are able to perform an energy performance assessment, some of them are related to the weather data analysis and they are used for making these data available for other software; other tools are used for collecting data for performing building energy audit, for enabling

parametric and optimisation analysis or for making air flow or detailed component simulations. Moreover, two kinds of software able to carry out the evaluation of the energy performance of a building can be found in the BEST's directory: one is based on dynamic simulations of the whole building-HVAC system (*Whole Building Energy Simulation, WBES, software*), the other is based on energy bills analysis.

Among all these tools, the most interesting for NZEB design are the WBES, a little fraction of all the tools reported in the BEST's directory. These tools are used for the prediction of the temporal evolution, under unsteady boundary conditions, of several physical parameters, enabling energy dynamic simulations. In this way, detailed information about the dynamic behaviour of the building coupled with its HVAC system are available and the evaluation of the impact of energy savings measures can be accurately analysed. The main differences among the WBES are related to:

- The list of the physical phenomena accounted for (i.e. shading effects, natural or mixed ventilation, air moisture transport/buffer, illuminance and so on);
- The kind of the adopted modelling (i.e. modelling based on lumped parameters, finite volume or transfer functions);
- The solver scheme (i.e. minimum time-step allowed, 2- or 3-dimensions geometry models and so on);
- Ability to model complex control systems;
- Possibility to evaluate occupant comfort and behaviour.

Generally, WBES tools do not allow a detailed prediction of comfort conditions, since the complete control of the local indoor conditions of a thermal zone needs a detailed reconstruction of the spatial distribution of humidity ratio, radiant temperature and air velocity among other parameters. To obtain this goal, a complete Computational Fluid Dynamics (CFD) simulation is generally needed, with an increase of the computational cost of the whole simulation which is obtained by coupling CFD and WBES by introducing the “*co-simulation*” concept. This concept describes simulations in which two or more software platforms are combined together with the aim to obtain detailed information about the observed system. For these reasons, another important feature required to WBES tools for being used for NZEB design is the ability to share information during the run-time simulation process with other software: in this way, not only detailed comfort assessment can be made (i.e. by coupling WBES tool with CFD), but also different WBES tools able to analyse only single physical phenomena could be coupled together and used for NZEB design.

Co-simulation is used also for solving multi-objective optimization problems, very frequent in the design of NZEB: in fact, WBES tool in some cases is not directly able to use optimisation algorithms. In these cases, multi-objective optimisation is obtained by using a specific external software (like

modeFRONTIER [15]) in order to drive the WBES tool through the optimization. By means of the optimisation algorithm implemented in a dedicated software, input data of dynamic simulations performed with WBES tool can be iteratively modified, until optimal solutions are found.

## 1.5 Time step discretization

The dynamic approach consists in the description of several physical phenomena by means of transient balance equations. The accuracy of the solution of these equations depends on the time step discretization adopted, that is related to the time constant of the analysed system.

As represented in Figure 1.2 a building is composed by a series of elements, like walls or roofs (indicated as 1 and 2), windows (3) and HVAC components (4 and 5), which are described by different transient equations.

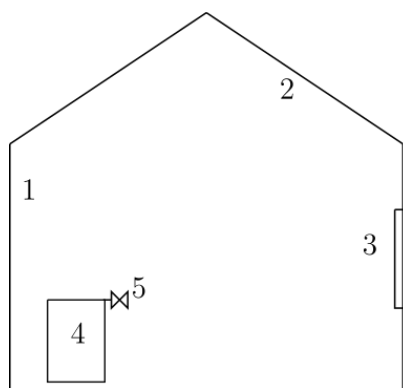


Figure 1.2. Example of elements composing a building-HVAC system, characterised by different time constants.

Generally, in a dynamic model, a transient equation related to  $i$ -th component of a building or HVAC system has the following generalized expression:

$$\frac{dT_i}{dt} = -B_i T_i + C_i \quad (1.1)$$

In this equation,  $T_i$  represents the dependent variable of interest, whilst  $B_i$  and  $C_i$  are coefficient not depending from  $T_i$ . As an example, equation (1.1) can describe the air thermal balance in a thermal zone; in this case  $T_i$  is the air temperature of the zone,  $B_i$  is the global heat transfer coefficient over the air thermal capacity and  $C_i$  represents the thermal fluxes not depending on the air temperature, like internal gains or solar radiation, scaled on the air thermal capacity.

The general solution of equation (1.1) can be expressed as the linear combination of the solution associated to the homogeneous equation and a steady-state particular solution of (1.1) as:

$$T_i = A_i e^{-B_i t} + \frac{C_i}{B_i} \quad (1.2)$$

where  $A_i$  is a constant that can be determined by means of an initial condition on  $T_i$ . From this equation, the time constant of the system,  $\tau_{ci}$ , can be derived as  $1/B_i$ .

The time constant indicates the characteristic time interval during which the system is able to react to a variation of its thermal conditions. Following the previous example, for the thermal balance of the air of a thermal zone the time constant is given by the ratio between the air capacity and the total heat loss coefficient. A similar equation is obtained for the dynamic analysis of massive envelope elements; again, the time constant of the element is given by the ratio between its thermal capacity and its thermal transmittance.

However, referring to the two examples described, even if the time constants have the same definition, as the thermal capacity of the massive element is at least three or four order of magnitude higher than that of the air, whilst heat loss coefficients are of the same order of magnitude, time constants assume very different values. In fact, the time constant related to the heat transfer that affects the air in the thermal zone is on the order of minutes, whilst heat transfer across massive elements has characteristic time interval of the order of hours. Therefore, a dynamic model of a building is composed by a set of very different time constants (one for each element of the analysed system): indoor air temperature has a time constant of minutes, the massive elements of hours, and HVAC elements, like thermostatic valves, are described by time constants of seconds.

As the time constant is a measure of the characteristic time interval of the considered physical phenomenon, accurate dynamic simulations, which are able to take into account all the dynamic phenomena involved in a building, must be obtained by considering a time step discretization lower than the smallest time constant of the whole system.

Due to the important discrepancy among the time constants involved in the building-HVAC system description, building models based on the dynamic approach can be solved in different ways, depending on the features of the numerical solver adopted. In detail, numerical solvers are characterised by the typology of time step (constant or variable) that are able to manage and by the ability to solve in a single environment several equations adopting different time steps for each equation.

Numerical solvers that adopt the same, constant time step discretization for the solution of the ordinary differential equations are the simplest. In this case, accurate solutions are obtained if the constant time step is less or of the order of magnitude of the lower time constant (which describes the fastest phenomenon). Nevertheless, usually the time step allowed by the solvers have a lower limit, which can depend on the models used for the building description. Moreover, it has to be remarked that, the lowest is the time step, the higher is the simulation time. For this reason, constant time steps are usually hourly or sub-hourly, making models based on this kind of solver not suitable for the simulation of building coupled with controlled HVAC system.

More complex solvers allow the use of variable time step. In this case, the solver refines the solution reducing the time step discretization if necessary, i.e. when faster phenomena became dominant on the other slower phenomena. As an example, when the HVAC system is off, the solver can adopt a time constant of few minutes, in order to evaluate correctly the internal air temperature variations, but when the HVAC system is on and the thermostatic valves open, the solver must be able to refine the solution adopting a time constant of seconds, in order to describe accurately the transient of the fastest phenomenon generated by the valve operation. In this way, accurate simulation of the whole building-HVAC system can be obtained with reasonable simulation time and by assuring accurate results.

Finally, some numerical solvers are able to solve different equations with different time step in the same numerical environment. Usually, this typology of solvers adopts two different time step discretization and equations are divided in two categories as a function of their time constant: equations related to slow transients are solved with the higher time step, whilst the remaining equations (concerning the HVAC system) with the lower one. By means of this kind of solver, between two consecutive time steps for the slow transients, fast transients are evaluated several times. In this way, the simulation time is lower than if a single time step is considered, but the solution may be less accurate, due to the fact that the coupling between building and HVAC system is simplified, as the equations related to the building and the HVAC systems are solved with different time steps.

### **1.6 Description of the main WBES tools**

After having listed the main characteristics required to a WBES tool for the NZEB design and having described different numerical solvers adopted for the solution of set of transients, three specific WBES tools, very diffuse in the thermal engineering community, are described (ESP-r, EnergyPlus, TRNSYS) in order to highlight their peculiarities and their suitability for NZEB design.

### 1.6.1 *ESP-r*

ESP-r is an open-source software, created in 1974 by the University of Strathclyde, for the building energy performance modelling. ESP-r is a whole building simulation software that enables the analysis of the interactions between envelope, external conditions, air flows, HVAC, control systems and comfort conditions of a building [16]. In ESP-r, each physical domain is analysed subdividing it in several sub-volumes, each of them described by mass, momentum and energy conservation equations. The domain sub-division is controlled by the user, defining different detail levels. In this way, in the early design phase, a thermal zone could be analysed as a single volume, in which air is perfectly mixed, whilst in more advanced design phases more sub-volumes could be considered for the same zone enabling the evaluation of air stratification in the zone. Increasing considerably the number of sub-volumes used for the description of a thermal zone, CFD analysis is possible, adopting also models for the descriptions of air turbulent flows (e.g.  $k-\epsilon$  model).

Finite difference method is adopted also for the HVAC system modelling. Again, HVAC components can be modelled by means of a single volume or with a higher number of volumes. Models of the main HVAC systems (solar [17], air conditioning [18]- [19] or cogeneration plants [20]- [21]) can be found in the ESP-r Database.

In ESP-r, the equations set describing all the physical phenomena considered (conduction, radiative heat transfer, air flows...) is processed simultaneously [22]. However, the different domains of a building are characterised by different time constants (i.e. envelope elements with higher thermal inertia and higher time constant compared to HVAC components). For reducing the simulation time, in ESP-r the modular solver uses different, but constant, time steps for solving building and HVAC system models. In this way, as an example, the energy balance equations of a thermal zone can be solved adopting an hourly time step, and within this time step, the state of the sub-systems characterized by time constants lower than 1 hour (i.e. HVAC systems) are evaluated a different number of times depending on the value of their time constant.

Multi-objective optimisation problems can be solved using ESP-r, but only coupling it to another software that contains optimisation algorithms, as demonstrated by Padovan and Manzan [23], who coupled the modeFRONTIER optimisation tool with ESP-r for the optimisation of a PCM enhanced storage tank in a solar domestic hot water system.

### 1.6.2 *EnergyPlus*

EnergyPlus is a modular, open-source software for the building energy performance modelling, created in 2001 and based on the more detailed sub-routines of two other WBES tools: DOE-2 and BLAST, developed by the US

Department of Energy (DoE) and by the US Department of Defence (DoD) [24]. The main feature of EnergyPlus is the absence of user-friendly Graphical User Interface (GUI): input data have to be inserted by means of an ASCII text. Actually, several GUI software, like DesignBuilder and OpenStudio, have been developed for the data insertion and for the output analysis by independent software developers.

EnergyPlus is built around three main modules: the Surface Heat Balance Manager (SHBM), the Air Heat Balance Manager (AHBM) and the Building Systems Simulation Manager (BSSM).

The SHBM adopts the Conduction Transfer Function (CTF) method for the determination of conductive heat transfer through each envelope element and, consequently, for the evaluation of its surface temperature. In CTF method the internal surface temperature and the internal heat flux are evaluated as a function of response factors, external heat flux and external surface temperature. It has to be remarked that response factors are constant coefficients evaluated once and depending on the time step selected by the user. Moreover, a limitation of the CTF method is that only surface temperature (indoor and outdoor) and heat flux are known, that means that no information can be obtained on the internal temperature distribution, which is fundamental for the prediction of interstitial condensation within the envelope elements. For these reasons, in addition to the CTF method, which is the default method used by SHBM, other algorithms based on finite difference methods are implemented in EnergyPlus.

The Air Heat Balance Manager is used for the prediction of the internal air temperature, that is evaluated solving the internal heat balance considering simultaneously both the convective and the radiative heat transfer mechanisms, assuming uniform air temperature (perfectly mixed air).

Finally, the Building Systems Simulation Manager is used for the simulation of the main HVAC components. The modelling of HVAC components is less detailed with respect to the building envelope description and most of the components are described by means of input-output correlations.

The main upgrade of EnergyPlus compared to DOE-2 and BLAST is represented by the Integrated Solution Manager (ISM) that enables the simultaneous solving of the three main modules (SHBM, AHBM and BSSM). In this way, there is a feedback between the calculation made by the HVAC modules and the loads calculation, that leads to a more accurate air temperature evaluation. Calculations are performed iteratively: firstly, thermal loads are evaluated assuming the internal air temperature as a constant equal to the set-point value, then the heat power released by HVAC components to the thermal zone is calculated, finally the internal air temperature is obtained by means of the balance between loads and HVAC delivered power.

Since envelope elements and HVAC components are characterised by different time constants, EnergyPlus performs load calculations (depending on



the interactions between building envelope and the external environment) considering hourly or sub-hourly (e.g. 15 minutes) time steps, whilst the HVAC system state is evaluated considering a different, variable time step, that cannot be defined by the user.

Co-simulations can be easily performed in EnergyPlus by means of the functional mock-up unit for co-simulation interface [25], enabling detailed comfort evaluations and indoor air quality assessment, as demonstrated by Dols *et al.* [26], who combined CONTAM with EnergyPlus for the evaluation of indoor contaminant distribution in a multi-zone building.

EnergyPlus does not provide any tools for managing of multi-objective optimisation problems. However, these problems can be solved coupling EnergyPlus with dedicated software, like GenOpt able to be coupled to any external program that writes input and output files in *txt* format. An example can be found in [27], where GenOpt has been coupled with EnergyPlus for evaluating the optimal PCM-drywall thickness that minimizes the annual energy consumption of a building in different climate.

### 1.6.3 TRNSYS

The TRaNsient SYstem Simulation (TRNSYS) program is a commercial component-based software created in 1975, by the joint work of several research institutions, like the Solar Energy Laboratory (SEL) of the University of Wisconsin-Madison, the Thermal Energy Systems Specialist (TESS, an engineering consulting company) and the French Centre Scientifique et Technique du Bâtiment (CSTB).

In TRNSYS, a dynamic model is built around by the adequate link between different “*Types*”, which are subroutines describing a specific component. Several TRNSYS libraries are available, the Standard one contains *Types* for the modelling of the main HVAC systems, electrical devices, hydrogen systems, solar energy systems and buildings. In particular, the building model is represented by a single *Type* (*Type* 56). Generally, the user has to set up the parameters of each *Type* involved in the model and to create the connections among the *Types*, in order to build a system. Since the building description can be very complex and the number of data required is very high, for *Type* 56 a dedicate tool named TRNBuild has been developed for driving the user in the data insertion and in the linking with the weather data *Types*.

The prediction of internal air temperature and thermal loads of each thermal zone is performed within *Type* 56, assuming a single air node for each thermal zone; in other words, the internal air is assumed to be perfectly mixed and no local information about the air temperature distribution in the zone is available. The temporal evolution of the surface temperature of an envelope component and the conductive heat transfer are predicted by means of constant coefficients

evaluated by means of the Mitalas transfer function method [28]. The number of these coefficients depends by a user parameter: the time base. The default value of the time base is one hour, whilst for heavy envelope component higher values are suggested. It has to be remarked that the time-base is used only for the evaluation of these parameters and it can differ from the fixed simulation time-step, set by the user. However, the time step cannot be greater than the time-base value [29].

Co-simulation is a very important method used for overcoming TRNSYS limitations. As an example, in TRNSYS the adoption of a Transfer Function Method for the modelling of the conduction within building elements does not allow the prediction of the temperature distribution and of the hygrothermal behaviour of these components. Ferroukhi *et al.* [30] solved this problem coupling COMSOL to TRNSYS, by means of Matlab; in this way the authors were able to predict the hygrothermal behaviour of the building and to evaluate mould health risk. Moreover, since a thermal zone is described only adopting a single air node, indoor air quality assessment (i.e. air temperature and contaminant distribution) becomes possible only by coupling TRNSYS with CFD software: as an example, Fan *et al.* [31] coupled ANSYS/FLUENT with TRNSYS for the evaluation of the indoor air quality and of thermal performance of a building in which a recovery ventilation system is used. Finally, co-simulation is used also for solving multi-objective optimisation problems; TRNSYS input and output files are compatible with GenOpt tool [32], but other platforms can be successfully used like Matlab [33] or the MOBO tool [34].

#### 1.6.4 Limitations and comparison of the main WBES

In the previous sections, the main characteristics of three popular WBES tools have been described, focusing on their capacity to meet the key features of NZEB design (dynamic approach, detailed comfort assessment, multi-objective optimisation problems). Since a common aspect of all WBES tool is to adopt a dynamic approach (even if with a different detail level) for the energy calculation of a building-HVAC system, Table 1-1 highlights the different ability of the three popular WBES tools to perform detailed comfort assessment and to solve multi-objective optimisation problems in stand-alone configuration. In addition, the typology of time step discretization (F means fixed, V variable) adopted during the simulation is reported.

Table 1-1. Main features of ESP-r, EnergyPlus and TRNSYS.

WBES	Detailed comfort assessment	Optimisation problems	Time step
ESP-r	✓	X	2-F
EnergyPlus	X	X	2-F-V
TRNSYS	X	X	1-F

As reported in Table 1-1, detailed comfort assessments are possible only using ESP-r, among the considered WBES tools. This is due to the fact that ESP-r is the only software able to sub-divide a thermal zone in several sub-volumes; in this way, the air temperature distribution and, consequently, the spatial distribution of comfort conditions can be predicted. On the contrary, in TRNSYS and EnergyPlus thermal zones are described by means of a single air node, so that a single mean air temperature can be evaluated and temperature distribution in a thermal zone can be obtained only by means of co-simulation with CFD software.

Co-simulation is also the only way to solve multi-objective optimisation problems for the three WBES considered here. The need of co-simulation for meeting the key features of the NZEB design represents a critical drawback of these tools: the need of several software can lead to an increase of the investment costs for the software license; moreover, expertise in all the coupled software is required, limiting the number of users able to perform these kinds of analysis. Finally, compatibility issues of different software and limitations due to the high computing time and difficulties on the handling of data exchange at different time steps cannot be neglected.

From Table 1-1 it can be noted that ESP-r and EnergyPlus adopt two different time step discretization: the bigger time step, defined by the user, refers to the time discretization for the evaluation of thermal zone loads and temperatures, whilst the lower time-step, that cannot be defined by the user, is related to the time discretization for the prediction of the HVAC system behaviour. The time step defined by the user is fixed and generally it ranges from few minutes to one hour; on the contrary, the second time step is fixed for ESP-r and variable in EnergyPlus. The use of two different simulation time steps for the evaluation of the dynamics of envelope and of HVAC systems represents a trade-off between accuracy and simulation time: in this way, the HVAC systems state is evaluated several times keeping constant the envelope state. On the other hand, TRNSYS adopts only a fixed time step for both envelope and HVAC systems analysis. Keeping in mind the observations about fixed and variable time steps described in section 1.5, it can be assessed that EnergyPlus allows the most accurate evaluation of the building (envelope and HVAC systems) behaviour, followed by ESP-r, whilst TRNSYS seems the most inaccurate. However, as remarked by Wetter [35], in traditional dynamic simulation software, like TRNSYS or EnergyPlus, the building and HVAC model is based on numerical solution algorithms that use discrete time representation of the building envelope dynamics that does not allow time step of the order of seconds, which is the typical time domain of the control system dynamics. That means that, in all the cases, the temporal evolution of the HVAC systems is not accurately simulated by these tools.

Finally, another important issue is the possibility to upgrade the WBES tool by adding new features by means of new components. Even if open-sourced codes

(i.e. ESP-r) and TRNSYS allow the creation of a new model, only user with high numerical skills can successfully attempt this effort, due to the specific program language adopted by each tool. The possibility to upgrade a tool in a simple way is another important feature required to a WBES tool in order to improve the diffusion of these tools among the designers.

In conclusion, the analysis of the most popular WBES tools puts in evidence the presence of three critical issues that can limit the diffusion of this approach among the NZEB designers: (i) the need of co-simulations involving different numerical tools for a complete analysis of a building-HVAC system, (ii) the different level of accuracy of the modelling of controlled systems linked to the limitations on the adoptable numerical time steps and (iii) the low level of customization of these tools.

### **1.7 Matlab/Simulink building performances simulation libraries**

During the last ten years a series of tools for dynamic simulations on energy building performances based on customized libraries developed for Simulink, a computational platform for multi domain simulation of dynamic systems integrated in Matlab, has been proposed. The choice of Matlab/Simulink as a framework for the development of libraries for building performance simulations is motivated by the main features of this computational environment.

First of all, Simulink contains a set of state-of-the-art Ordinary Differential Equations (ODE) solvers that allows the modelling of dynamic continuous, discrete and hybrid systems in which the time-dependent governing equations can be solved in time by using both fixed or variable time steps. Moreover, default libraries composed by blocks for the modelling of the most common controllers are already present in Simulink. New libraries consisting of customised blocks can be easily implemented in Simulink, since Simulink adopts a graphical programming language, making the model development intuitive even for users without a specific expertise in complex language programming (i.e. C or Fortran). In addition, as Simulink is integrated in Matlab, all Matlab toolboxes can be used in Simulink, enhancing Simulink modelling capabilities. Furthermore, Matlab is equipped with many tools that can be used for solving optimisation problems: Optimisation Toolbox and Global Optimisation Toolbox can be used for solving multi-objective optimisation adopting different algorithms (like Genetic Algorithm, Particle Swarm Algorithm or Linear Search Algorithm). Besides, the advanced features of Matlab for post processing can help the designers to have a better understanding of the simulation results.

Finally, the problem due to the long simulation time required for a single annual simulation for complex models, that can make optimisation problems unaffordable [36], can be overcome in Matlab reducing the complex model to a

simplified one (meta-model) by means of several toolboxes, like the System Identification Toolbox, the Neural Network Toolbox, the Design and Analysis of Computer Experiment (DACE) Toolbox or the Statistics and Machine Learning Toolbox, as demonstrated by Prada *et al.* [37].

From this brief description of Matlab capabilities, it becomes evident how all the main problems evidenced by the most popular WBES tools (co-simulation, optimization and customization) can be solved by using Matlab/Simulink as framework for the development of a specific blockset devoted to the analysis of energy building performances. In fact, the need of co-simulation for having more detailed information about air temperature distribution in a thermal zone can be solved in Matlab by considering the possibility to model all kinds of equations within this computational platform; furthermore, optimisation problems can be managed by using dedicated Matlab toolboxes which can easily recall Simulink. In addition, the native capability of Simulink to use variable time steps, even in the order of seconds, and the presence of blocks devoted to the modelling of the most diffuse control systems makes it a suitable platform for the analysis of the “building-HVAC” system; finally, the Simulink graphical programming language facilitates the creation of new customized blocks even to users without specific skills in computational languages.

For these reasons, Matlab has been individuated as a promising environment for developing a comprehensive tool for dynamic simulations of complete “building-HVAC” systems by many authors (Morini and Piva [38]- [39] and Ahmad *et al.* [40]).

In the past, several building performance Simulink libraries, like SIMBAD, CARNOT, IBPT and HAMBASE have been proposed, but, up to now, a series of issues have limited their diffusion. In the following paragraphs, a summary of the main features of these software (and their main drawbacks) is presented.

### **1.7.1 IBPT**

The cooperation of the Building Physics research groups of Chalmers University of Technology in Gothenburg (Sweden) and the Department of Civil Engineering of the Technical University of Denmark in Copenhagen led to the development, in 2002, of the International Building Physics Toolbox (IBPT). The IBPT toolbox is an open source and free of charge Matlab toolbox that contains a Simulink library. Since the focus of IBPT is the Heat, Air and Moisture (HAM) transfer analysis in buildings, the IBPT Simulink library is composed by detailed dynamic models of the envelope elements, but heating/cooling systems are roughly modelled, neglecting the heat generation and the hydraulic loop presence. However, as an open source toolbox, new and customized blocks can be easily developed, adopting the data exchange formats (seven different data arrays) defined in the main documentation of the toolbox [41].

Nik *et al.* [42], used IBPT for the evaluation of hygrothermal performance and mould growth risk in ventilated attics considering possible climate change in Sweden; IBPT has been used also by Kalagasidis [43] for the evaluation of thermal performance of phase change materials in buildings and by Muresan *et al.* [44] for the study of the impact on energy consumption of a radiant floor heating and a panel radiator.

The main drawbacks of IBPT are related to the manual data block insertion and the building model development, that is achieved by the manual link of IBPT library blocks. These two features make the data insertion and the model development the most problematic step of the design phase. Moreover, the adoption of a fixed time-step required by the finite control volume method used for the evaluation of one-dimensional HAM transfer among the walls [45] limits the possibility to analyse accurately the control system behaviour in affordable simulation time. Finally, the thermal zone models implemented in IBPT do not allow the evaluation of indoor air temperature spatial distribution, that can be determined only by means of specific co-simulations involving CFD.

### 1.7.2 CARNOT

The Conventional And Renewable eNergy Optimization Toolbox (CARNOT) blockset is a Simulink library developed by the Solar Institute Juelich and commercially available since 1999 [46]. The development of CARNOT was initiated by financial support of Viessmann GmbH, one of the most popular German manufacturer and market leader of house heating equipment. However, the success of this numerical tool has been scarce as proved by the actual limited diffusion of this library (limited to German countries).

By means of the CARNOT blockset detailed HVAC system modelling is possible: the modelling of the hydronic loops is obtained thanks to pre-set dynamic models of pipes, valves, pumps and flow mixers/diverters, as well as boilers, solar collectors, chillers and heat pumps models, emitters and storage available in CARNOT. In order to simulate accurately heating/cooling systems, CARNOT allows the use of variable time step, that can decrease to sub-second range enabling the study of highly dynamic systems, as controllers.

The CARNOT blockset has been mainly used for the evaluation of the HVAC systems energy performances: solar air collector have been considered by Delahaye *et al.* [47]; Ochs *et al.* [48] analysed heat pumps coupled to ground heat exchangers, whilst façade integrated micro-heat pump in combination with mechanical ventilation with heat recovery are studied by Dermentzis *et al.* [49].

In addition to the set of blocks representative of the most important HVAC devices, in CARNOT only simplified blocks for the building modelling are available up to now. This represents an important drawback of CARNOT, since a correct evaluation of the integrated building-HVAC system can be achieved only

by means of a detailed building and HVAC system modelling. Moreover, the absence of a detailed building model that enables the evaluation of the spatial distribution of the indoor air temperature leads to the need of co-simulation in which CFD models are involved. Last but not least, another critical aspect of this Simulink blockset is related to the model creation which requires a heavy input phase obtained by connecting manually the different blocks and by using input data lists contained in specific Matlab scripts.

### 1.7.3 HAMBASE

The development of the Heat Air and Moisture model for Building And Systems Evaluation (HAMBASE) starts in 1987 with the publication of ELAN [50], a model for the calculation of the indoor air temperature and of the heating and cooling energy needs in multi-zone buildings. Later, de Wit developed a separate model for the simulation of the indoor air humidity, called AHUM [51]. Only in 1992 these two models were combined in the WAVO model [52] and implemented in the Matlab environment; several upgrades follow, according to the evolution of Matlab capabilities, and in 2004 the WAVO model is definitively renamed HAMBASE [53]. There are three versions of HAMBASE: the HAMBASE continuous model, the HAMBASE\_R model used for research purpose, in which finite differences discretization is adopted, and HAMBASE\_S in which Simulink is used as computational environment.

The peculiarity of HAMBASE\_S is that the implementation in the Simulink environment enables the detailed evaluation of HVAC installations and of the control systems. In order to reduce the simulation time, the evaluation of heat fluxes through the envelope are performed considering a constant time step, generally of one hour, whilst the HVAC system behaviour is estimated according to a variable time step. In this way, highly dynamic systems are accurately simulated, slightly reducing the envelope behaviour accuracy, in limited simulation times.

HAMBASE has been mainly used in problems focused on the control systems behaviour: as an example, Schellen and Van Schijndel [54] determined the optimal set-point control for an all-air heating system in a church with the aim to minimize the moisture negative effects on a monumental wooden organ. More recently, by means of HAMBASE several control methods have been analysed with the aim to reduce the energy consumption for heating and cooling in NZEB increasing the energy self-consumption [55].

As for the previous toolbox based on Simulink, the main drawback is represented by the creation of the building modelling, since the input data for the building description are inserted by means of a series of specific m-files, and blocks have to be manually linked each to other. Moreover, air and moisture spatial distribution within a thermal zone can be in principle obtained only

coupling HAMBASE with CFD models, as done by Schellen and Van Schijndel [54], where HAMBASE has been coupled with COMSOL.

### 1.7.4 SIMBAD

The SIMulator of Building And Devices (SIMBAD) toolbox is a commercial Simulink library mainly addressed to the simulation and the test of HVAC control systems, developed by the Centre Scientifique et Technique du Bâtiment of Marne la Vallée (France) since 1997 [56]. The toolbox has a modular structure and the library is composed by models for the simulation of the main HVAC devices, from the heat generation sub-system (boilers, solar collectors, heat pumps...) to the storage, distribution (i.e. pipes, valves, pumps ...) and emitters. In addition to these models, the toolbox is composed by different thermal zone models, characterised by a different detail level in the description of building heat transfer phenomena. In particular, a thermal zone can be modelled considering a single air node or sub-dividing the zone into several volumes, enabling the analysis of air temperature stratification [57].

One of the main peculiarities of the SIMBAD toolbox concerns the creation of the building model and the data input phase. Until 2005, it was possible to model multi-zone buildings only by manually coupling several mono-zone blocks. Since this procedure has been recognized as an important source of mistakes, El Khoury *et al.* [58] developed, in Visual Basic environment, SIMbad Building Description Interface (SIMBDI), a graphical user interface that allows the user to draw the building and to enter all input data interactively. By means of SIMBDI, the user is driven during the introduction of the input parameters; the program automatically uses the input data in vectors and matrixes needed by the SIMBAD multi-zone building model for the solution of the set of the governing equations. In this way, the complete model of a building-HVAC system can be easily obtained even by users with limited knowledge of Simulink.

Nevertheless, the weak point of the SIMBAD toolbox is still represented by the building modelling. In fact, even adopting the most detailed building model available, some important simplifications are present: as an example, in the window model, the window solar transmittance and absorbitivity are assumed to be constant, whilst they depend on the angle of incidence of the solar radiation [58]. For this reason, Riederer *et al.* [59] proposed a procedure for coupling TRNSYS with SIMBAD, by importing TRNSYS building model in Simulink, and then adopting SIMBAD HVAC models. However, since both TRNSYS and SIMBAD are commercial software, this solution is economically very expensive.

Thanks to its ability to model and simulate new control systems, SIMBAD has been recently used for the development and the evaluation of the performance of different control strategies like the supervisory control strategy based on feedforward neural networks proposed by Ahmed *et al.* [60], or the Global Model



Based Anticipative Building Energy Management System (GMBA-BEMS), whose goal is the minimisation of the daily energy cost without affecting thermal comfort conditions [61].

## 1.8 Constraints of Matlab/Simulink libraries

In the previous section, four Matlab toolboxes for the building energy performance simulation, developed in the Simulink environment, have been described. As indicated by Table 1-2, all these tools, except IBPT, adopt ODE solvers that enable the use of variable time steps. The different time step discretization adopted by IBPT reflects the specific focus of IBPT compared to the other toolboxes. In fact, IBPT contains detailed building models, but simulates HVAC system roughly, considering only the emission sub-systems; on the contrary CARNOT, HAMBASE\_S and SIMBAD are more focused on the HVAC systems and on their control systems, considering only simplified building models.

Table 1-2. Main features of Simulink toolboxes for building performance simulation.

Toolbox	Use of variable time step	Building data insertion	Limitations
IBPT	No	Manual	Rough HVAC system models
CARNOT	Yes	Script	Simplified building model
HAMBASE_S	Yes	Script	Adoption of hourly fixed time step for building evaluation
SIMBAD	Yes	GUI	Simplified building model

The main constraint that limits the diffusion of these Simulink libraries is represented by the creation of the building model in Simulink and the input data insertion. As can be seen in Table 1-2, the building data insertion is done manually in IBPT, whilst in CARNOT and HAMBASE\_S data are written in a script. However, the more complex is the building, the greater is the possibility to make mistakes during the compilation of the input *m-files*. Only in SIMBAD a graphical interface has been developed for helping the user to describe the building. Nevertheless, for all these libraries, blocks have to be connected each other manually, making the generation of the complete model very time consuming and requiring to the user a good expertise in Simulink.

## 1.9 Thesis outline

This Thesis deals with the description of a new open Matlab toolbox, developed in the Simulink environment, called ALMA Building Energy Simulation Toolbox (ALMABEST). ALMABEST has been developed with the aim

to remove the main constraint that limit the diffusion of Simulink libraries in the building performance simulation field: the building modelling.

In *Chapter 2* ALMABuild, which is the tool of ALMABEST dedicated to the building modelling and represents the focus of this dissertation, is presented. In *Chapter 2* it is evidenced that, contrary to the other tools based on Simulink, ALMABuild is composed by a Simulink library and by a set of Graphical User Interfaces (GUIs). Illustrating the steps for the creation of the building model driven by GUIs, the benefits due to the use of GUIs, in terms of easiness of the data insertion and the automatic implementation of the building model in the Simulink desktop, are emphasized. Moreover, the main blocks of the ALMABuild library are described, given details on their mathematical models and remarking the connections to the other ALMABuild blocks, listing the input and output bus signals required.

*Chapter 3* deals with the validation of ALMABuild obtained following the BESTEST procedure. This procedure used for the benchmark of the main WBES tools available in the market, consists of three steps: (i) analytical validation; (ii) empirical tests and (iii) intermodel comparison. Results of these three benchmark steps are reported and discussed; in particular, performing the third step, which consists in the comparison of the numerical predictions of the testing to the results obtained by a set of reference software for univocally-defined cases, the BESTEST procedure has been critically analysed, emphasizing the need to periodically update the set of reference software for obtaining an accurate state-of-the-art validation procedure. Therefore, in *Chapter 3* are described the benchmarks of ALMABuild carried out by running it against EnergyPlus and the new hourly model proposed by the EN ISO 52016 [62].

The description of detailed models, implemented in ALMABuild in addition to the simple model, for solving the thermal balance of a zone, enabling the evaluation of the spatial distribution of the radiative, air and operative temperature within a zone is reported in *Chapter 4*. Furthermore, the application of these detailed models is explored by means of two case study. The first case study deals with the determination of the effects of six different heat emitters (from radiant floor to all-air systems) to the indoor local comfort conditions during all the heating season, considering two different envelope insulation levels. On the other hand, in the second case study, the impact of the indoor temperature sensor position on both indoor local comfort conditions and emitter dynamics is evaluated for two different radiator sizes and three different control strategies by means of numerical simulations for the heating season.

In *Chapter 5* the use of ALMABEST coupled to the Matlab Optimisation Toolbox is explored by means of five case-studies. In particular, four single-objective optimizations are performed to find the optimal building configuration (modifying different parameters) that determines the lowest total annual energy consumptions. By adopting the *Brute force* method, the solution found by the

optimization algorithm is verified. In addition, before running the optimization algorithm, few numerical simulations are performed with the aim to evaluate the dependency of the output parameter to the input one. Finally, a multi-objective optimization is carried out with the aim to optimize two contrasting goals: minimization of the energy demand and maximization of indoor comfort conditions. By means of this case-study it is demonstrated how the analysis of the dependencies of the objective functions to the input parameters can lead to a reduction of the design parameter space, speeding up the optimization calculations.

The occupant interactions with the building and their implications on the energy consumptions and indoor comfort conditions are the focus of *Chapter 6*. More in detail, in *Chapter 6* windows operations (openings and closings) due to the occupant are considered. Analysing the sensitivity of both heating energy consumptions and indoor comfort conditions to different building parameters (like the window typology, shadings, insulation thickness) it is evidenced that a lower sensitivity of the objective functions to the design parameters is obtained if the occupant behaviour is taken into account. Moreover, multi-objective optimizations are performed both considering and neglecting the occupant behaviour, highlighting the influence of the occupant behaviour on the Pareto frontiers. Furthermore, a robustness index, that evaluates the sensitivity of objective functions to the occupant behaviour, is proposed and adopted for the definition of building configurations occupant-free (i.e. building configurations whose energy and comfort performance are not affected by the occupant behaviour).

Finally, general conclusions on this work are presented in addition to future developments of the ALMABuild library.



# ALMABuild description

---

## Abstract

ALMA Building Energy Simulation Toolbox (ALMABEST) is the Matlab toolbox developed in this PhD Thesis operating in the Simulink environment for the simulation of the behaviour of coupled building-HVAC systems under dynamic thermal conditions. ALMABEST is composed by two libraries: ALMABuild and ALMAHVAC, that are used for the modelling of buildings and of the main components of HVAC systems, respectively. Both ALMABuild and ALMAHVAC are composed by a series of Simulink blocksets and by a set of Graphical User Interfaces (GUIs).

This *Chapter* is focused on the description of ALMABuild; by the illustration of the procedure for the creation of a building model by means of ALMABuild, the ALMABuild rationale and the main advantages linked to the use of Graphical User Interface (GUI) are emphasized. The description of the main blocks of the ALMABuild library is presented. The main feature of ALMABuild consists in the development of a series of *m-files* that, thanks to a series of GUIs, automatically implements the building model in the Simulink desktop. These *m-files* enable to recall automatically blocks from both Simulink and ALMABuild libraries. The blocks are properly linked each other by the *m-files* and specific parameters are set in an automatic way. In this way, the creation of the whole building modelling driven by these GUIs becomes fast and safe, with a reduced probability to make mistakes for non-expert users.

---

## 2.1 Simulink environment and ALMABEST library

Simulink is a graphical programming environment, developed in Matlab, for the modelling of multi-domain dynamic systems. The main characteristic of Simulink is the creation of dynamic models by means of an intuitive programming language based on a series of blocks which are coupled each to other thanks to graphical links. Simulink is based on a library of blocksets, shown in Figure 2.1. Each blockset is focused on a specific aspect and it is composed by a series of elementary blocks: as an example, in the *Sources* blockset input blocks useful for the creation of constant or time-dependent signals and blocks which recall variables defined in the Matlab workspace can be found. In the *Math Operations* blockset all the blocks that enable the main mathematical operations, (i.e. sum, subtraction, product and division) among signals are collected.

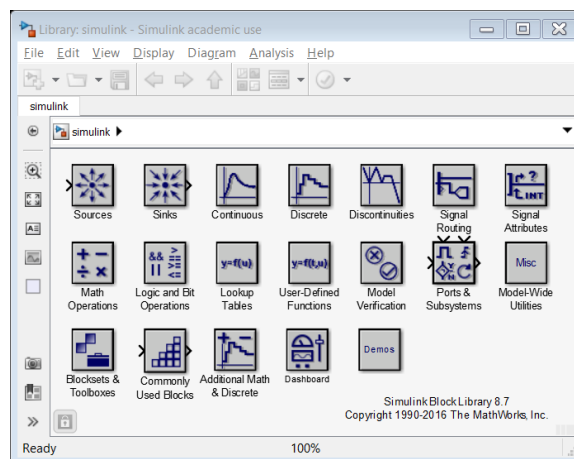


Figure 2.1. Simulink library.

Simulink is mainly used for its ability to easily solve systems of time-dependent ordinary differential equations. As an example, equations expressed as:

$$\frac{dT}{dt} = AT + B \quad (2.1)$$

where  $A$  and  $B$  are coefficients that can depend by several parameters, can be easily managed in Simulink by using a series of elementary blocks, as shown in Figure 2.2.

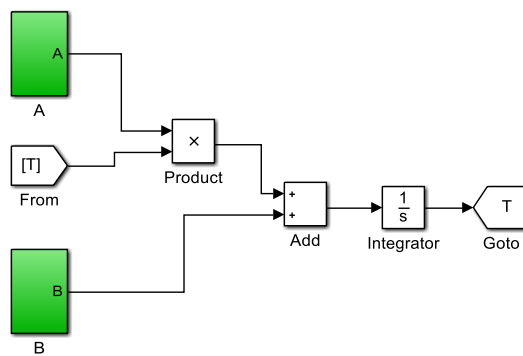


Figure 2.2. Example of a simple model implemented in Simulink.

For sake of clearness, the dependent variable (signal  $T$ ) is the output of the *Integrator* block.  $T$  is connected to the *Product* block by recalling its value from the output of the *Integrator* block by means of a *Goto* block linked to a *From* block. In this way, the direct link between the *Integrator* and *Product* blocks is avoided and no graphical links are present in the Simulink desktop. Moreover, in Figure 2.2 it can be noted that two kinds of blocks can be found in the model: white blocks are the elementary blocks available in the Simulink library, whilst green blocks are customized subsystems, which the user can build by means of elementary blocks. Customized subsystems can be created as well as customized libraries; in this way a Simulink model can be developed linking blocks originated from different libraries. In Simulink, a complete building model can be easily obtained by means of blocks linked to different building elements. This is the main idea of ALMABEST, where customized subsystems are used for the modelling of buildings and HVAC systems.

In Figure 2.3 the hierarchical structure of ALMABEST can be appreciated. ALMABEST is composed by two libraries: ALMABuild, used for the building modelling, and ALMAHVAC, adopted for the simulations of HVAC components. Each library consists of specific blockset devoted to specific aspects (i.e. weather data collection, thermal balance of the envelope elements and so on), which are composed by a series of subsystem. Finally, each subsystem contains a set of elementary blocks that are related to specific aspects of the building modelling.

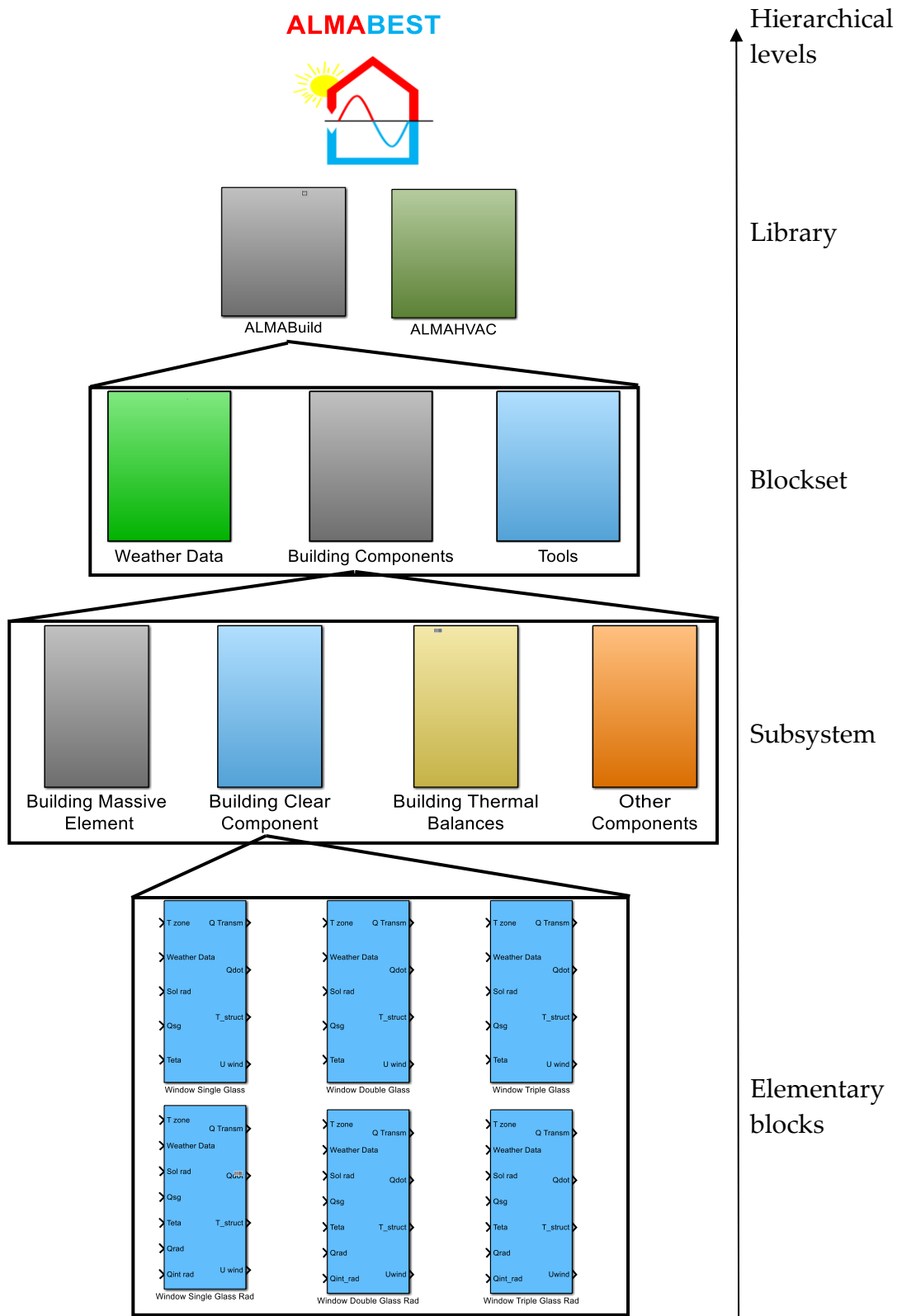


Figure 2.3. ALMABEST hierarchical levels.



## 2.2 Development of the building model

Starting from the blocks contained in the ALMABEST library (an overview of the ALMABEST library is given in *Appendix C*), the model of a building coupled with its HVAC system can be implemented in Simulink by selecting from the library a series of specific elementary blocks, properly linking each to other and by setting for each block the required parameters. In this way, the user can easily implement in the Simulink desktop a complex building model without to be called to develop new subsystems. This job can be done even by users with limited expertise about numerical solvers.

Let's to implement in Simulink the dynamic model of the building represented in Figure 2.4. This building is composed by two floors; in the first floor two thermal zones (i.e. bathroom and kitchen) can be found, whilst the second floor consists of a single thermal zone, i.e. bedroom.

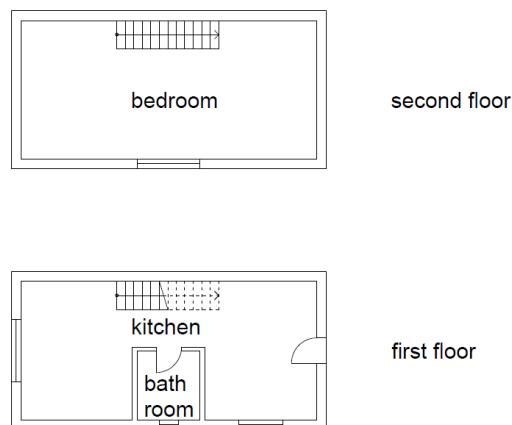


Figure 2.4. Plant of a two-stage building.

In Figure 2.5 the model of the two-stages building implemented in the Simulink desktop by means of the ALMABEST library is represented. In Figure 2.5 it is evident that the structure of the building model, shown in the Simulink desktop, is built around four different kinds of subsystems:

- The *Climatic Data* subsystem (in green in Figure 2.5);
- The *Thermal Zone* subsystems (in yellow in Figure 2.5);
- The *Intersections* subsystem (in red in Figure 2.5);
- The *HVAC* subsystem (in white in Figure 2.5).

In the *Climatic Data* subsystem the weather data, like external air temperature, wind velocity and incident solar radiation, are evaluated and aggregated in defined bus signals.

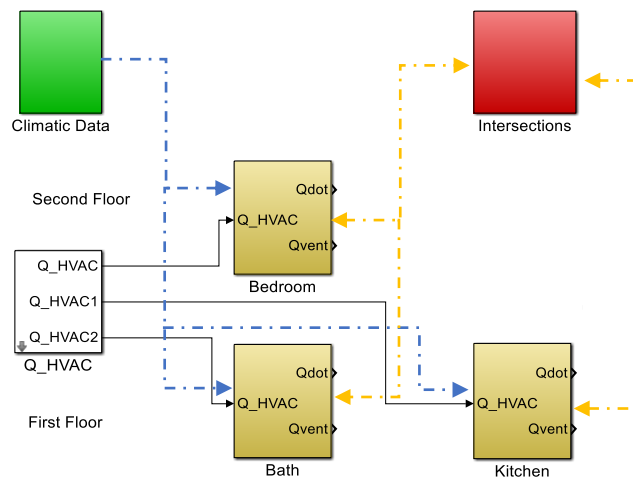


Figure 2.5. Simulink model of the two-stage building developed by means of ALMABEST.

In the *Thermal Zone* subsystem the thermal balance of a zone is solved and the indoor temperature and the heat fluxes which are present in the thermal zone are calculated. On the contrary, the *Intersections* subsystem allows to model the heat transfer across the envelope elements which separate different thermal zones (i.e. partition walls between bathroom and kitchen and the ceiling that divides the first floor from the second one). Finally, the *HVAC* subsystem contains the model of the HVAC system. Observing Figure 2.5, two kinds of wires can be noted. The solid black wires are used for a direct connection between two subsystems. This is the case of the *HVAC* subsystem, whose output ports are linked to the input ports of the *Thermal Zone* subsystems, determining the coupling between the building and the HVAC system. On the contrary, the dashed wires in Figure 2.5 (not represented in the Simulink desktop) evidence the connections performed by using the *Goto* and *From* blocks. As emphasized by Figure 2.5, *Goto* and *From* blocks are used to share the weather data defined in the *Climatic Data* subsystem to the *Thermal Zone* subsystems, as well as for coupling the *Thermal Zone* subsystems with the blocks contained in the *Intersections* subsystem. In this case double arrow wires are represented in Figure 2.5 in order to stress that the envelope elements contained in the *Intersection* block are part of the thermal zones (bidirectional exchange of signals among the blocks).

In the building model created with ALMABEST, *Goto* and *From* blocks are widely used, in order to eliminate from the Simulink desktop a series of wire connections among the blocks useless for the comprehension of the model. In this way, the clearness of the model is preserved.

## 2.3 Bus signals used in ALMABuild

In the Simulink building model represented in Figure 2.5 the signals exchanged between blocks by direct link (solid wires in Figure 2.5) or by means of the *From* and *Goto* blocks (dotted lines) are generally composed by many parameters. Due to the huge number of scalar values that are required by the ALMABEST blocks, the signals exchanged among the blocks are grouped in a series of customized “buses”. In this way, a clear layout of the building model can be obtained in the Simulink desktop. In Table 2-1, the main bus signals used in ALMABuild are listed together with the general information that they provide. The reader can find in *Appendix B* a complete description of all the different buses used for the block connections in ALMABEST.

Table 2-1. ALMABuild bus signals.

Name of the bus signal	Collected information
Weather Data Bus	Ambient conditions
Sun bus	Sun conditions
Solar Radiation Bus	Components of incident solar radiation
Temperature zone bus	Air and mean radiant temperature of the thermal zone
Superficial temperature bus	Temperature of internal and external surface of envelope element
Power bus	Heat fluxes
Ventilation bus	Thermal flux and airflow due to Ventilation

As it can be seen by Table 2-1, each bus collects information related to a particular physical aspect (i.e. outdoor conditions, heat fluxes...) or to a building component (i.e. envelope elements, thermal zone...). Anyway, customized bus signals are used not only in ALMABuild, but also in other Simulink based tools described in *Chapter 1* like SIMBAD, HAMBASE and CARNOT. In order to obtain the possibility to link other Simulink libraries with ALMABuild, conversion blocks able to translate customized bus of Simulink tools to ALMABuild buses and vice versa are provided in the ALMABuild library. In particular, due to a collaboration with the research team Unit for Energy Efficient Building of the University of Innsbruck (Austria), the ALMABuild library contains blocks that converts the CARNOT *S-vector* to the *Power bus* and the *Ventilation bus* of ALMABuild. In this way, it becomes possible to couple ALMABuild blocks with the CARNOT ones. However, it should be remarked that conversions block can be easily developed also for coupling ALMABuild with other Simulink-based tools, by removing all the constraints to the diffusion of this new tool.

## 2.4 Building model in ALMABuild

The ALMABuild library, which is represented in Figure 2.6, is composed by three main blocksets: *Climatic Data*, *Building Components* and *Tools*.

The *Weather Data* blockset consists of blocks that are useful for the calculation of weather-related physical entities, like the incident solar radiation, or for the upload of external weather data (i.e. Test Reference Year of a specified site) in the Simulink project.

The *Building Component* blockset is composed by elementary dynamic models of building envelope elements (walls, roofs, windows...).

Finally, blocks for the evaluation of comfort conditions in a thermal zone and other blocks used for the building modelling are collected in the *Tools* blockset. A description of all the elementary blocks which are present in the ALMABuild library is reported in *Appendix C*.

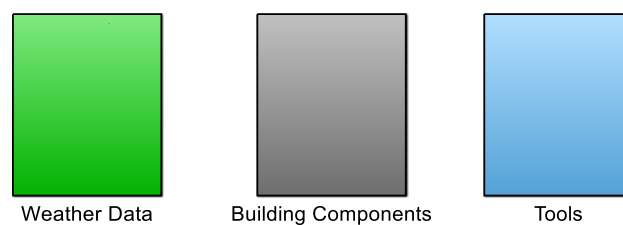


Figure 2.6. ALMABuild library main level.

The model of a building, even if simple, is always obtained by using a large number of blocks. In Figure 2.7 the blocks involved for the description of a thermal zone (i.e. Bedroom) are shown. For the description of a thermal zone, a series of blocks linked to the single envelope elements (walls, roof...) are used together with a block able to make the balance of the heat fluxes present in the zone. In ALMABuild, since blocks concerning different typologies of envelope elements require different data (i.e. wall stratigraphy or optical and gap gas properties for windows) and each envelope element of the building differs to the other in terms of exposition (i.e. internal, external or to ground), slope (i.e. vertical, inclined or horizontal) and area, a large amount of parameters must be set for each elementary block composing the building model. As it is shown in Figure 2.7, in the Simulink desktop a complete model is characterised by a large number of blocks and wires by means of which the data are exchanged among the blocks. Therefore, the possibility to make mistakes during the manual implementation of blocks and wires becomes very high. In addition, the building model construction becomes time consuming in case of a complex building geometry.

These kinds of problems are common to the tools for dynamic energy simulations based on Simulink environment. In fact, as discussed in *Chapter 1*

when analysing the constraints of WBES tools based on Simulink, the data insertion in these tools is usually obtained manually or by means of *m-files*, except in SIMBAD where a series of GUIs is adopted for the introduction of the input data. In ALMABuild, like in the last versions of SIMBAD, the introduction of the building input data is obtained by means of Graphical User Interfaces (GUIs), developed in Matlab. However, the main advantage of ALMABuild with respect to SIMBAD is that the creation of the Simulink model is completely automatized. In addition, in ALMABuild a series of specific interfaces have been developed to allow to the user to modify the input data, adding or erasing elements or thermal zones.

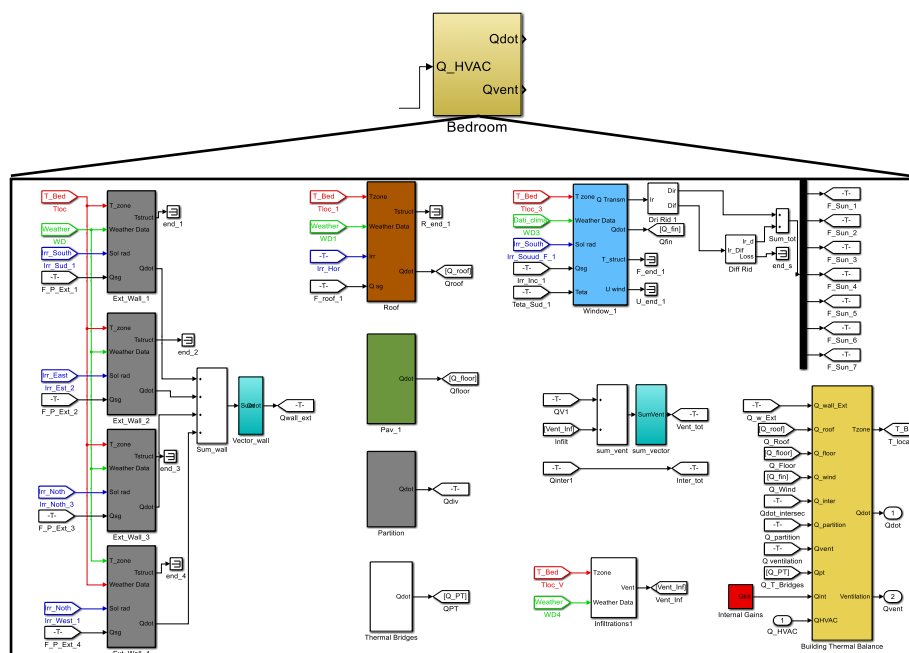


Figure 2.7. Example of models that compose a *Thermal zone* block.

Starting from the main interface of ALMABuild, represented in Figure 2.8, the user is driven towards the construction of the building energy model by a series of specific interfaces, each one linked to a specific aspect of the building modelling.

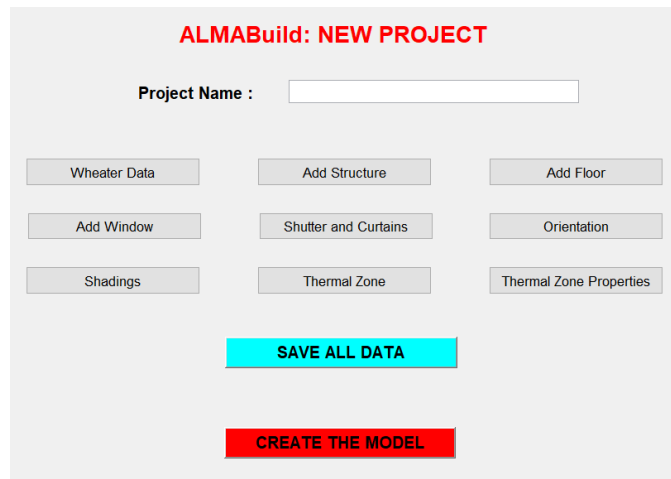


Figure 2.8. ALMABuild main interface.

Now, following the procedure driven by the GUIs, the implementation of the building model in Simulink is described together with the rationale of the main ALMABuild blocks.

## 2.5 Weather data

The first step for the creation of the building modelling driven by the ALMABuild GUIs consists in the definition of the weather data. By means of the *Weather Data* GUI, the user can import the weather data from the METEONORM database [63] or, only for Italy, from the CTI database [64] selecting the location of the building. In addition, the user can define the solar albedo of the location. In this way, all the weather information are imported from weather database and collected in a Matlab structure, labelled *Ambient\_Data*.

Information collected in the *Ambient\_Data* are managed by the elementary blocks composing the ALMABuild *Weather\_Data* blockset. As it is shown in Figure 2.9, the *Weather\_Data* blockset is composed by two kinds of blocks: reader (*Weather Data Reader* and *Solar Radiation Reader*) and calculator (*Solar data* and *Solar Radiation Calculator*).

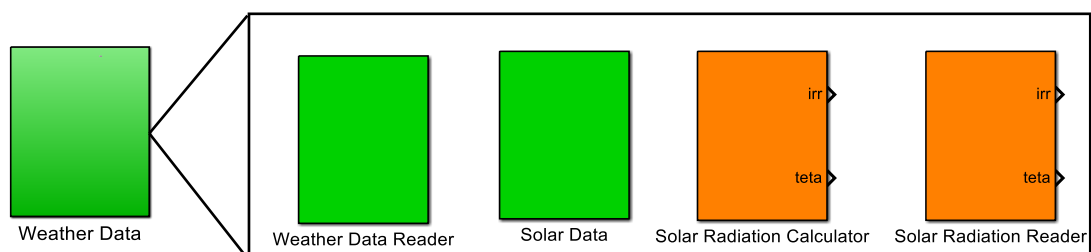


Figure 2.9. Exploded of the *Weather Data* block of the ALMABuild library.

Calculator blocks are used for the evaluation of the annual profile of the instantaneous incident solar radiation for each orientation (defined in the *Orientation* GUI) of the envelope elements. This calculation is performed once,

during the creation of the building modelling in the Simulink desktop and the obtained results are added to the *Ambient\_Data* structure. In this way, a *Climatic Data* block can be created in a Simulink project by means of a series of “readers” blocks which interacts with the *Ambient\_Data* structure, as shown in Figure 2.10. For a specific project, the creation of the *Climatic Data* block allows to calculate and collect in the *Ambient\_Data* structure all the weather parameters useful for the thermal balance of each zone. The calculation of all the quantities of interest is done “all at once” for the whole period of the simulation (i.e. one year). In this way, the computational effort during the building energy simulations is reduced, since the incident solar radiation as well as all the other weather data are already available as an input data for the whole duration of the simulation.

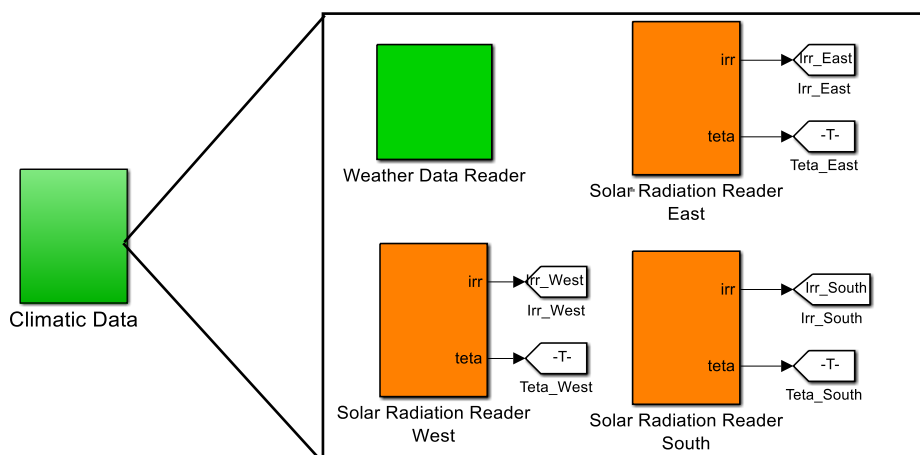


Figure 2.10. Exploded of the *Climatic Data* block for a building characterised by three orientations (East, West, South).

### 2.5.1 Weather Data Reader block

The *Weather Data Reader* block is used for creating the *Weather Data Bus*, which contains all the information about the external environment conditions. The *Weather Data Bus* is created by importing in Simulink the data collected in the *Ambient\_Data* structure, that has to be defined in the base workspace. This structure is composed by 15 fields, by means of which information about the building location (name of the city, latitude, longitude and albedo) and weather data are collected. In addition to weather data reported in the *Ambient\_Data* structure, the *Weather Data Bus* contains also the fictive sky temperature, that is evaluated in the *Weather Data Reader* block as a function of the outdoor vapour pressure, according to UNI TS 11300-1:2004 [65]. As it can be noticed by looking at Figure 2.11, the *Weather Data Reader* block does not have any output port; in fact, the *Weather Data Bus* is connected to the other blocks of the building model by means of a *Goto* block.

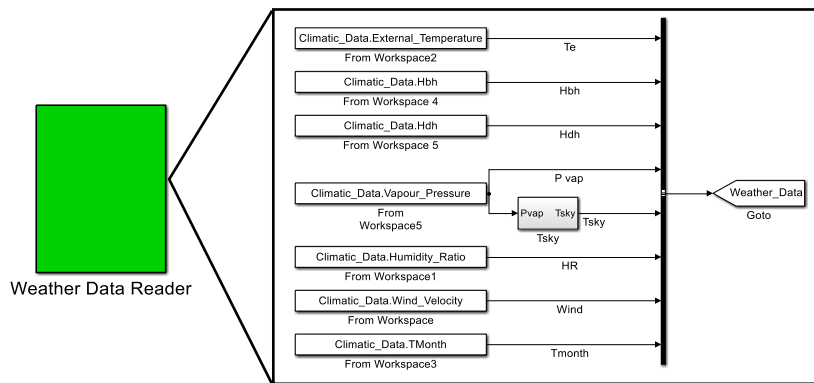


Figure 2.11. Weather Data Reader block.

### 2.5.2 Solar Data block

In the *Solar Data* block the weather data are processed for the evaluation of parameters, collected in the *Sun bus*, related to the sun position. These parameters are required for the calculation of the incident solar radiation on a surface. In Figure 2.12, the structure of the *Solar Data* block, which is composed by seven subsystems, can be seen.

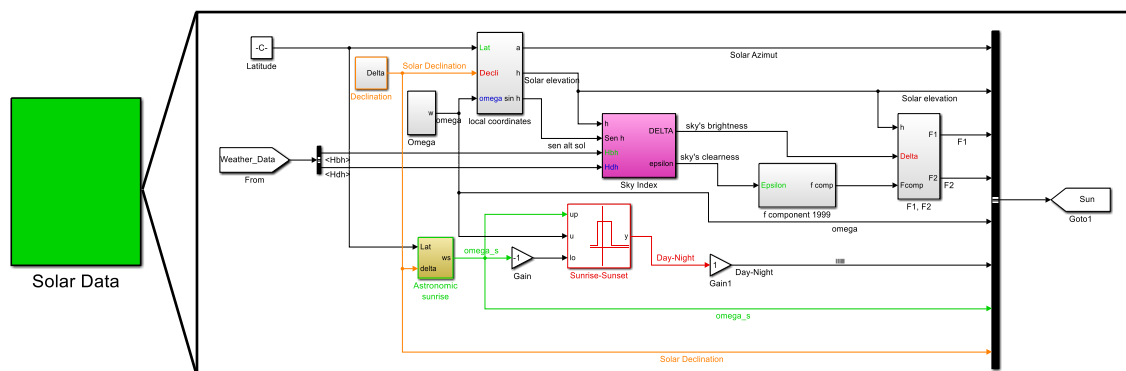


Figure 2.12. Solar Data block.

The solar azimuth and solar elevation angles, the first two signals of the *Sun bus*, define the sun position in the sky; they are evaluated as a function of the latitude of the building location, the solar declination (estimated by the approximate equation proposed by Cooper [66]) and solar hour angle. The angle shift between solar and standard time, evaluated adopting the equation of time proposed by Spencer [67], is taken into account.

In the *Sky Index* subsystem, the sky's clearness ( $\epsilon$ ) and brightness ( $\Delta$ ), introduced by the Perez model [68], are evaluated from the solar elevation and the beam and diffuse solar radiation on a horizontal plane ( $H_{bh}$  and  $H_{dh}$ ) by means of the following relations:



$$\epsilon = \frac{\frac{H_{dh} + \frac{\pi}{2} - \psi}{H_{dh}} + 1.041 \left( \frac{\pi}{2} - \psi \right)^3}{1 + 1.041 \left( \frac{\pi}{2} - \psi \right)^3} \quad (2.2)$$

$$\Delta = \frac{H_{dh} AM}{H_{et}} \quad (2.3)$$

where  $\psi$  is the solar elevation,  $H_{et}$  is the extra-terrestrial irradiance and  $AM$  is the relative optical airmass, evaluated by the relation proposed by Pickering [69] :

$$AM = \frac{1}{\sin \left( \psi + \frac{244}{165 + 47\psi^{1.1}} \right)} \quad (2.4)$$

From the sky condition indexes, the two parameters ( $F_1$  and  $F_2$ ) used in the Perez model [68] for the estimation of the diffuse component of the incident solar radiation on a surface are estimated and collected in the *Sun bus*. The day-night coefficient, which is one if the sun is over the horizon, otherwise it is equal to zero, is also evaluated. Even this signal is collected in the *Sun bus*, as well as the solar hour angle, the solar hour angle of the astronomic sunrise and the solar declination angle.

As the *Weather Data Reader* block, the *Solar Data* block has no input and output ports; as it can be seen in Figure 2.12, the *Weather Data Bus* is called by the other blocks by means of a *From* block and the output, which is the *Sun bus*, is available to the other blocks thanks to a "Goto-From" ghost link.

### 2.5.3 Solar Radiation Calculator and Solar Radiation Reader block

The *Solar Radiation Calculator* and the *Solar Radiation Reader* blocks are used for the creation of the *Solar Radiation Bus*, which is composed by the beam, diffuse and reflected components of the incident solar radiation, and by the angle of incidence of the solar radiation on a surface.

In the *Solar Radiation Calculator* block the beam, diffuse and reflected components and the angle of incidence of the solar radiation over a surface are evaluated using as inputs the values contained in both the *Sun Bus* and the *Weather Data Bus*, as it can be seen in Figure 2.13, where these signals are evidenced by orange and cyan wires. This block requires as parameters the angles of slope and azimuth of the surface for which the incident solar radiation has to be estimated, together with the albedo and the latitude of the location.

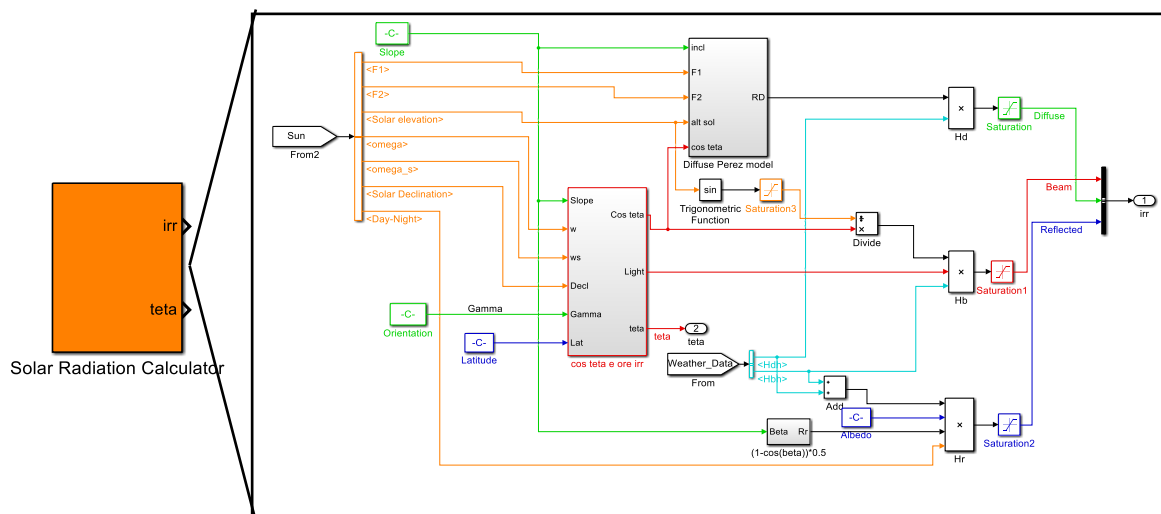


Figure 2.13. Solar Radiation Calculator model.

First of all, the angle of incidence ( $\theta$ ) is evaluated as a function of the azimuth ( $\gamma$ ) and slope ( $\beta$ ) of the surface and of the latitude ( $\varphi$ ) the solar hour angle ( $\omega$ ) and of the declination angle ( $\delta$ ) by using the following relationships:

$$\theta = \arccos(u \cos \omega + v \sin \omega + t) \quad (2.5)$$

$$\begin{cases} u = \sin \delta (\sin \varphi \cos \beta - \cos \varphi \sin \beta \cos \gamma) \\ v = \cos \delta (\cos \varphi \cos \beta - \sin \varphi \sin \beta \cos \gamma) \\ t = \cos \delta \sin \beta \sin \gamma \end{cases} \quad (2.6)$$

Beam radiation is calculated as the product of the direct solar radiation on a horizontal plane with the geometric factor defined as the ratio between the cosine of the incident angle and the sine of the elevation angle [70].

As for the beam radiation, also the tilted diffuse radiation is estimated evaluating its ratio with the diffuse radiation on a horizontal plane. In literature, isotropic and anisotropic models for the estimation of this ratio can be found. In isotropic models (like Koronakis [71], Liu and Jordan [72] and Badescu [73] models among others) the diffuse sky radiation is assumed to be uniform over the sky dome and, consequently, the tilted diffuse radiation depends on the fraction of the sky dome seen by the surface. On the contrary, in anisotropic models (i.e. Perez [68], Hay and Davies [74] and Reindl [75] as example) the sky dome is divided in at least two main zones: the circumsolar region, which is the region of the sky near the solar disk, and the rest of the sky in which the diffuse radiation is assumed to be isotropic. Among these models, the anisotropic Perez model has been implemented in the *Solar Radiation Calculator* block, since it has

been recognised by several authors (see [76]- [77]) as one of the most accurate solar model for the computation of the diffuse radiation over a tilted surface.

Finally, the reflected component of the solar radiation ( $H_{refl}$ ) is estimated from the total radiation on a horizontal surface assuming isotropic reflections:

$$H_{refl} = (H_{dh} + H_{bh}) \frac{1 - \cos \beta}{2} \xi \quad (2.7)$$

where  $\xi$  is the albedo of the surroundings.

If the incident solar radiation on a surface, in all its components, is already available from measures or previous calculations, the *Solar Radiation Bus* can be created by means of the *Solar Data Reader* block. In this block, no calculations are performed but data, defined in the block mask, are only arranged in order to form the *Solar Radiation Bus*. In the same way, also the temporal profile of the angle of incidence has to be defined.

## 2.6 Opaque envelope elements in ALMABuild

Following the layout of the ALMABuild main interface (see Figure 2.8), after the selection of the weather data, the structures, i.e. the massive envelope elements, that compose the building can be defined by means of the Structure GUI represented in Figure 2.14.

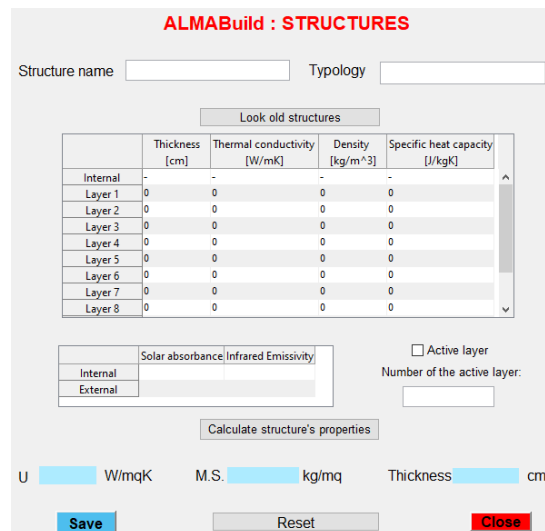


Figure 2.14. Structure GUI used for the definition of main characteristics of massive elements.

As it can be seen in Figure 2.14, it is required to give a label to each massive envelope element and to select its typology among the following categories:

- External wall;
- Internal wall, i.e. a wall between two adjacent thermal zones;

- Internal partition, that is a wall within a thermal zone;
- Ceiling (or internal floor);
- Roof.

Then, massive element stratigraphy, radiative coefficients for both solar and infrared radiation, and eventually the position of the active layer can be defined, and from these data thermal transmittance, superficial mass and total thickness of the element are calculated.

Slab-on-grade floor, that is not listed among the categories defined in the Structure GUI, is described by means of a dedicated GUI in which, in addition to the data required for every massive envelope elements, information needed for the evaluation of the floor equivalent thermal transmittance, obtained by following the calculation procedure described in the EN ISO 13370 [78], can be inserted.

### ***2.6.1 Modelling of envelope elements in ALMABuild***

Dynamic building modelling is generally obtained by considering all the envelope elements which are present in a thermal zone. Each envelope element is characterised by a specific thermal inertia (i.e. walls, windows), optical properties (an element could be clear or opaque to solar radiation) and all the three heat transfer mechanisms (conduction, convection and radiation) are involved. In many cases the number of elements involved in the definition of a thermal zone can be very large but, despite the complexity of the physical issues concerned, building thermal energy simulations are required to be fast and computationally efficient in order to be used in long simulations (one year or more), in predictive control algorithm and for performing multi-objective optimisations.

In the literature, many building models are available according to various techniques: some of them require the monitoring of data inside a thermal zone, by means of which statistical model are developed based on various techniques like artificial neuronal network [79], support vector machine [80] and multiple linear regression [81], whilst others are based on equations derived from physical laws. Within the physical model techniques, one of the most employed approach for simulating the heat transfer in buildings is the utilization of models based on thermal resistances (R) and thermal capacitances (C). These models, known as RC models, labelled according to the number of thermal resistances and capacities considered, offer low computational demand and are characterised by simplicity and transparency. Within these models, two different categories can be individuated: the Lumped Parameters Whole Room (LPWR) models and the Lumped Parameters Construction Element (LPCE) models.

In LPWR models the thermal behaviour of a zone is evaluated lumping the whole zone, achieving the lowest computational effort and consequently the lowest simulation time. As an example, in 1987 Crabb *et al.* [82] proposed a 3R2C

model for the simulation of a thermal zone: a thermal resistance takes into account thermal losses due to conduction within light envelope elements and ventilation, whilst the remaining two thermal resistances are used for the modelling of heat losses in heavy building components; the two thermal capacitances are related to the thermal capacity of the building structures and of the air in the thermal zone. In 1993, Tindale [83] suggested a third order lumped models (that means that three capacitances are considered) in order to improve the accuracy with respect to the 3R2C model when considering heavyweight buildings. However, more recently Nielsen [84] developed a 2R2C model demonstrating that a second order model is accurate enough for a fast evaluation of the energy performance of a building in the early stages of the building design. Moreover, the standard EN ISO 13790 [85] proposed a method based on a first order model, the 5R1C model, that has been adopted as reference by several researchers. Even if some upgrades to this model have been suggested, like for the analysis of a double skin natural and mechanical ventilated cell [86], some researchers pointed out the inconsistency of the model for the analysis of intermittent use of heating and cooling systems [87], and for heavyweight building envelope [88].

On the other hand, in LPCE models each building massive element is described by means of a RC model and a thermal zone is modelled aggregating single RC models. Even in this case, models of different orders can be found: Lorenz and Masy [89] proposed in 1982 a 2R1C model, Gouda *et al.* [90] improved this model to a 3R2C model, Mara *et al.* [91] increased again the number of capacitance suggesting a 6R3C model and finally Fraisse *et al.* [92] derived from a 3R2C model a fourth order model, 3R4C. The discretization of the massive elements for the evaluation of the thermal resistances and capacitances of the aforementioned models is done by means of analytical rules in all the cases, except in the 3R2C model proposed by Gouda *et al.* [90]. In this case, the five required parameters are estimated by means of an optimisation algorithm that minimise the discrepancies of the thermal response of the wall evaluated through a 20<sup>th</sup>-order reference model and the reduced-order model (second order). The thermal response of a wall is estimated imposing a step disturbance of both external temperature and internal heat flux. More recently, Underwood [93] suggested an upgrade of the tuning algorithm for the evaluation of the 3R2C model parameter: the reference model is solved with a rigorous finite-difference method. In this tuning algorithm, continuous excitations in both the side of the wall are considered simultaneously. As a consequence, a multi-objective algorithm for the model parameter estimation is required, since the discrepancies of the thermal response of the wall are to be reduced on both the internal and external side.

Finally, in the new Standard EN ISO 52016 [62], that replaces EN 13790 for the assessment of the energy performance of building, a LPCE RC model is

proposed. This model consists in the description of opaque elements with a general 4R5C model, that is reduced to a first order model (the capacity is different from zero only in one node) if the mass is concentrated at the internal or external side. Only in the case of elements with equally distributed mass, all the nodes of the 4R5C model have a capacities higher than zero.

In ALMABuild, a LPCE method for the description of the building has been implemented since it has been recognized that LPWR models are not suitable for the assessment of the energy performance of building and for the evaluation of the indoor comfort conditions. This is confirmed by the replacement of the standard EN 13790 based on LPWR with the EN ISO 52016 which proposes a LPCE model. In fact, LPWR models do not provide essential information, like the distribution of the surface temperature of the different building elements of a thermal zone, now required even in the earlier stage of the NZEB design building.

The LPCE models used for the building description in ALMABuild are collected in the *Building Components* blockset. As shown in Figure 2.15, this blockset consists of four kinds of blocks: the *Building Massive Element* (BME) block, the *Building Clear Component* (BBC) block and the *Building Thermal Balance* (BTB) block and the *Other Components* block.

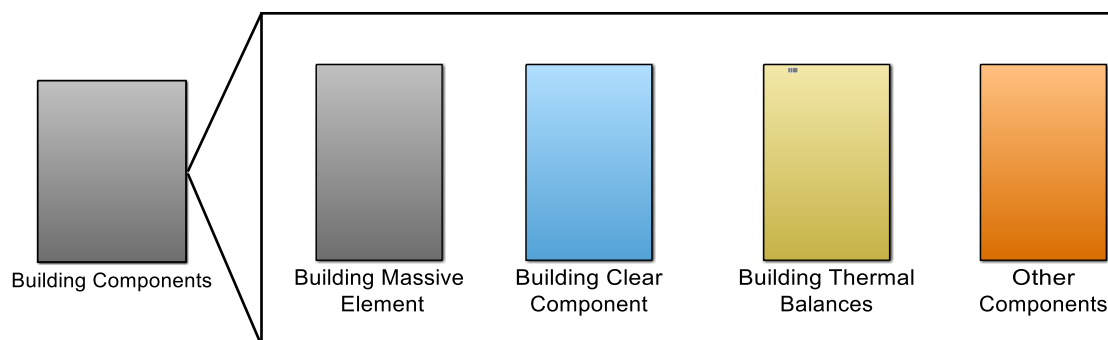


Figure 2.15. Blocks composing the *Building Components* blockset.

### 2.6.2 *Building Massive Element block*

The Building Massive Element subsystem is composed by elementary blocks used for the modelling of opaque envelope elements, like walls, roofs and floors, according to a 3R4C model. By the comparison of this model to the recent LPCE models proposed, two relevant differences can be found: first of all, the model implemented in a BME block is a fourth-order model instead of a reduced-order model; secondly, the parameter estimation is based on a new analytical procedure for the discretization of multi-layered structures. A fourth-order model has been preferred to a reduced-order model since the analysis conducted by Fraisse *et al.* [92] evidenced that a second order model is not accurate enough

in the evaluation of the superficial temperature of both the side of a wall when considering variation in the internal temperature. As described in the previous Section, in the recent LPCE models proposed the parameter estimation is achieved by means of tuning algorithms based on optimisation approaches. On the contrary, in the 3R4C model implemented in ALMABuild, a new analytical procedure for the discretization of multi-layered structures has been developed with the aim to obtain more meaningful parameters values, not requiring to perform additional simulations considering different models or different computational platforms.

The analytical procedure for the calculation of the thermal resistances and capacitances of the 3R4C model implemented in the BME block consists in the determination of the position of the four nodes in a multi-layer element, as represented in Figure 2.16.

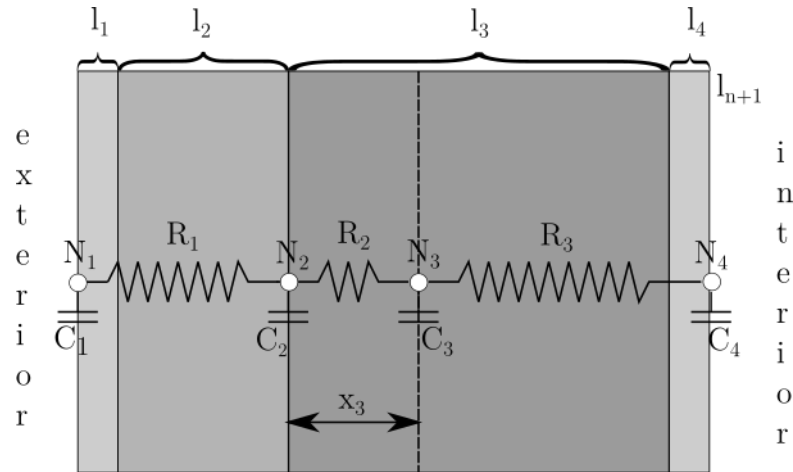


Figure 2.16. Equivalent 3R4C network associated to an opaque envelope building.

As shown in Figure 2.16, the first and the last node are placed on the external and internal surface of the wall, whilst the second and the third nodes are placed within the wall.

More in detail, nodes 2 and 3 are positioned at the interface between the insulation layer and the massive layer and where the first quarter of the total wall heat capacity is reached, starting from the external side.

By knowing the number of wall layers ( $nl$ ) and the physical properties ( $\rho_i$ ,  $c_i$ ) and thickness ( $d_i$ ) of each  $i$ -th wall layer, it is possible to calculate the total thermal capacity of the wall ( $C_{tot}$ ), by means of the relation:

$$C_{tot} = \sum_{i=1}^{nl} \rho_i c_i d_i \quad (2.8)$$

The position ( $x_c$ ) and the wall layer ( $l_c$ ) in which the first quarter of the total thermal capacity of the wall is reached can be found thanks to the following relationship:

$$\left\{ \begin{array}{l} \sum_{i=1}^j \rho_i c_i d_i + \rho_{j+1} c_{j+1} x_{j+1} = C_{tot} / 4 ; \quad j \in [1, nl-1], \quad x_{j+1} \in [0, d_{j+1}] \\ l_c = j+1; \quad x_c = \sum_{i=1}^j d_i + x_{j+1} \end{array} \right. \quad (2.9)$$

where the layers are counted starting from the external wall layer ( $i=1$ ).

The position of the thermal insulation is found by comparing the thermal conductivity of each wall layer:

$$l_{is} : \lambda(l_{is}) = \min(\lambda(l_j)); \quad j \in [1, nl] \quad (2.10)$$

Now, the positions of the internal nodes  $N_2$  and  $N_3$  can be obtained as:

$$\left\{ \begin{array}{l} N_2 = \min \left( \sum_{i=1}^{l_{is}} d_i, \sum_{i=1}^{l_c-1} d_i + x_{j+1} \right) \\ N_3 = \max \left( \sum_{i=1}^{l_{is}} d_i, \sum_{i=1}^{l_c-1} d_i + x_{j+1} \right) \end{array} \right. \quad (2.11)$$

After having determined the position of the four nodes of the RC network, thermal resistances that connect two adjacent nodes ( $R_j$ ) are calculated as the sum of the thermal resistances of the BME layers that are contained within the two considered nodes, whilst thermal capacitance of a node is estimated as the sum of half the thermal capacity of the layers adjacent to the node.

In ALMABuild all the massive envelope components are described by this 3R4C model, except for “slab on grade” elements. Actually, floors on ground are modelled by means of the above mentioned 3R4C network in which the external node, which faces to the ground, is jointed to an additional RC network, as represented in Figure 2.17. This additional network is composed by three capacitive nodes, that represent the first 0.5 m depth of ground (ground layers), and a non-capacitive node, which describes a virtual layer. The ground and virtual layers compose the 3R3C model that is used for taking into account the dynamic behaviour of the ground under the floor, in agreement with the annex F of the Standard EN ISO 13370 [78].



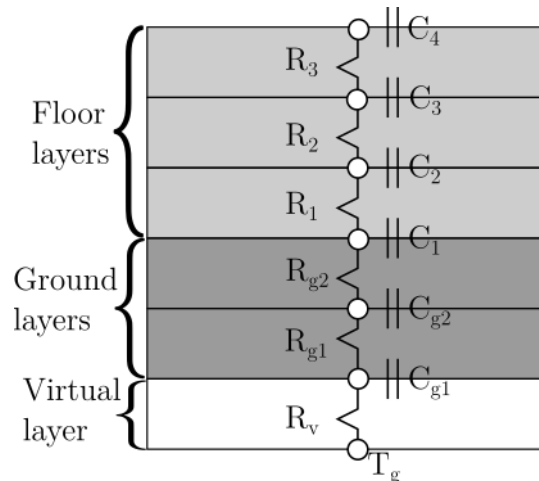


Figure 2.17 Floor on ground RC network.

The two ground layers are equally distributed in the 0.5 m depth of ground, which means that each layer is 0.25 m thick. Thermal capacitance and thermal resistance of the ground layers are evaluated as for the 3R4C model. On the contrary, the thermal resistance of the virtual layer ( $R_v$ ) is estimated by means of:

$$R_v = \frac{1}{U} - R_{si} - R_f - R_g \quad (2.12)$$

where  $U$  is the equivalent thermal transmittance of the floor,  $R_{si}$  is the internal surface resistance,  $R_f$  is the total thermal resistance of the floor layers and  $R_g$  is the thermal resistance of the 0.5 m of ground. The non-capacitive node represents the undisturbed ground and it is characterised by a constant temperature,  $T_g$ , set as the mean annual external temperature.

If the massive envelope element contains an active layer (such as in case of radiant floor, ceilings or walls), an additional capacitive node is inserted in the RC network in correspondence of the middle of the active layer. As represented in Figure 2.18, an internal heat gain insists on this node, which is the power delivered by the HVAC system to the node.

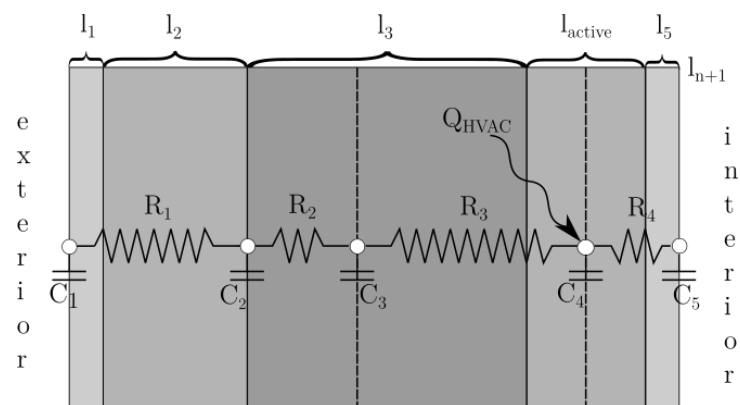


Figure 2.18. Equivalent RC network related to an opaque element with an active layer ( $l_{active}$ ).

It has to be remarked that the equations that are used for the modelling of massive elements by means of BME block concern only the heat transfer mechanisms across walls. In fact, during the PhD period, models for the analysis of the mass transfer mechanisms, across the envelope elements was not developed. This means that, at the moment, in ALMABuild the analysis of the water vapour storage and transmission phenomena can be considered only in a very simplified way. Anyway, since it is recognised the importance of mass transfer mechanisms across walls for the water condensation risk assessments and for the evaluation of the indoor air comfort conditions, the development of models for the analysis of mass transfer phenomena is planned for the next period.

In BME blocks, represented in Figure 2.19, convective and radiative heat transfer between the external surface of the element and the external surroundings are evaluated considering the respective heat transfer coefficient according to EN 6946 [94], whilst the radiative heat transfer between external surface of the element and sky is written in agreement with UNI 11300-1 [65] as follows:

$$\begin{cases} \varphi_{sky} = h_r F_r (T_e - T_{sky}) \\ h_r = \varepsilon \sigma_0 \frac{(T_e + 273)^4 + (T_{sky} + 273)^4}{T_e - T_{sky}} \\ F_r = \frac{1 + \cos \beta}{2} \end{cases} \quad (2.13)$$

where  $h_r$  is the radiative heat transfer coefficient for long-wave heat transfer,  $F_r$  is the view factor of the external surface of the element to the sky,  $T_{sky}$  is the “fictive” sky temperature,  $\varepsilon_s$  is the emissivity of the element,  $\sigma_0$  is the Stefan-Boltzmann constant and  $\beta$  is the slope of the envelope element.

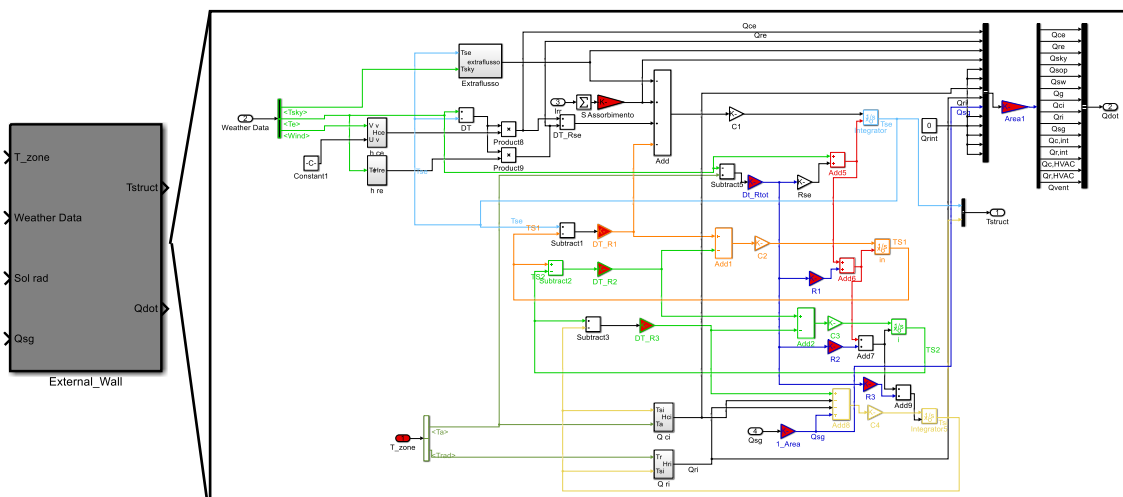


Figure 2.19. BME block of an external wall.

Even the convective heat transfer between the internal surface of an envelope element and the internal surrounding is evaluated considering the convective heat transfer coefficient reported in EN 6496 [94]. The radiative heat transfer is estimated in two different models. In the first model, the radiative heat transfer between the internal surface of an envelope element and the internal surrounding is evaluated adopting the radiative heat transfer coefficient for internal surfaces in agreement with EN 6496. On the contrary, the second model is based on the calculation of the view factors among the internal surface of the thermal zone; in this case the internal radiative heat transfer is an input data, and the detailed radiative model has to be selected, as it is described later.

In BME blocks, the external heat flux due to solar radiation is given by the product of the sum of the three components of the incident solar radiation with the solar absorbance of the envelope element, whilst the internal solar heat flux due to the solar radiation that is transmitted by clear elements is an input data of the block.

Since massive envelope elements can be passive or active surfaces, they can have different exposition and consequently different boundary conditions (i.e. walls can divide the thermal zone from the external environment or from other thermal zones, whereas floors can be in contact with the ground...) and since different models can be selected (i.e. simple or detailed radiative models), in ALMABuild library several BME blocks can be found.

However, all these blocks require almost the same input data and give the same outputs. As shown in Figure 2.19 which represents the BME block for an external wall, four inputs are required and two are the outputs. The first input is the *Temperature zone bus* that is composed by the air and the mean radiant temperature of the thermal zone; whilst the second input is the *Weather Data bus*. The third input required is the *Solar Radiation Bus*, that collects the three components of the incident solar radiation over the considered surface, and finally, the last input is represented by the solar radiation transmitted by the clear elements of the thermal zone that strikes the internal surface of the considered envelope element.

The outputs of a BME block are the *Superficial temperature bus* that contains the external and internal surface temperature of the envelope element described by the block and the *Power bus*, in which the values of all the thermal fluxes on both the external and internal side of the element are collected.

## 2.7 Windows in ALMABuild

Similarly to massive envelope elements, interfaces have been developed for the insertion of data related to windows composing a building. As it can be seen in Figure 2.20, for each window it is required to define a label, the total thermal

transmittance and the number of panes that compose the window. Based on the number of panes of the widows, the tables of the Window GUI are modified.

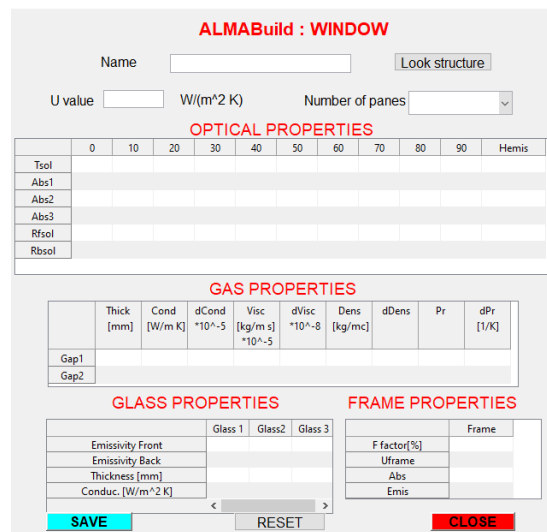


Figure 2.20. Window GUI, for the definition of characteristics of clear envelope elements.

Then, the user can insert all the data related to the angular dependency of optical properties of the glasses (described in Table 2-2), the thermal properties of the gas in the gap between two glasses (see Table 2-3), of glasses (see Table 2-4) and frame (see Table 2-5). Contrary to opaque massive elements described above, for which the thermal properties of each layer are common data reported in technical sheets, the required window elements properties need to be evaluated by means of dedicated software like WINDOW [95]. Since windows can consist of additional elements like shutters and curtains, additional dedicated GUI are developed for the data insertion related to these elements.

Table 2-2. Optical window properties.

Label	Description
<b>Tsol</b>	Window solar transmittance
<b>Abs 1</b>	Solar absorbance of glass 1 (glasses are numbered from outdoor to indoor)
<b>Rfsol</b>	Reflectivity of surface facing toward outside
<b>Rbsol</b>	Reflectivity of the surface facing toward the interior of a building

Table 2-3. Gas gap properties

Label	Description
<b>Thick</b>	Thickness of the gap
<b>Cond</b>	Thermal conductivity of the gas
<b>dCond</b>	Derivative of the thermal conductivity of the gas to the temperature
<b>Visc</b>	Gas viscosity
<b>dVisc</b>	Gas viscosity to the temperature
<b>Dens</b>	Density of the gas
<b>dDens</b>	Derivative of the gas density
<b>Pr</b>	Prandtl number of the gas
<b>dPr</b>	Derivative of the Prandtl number of the gas to the temperature

Table 2-4. Glass properties.

Label	Description
<b>Emissivity front</b>	Infrared emissivity of the surface facing toward the outside
<b>Emissivity front</b>	Infrared emissivity of the surface facing toward the inside
<b>Thickness</b>	Thickness of the glass
<b>Conductance</b>	Thermal conductance of the glass

Table 2-5. Frame properties.

Label	Description
<b>F factor</b>	Frame factor
<b>Uframe</b>	Thermal transmittance of the frame
<b>Abs</b>	Solar absorbance of the frame
<b>Emis</b>	Infrared emissivity of the frame

### 2.7.1 Building Clear Component block

Building Clear Component blocks are the elementary blocks composing the Building Clear Component subsystem represented in Figure 2.15. BCC blocks contain the physical model of light clear building elements (i.e. windows). As a window is composed by several materials with different thermal and optical properties, BCC blocks are composed by different physical models. More precisely, BCC blocks include models of: (i) frame, (ii) glass and (iii) gas contained in the cavity between two panes.

The frame is modelled by means a reduced order RC network, similar to the one used in BME: two capacitive nodes (located in the internal and external surface of the frame) and a single thermal resistance composes the 1R2C model. The same thermal fluxes considered in BME block are taken into account in the frame model, except the internal solar heat flux, that is neglected.

The thermal behaviour of the clear fraction of a window is modelled in a BCC block by means of the glass and gas models, that are merged in a single RC network. In ALMABuild each typology of window (single, double or triple pane) is modelled with a customized RC network. A 1R2C network is used for the modelling of single and double pane windows. For single pane window, the two capacities are located in the external and internal surface of the pane, enabling the evaluation of the temperature of the internal and external surfaces.

On the contrary, in the 1R2C network for double pane window the nodes are located in the middle of each pane, in this way it is possible to evaluate the dynamic trend of the temperature of each pane. Finally, for a triple glass window, the temperature of each pane is obtained considering a 2R3C model, in which again the capacitive nodes are located in the middle of each pane.

It has to be remarked that, contrary to the main WBES tools in which the thermal inertia of the window is neglected, by means of the RC network of BCC blocks the thermal capacity of each glass, even if low, is taken into account. Therefore, for double and triple pane windows, the capacitance of each node is

the total thermal capacity of the modelled glass, whilst for the single pane window, the two capacitances are set to half the capacity of the window.

Thermal resistances, as for BME block, connect two adjacent nodes and, except for the case of a single glass window, are related to the radiative and convective heat transfer among the gas cavity, neglecting the conduction in the glass. The radiative heat transfer coefficient is evaluated considering the radiative heat exchange between two grey infinite planes:

$$h_{rad} = \frac{(T_m + 273)^3 4\sigma_0}{1 - \frac{1}{\varepsilon_{s1}} - \frac{1}{\varepsilon_{s2}}} \quad (2.14)$$

where  $T_m$  is the mean temperature of the panes that delimit the cavity,  $\sigma_0$  is the Stefan-Boltzmann constant and  $\varepsilon_s$  is the emissivity of the panes.

On the other hand, the convective heat transfer coefficient is determined by means of the gas-cavity model. In ALMABuild, the experimental correlation proposed by Elsherbiny [96] for the Nusselt number for vertical windows is adopted:

$$Nu = \left[ 1 + (0.0303Ra^{0.402})^{11} \right]^{0.091} \quad \text{for } Ra < 2 \times 10^5 \quad (2.15)$$

Considering the expression of the radiative and convective heat transfer coefficient in the gas cavity, it can be noted that they depend on the temperature of the pane, that is not constant during the simulations. As a consequence, contrary to massive envelope elements, windows are characterised by a variable thermal transmittance.

Windows are clear components, that means that they transmit a fraction of the incident solar radiation to the thermal zone. Moreover, a fraction of the incident solar radiation is absorbed by panes. The evaluation of the optical behaviour is modelled considering the solar absorptance of each pane, the solar transmittance and the back and inward solar reflectance of the overall window system, composed by several panes. All these parameters are function of the angle of incidence, but also the hemispherical average value is needed to correctly estimate the optical behaviour of a window with the diffuse solar radiation [97]. It has to be remarked that, since each pane absorbs a fraction of the incident solar radiation, the nodes of the RC network are characterised by an additional power source in order to take into account this thermal flux. The convective and radiative heat transfer with the external and internal surrounding and the long-wave radiative heat transfer with the sky are evaluated as for BME blocks.

In Figure 2.21, that represents the BCC block of a double pane window, input and output required by a BCC block can be appreciated. The first four inputs are

the same of a BME block: the *Temperature zone bus* is the first output, followed by the *Weather Data bus*, *Solar Radiation Bus* and by the secondary solar radiation that strikes the internal surface of the window. The last input required is the angle of incident of the solar radiation, since optical properties of the window depend on it.

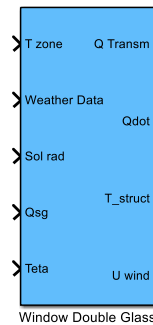


Figure 2.21. BCC block for a double pane window.

Four are the outputs of a BCC block: the first,  $Q Transm$ , is a vector composed by the direct and the diffuse solar radiation transmitted by the window to the thermal zone. This output is directly linked to *Direct Distribution block*, collected in the *Other Components* blockset, that is used for the evaluation of the share of the entering solar radiation that strikes the internal surface of each envelope element of the thermal zone. The second and the third outputs are the *Power bus* and the *Superficial temperature bus*, which is composed by the superficial temperature of the clear part of a window, since generally it is the main component of a window. Finally, the last output is the thermal transmittance of the window that, as remarked previously, is not a constant value but it changes dynamically, as a function of the pane temperature.

### 2.7.2 Distribution of the incoming solar radiation

Windows are clear components so, contrary to opaque elements, not only they absorb and reflect, but they also transmit a fraction of the incident solar radiation to the inside. Solar Gains (SG) are the incoming solar radiation that is absorbed by the internal surface of opaque envelope elements, that can also reflect the radiation. The evaluation of solar gains for each envelope element ( $SG_i$ ) is performed in ALMABuild by means of the *Direct distribution* and the *Diffuse distribution* blocks. In a building model, a *Direct distribution* block is needed for each window, whilst only a *Diffuse distribution* block is required for each thermal zone.

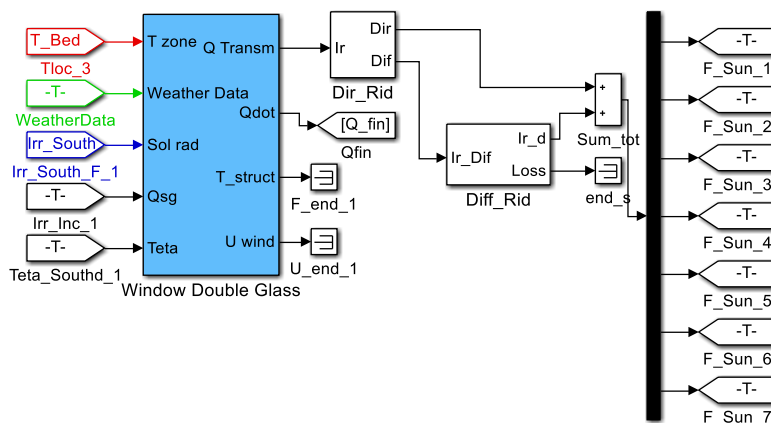


Figure 2.22. Connections of a BCC block to *Direct* and *Diffuse distribution* blocks.

As represented in Figure 2.22, the first output of the window block, that is the vector composed by the direct and diffuse component of the solar radiation transmitted by a window, is the input of the *Direct distribution* block. In this block, the direct component of the incoming solar radiation is split over all the opaque surfaces of the envelope elements of the thermal zone, except for those components that have the same exposition of the considered window. In this way, the direct solar radiation transmitted by a window can't strike the wall that contains the window. The direct solar gain ( $SG_b$ ) of an envelope element, that represent the fraction of the incoming solar radiation absorbed the opaque element, is calculated as the product between the surface fraction, evaluated as the fraction of the area of the  $i$ -th element ( $A_i$ ) to the total opaque area of the thermal zone ( $A_{tot,opaque}$ ) and the solar absorptance coefficient of the internal side of the  $i$ -th element ( $\alpha_i$ ), as:

$$SG_{b,i} = \frac{A_i}{A_{tot,opaque}} \alpha_i \quad (2.16)$$

As it can be noted by Figure 2.22, the *Direct distribution* block has two outputs: the first is a vector composed by the direct solar radiation absorbed by the internal side of each envelope element of the thermal zone, whilst the second output is the diffuse solar radiation entering in the thermal zone. The incoming diffuse solar radiation is evaluated as the sum of the diffuse component of the transmitted solar radiation and the fraction of the direct solar radiation diffusively reflected by the internal side of the opaque element of the thermal zone.

In the *Diffuse distribution* block, whose input is the second output (or the sum of the second output in case of more than one window in the thermal zone) of the *Direct distribution* block, the solar fractions for the diffuse radiation are evaluated following a calculation method based on the model described by Judkoff and Neymark [98].



The solar gain of the  $i$ -th surface element for diffuse radiation ( $SG_{d,i}$ ) is calculated as the sum of four coefficients, as evidenced by:

$$SG_{d,i} = B1_i + B2_i + B3_i + BR_i \quad (2.17)$$

The first term of Equation (2.17) describes the first “bounce” of the entering diffuse solar radiation, assuming that all the shortwave radiation strikes only the floor. For this reason, the first term of the equation is equal to the solar absorptivity for floors, otherwise it is set to zero.

The second term,  $B2_i$ , is related to the second “bounce”, due to the reflection of the solar radiation on the floor. The terms  $B2_i$  are evaluated by means of the following relationships:

$$\begin{cases} B2_i = (1 - \alpha_{fl}) \alpha_i \frac{A_i}{A_{tot, no\ floor}} & \text{if } i \neq \text{floor} \\ B2_i = 0 & \text{if } i = \text{floor} \\ B2_{i, loss} = (1 - \alpha_{fl}) \tau_{s,i} \frac{A_i}{A_{tot, no\ floor}} & \text{if } i = \text{window} \end{cases} \quad (2.18)$$

The reflected solar radiation is distributed over both opaque and clear envelope elements of the thermal zone in proportion to the surface fraction, evaluated in this case considering the total area (clear and opaque) of the internal surface of the thermal zone, not considering the floors area. In (2.18)  $\alpha_{fl}$  is the mean solar absorptivity coefficient of floors, whilst  $\alpha_i$  and  $\tau_{s,i}$  are the solar absorptivity and transmissivity coefficient of the  $i$ -th surface. Moreover, it can be noted that  $B2$  is set to zero for floors, and for windows and additional term is evaluated ( $B2_{i, loss}$ ), for taking into account the fact that a fraction of the reflected shortwave radiation that hits the window is lost since it is transmitted to the external ambient.

The term  $B3_i$  takes into account the third “bounce” in a similar way to  $B2_i$  but considering also the floor. Again, the remaining shortwave radiation is distributed over the surface in proportion to the surface fraction, in which the total internal area of the thermal zone is considered, The terms  $B3_i$  are evaluated as:

$$\begin{cases} B3_i = (1 - \alpha_{fl} - \sum_i B2_i) \alpha_i \frac{A_i}{A_{tot}} \\ B3_{i, loss} = (1 - \alpha_{fl} - \sum_i B2_i) \tau_{s,i} \frac{A_i}{A_{tot}} \end{cases} \quad (2.19)$$

Finally, the last term of (2.17) is used for modelling all the remaining bounces, distributing the remaining shortwave radiation considering the calculated  $B3_i$  terms, as:

$$BR_i = \left(1 - \alpha_{\beta} - \sum_i B2_i - \sum_i B3_i\right) \frac{B3_i}{\sum_i B3_i} \quad (2.20)$$

As shown in Figure 2.22, the *Diffuse distribution* block has two outputs. The first output is a vector that contains the values of the diffuse solar radiation absorbed by the envelope element of the thermal zone, calculated as the product of the solar fractions of each envelope element to the transmitted diffuse radiation. The second output of the *Diffuse distribution* block represents the energy losses due to the solar radiation transmitted back to the external ambient. Moreover, from the Figure 2.22 it is possible to appreciate that the vectors containing the direct and diffuse solar radiation absorbed by each envelope component are summed up and then split into their components in order to link each thermal flux to the corresponding building element block by means of a *Goto* command.

## 2.8 Shadings

As it can be appreciated in Figure 2.8, ALMABuild provides GUIs also for the definition of shadings that can affect envelope elements, typically windows. By means of the dedicated interface, the user can define the geometry of the shading object, verifying the geometry thanks to a graphical representation of the building and of the shading device based on the data inserted, like the building represented in Figure 2.23.

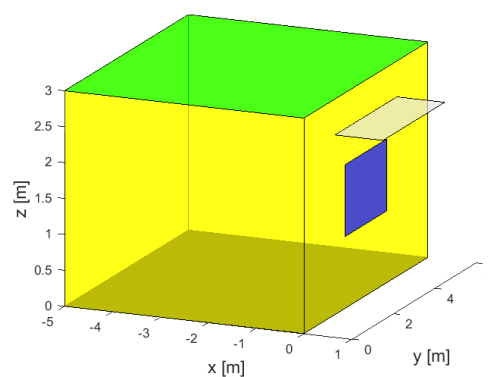


Figure 2.23. Graphical representation of a building with a horizontal shading device (in grey), obtained by the ALMABuild shading GUI.

In order to reduce the computational effort of building energy simulations, as for the evaluation of the incident solar radiation, also the calculation of the annual shading factor profile is automatically performed by a Matlab script only

once, during the implementation of the building model in the Simulink desktop. The user can select the daily time step discretization for the calculation of the annual shading factor profile: calculation can be performed for every day of a year, or for representative days (e.g. one day every one or two weeks). For each day, the calculation of the shading profile is carried on considering a time step of 10 minutes. The evaluated annual shading profile is stored, together with other information related to the envelope element affected by the shading device, in a Matlab structure. In this way, the annual shading factor profile is an input data that is imported in the Simulink desktop from the Matlab workspace.

### 2.8.1 Shading model

Overhangs and external blocks (buildings, trees...) can affect the thermal behaviour of a thermal zone, reducing the incident solar radiation over the external opaque and clear surfaces of the thermal zone. In fact, in these cases, the incident solar radiation,  $H_{tot,inc}$ , is expressed as:

$$H_{tot,inc} = H_b SH_b + H_d SH_d + H_{refl} \quad (2.21)$$

where  $SH$  is the instantaneous shading factor, that is generally defined as:

$$SH = \frac{A_w - A_{sh}}{A_w} \quad (2.22)$$

where  $A_w$  is the area of the surface for which the shading factor is defined, and  $A_{sh}$  is the shaded area of the surface.

Since the area of the considered surface is constant and an input data, the estimation of the instantaneous shading factor requires the calculation of the variable shaded area.

For the beam component of the incident solar radiation the shaded area is evaluated by the projection of the obstruction to the envelope surface plane, as a function of the sun position and of the geometry of the system. The geometry of the system is defined by the coordinates of the edges of the envelope surface and of the obstruction in a cartesian reference system in which the x-axis is oriented toward the South and the y-axis to East. Considering these assumptions, the plane that contains the envelope surface is expressed as:

$$a \cdot x + b \cdot y + c \cdot z = 0 \quad (2.23)$$

where coefficients  $a$ ,  $b$  and  $c$  are defined as functions of slope ( $\beta$ ) and azimuth ( $\gamma$ ) of the surface:

$$\begin{cases} a = \cos \gamma \sin \beta \\ b = \sin \gamma \cos \beta \\ c = \cos \beta \end{cases} \quad (2.24)$$

For an arbitrary point of coordinates  $(x_0, y_0, z_0)$ , the parametric equation of the projective line is:

$$\begin{cases} x = x_0 + l \cdot t \\ y = y_0 + m \cdot t \\ z = z_0 + n \cdot t \end{cases} \quad (2.25)$$

where  $t$  is the equation parameter and coefficients  $l$ ,  $m$  and  $n$  are functions of the sun position, defined by the solar azimuth ( $\gamma_s$ ) and elevation ( $\psi$ ), as evidenced by:

$$\begin{cases} l = \cos \gamma_s \sin \psi \\ m = \sin \gamma_s \sin \psi \\ n = \cos \psi \end{cases} \quad (2.26)$$

From the intersection between the plane of the surface defined in (2.23) and the projection line (2.25) the shadow coordinates on the surface plane can be determined, and consequently the shadow area contained in the surface,  $A_{sh}$ . Then, by means of (2.22) the shading factor for beam radiation is evaluated.

For the calculation of the instantaneous shading factor for the diffuse radiation the sky dome is divided into several cells, whose position is defined by the azimuth and the elevation angle of the central point of the cell. In this way, for each cell, the shadow area on the surface and the shading factor is evaluated adopting the same approach used for the beam radiation. Then, the total shading factor for diffuse radiation ( $SH_d$ ) is evaluated as the mean of shading factors of each cell weighed on the sky radiance, by:

$$SH_d = \frac{\sum_i SH_i H_i}{H_{dh}} \quad (2.27)$$

where  $SH_i$  is the shading factor of the  $i$ -th sky dome cell,  $H_i$  is the sky radiation of the  $i$ -th sky dome cell, estimated by the anisotropic sky radiance model proposed by Brunger and Hooper [99], and  $H_{dh}$  is the diffuse solar radiation on horizontal plane.

## 2.9 Definition of thermal zones

After having defined the weather data, the thermal properties of both opaque and clear envelope elements and the characteristics of eventual shadings devices, data about the thermal zones in which the building is divided can be inserted. Again, for this purpose, a set of GUIs have been developed.

Firstly, it is required to define the number of floors composing the building, and to label each floor, starting from the bottom floor. Then, for each floor, labels of thermal zones located in the considered stage can be defined. Now, the user can insert the main properties of each thermal zone, by means of the GUI represented in Figure 2.24.

Figure 2.24. Thermal zone properties GUI.

As it can be seen in this figure, a pop-up menu is used for the selection of the thermal zone, and internal air volume and initial air temperature can be defined. On the contrary, internal gains profile, characteristics of air ventilation and thermal bridges are inserted by means of dedicated GUIs. Moreover, as it can be appreciated in Figure 2.24, the user can select the kind of model by means of which the thermal zone is simulated. The *simple model* is the most used and consists in the evaluation of both the convective and radiative temperature of the zone, whilst the *radiative model* is used for the estimation of the spatial distribution of the radiative temperature in the thermal zone. The *convective model*, as the radiative, is used for the determination of the spatial distribution of the air temperature, taking into account the convective airflows and, lastly, the *fully detailed model* is adopted for the estimation of the spatial distribution of both the radiative and convective temperature. Finally, by means of a pop-up menu, the user can select the typology of evaluation that has to be performed for the considered thermal zone: it is possible to evaluate the temperature of the thermal zone or the ideal power that a convective HVAC system has to provide to the

zone to guarantee a defined air temperature profile. This last option is available only for *simple* or *radiative detailed models*.

Based on the typology of model selected by the user for the building energy simulation, different geometry information are needed. In Figure 2.25 the GUI for the insertion of geometry data, if the simple model of the thermal zone is selected, is represented. In this figure it can be noted that the thermal zone is defined specifying for each envelope element, characterised by its typology and label (first two columns in the table of Figure 2.25), its orientation and area, that has to be calculated manually. Data required if *radiative*, *convective* or *fully detailed model* is selected are described in *Chapter 4*.

**ALMABuild : Thermal zone geometry:  
Simple model**

Floor **Second**      Thermal zone **Bedroom**

Remark: Surfaces are considered referring to the OUTDOOR SIDE

	Typology	Structure	Area (m <sup>2</sup> )	Orientation	Shading
1	External Wall	Ext_1	10.8000	East	Absent
2	External Wall	Ext_1	8.8000	South	Absent
3	External Wall	Ext_1	10.8000	West	Absent
4	External Wall	Ext_1	10.8000	North	Absent
5	Internal floor	Ceil	10	Kitchen	Absent
6	Internal floor	Ceil	6	Bathroom	Absent
7	Roof	Roof_1	16	Horizontal	Absent
8	Window	Window	2	South	Absent
9	Select	Select	0	Select	Select

**Save and close**

Figure 2.25. GUI for the insertion of the thermal zone geometry for simple model.

### 2.9.1 Building Thermal Balance block

In *Section 2.6.1* it has been remarked that the building modelling in ALMABuild is achieved adopting the LPCE model. By means of this typology of models, buildings are described simulating the dynamic behaviour of all its envelope elements, evaluating thermal fluxes that affects each envelope element and calculating the superficial temperature of it by means of equations as:

$$q_{cd,j} + q_{conv,j} + q_{sg,j} + q_{rad,j} = C_{si,j} \frac{dT_{si,j}}{dt} \quad j \in [1, N] \quad (2.28)$$

where  $q_{cd,j}$  is the heat transfer for unit area due to conduction through the  $j$ -th element,  $q_{conv,j}$  and  $q_{rad,j}$  are the convective and radiative heat transfer between the internal surface of the element  $j$  and indoor surroundings,  $q_{sg,j}$  is the power

related to solar gains, whilst  $C_{si,j}$  and  $T_{si,j}$  are the thermal capacity and temperature of the internal surface of the element  $j$ . Anyway, LPCE models require an additional equation for the estimation of the air temperature, that in general is evaluated as:

$$Q_v + Q_{conv} + Q_{HVAC} + Q_{int} = C_a \frac{dT_a}{dt} \quad (2.29)$$

where  $Q_v$  is the heat transfer due to ventilation with the outdoor,  $Q_{conv}$  is related to the convective heat transfer with the internal surface of the envelope elements,  $Q_{HVAC}$  is the power provided by a HVAC system,  $Q_{int}$  is power due to internal gains, whilst  $C_a$  and  $T_a$  are the thermal capacity and temperature of the air.

Therefore, the description of a thermal zone, composed by  $N$  envelope elements, consists of  $N$  equations (2.28) and one equation for air (2.29). Anyway, the number of unknown variables is  $N+2$ :  $N$  superficial temperatures  $T_{si}$ , the air temperature  $T_a$  and the power provided by the HVAC system,  $Q_{HVAC}$ . Thus, it is required to fix one variable for solving the thermal balance of a zone. If the air temperature is set, the ideal power required to the HVAC system to guarantee the chosen air temperature can be evaluated. On the contrary, if the power provided by the HVAC system is set, it is possible to estimate the air temperature of the thermal zone by solving the set of  $N+1$  equations.

In ALMABuild, the set of  $N$  equations related to the envelope elements of a thermal zone are implemented by means of BME and BCC blocks, whilst the equation related to the air temperature of the zone is implemented in elementary blocks of the Building Thermal Balance subsystem, where the thermal balance of the zone is solved aggregating information related to the  $N$  equations for the envelope elements. Since different kinds of models can be selected by means of the Thermal Zone GUI, in the ALMABuild library different BTB blocks can be found. However, in this Chapter only the BTB blocks related to the thermal balance labelled *simple model* are described, whilst the others are described in Chapter 4.

### 2.9.2 BTB simple model

In the BTB simple model, the thermal balance of a zone is solved according to a two-stars model: one-star model is used for the evaluation of the convective temperature whilst the second is related to the radiative temperature of the zone. The star model representing the convective thermal balance of the thermal zone is shown in Figure 2.26.

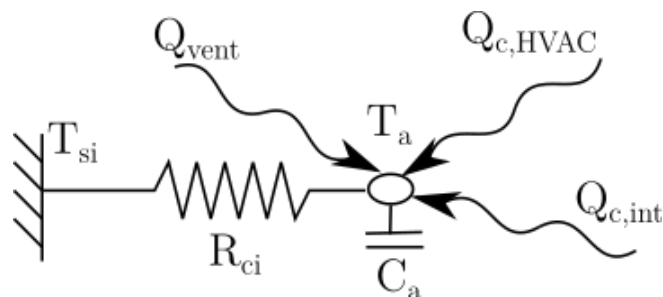


Figure 2.26. Convective star node.

In this figure it is possible to see that the convective node is capacitive and all the convective heat fluxes of the thermal zone insist on it: (i) the convective heat transfer of the internal surface of each envelope element with the internal surroundings ( $Q_{ci}$ ); (ii) the heat transfer due to ventilations and/or air infiltrations ( $Q_{vent}$ ) and (iii) the convective fraction of the power delivered by the HVAC system ( $Q_{c,HVAC}$ ) or (iv) by internal gains ( $Q_{c,int}$ ).

From the star network represented in Figure 2.26, the convective heat balance equation can be written as:

$$\sum Q_{ci} + \sum Q_{vent} + \sum Q_{c,HVAC} + \sum Q_{c,int} = \rho_a c_a V \frac{dT_a}{dt} \quad (2.30)$$

From (2.30) it is possible to see that the convective temperature of the zone depends on the heat capacity of the air, given by the product of the air density ( $\rho_a$ ), the specific heat capacity ( $c_a$ ) of the air and the net volume of the thermal zone ( $V$ ). It is important to remark that, the convective temperature evaluated solving (2.30) has the physical meaning of the air temperature of the thermal zone, assuming a homogenous distribution of the temperature inside the zone.

On the other hand, the radiative temperature estimated by means of the star model represents the mean radiative temperature evaluated in the centre of the thermal zone. In Figure 2.27a the delta network scheme representing the radiative heat transfer among three surfaces is depicted. In this figure it is possible to note that each surface is connected (i.e. heat transfer is accounted) to the others by means of thermal resistances. The values of these thermal resistances depend not only on the radiative heat transfer coefficient but also on the view factors between the surfaces. However, since the calculation of the view factors is time consuming and requires the complete definition of the geometry of the thermal zone, by means of the edge coordinates of each surface, the delta connection is replaced by the star network, represented in Figure 2.27b.



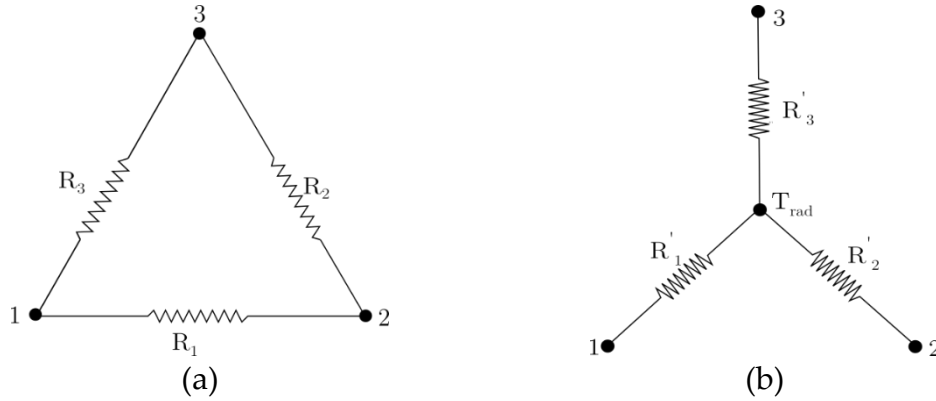


Figure 2.27. Radiative exchange between three surfaces, delta (a) and star (b) network.

By means of this network, each surface is characterised only by the heat transfer with the central node of the star network, which represents the mean radiative temperature of the zone. As represented in the figure, the thermal resistances that connect each surface to central node ( $R'_i$ ) are different to the respective one of the delta-connection; actually, the thermal resistances of the star network ( $R'_i$ ) depend only on the radiative heat transfer coefficient, since the view factor between a surface to the central node is unitary. In this way, the view factor calculation is not required. It has to be remarked that the delta-star transformation gives exact results only for a three-surface enclosure, whilst for more surfaces the star network results are approximations of the exact results obtained with the delta connection. However, it has been demonstrated that for the analysis of radiant exchange between surfaces in buildings the star network is satisfactory [100].

The mean radiative temperature is evaluated solving the radiative heat balance of the thermal zone:

$$\sum Q_{ri} + \sum Q_{r,HVAC} + \sum Q_{r,int} = \frac{dT_r}{dt} \quad (2.31)$$

From (2.31) it can be seen that the radiative temperature depends only on the radiative heat fluxes of the thermal zone due to HVAC system ( $Q_{ri}$ ), internal gains ( $Q_{r,HVAC}$ ) and the heat transfer with the surface of the envelope elements ( $Q_{r,int}$ ). Moreover, equation (2.31) highlights that no heat capacity is considered, since as represented in Figure 2.27(b) the radiative node is non-capacitive. However, it has to be remarked that, caused by numerical issues, in the ALMABuild BTB block a little heat capacity is considered also for the radiative node, not affecting the solution.

In Figure 2.28, two BTB blocks that implement the simple thermal balance model are represented. The inputs of these blocks are the sum of the *Power Bus* related to different categories of buildings elements or thermal fluxes. As an example, the first input of both the blocks is the sum of the *Power Bus* that

concerns external walls, whilst the second output is referred to roofs. In this way, by means of the *Power Bus* each BME and BCC block is linked to the BTB block, implementing the set of  $N+1$  equations necessary for solving the thermal balance of the zone, as described above. Inputs of the BTB blocks are not only related to envelope elements but also to different kinds of thermal fluxes. As an example, the seventh and the ninth inputs concern the *Ventilation Bus* and the *Power bus* describing the internal heat gains respectively. However, comparing the inputs of these blocks, it can be observed that the last input is different: the block on the left in Figure 2.28, labelled *Temperature evaluation*, requires as input the *Power Bus* related to the HVAC system, whilst the BTB block on the right, labelled *Ideal Power*, uses as input the air temperature, that has to be set. This is due to the fact that, as described before, for solving the thermal balance of the zone, the air temperature or the power provided to the thermal zone by the HVAC system has to be fixed. Thus, in the BTB block labelled *Temperature evaluation*, the air and the radiative temperatures are calculated by equations (2.30) and (2.31), whilst in the *Ideal Power* block, the convective fraction of the HVAC system, required for maintaining the air temperature to the set imposed by the last input, is evaluated by means of (2.30). On the contrary, in the *Ideal Power* block the radiative temperature, that is not set by the last input, is evaluated by (2.31) and the radiative component of the HVAC power is set to zero.

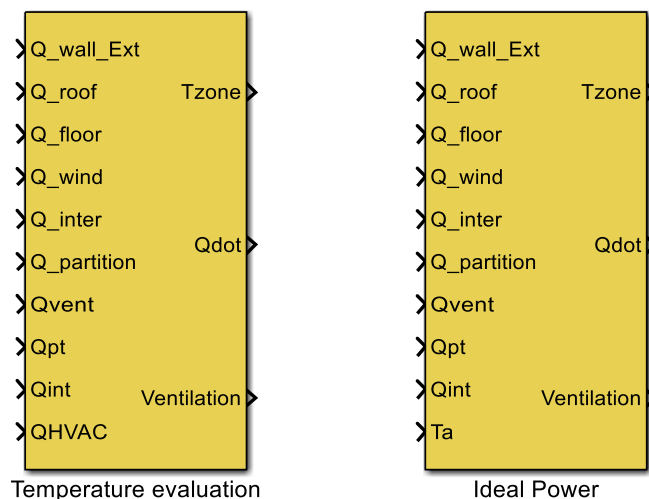


Figure 2.28. BTB blocks for the evaluation, by means of the simple model, of the temperature of the zone (left block) and of the ideal power for fixed thermal zone conditions (right block).

Finally, as it can be appreciated by Figure 2.28, both the kinds of BTB blocks have the same outputs: the *Temperature zone bus*, the total *Power bus* of the zone and the *Ventilation bus*.

## 2.10 Implementation of the building model

The data inserted by the user concerning the weather, the envelope elements and thermal zones of the building are collected in two Matlab structures by means of the *SAVE ALL DATA* button of the ALMABuild main interface, as represented in Figure 2.8. Weather data are collected in the *Climatic\_Data* structure, whilst all the information about envelope elements and thermal zones are collected in the *Building\_Data* structure.

Then, the building model can be implemented in the Simulink desktop just by means of the *CREATE THE MODEL* command of the ALMABuild main interface. Firstly, all the yearly calculations related to the evaluation of the incident solar radiation over a surface and of the shading factors are automatically performed and the obtained profiles are added to the *Ambient\_Data* and the *Building\_Data* structure, respectively. In this way, the computational effort, and consequently the time required for simulations is reduced, since shadings and solar radiation information needs only to be recalled as data and not evaluated time by time.

Then, by means of a series of *m-files* (an example of these codes is reported in *Appendix D*), the building model is implemented in the Simulink desktop, importing all the necessary blocks from both the Simulink and ALMABuild libraries, properly linking them and setting for each block the proper parameters, based on the data previously inserted by the user. In this way, the creation of the building model in the Simulink desktop is totally automatic, making the building modelling faster compared to a manual implementation and drastically reducing mistakes due to data insertion or block linking. Moreover, it has to be highlighted that all the procedure for the building modelling with ALMABuild does not require any Simulink expertise of the user. Finally, it can be remarked that, during the implementation of the building model in the Simulink desktop, a customized ALMABuild function is defined among the *PreFcn* property of the Simulink model, in order to make available weather and shading data if the simulations intervals higher than one year.

## 2.11 Conclusions

In this *Chapter*, ALMABuild, a Matlab tool for the building modelling in Simulink that composes the ALMABEST tool, has been described. Contrary to the other tools that can be found in the literature ALMABuild consists of both a Simulink library and a set of Graphical User Interfaces (GUIs).

The building modelling in ALMABuild is based on the Lumped Parameter Construction Element (LPCE) approach, that consists in the description of a building by the modelling of all its envelope element. Thus, the ALMABuild library is composed by a set of blocks used for the modelling of walls, roofs and

ceilings (Building Massive Elements blocks), windows (Building Clear Components blocks) and for solving the thermal balance of the zone, according to different models (Building Thermal Balance blocks).

The main novelty introduced by ALMABuild is represented by its approach for the building modelling: user is driven in the insertion of the data by the GUIs that also recalls a series of *m-files*. By means on these *m-files*, based on the data defined by the user, the building modelling is automatically implemented in the Simulink desktop, by importing all the necessary blocks from both the Simulink and ALMABuild libraries and properly linking them and setting the parameters. In this way, the main drawback that limits the diffusion of Simulink tools described in *Chapter 1* is overcome.

## ALMABuild validation

---

### Abstract

In this *Chapter*, the benchmark of the ALMABuild library, conducted following the Building Energy Simulation Test (BESTEST) procedure reported by Judkoff and Neymark [98], is described.

Firstly, results of analytical and empirical tests, used for the validation of the ALMABuild *Building Massive Elements* block, are presented. Then, comparative tests for a series of univocally defined cases, described in the BESTEST report, with a reference software list of both BESTEST and ASHRAE Standard 140 [101] are carried out. For all the considered cases ALMABuild predictions are always within the maximum and minimum threshold values, confirming the validity of the models used in this tool. Anyway, the comparison with the BESTEST and ASHRAE Standard 140 reference software pointed out that the BESTEST reference results and software must be periodically updated for obtaining an accurate state-of-the-art validation of new software. In fact, the reference software list recalled by BESTEST contains codes based on outdated models and a great discrepancy among the reference results can be observed. For these reasons, additional benchmarks of ALMABuild are performed, running it against EnergyPlus and the new hourly method proposed by the recent European Standard EN ISO 52016 [62]. Results show a good agreement between ALMABuild and EnergyPlus, whilst the comparison with EN ISO 52016 evidenced the inadequacy of the new simplified hourly model proposed, especially for heavyweight buildings.

---

### 3.1 The BESTEST procedure

The Building Energy Simulation Test (BESTEST) procedure is a validation methodology for whole building simulation software that has been developed by the Model Evaluation and Improvement International Energy Agency (IEA) Experts Groups in the first years of 1990s. In fact, the increasing calculation power of computers and the drop of their prices led to the development of a large number of building energy software. However, the physical models adopted for the development of these programs and, consequently, their main assumptions and simplifications were usually not clearly described. Moreover, in the first building energy software only few information about the limitations of the implemented algorithms were available to the users. The lack of information and the great, unexplained, discrepancies between the predictions performed with these tools if applied to the same test case, led to the need of a shared and detailed common benchmark method.

The BESTEST method, fully described by Judkoff and Neymark [98], consists in three different kinds of tests:

- analytical verification, in which software predictions are compared to analytical solutions for simple reference cases;
- empirical validation, in which the agreement between numerical predictions and measured real data is evaluated;
- comparative testing, in which the results obtained with a software are compared to the ones obtained with other codes.

The main advantages of analytical verifications are the absence of uncertainty on inputs and outputs, and the fact that this typology of test is fast and inexpensive. Nevertheless, analytical solutions can be derived only for simple cases, in which single heat transfer mechanism, under simplified boundary conditions, are considered.

Empirical validations require the set-up of an experimental apparatus that makes this kind of test expensive and time consuming. Moreover, inputs and outputs, as they are experimentally measured, are affected by uncertainty related to the accuracy of the monitoring equipment. In these cases, all kinds of heat transfer mechanisms are taken into account at the same time, enabling the comparison of the numerical predictions to real behaviour of buildings.

Finally, inter-model comparisons can be performed adopting any level of complexity. However, it has to be remarked that, in this case, the results obtained by the reference models cannot be assumed as the “truth”, since reference model results are based on accepted current state-of-the-art models, which are upgraded time by time.

In the BESTEST procedure, analytical verifications, empirical validations and inter-model comparisons must be performed systematically, following the scheme represented in Figure 3.1.

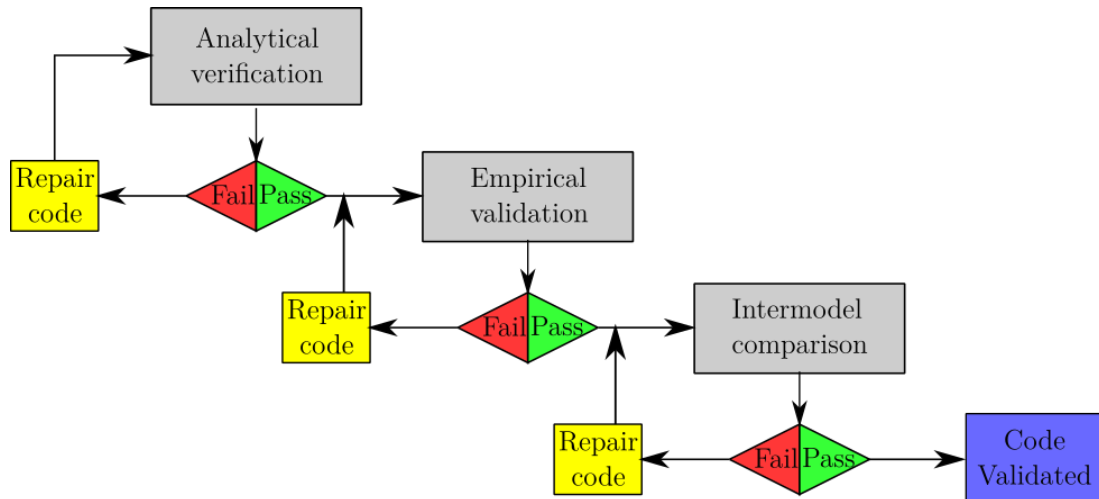


Figure 3.1. BESTEST validation scheme.

As evident in Figure 3.1, analytical verifications are considered the first step of this benchmark procedure. Only if analytical verifications give a positive result the numerical code is tested by using empirical validation data, in order to correct errors that cannot be detected considering only single heat transfer mechanisms or simplified boundary conditions, like in analytical tests. After these two steps, the software is run against reference software, in well-defined reference cases, with the aim to ensure that the numerical results of the new software are in good agreement with those obtained with the most diffuse software for dynamic building energy simulations (which were yet tested following the BESTEST procedure).

Thanks to its systematic approach, the BESTEST procedure has been followed for the validation of the main whole building energy simulation programs, like TRNSYS, ESP-r, EnergyPlus and DeST [102]. Moreover, this procedure has also been inserted in the Standard ASHRAE 140 [101].

## 3.2 Analytical verifications

The first step of the validation procedure of the ALMABuild library following the BESTEST procedure consists in the comparison of the ALMABuild numerical predictions with analytical solutions. This comparison is performed considering the problem related to the determination of the dynamic trend of the indoor air temperature in a cubic room during a variation of the external air temperature from 20 °C to 30 °C in one hour. The cubic room, whose side is one-meter long, is composed by floor, ceiling and four identical vertical walls, no windows are present. Floor and ceiling have the same composition and the same boundary conditions applied to the walls. Four different wall compositions are considered, as reported in Table 3-1. In the first two cases, envelope elements are composed by a single layer, brick in Case#1 and thermal insulation in Case#2. Then, multi-

layered walls, given by combinations of bricks, insulation and plaster layers are considered: in Case#3 bricks are in the external layer, whilst in Case#4 they are in the internal one.

Table 3-1. Wall stratigraphy for the room considered in the ALMABuild analytical verification.

Case #	d [cm]	$\lambda$ [W/(m K)]	$\rho$ [kg/m <sup>3</sup> ]	c [kJ/(kg K)]
1	20	1.2	2000	1.0
2	10	0.04	50	1.0
3	20 (ext)	1.2	200	1.0
	10	0.04	50	1.0
	0.5 (int)	0.14	800	1.5
4	0.5 (ext)	0.14	800	1.5
	10	0.04	50	1.0
	20 (int)	1.2	2000	1.0

The emissivity of the room walls is imposed equal to zero in order to eliminate radiative contributions, whilst the internal and external convective heat transfer coefficients of each element are set to 2.5 and 8 W/(m<sup>2</sup>K) respectively. The incident solar radiation on the external walls is neglected, as the air flow rate due to ventilation. There are no HVAC systems in the room that, consequently, is in free-float conditions.

The analytical solution of this problem is obtained by applying the procedure proposed by EN ISO 13791 [103] for the analysis of the unsteady heat conduction through multi-layered opaque walls. The comparison between the instantaneous indoor air temperature calculated by ALMABuild and the analytical solution reported by EN ISO 13791 is shown in Table 3-2 at fixed time intervals, starting from the instant in which the external air temperature begins to rise (t=0). The comparison has been repeated four times, considering the four different wall compositions described in Table 3-1.

Table 3-2. Comparison between analytical [103] and numerical values of the indoor air temperature (in °C) obtained with ALMABuild.

		Time [h]									
		2		6		12		24		120	
		T	$\Delta\%$	T	$\Delta\%$	T	$\Delta\%$	T	$\Delta\%$	T	$\Delta\%$
Case #1	Analytical	20.04	0.15	21.26	0.09	23.48	-0.17	26.37	0	30.00	0
	ALMABuild	20.07		21.28		23.44		26.37		30.00	
Case #2	Analytical	25.09	-0.20	29.63	0	30.00	-0.03	30.00	0	30.00	0
	ALMABuild	25.04		29.63		29.99		30.00		30.00	
Case #3	Analytical	20.00	0.05	20.26	0.5	21.67	0.09	24.90	-0.28	29.95	0
	ALMABuild	20.01		20.36		21.69		24.83		29.95	
Case #4	Analytical	20.00	0	20.06	0.05	20.25	-0.10	20.63	-0.15	23.17	-0.04
	ALMABuild	20.00		20.07		20.23		20.60		23.16	

The results collected in Table 3-2 show a good agreement between the analytical and the numerical results obtained with ALMABuild, with absolute



percentage difference between the results lower than 0.5%. In particular, it can be noted that the maximum difference between analytical and numerical results, obtained in hour 6 for Case#3, is equal to 0.1 K, whilst for the other cases, discrepancy is less than 0.05 K. The results shown in Table 3-2 confirm the good accuracy of the model adopted in the *Building Massive Element* (BME) blocks, based on a 3R4C model, both for single and multi-layer building element compositions.

### 3.3 Empirical validation

Following the BESTEST method, after the analytical verification, results obtained by BME blocks of ALMABuild are compared to empirical data. The empirical validation of BME blocks is performed considering a series of measurements obtained during the in-situ determination (performed in February) of the thermal transmittance of an external vertical wall. This wall (whose stratigraphy is reported in Table 3-3) has a North exposure and is an envelope component of a building located in Bologna (Italy).

Table 3-3. Stratigraphy of the measured wall.

Layer	d [cm]	$\lambda$ [W/(m K)]	$\rho$ [kg/m <sup>3</sup> ]	c [kJ/(kg K)]
Plaster	1.5	0.99	1800	1
Brick	28	0.79	1800	0.84
Plaster	1.5	0.99	1800	1

The experimental set-up, shown in Figure 3.2, adopted for the in-situ measurement of a wall thermal transmittance consists in a commercial device (*Optivelox Thermozig*) composed by a heat flow meter (labelled 1 in Figure 3.2), two Pt1000 RTD sensors (class 1/3 B), labelled 2 and 3, two temperature sensors for outdoor and indoor air (4 and 5) and a data acquisition system (6 in Figure 3.2).

The empirical validation of the ALMABuild BME block has been conducted by imposing as boundary conditions the dynamic trend of the internal and external air temperature measured during the test. The hourly profiles of solar radiation on the external wall and of internal gains, considering also the power released by the radiators, are represented in Figure 3.3a and Figure 3.3b respectively. The dynamic trend of the wall temperature on the internal wall side has been calculated and compared with the experimental values.

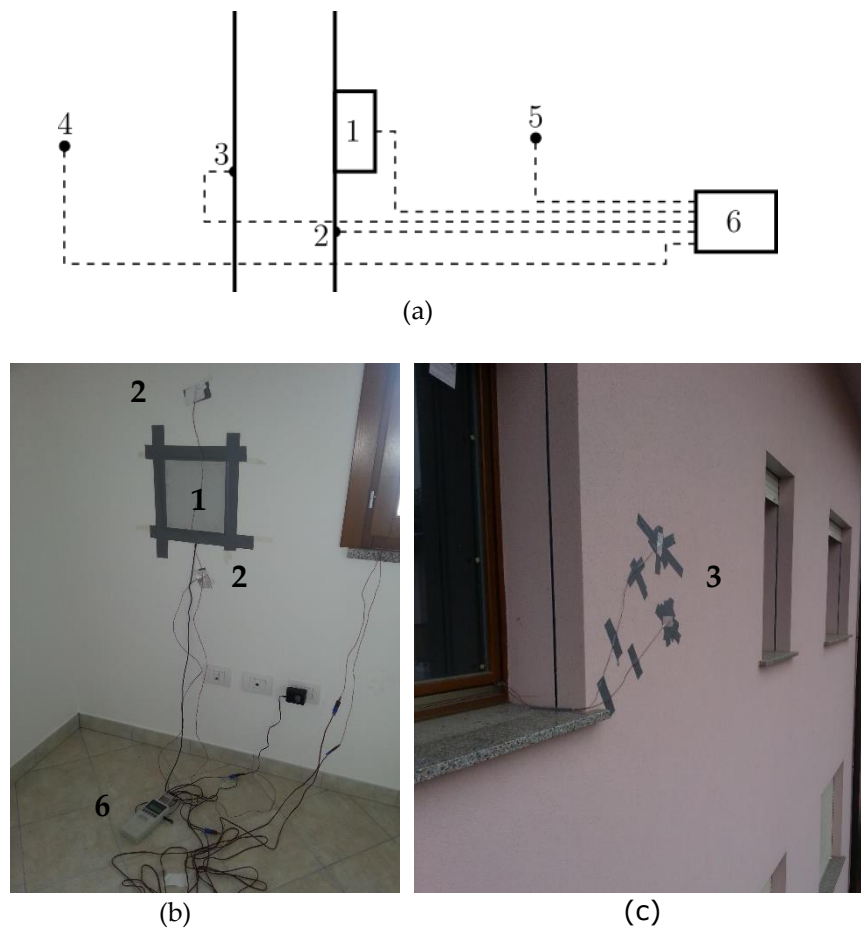


Figure 3.2. (a), (b) and (c): Experimental set-up. (1) is the heat flow meter that, together with the Pt1000 RTD sensors (2) and (3), composes the Optivelox ThermoZig, (4) and (5) are outdoor and indoor air temperature sensor and (6) is the data acquisition system.

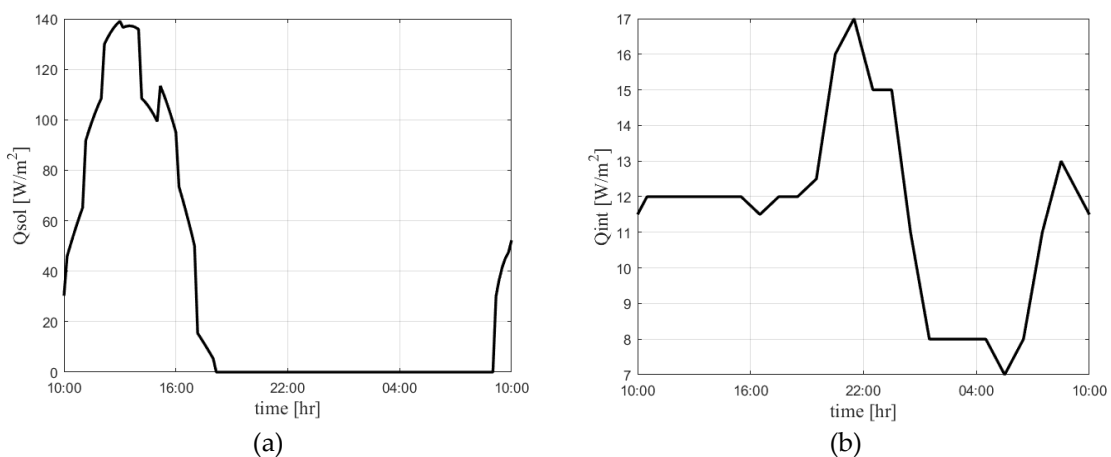


Figure 3.3. Hourly profile for the incident solar radiation over the wall (a) and of internal heat gains (b) used for the evaluation of the internal wall surface temperature with ALMABuild.

In Figure 3.4 the internal surface temperature of the wall obtained by means of numerical simulations performed using ALMABuild is compared with the

measured values collected during one day (24 h) in which the outdoor air temperature varied from 12°C (at 3:00 p.m.) to 7°C (at 6:00 a.m.). In Figure 3.4 the experimental temperature data are shown together with their uncertainty ( $\pm 6\%$ ) calculated by means of the theory on the propagation of errors [104], starting by the uncertainty values declared by the manufactures of the sensors used during the tests.

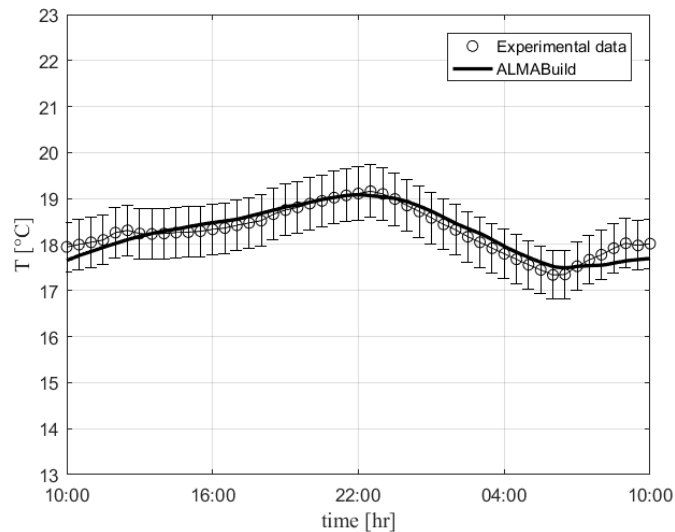


Figure 3.4. Comparison between the empirical data and the numerical result obtained using ALMABuild in terms of internal surface temperature of the wall.

By observing Figure 3.4 it is possible to appreciate how the prediction of the internal surface temperature of the wall obtained by using ALMABuild is in good agreement with the experimental data, if one considers that the numerical results are always within the error band of the temperature data. It can only be pointed out that, in the last two hours of the measured interval, numerical results, even if within the error band of the experimental data, show rising trend that is slightly lower than that measured.

Nevertheless, the good agreement between numerical and empirical results confirm the validity and the accuracy of the procedure for the modelling of massive envelope elements followed by the BME block of the ALMABuild library, even in presence of multiple heat transfer mechanisms activated across the wall and of complex boundary conditions, like in the described experimental test.

### 3.4 Comparative tests

The third, and last, step of the BESTEST method consists in the comparison of the numerical results obtained by using the software being validated, with the results obtained with other codes. In the BESTEST report [98], a series of cases univocally defined are collected, together with the results obtained for each case

by some software assumed as reference for the dynamic building energy simulations. In this way, it becomes possible to compare the results obtained with ALMABuild to those obtained for the same cases by different reference software. In the BESTEST report of 1995, eight reference software are indicated: ESP-r, TRNSYS, DOE2, SRES/SUN, SERIRES, S3PAS, TASE and BLAST. However, it can be observed that this set of reference software could be considered as representative of the state-of-the-art of the building energy simulation in 90's but not today, due to the evolution of the physical models used in that software. For this reason, ASHRAE Standard 140 [101] proposed an updated set of reference software, which is considered in the benchmark described in this Thesis. In the following, the results collected in this Standard are labelled as BESTEST.

The set of test cases specified in the BESTEST report consists of 40 cases, that progress systematically from extremely simple to more complex and realistic cases. For each test case, the BESTEST report specifies all the input data, like the hourly external weather data, building geometry, internal gains, composition of each envelope element and air ventilation. The simplest cases are used for diagnostic purposes; in fact, single heat transfer mechanisms are added from one case to the following, in order to easily detect errors in the physical modelling. On the contrary, the following fourteen qualifications tests are more realistic, and are used to test the ability of the software to take into account, at the same time, different heat transfer mechanisms and to model building features, like different windows positions, shading devices and different control strategies.

By adopting the same notation of the BESTEST report, the comparative qualification tests selected for the ALMABuild benchmark are listed in Table 3-4. From Table 3-4 it can be noted that the qualification cases (not considering the free float cases) selected for the ALMABuild validation are 13: only Case 990, that is related to the ground coupling, has not be considered.

As indicated in Table 3-4, the envelope element's composition changes among the tests; in particular, the heat capacity and the density of the building elements are modified, whilst the total thermal transmittance is constant over the cases. In this way, the ability of the software to model both heavy and light buildings is tested. As reported in Table 3-4, in the qualification tests different control strategies of the ideal HVAC system integrated to the building are considered. As defined in the BESTEST report, adopting the "*Dead-Band*" control strategy the HVAC system is switched on in the heating mode if the internal air temperature is less than 20 °C, whilst if the internal air temperature is higher than 27 °C the HVAC system works on cooling mode. With the "*Setback*" control strategy a night attenuation is imposed for the heating mode, whilst the cooling mode is the same of the "*Dead-Band*" control strategy. Finally, the "*Venting*" control strategy is characterised by an hourly profile of the air ventilation and the HVAC system works only in cooling mode from 7 a.m. to 6 p.m., if the internal air temperature is higher than 27 °C.

Table 3-4. List of the qualification cases analysed during the comparative tests.

Case	Envelope composition	Position of the windows	Window Shadings	Control strategy	
600	Lightweight	South	No	Dead band	
610	Lightweight	South	H	Dead band	
620	Lightweight	East, West	No	Dead band	
630	Lightweight	East, West	H-V	Dead band	
640	Lightweight	South	No	Setback	
650	Lightweight	South	No	Venting	
900	Heavyweight	South	No	Dead band	
910	Heavyweight	South	H	Dead band	
920	Heavyweight	East, West	No	Dead band	
930	Heavyweight	East, West	H-V	Dead band	
940	Heavyweight	South	No	Setback	
950	Heavyweight	South	No	Venting	
600FF	Lightweight	South	No	Free-Float	
650FF	Lightweight	South	No	Free-Float and venting	
900FF	Heavyweight	South	No	Free-Float	
950FF	Heavyweight	South	No	Free-Float and venting	
960	Back zone	Lightweight	No	No	Dead band
	Sun zone	Heavyweight	South	No	Free Float

Cases labelled FF are the free-float cases, in which the HVAC system is switched off and only the air ventilation conditions can change if the control strategy is “*Venting*” (imposing an hourly profile of the air infiltration rate). For case 960 in which two thermal zones are present, the adopted conditions during the numerical tests are indicated in Table 3-4 separately for the back zone and the sun zone.

As suggested by BESTEST, the building geometry reported in Figure 3.5 has been used during the numerical tests. The reference room is characterised by a horizontal roof, a near-adiabatic slab-on-ground floor and two windows, both inserted in the South wall. In order to model the near-adiabatic slab-on-ground floor, a thick (1 m) under-floor thermal insulation layer has been considered in the numerical runs of ALMABuild. For Cases 620, 630, 920 and 930 the position of the windows is different from the building geometry reported in Figure 3.5; in these cases, a window both in the East and the West wall is present. For case 960, two thermal zones are considered by adding the room indicated with dashed lines in Figure 3.5. In this last case the original South wall becomes an internal wall (without windows) which separates the room considered in the other cases (Back zone) from the additional zone having two windows on the South Wall (Sun Zone).

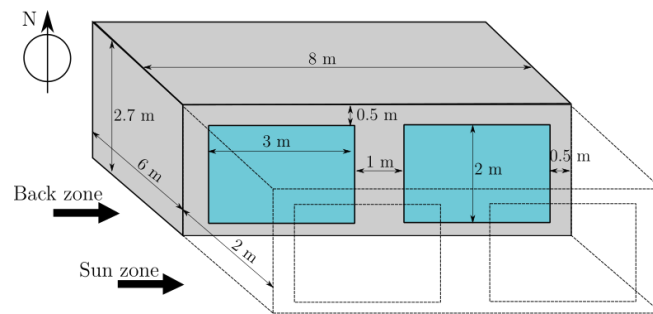


Figure 3.5. The reference building geometry indicated by BESTEST for software verification.

The geometry of the shading devices that are present in cases 610, 630, 910 and 930 is represented in Figure 3.6. In particular, for cases 610 and 910, characterised by two windows in the South wall, there is a single horizontal shading device (Figure 3.6a); whilst for cases 630 and 930, for both the windows in the East and West wall, the shading device is composed by a horizontal and two vertical overhangs (Figure 3.6b).

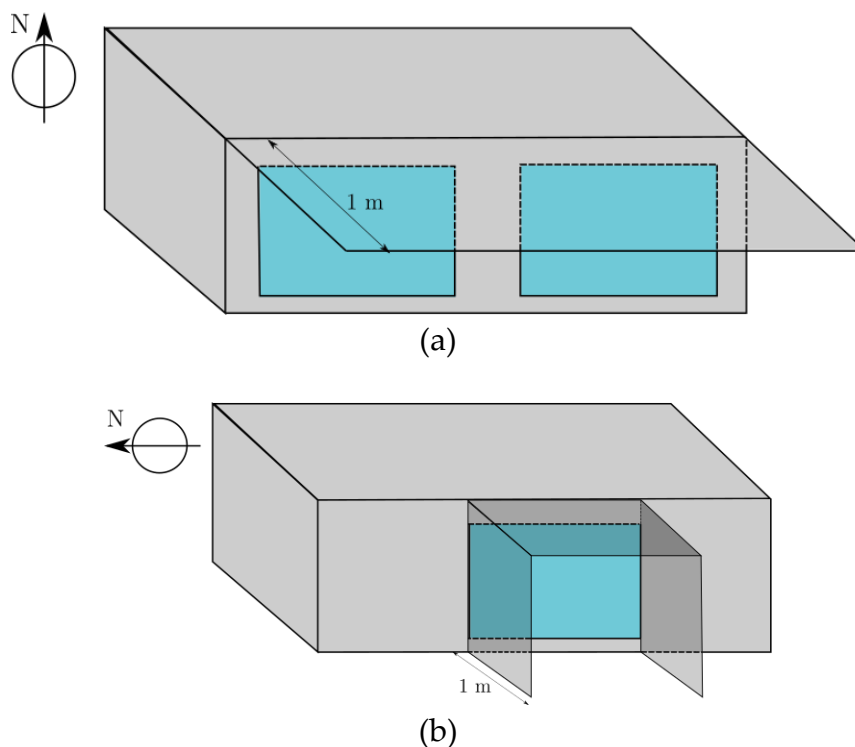


Figure 3.6. Horizontal shading device for cases 610 and 910 (a); vertical and horizontal shading devices for cases 630 and 930.

For each case, the weather data are the same and the Typical Meteorological Year (TMY) is supplied by the BESTEST report. The building is located in Denver (Colorado, USA), which is characterised by cold clear winters and hot dry summers. The minimum, maximum and mean annual temperatures are  $-24.4\text{ }^{\circ}\text{C}$ ,

35 °C and 9.7 °C respectively, whilst the mean and maximum daily temperature ranges are 14.2 °C and 29.4 °C.

In agreement with the procedure suggested by the BESTEST report, the comparative test was firstly performed focusing the attention on the evaluation of the incident solar radiation on opaque and transparent external building surfaces. Then the comparative test was carried out considering the solar transmission of the clear components, both neglecting and taking into account window overhangs. Finally, comparative test dealt with the analysis of the hourly free-float internal air temperature, the energy consumption and the power peak released by the HVAC system to the room both for heating and cooling conditions.

### 3.4.1 Validation of the solar contributions on the external surfaces

The first comparative test is related to the calculation of the incident solar radiation on external building surfaces. In fact, the weather data contained in the TMY file provide only the hourly profiles of the beam and diffuse incident solar radiation on horizontal plane. Table 3-5 shows the predicted incident annual solar radiation (divided for orientation) on external opaque and clear elements of the building shown in Figure 3.5, obtained with ALMABuild and the reference software. In this case the reference software collected in the ASHRAE Standard 140 are the same listed in the BESTEST report of Judkoff and Neymark [98].

From Table 3-5, it can be noted that, for each surface orientation, the annual incident solar radiation predicted by ALMABuild is in good agreement with the values indicated by the other software. In fact, the values obtained with ALMABuild are always within the maximum and the minimum values obtained with the reference software.

Table 3-5. Annual incident solar radiation [kWh/(m<sup>2</sup> year)] on the external walls of the building of Figure 3.5 obtained by using the reference software and ALMABuild.

	North	East	West	South	Horizontal
ESP	427	959	1086	1456	1797
DOE2	434	1155	1079	1566	1831
SRES/SUN	456	1083	1003	1476	1832
SERIRES	407	1217	857	1468	1832
S3PAS	457	1082	1002	1474	1832
TRNSYS	367	1101	1012	1522	1832
TASE	453	962	1090	1468	1832
<b>ALMABuild</b>	<b>393</b>	<b>1116</b>	<b>1073</b>	<b>1566</b>	<b>1831</b>
$\Delta_{\max}$ [%]	16.3	14.1	20.1	7.0	1.9
Software	S3PAS	TASE	SERIRES	SERIRES/TASE	ESP

As it can be observed in Table 3-5, the maximum absolute differences between ALMABuild and the reference software are obtained considering the SERIRES

and TASE software, except for the horizontal and north surfaces, for which ESP and S3PAS codes determines the higher discrepancies with ALMABuild. All these codes are no more used, except ESP for which updated version can be found.

However, considering for each orientation the mean values among the software the maximum absolute difference is less than 8%, confirming that the calculations made by means of the ALMABuild *Climatic Data* block by starting from the conventional weather data can be considered accurate as well as the calculations performed by the reference programs.

After the annual evaluation of the incident solar radiation, the corresponding hourly values obtained from ALMABuild have been compared with the data reported by ASHRAE Standard 140 for the South and West external envelope elements. In order to test the ALMABuild solar model in different sky conditions, the prediction of the hourly solar radiation was performed by considering a clear and a cloudy day, following the specific BESTEST indications on this point. In Figure 3.7, the minimum and maximum hourly incident solar radiation profile given by the ASHRAE Standard 140 and the hourly profile obtained using ALMABuild for a clear and cloudy day are shown.

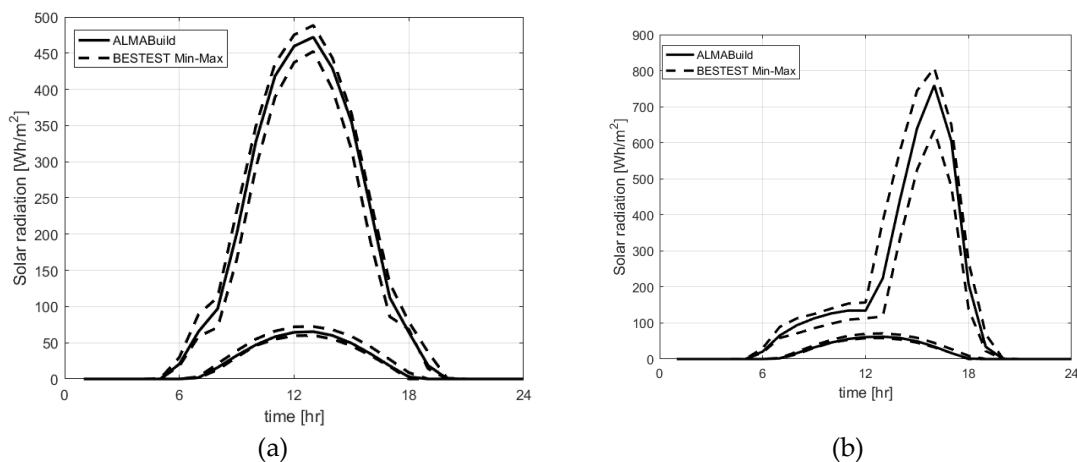


Figure 3.7. Hourly incident solar radiation during a clear (higher profile) and cloudy (lower profile) day for: South (a) and West (b) orientation.

As shown in Figure 3.7a, the ALMABuild trend of the hourly incident solar radiation on a surface with South orientation, for both clear and cloudy days, is always within the maximum and minimum BESTEST profiles, represented by the higher and lower profiles respectively. Same assessments are obtained considering the hourly incident solar radiation on a West surface, depicted in Figure 3.7b.

In conclusion, the data reported in Table 3-5 and Figure 3.7 confirm that the calculation procedure followed by the ALMABuild *Solar Radiation Calculator*



block can be considered validated as well as the solar model implemented in ALMABuild.

### 3.4.2 Validation of the optical model for clear component

The second comparative test is related to the evaluation of the solar radiation transmitted by the windows of the reference room. The global solar radiation transmitted by a window to a thermal zone depends on the optical properties of each single glass layer. As described in *Chapter 2*, the calculation of the solar transmission of a clear component is performed in ALMABuild, like almost all the main software used for building dynamic simulations, by means of a model that requires as input data the global optical properties of the window (absorbance, transmittance and reflectance), depending on the angle of incident of the solar radiation. These data can be obtained using a dedicated software (i.e. Window [95]) or found in technical glass data sheets. In the BESTEST report the optical properties of both the single glass layer and of the whole window are fully defined in order to avoid a detailed analysis of the optical behaviour of the glass layers. In this way, the comparison performed using the BESTEST method is focused on the calculation of the transmitted solar radiation across the clear building elements and its repartition within the internal surface of the walls of the room. Since in the considered cases the window is in the South wall (or in the West and East wall for Cases 620 and 920), in Table 3-6 the annual transmitted solar radiation for South and West orientation are reported, according to the BESTEST report. The results obtained with ALMABuild are compared in Table 3-6 with the results obtained with the reference software cited by BESTEST, that are the same listed in the ASHRAE Standard 140 for this comparison. It is possible to note that ALMABuild gives results in good agreement with the data obtained by the reference software with a deviation from the mean value of 5.5% and 4.8% for the South and West orientations.

Table 3-6. Annual solar radiation [kWh/(m<sup>2</sup> year)] transmitted by the reference windows, and its mean annual transmissivity coefficient.

	Annual transmitted solar radiation		Annual transmissivity coefficient	
	South	West	South	West
ESP	946	732	0.65	0.674
DOE2	1051	735	0.671	0.681
SRES/SUN	962	689	0.652	0.687
SERIRES	954	563	0.65	0.657
S3PAS	926	642	0.628	0.641
TRNSYS	984	662	0.647	0.654
TASE	914	706	0.623	0.648
ALMABuild	<b>1015</b>	<b>708</b>	<b>0.648</b>	<b>0.659</b>
$\Delta_{\max}$ [%]	10	20.5	3.9	4.2
Software	TASE	SERIRES	TASE	SRES/SUN

In addition to the annual transmitted solar radiation, in Table 3-6 the mean annual transmissivity coefficient of the window, evaluated as the ratio between the annual transmitted solar radiation over the incident solar radiation for the considered orientation, is reported for the reference software and ALMABuild. This additional comparison is necessary for the assessment of the accuracy of the calculation of the window transmissivity; in fact, the comparison of the annual transmitted solar radiation is affected by the evaluation of the incident solar radiation. From the results collected in Table 3-6, it is possible to appreciate that the evaluation of the annual transmissivity coefficient performed by ALMABuild is in very good agreement with the evaluations obtained with the reference software; the absolute deviation from the mean value is of 0.3% and 0.6% for the South and West orientations.

Anyway, from Table 3-6 it can be noted that the maximum absolute differences between ALMABuild and reference software predictions ( $\Delta_{max}$ ) are large considering the annual transmitted solar radiation, with values up to 20.5% for West orientation. It has to be noted that the maximum discrepancies are obtained again for SERIRES and TASE software, in addition to SRES/SUN for the evaluation of the annual transmissivity coefficient for West orientation.

The comparison of the annual transmitted solar radiation and of the mean annual transmissivity window coefficient shows how ALMABuild results are very close to the mean values of the references results, allowing to consider the optical model implemented in the BCC block of the ALMABuild library as validated.

### ***3.4.3 Validation of the shading model***

After the comparison of the results related to the prediction of the incident solar radiation over a surface and of the solar radiation transmitted by the window, the following step of the BESTEST comparative test consists in the validation of the shading model. This test is performed comparing the solar radiation transmitted by windows in South and West expositions, considering the overhangs represented in Figure 3.6. Again, as for the validation of the optical model for clear components, both the annual transmitted solar radiation and the mean annual shading factor evaluated by ALMABuild are compared to the predicted values obtained with the reference software listed in the BESTEST report and in the ASHRAE Standard 140. The mean annual shading factor,  $SF$ , is defined as:

$$SF = 1 - \frac{Q_{sol,sh}}{Q_{sol,unsh}} \quad (3.1)$$

where  $Q_{sol,sh}$  is the annual solar radiation transmitted by the window, considering the shadings, whilst  $Q_{sol,unsh}$  is the transmitted solar radiation for the unshaded case. Considering the results collected in Table 3-7, it is possible to note that the annual transmitted solar radiation predicted by ALMABuild is within the results obtained with the reference software for both South and West orientations, and the absolute deviation from the mean value is of 1.6% and 5.2% respectively.

Table 3-7. Annual solar radiation [kWh/(m<sup>2</sup> year)] transmitted by the reference shaded windows, and the mean annual shading factor.

	Annual transmitted solar radiation		Mean annual shading factor	
	South	West	South	West
ESP	785	599	0.17	0.182
DOE2	831	481	0.209	0.346
SRES/SUN	803	554	0.165	0.196
SERIRES	775	441	0.188	0.216
S3PAS	757	431	0.183	0.329
TRNSYS	782	438	0.205	0.339
TASE	809	469	0.115	0.336
<b>ALMABuild</b>	<b>804</b>	<b>513</b>	<b>0.208</b>	<b>0.275</b>
$\Delta_{max}$ [%]	5.8	16.8	44.7	33.8
Software	S3PAS	ESP	TASE	ESP

Analysing the predictions of the mean annual shading factor, performed by the reference software, a large spread among the results can be appreciated: the maximum absolute deviation from the mean value is 35% in both South and West orientations, revealing large discrepancies in the different shading models adopted by the reference software. However, the ALMABuild predictions are within the reference range and the absolute deviation from the mean value is 18% and 1% for South and West orientations respectively.

Even in this case, the maximum absolute difference between ALMABuild and the reference software ( $\Delta_{max}$ ) is evidenced for S3PAS and TASE, together with ESP.

From the good agreement between the results obtained comparing ALMABuild with respect to the ones obtained by the reference software, the ALMABuild shading model for both horizontal (for windows with South orientations) and vertical overhangs, and for shadings due to multiple overhangs (as in the case of window with West orientation) can be considered as validated.

#### 3.4.4 Thermal zone balance validation in free-float temperature conditions

The fourth comparative test suggested by BESTEST, concerns the prediction of the trend of internal air temperature in a room in free-floating conditions. Since this parameter is obtained as result of an energy balance among the heat fluxes

exchanged by all the elements involved in the thermal zone, the comparison of the indoor air temperature becomes a method for the verification of the correct solution of the energy balance of a thermal zone. This last step is very important for assessing the reliability of ALMABuild, because the internal air temperature is correctly evaluated only if all the heat fluxes are calculated in a proper way and if the thermal inertia of all the envelope components is adequately taken into account.

In Table 3-8 for each case analysed, the annual mean, maximum and minimum indoor air temperature values obtained by using ALMABuild (adopting the BTB block based on the *simple model*, see *Chapter 2*) are reported together with the maximum and minimum threshold values obtained for the same cases by the reference software cited by ASHRAE Standard 140 [101].

Table 3-8. Annual internal air temperature values (°C) obtained for free-float (FF) BESTEST cases compared with the minimum and maximum threshold values indicated by BESTEST.

	Case 600 FF	Case 900 FF	Case 650 FF	Case 950 FF	Case 960 Sun zone
	<b>Mean annual value</b>				
<b>Max threshold</b>	27.4	27.5	20.8	15.3	30.5
<b>Min threshold</b>	24.2	24.4	18.0	14.0	26.4
<b>Average</b>	25.3	25.5	18.9	14.5	28.2
<b>ALMABuild</b>	<b>25.6</b>	<b>25.8</b>	<b>18.7</b>	<b>14.3</b>	<b>29.3</b>
	<b>Minimum annual value</b>				
<b>Max threshold</b>	-15.6	-1.6	-21.0	-17.8	6
<b>Min threshold</b>	-18.8	-6.4	-23.0	-20.2	-2.8
<b>Average</b>	-17.6	-3.7	-22.4	-19.3	2.3
<b>ALMABuild</b>	<b>-17.7</b>	<b>-2.1</b>	<b>-22.8</b>	<b>-19.7</b>	<b>2.1</b>
	<b>Maximum annual value</b>				
<b>Max threshold</b>	75.1	46.4	73.5	38.5	55.3
<b>Min threshold</b>	64.9	41.8	63.2	35.5	48.9
<b>Average</b>	67.7	43.7	66.1	36.6	50.5
<b>ALMABuild</b>	<b>69.3</b>	<b>44.2</b>	<b>67.9</b>	<b>36.3</b>	<b>54.4</b>

As reported in Table 3-8, the results obtained with ALMABuild are in between the minimum and maximum threshold values defined by BESTEST in each case. More in detail, analysing the mean annual indoor temperature, it can be noted that ALMABuild results are very close to the average values: for Case 600FF and 900FF ALMABuild results are only 0.3 K higher than the average values, whilst for Case 650FF and 950FF the absolute deviation is even smaller, equal to 0.2 K. On the contrary, referring to the sun zone of Case 960, the discrepancy of the ALMABuild result to the average value is 1.1 K but again the ALMABuild result is contained within the BESTEST range.

Referring to the minimum annual indoor temperature, results obtained with ALMABuild for Cases 600FF and 960 are very close to the average values (-0.1 K

and  $-0.2$  K respectively), whilst the maximum absolute deviation from the average values is observed for Case 900FF, for which the ALMABuild results is  $1.6$  K higher than the mean.

Finally, considering the maximum annual indoor temperature, higher deviations from the average values can be observed: for Case 900FF and 950FF the deviation is less than  $0.5$  K, whilst for Case 600FF, 650FF and 960 the discrepancies are  $1.6$  K,  $1.8$  K and  $3.9$  K respectively. It can be noted that the higher discrepancies occur in cases in which the difference between the minimum and maximum BESTEST threshold values are around  $10$  K. These cases are characterised by the lightweight envelope composition: in fact, in light buildings, the maximum indoor temperature is deeply dependent on the incident solar radiation, whose evaluation differs from the reference BESTEST programs. Solar radiation is the main responsible of the maximum indoor temperature even for the Sun Zone of Case 960; in fact, even if this thermal zone is composed by external heavyweight walls, the room is not so big as in the other cases and the thermal capacity do not differs significantly from the lightweight cases, keeping constant the solar radiation transmitted by the windows.

In addition to evaluation of the mean, minimum and maximum annual indoor temperature, the BESTEST procedure requires also the comparison of the hourly profile of the indoor temperature for two specific days.

Figure 3.8a shows the hourly profile of the internal temperature evaluated with ALMABuild (solid line) compared with the maximum and minimum profiles (dashed lines) reported by the BESTEST report for case 600FF. In the same way, Figure 3.8b represents the hourly profile evaluated for case 900FF.

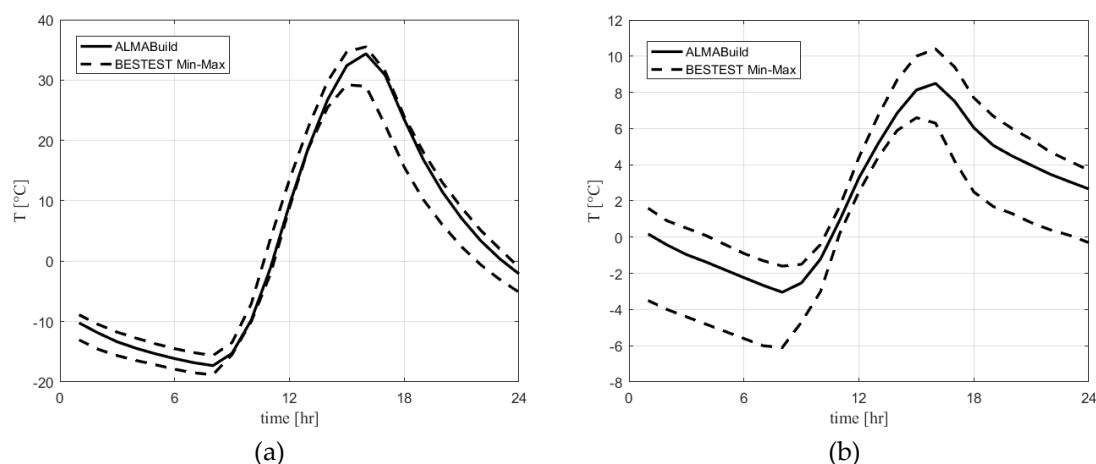


Figure 3.8. Trend of hourly free-floating internal air temperature for Case 600FF (a) and Case 900FF (b): comparison with the BESTEST limits.

Since case 600FF differs from case 900FF only for the external wall composition (see Table 3-4), comparing these two figures it is possible to appreciate the effect of the thermal inertia of the walls on the internal air temperature trend. It can be noted that the amplitude of the variation of the

internal air temperature is very high ( $\pm 25$  K) in Case 600FF (lightweight walls), whilst for the Case 900FF (heavyweight wall) this variation is limited to few kelvin ( $\pm 6$  K). Also in these cases the temperature profile obtained with ALMABuild is in good agreement with the BESTEST results; for this reason, the *thermal zone* block (based on the *simple model* BTB block) of the ALMABuild library, can be considered as validated.

Figure 3.9 shows the hourly profiles obtained for cases 650FF (a) and 950FF (b) for a clear hot day.

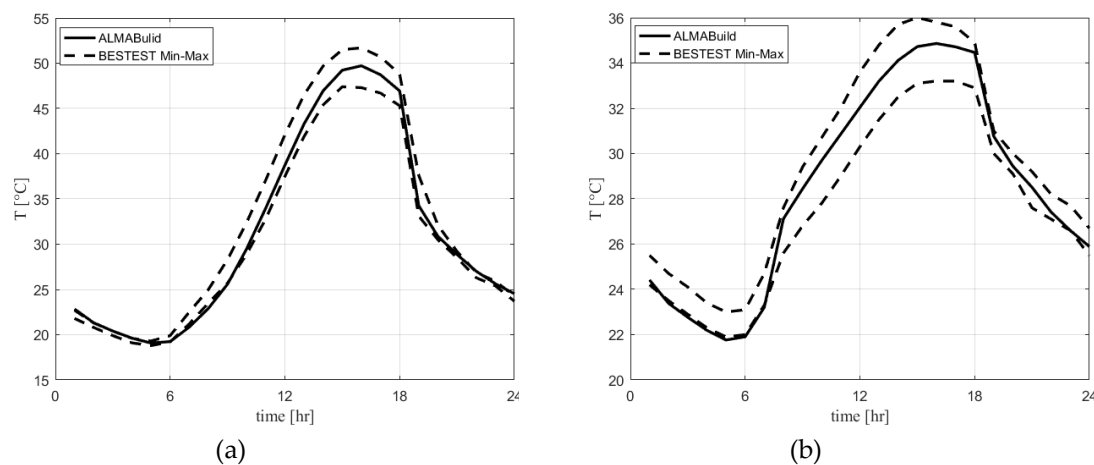


Figure 3.9 Trend of hourly free-floating internal air temperature for case 650FF (a) and case 950FF (b): comparison with the BESTEST limits.

As quoted in Table 3-4, case 650FF and 950FF have the same wall composition of case 600FF and 900FF respectively but with an extra intermittent air ventilation profile. From the results reported in Figure 3.9, it is possible to appreciate that, also for cases 650FF and 950FF, ALMABuild results are within the BESTEST limits, except from 7 to 8 for Case 650FF (see Figure 3.9a) for which ALMABuild predictions are slightly lower than the BESTEST minimum threshold (discrepancies are lower than 0.5 K), and during the first hours of the day for Case 950FF (see Figure 3.9b), for which ALMABuild predictions are lower than BESTEST minimum threshold of around 0.1 K. Therefore, even if the ALMABuild predictions not always are contained in the BESTEST range, it can be assessed that the effects due to the presence of an intermittent air ventilation profile are correctly modelled by ALMABuild.

### 3.4.5 Thermal zone balance validation in presence of an ideal HVAC system

The last comparative test is related to the evaluation of the behaviour of a room in which an ideal HVAC system for heating and cooling is working adopting different control strategies. The considered HVAC system is characterised by a unitary efficiency and by an infinite power; only sensible loads

are considered. The annual energy exchanged from HVAC system and indoor air during cooling and heating and the annual peaks of heating and cooling loads in the room are evaluated for the non-free-float cases in order to test the software capability to implement correctly different control strategies and to couple the building to the HVAC system. The comparison between the annual energy demand predicted by using ALMABuild and the minimum, maximum and average values obtained with the software referenced by ASHRAE Standard 140 for lightweight buildings is reported in Table 3-9 and in Table 3-10, for heating and cooling respectively.

Table 3-9. Annual Heating Load (MWh) obtained for non-free-float lightweight BESTEST cases compared with the minimum and maximum threshold values indicated by BESTEST.

Case	600	610	620	630	640	650
<b>BESTEST Minimum</b>	4.296	4.355	4.613	5.05	2.751	0
<b>BESTEST Maximum</b>	5.709	5.786	5.944	6.469	3.803	0
<b>BESTEST Average</b>	5.046	5.098	5.328	5.686	3.135	0
<b>ALMABuild</b>	<b>4.857</b>	<b>5.126</b>	<b>5.151</b>	<b>5.627</b>	<b>3.15</b>	<b>0</b>
<b>Difference</b>	-3.7%	0.5%	-3.3%	-1%	0.5%	0
<b>Within range</b>	Yes	Yes	Yes	Yes	Yes	Yes

Referring to Table 3-9 it can be noted that the ALMABuild results are always within the BESTEST range. More in detail, the ALMABuild predictions are very close to the average BESTEST values: the maximum absolute deviation from ALMABuild and the average BESTEST values is 3.7% (for Case 600), whilst for Case 610 and 640 the deviation is 0.5%. In Case 650 the absence of heating demand is due to the fact that, as reported in Table 3-4, in this case the HVAC system works only on cooling mode.

Table 3-10. Annual Cooling Load (MWh) obtained for non-free-float lightweight BESTEST cases compared with the minimum and maximum threshold values indicated by BESTEST.

Case	600	610	620	630	640	650
<b>BESTEST Minimum</b>	6.137	3.915	3.417	2.129	5.952	4.816
<b>BESTEST Maximum</b>	8.448	6.139	5.482	3.701	8.097	7.064
<b>BESTEST Average</b>	7.053	5.144	4.416	2.951	6.79	5.708
<b>ALMABuild</b>	<b>6.958</b>	<b>4.919</b>	<b>4.156</b>	<b>2.629</b>	<b>6.758</b>	<b>5.723</b>
<b>Difference</b>	-1.3%	-4.4%	-5.9%	-11%	-0.5%	0.3%
<b>Within range</b>	Yes	Yes	Yes	Yes	Yes	Yes

Considering the predictions of the annual cooling demand, reported in Table 3-10, higher deviation of the ALMABuild results from the average BESTEST

values are observed, even if in all the cases ALMABuild predictions are within the BESTEST range. However, except for Case 620 and 630, the absolute deviation is lower than 5%.

The same comparisons performed for the lightweight buildings are repeated also for buildings with heavyweight envelope elements. In Table 3-11 the predictions of the annual heating demand obtained by using ALMABuild, together with the BESTEST minimum, maximum and average results are reported. From the data collected in this Table, it can be noted that the ALMABuild results are always within the BESTEST range. In particular, absolute deviations from the average BESTEST values less than 5% are observed for Case 910, 920 and 930, whilst for Case 900 and 940 higher deviation are remarked. Nevertheless, the higher deviation for these two cases are mainly due to the low absolute value of the average value. In Case 950 there is no heating demand since, as reported in Table 3-4, the HVAC system works only on cooling mode.

Table 3-11. Annual Heating Load (MWh) obtained for non-free-float heavyweight BESTEST cases compared with the minimum and maximum threshold values indicated by BESTEST.

Case	900	910	920	930	940	950
<b>BESTEST Minimum</b>	1.17	1.512	3.261	4.143	0.79	0
<b>BESTEST Maximum</b>	2.041	2.282	4.3	5.335	1.411	0
<b>BESTEST Average</b>	1.649	1.951	3.828	4.603	1.086	0
<b>ALMABuild</b>	<b>1.456</b>	<b>1.886</b>	<b>3.674</b>	<b>4.570</b>	<b>0.997</b>	<b>0</b>
<b>Difference</b>	-12%	-3.4%	-4%	-0.7%	-8%	0
<b>Within range</b>	Yes	Yes	Yes	Yes	Yes	Yes

Analysing the prediction of the annual cooling demand, reported in Table 3-12, much higher deviations of the ALMABuild results to the average BESTEST values are observed; however, ALMABuild predictions are always within the BESTEST range.

Table 3-12. Annual Cooling Load (MWh) obtained for non-free-float heavyweight BESTEST cases compared with the minimum and maximum threshold values indicated by BESTEST.

Case	900	910	920	930	940	950
<b>BESTEST Minimum</b>	2.132	0.821	1.84	1.03	2.079	0.387
<b>BESTEST Maximum</b>	3.669	1.883	3.313	2.238	3.546	0.921
<b>BESTEST Average</b>	2.826	1.521	2.684	1.15	2.725	0.635
<b>ALMABuild</b>	<b>2.714</b>	<b>1.262</b>	<b>2.453</b>	<b>1.424</b>	<b>2.561</b>	<b>0.537</b>
<b>Difference</b>	-3.9%	-17%	-8.6%	-24%	-6%	-15%
<b>Within range</b>	Yes	Yes	Yes	Yes	Yes	Yes



The greatest deviations from the BESTEST average values are referred to Case 910 (-17%) and 930 (-24%), which are characterised by the adoption of shading devices. The predictions of the annual cooling demand for Case 900, 920 and 940 are the closest to the average BESTEST values; their absolute deviations are less than 10%. Finally, for Case 950 a deviation of 15% is observed, but it is mainly due to the very low absolute value of the cooling demand, in fact the absolute difference between ALMABuild and the BESTEST average is around 0.1 MWh.

After the comparison of the annual heating and cooling loads, the BESTEST procedure requires the evaluation of the annual heating and cooling power peaks, with the aim to compare the dynamic behaviour of the building with different boundary conditions and adopting different control strategies. In Table 3-13, the predicted annual heating peak for lightweight buildings obtained using ALMABuild are compared to the results of the BESTEST reference software. From Table 3-13, it can be noted that the ALMABuild results are always within the BESTEST range; moreover, ALMABuild results are very close to the average BESTEST values: the absolute deviations are less than 6.5%.

Table 3-13. Annual Heating Peak (kW) obtained for non-free-float lightweight BESTEST cases compared with the minimum and maximum threshold values indicated by BESTEST.

Case	600	610	620	630	640	650
<b>BESTEST Minimum</b>	3.437	3.437	3.591	3.592	5.232	0
<b>BESTEST Maximum</b>	4.354	4.354	4.379	4.28	6.954	0
<b>BESTEST Average</b>	3.952	3.947	3.998	3.949	5.903	0
<b>ALMABuild</b>	<b>3.735</b>	<b>3.723</b>	<b>3.744</b>	<b>3.739</b>	<b>5.524</b>	<b>0</b>
<b>Difference</b>	-5.5%	-5.5%	-6.4%	-5.3%	-6.4%	0
<b>Within range</b>	Yes	Yes	Yes	Yes	Yes	Yes

Table 3-14. Annual Cooling Peak (kW) obtained for non-free-float lightweight BESTEST cases compared with the minimum and maximum threshold values indicated by BESTEST.

Case	600	610	620	630	640	650
<b>BESTEST Minimum</b>	5.965	5.669	3.63	3.072	5.884	5.831
<b>BESTEST Maximum</b>	7.188	6.673	5.096	4.116	7.126	7.068
<b>BESTEST Average</b>	6.535	6.090	4.393	3.688	6.478	6.404
<b>ALMABuild</b>	<b>6.743</b>	<b>6.115</b>	<b>4.166</b>	<b>3.571</b>	<b>6.697</b>	<b>6.323</b>
<b>Difference</b>	3.2%	0.4%	-5.2%	-3.2%	3.4%	-1.2%
<b>Within range</b>	Yes	Yes	Yes	Yes	Yes	Yes

Similar conclusions can be assessed considering the predictions of the annual cooling peak. As reported in Table 3-14, the ALMABuild results are within the

BESTEST range, and the absolute deviation from the average BESTEST values is even smaller than for the evaluation of the heating peaks. In fact, expect for Case 620, in which a deviation of 5.2% is observed, for the remaining cases the deviation is around 3% (Case 600, 630 and 640) or 1% (Case 610 and 650).

As done for cases with lightweight buildings, comparison of the heating and cooling peak loads is performed also for heavyweight buildings. In Table 3-15, ALMABuild predictions of the annual heating peak are compared to the BESTEST values. Again, ALMABuild results are within the BESTEST range. Moreover, the absolute deviations from the average BESTEST values are slightly higher than the cases with lightweight buildings. In fact, in the lightweight cases the absolute deviations are around 6%, whilst for the heavyweight buildings are around 7%.

Table 3-15. Annual Heating Peak (kW) obtained for non-free-float heavyweight BESTEST cases compared with the minimum and maximum threshold values indicated by BESTEST.

Case	900	910	920	930	940	950
<b>BESTEST Minimum</b>	2.85	2.858	3.308	3.355	3.98	0
<b>BESTEST Maximum</b>	3.797	3.801	4.061	4.046	6.428	0
<b>BESTEST Average</b>	3.452	3.459	3.738	3.733	5.414	0
<b>ALMABuild</b>	<b>3.203</b>	<b>3.208</b>	<b>3.456</b>	<b>3.498</b>	<b>4.97</b>	<b>0</b>
<b>Difference</b>	-7.2%	-7.3%	-7.6%	-6.3%	-8.2%	0
<b>Within range</b>	Yes	Yes	Yes	Yes	Yes	Yes

Considering the evaluation of the cooling peak, similar conclusions can be assessed. From the results collected in Table 3-16, it can be appreciated that the maximum deviation of the ALMABuild results from the BESTEST average values, observed for Case 910, is around 12%. However, ALMABuild results are always contained in the BESTEST range.

Table 3-16. Annual Cooling Peak (kW) obtained for non-free-float heavyweight BESTEST cases compared with the minimum and maximum threshold values indicated by BESTEST.

Case	900	910	920	930	940	950
<b>BESTEST Minimum</b>	2.888	1.896	2.385	1.873	2.888	2.033
<b>BESTEST Maximum</b>	3.932	3.277	3.505	3.08	3.932	3.17
<b>BESTEST Average</b>	3.46	2.676	3.123	2.526	3.46	2.724
<b>ALMABuild</b>	<b>3.655</b>	<b>3.0</b>	<b>2.862</b>	<b>2.405</b>	<b>3.631</b>	<b>2.532</b>
<b>Difference</b>	5.6%	12%	-8.4%	-4.8%	4.9%	-7.6%
<b>Within range</b>	Yes	Yes	Yes	Yes	Yes	Yes

The results collected from Table 3-9 to Table 3-16 show that the ALMABuild predictions of annual heating and cooling energy demand and thermal power peaks for both light and heavyweight buildings are always contained within the BESTEST range reported in ASHRAE 140 [101]. Therefore, it is possible to assess that the validity of the algorithms implemented in ALMABuild for the energy balance of a thermal zone and the ability of the program to model different control strategies and boundary conditions is confirmed by these comparative tests.

Finally, in Table 3-17 is reported the comparison between ALMABuild and the BESTEST reference software for the evaluation of the annual heating and cooling energy demand and power peak for Case 960. As described in Table 3-4, in this case the building is composed by two zones: the Back Zone is equipped with a HVAC system, whilst the Sun Zone is in free-float conditions. Analysing the results collected in Table 3-17, it can be noted that even in this case ALMABuild predictions are within the BESTEST range; however, a great deviation from the average BESTEST values is observed for the evaluation of the cooling energy demand (-37%) and power peak (-21%). In fact, these two predictions are slightly above the minimum BESTEST threshold. Nevertheless, these results allow to consider the ALMABuild algorithms for the evaluation of multi-zone buildings as validated.

Table 3-17. Annual heating and cooling load [MWh] and peak [kW] for back zone of Case 960, compared with the minimum and maximum threshold values indicated by BESTEST.

Case	Heating load	Cooling load	Heating peak	Cooling peak
<b>BESTEST Minimum</b>	2.144	0.4113	2.41	0.953
<b>BESTEST Maximum</b>	3.373	0.895	2.863	1.422
<b>BESTEST Average</b>	2.709	0.669	2.686	1.210
<b>ALMABuild</b>	<b>2.788</b>	<b>0.416</b>	<b>2.605</b>	<b>0.955</b>
<b>Difference</b>	2.9%	-37%	-3.0%	-21%
<b>Within range</b>	Yes	Yes	Yes	Yes

### 3.5 Comparison with other references

Analysing the maximum and minimum BESTEST threshold values collected from Table 3-9 to Table 3-17, a great discrepancy can be observed. More in detail, as reported in Table 3-18, discrepancies between maximum and minimum threshold values, for each qualification case, go from the 16% to more than 100%: the highest differences concern the annual cooling energy for the heavyweight buildings, whilst the lowest discrepancies are related to the heating power peak for lightweight buildings.

Table 3-18. Discrepancy [%] between the maximum and minimum BESTEST threshold values for all the qualification tests. Highest and lowest discrepancies are evidenced in bold.

Case	600	610	620	630	640	650	900	910	920	930	940	950	960
Heating load	28	28	25	25	34	-	53	39	27	26	57	-	46
Cooling load	33	43	47	53	32	39	54	70	55	<b>105</b>	54	84	72
Heating peak	23	23	20	17	29	-	27	27	20	19	45	-	17
Cooling peak	19	<b>16</b>	33	28	19	19	30	52	36	48	30	42	39

Therefore, for some cases, due to the great spread between the reference results, the BESTEST procedure is not really strict. This is due to the fact that BESTEST and ASHRAE 140 reference software lists contain outdated codes, like SERIRES, S3PAS and TASE, that are no more used. It has to be underlined how the highest discrepancies between ALMABuild and BESTEST results have been observed just referring to these software and the outdated version of ESP-r. In fact, in both the BESTEST and ASHRAE 140 reference software lists the updated version of reference software are omitted as well as recent software for the dynamic building energy simulation, like EnergyPlus. Therefore, in order to obtain a stricter verification, with converging reference threshold values, the reference software list should be periodically updated, eliminating codes based on outdated models and introducing new software recognized as reliable and well diffused.

For these reasons, with the aim to have an additional benchmark of the ALMABuild library, a comparison with other references is performed. In particular, the ALMABuild predictions are compared to the results obtained with EnergyPlus and the hourly method proposed by the recent European Standard EN ISO 52016 [62]. The BESTEST qualification cases are considered for this comparison. Predictions of the annual heating and cooling energy demand and power peak obtained with EnergyPlus are available for the version 8.3.0 [105], whilst in EN 52016 are collected the results obtained with the hourly method proposed only for Cases 600, 640, 900 and 940.

In Figure 3.10, the annual energy demand for heating (positive values) and cooling (negative values) predicted by EnergyPlus, EN 52016 and ALMABuild for the lightweight cases are represented, together with the minimum and maximum BESTEST threshold values (dashed lines).

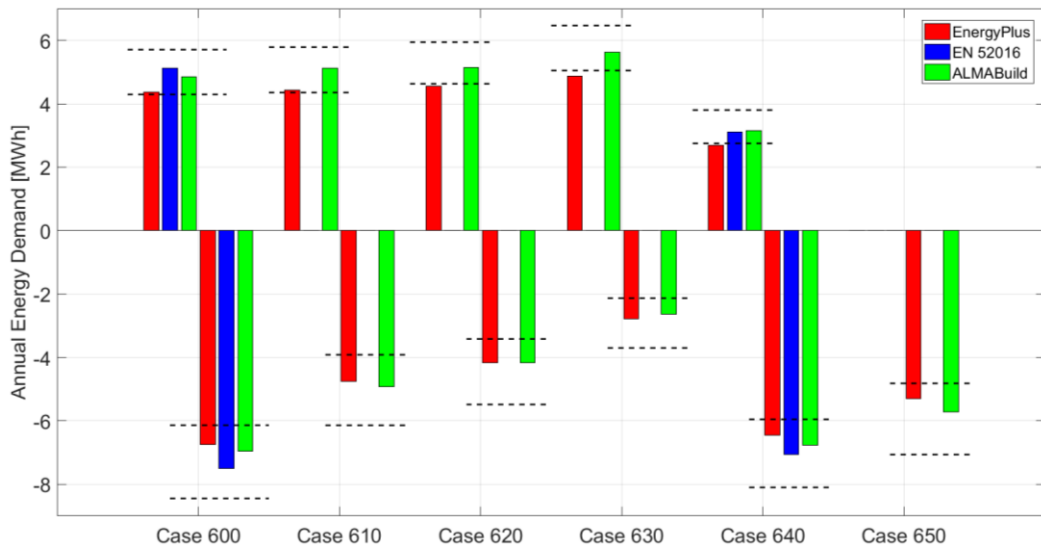


Figure 3.10. Comparison of the annual energy demand [MWh] predicted by EnergyPlus, the Standard EN 52016 and ALMABuild for lightweight BESTEST buildings.

In this figure it is possible to appreciate that the results obtained with the new hourly method described by EN ISO 52016 (for the cases for which results are available), like the ALMABuild results, are within the BESTEST range, whilst EnergyPlus do not. More in detail, EnergyPlus slightly underestimates the annual heating load for Cases 620, 630 and 640; on the contrary the predicted annual cooling load is always within the BESTEST range. Discrepancies between ALMABuild and EnergyPlus go from the 10% (Case 600) to 15% (Case 640) for the heating loads, whilst for the cooling energy demand deviations are less than 5%, except for Case 630, for which the difference between ALMABuild and EnergyPlus is 6%. Also the results obtained with the new European Standard are close to the ALMABuild predictions: the maximum deviation, equal to 8%, is observed for the evaluation of the cooling load in Case 600.

Predictions of the annual energy demand for the BESTEST heavyweight buildings and the multizone case, obtained with ALMABuild and the additional references are reported in Figure 3.11

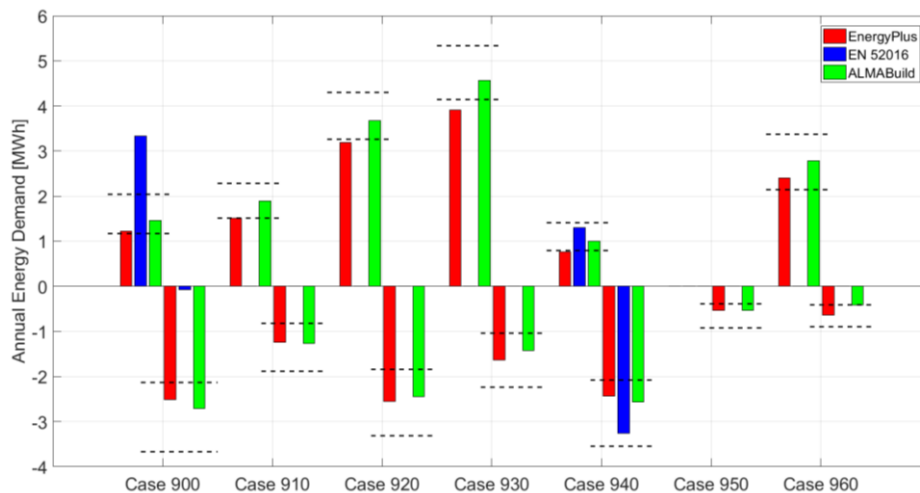


Figure 3.11. Comparison of the annual energy demand [MWh] predicted by EnergyPlus, the Standard EN 52016 and ALMABuild for heavyweight BESTEST buildings.

In this figure it can be noted that, as previously demonstrated, the ALMABuild results are within the BESTEST range, whilst EnergyPlus and EN 52016 do not. Again, as for lightweight buildings, the EnergyPlus annual heating loads are always around the minimum BESTEST threshold values, and from Case 910 to Case 940 the EnergyPlus predictions are lower the BESTEST range. On the contrary, the evaluation of the cooling energy demand by means of EnergyPlus is always within the BESTEST range. Comparing EnergyPlus and ALMABuild heating demand predictions, the minimum deviation is observed for Case 920 (+13%), whilst the maximum occurs for Case 940 (+23%). On the contrary, regarding the annual cooling loads, discrepancies are around 5%, except in Case 930 (-15%) and Case 960 (-54%).

Considering the EN 52016 results, it can be noted that, for Case 940 predictions are within the BESTEST range, even if a large discrepancy with ALMABuild, around 30% for both the cooling and heating demand there exists. However, in Case 900, EN 52016 predictions are very far from the BESTEST range: the heating demand is too high (+129% with respect to ALMABuild) and the cooling load is too lower (-97%).

The predictions of the heating and cooling power peak delivered by the ideal HVAC system for lightweight buildings, reported in Figure 3.12, show a good agreement among the different numerical method considered. In fact, for ALMABuild, EnergyPlus and EN 52016 the results are always contained within the BESTEST range. Moreover, the discrepancies between ALMABuild and EnergyPlus are around 0.5% for the heating power peak and around 5% for the cooling one, except the heating power peak evaluation in Case 640, for which a deviation of 14% is observed. Comparing the EN 52016 predictions to the ALMABuild ones, deviations are around 20% for the heating power peak and around 6% for the cooling.

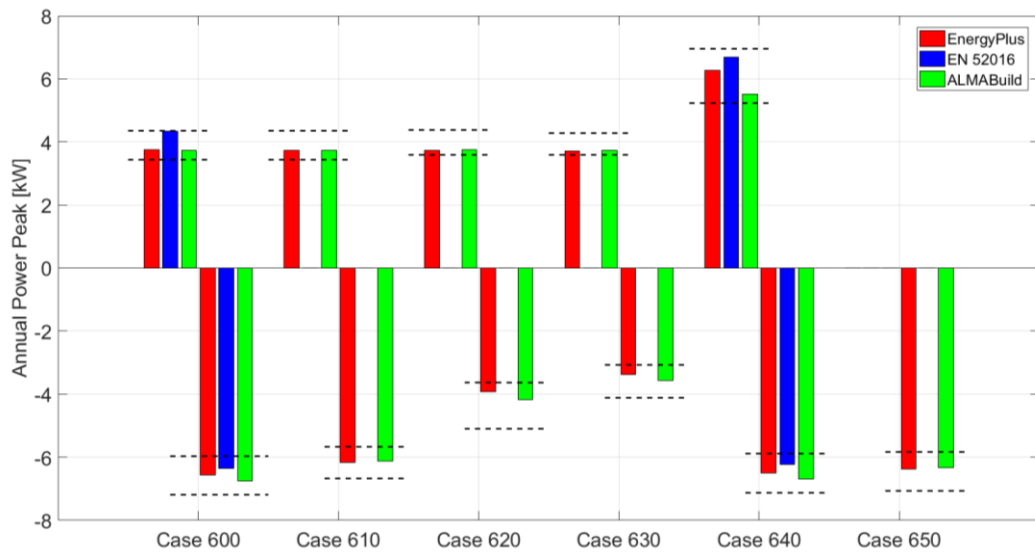


Figure 3.12. Comparison of the annual power peak [kW] predicted by EnergyPlus, the Standard EN 52016 and ALMABuild for lightweight BESTEST buildings.

Finally, in Figure 3.13 are shown the heating and cooling power peaks predicted for the BESTEST heavyweight cases. In this figure it can be appreciated that ALMABuild and EnergyPlus results are always within the BESTEST range, whilst EN 52016 predictions are always higher than the BESTEST range. In particular, for Case 940 the difference between ALMABuild and EN 52016 heating peak prediction is very high (+97%), whilst in the other case the deviation is around 20%; on the contrary deviations for the cooling power peak for both Case 900 and 940 are around 11%. On the other hand, the discrepancies between ALMABuild and EnergyPlus for the heating peak evaluation are very low: the maximum absolute deviation is 3%. Larger deviations are observed for the cooling peak estimations: the difference between ALMABuild and EnergyPlus are less than 10%, except for Case 910 (+14%) and Case 960 (-20%).

From the results reported from Figure 3.10 to Figure 3.13, some general conclusions can be assessed. First of all, it can be noted that the predictions obtained with a wide diffuse software for the building energy simulation like EnergyPlus not always are contained within the BESTEST range. This fact underlines that the BESTEST procedure should be updated taking into account the most recent programs for building energy simulations. However, the comparison between ALMABuild, whose results are always contained in the BESTEST range, and EnergyPlus shows a good agreement among these programs, with discrepancies generally lower than 10%, confirming the validity of the numerical models implemented in ALMABuild. The maximum differences between these two software are observed in Case 960, in which a multizone building is considered.

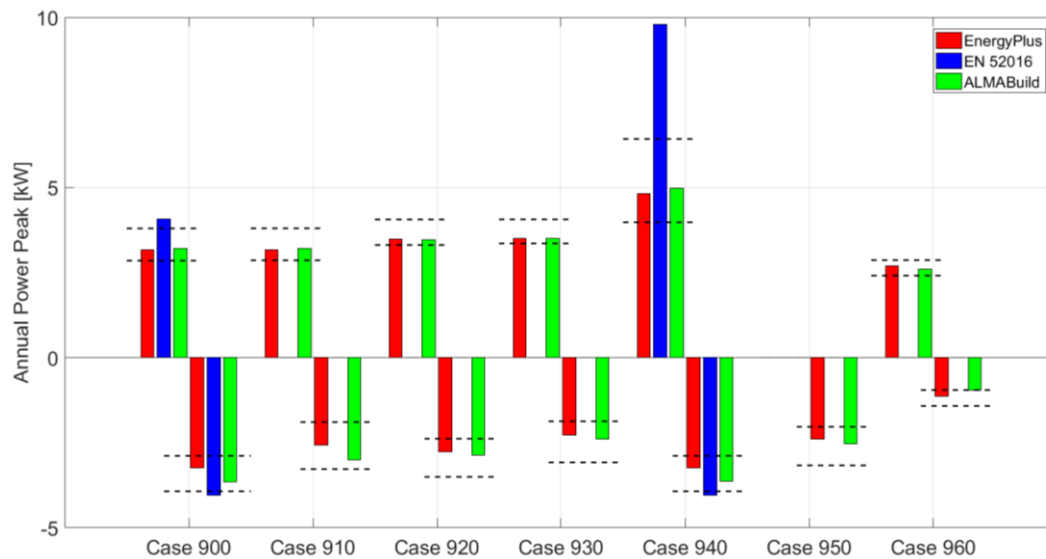


Figure 3.13. Comparison of the annual power peak [kW] predicted by EnergyPlus, the Standard EN 52016 and ALMABuild for heavyweight BESTEST buildings.

On the contrary, the comparison between ALMABuild and the new hourly model proposed by EN 52016, is less significative. This is due not only to the few Cases for which results obtained with the new hourly model are available, but also because, as it has been demonstrated, predictions obtained following the EN 50126 for heavyweight buildings are significantly out from the BESTEST range, revealing some problems to model correctly the thermal inertia of buildings. In fact, even if the rationale of this Standard is the same followed in ALMABuild (the building is divided in thermal zones, each building element of a zone is studied by using a RC model and the heat fluxes across these elements are combined to obtain the energy loads and the internal air temperature of the thermal zone), there are important differences between the 3R4C model adopted in ALMABuild (described in *Chapter 2*) and the RC model proposed in the Standard.

The main differences between the ALMABuild RC network adopted in the BME blocks and the 4R5C network proposed by the EN 52016 for the wall modelling concern the evaluation of the total capacity of the wall and its distribution to each node. In EN 52016, the value of the total capacity of the envelope element is obtained by classifying each element by means of definitions reported in Table 3-19. From Table 3-19, it can be remarked that, contrary to the procedure followed in ALMABuild, adopting the method proposed by EN 52016, the total capacity of massive envelope elements is not equal to the actual capacity of the element, but it is set to a specific constant value.



Table 3-19. Specific heat capacity of massive envelope elements, according to EN 52016 [62].

Class	Description	C [kJ/(m <sup>2</sup> K)]
Very light	Element containing no mass layers, other than e.g. plastic board	50
Light	Element containing no mass components other than 5 to 10 cm lightweight brick or concrete, or equivalent	75
Medium	Element containing no mass components other than 10 to 20 cm lightweight brick or concrete, or less than 7 cm solid brick or heavyweight concrete, or equivalent	110
Heavy	Element containing 7 to 12 cm solid brick or heavyweight concrete, or equivalent	175
Very heavy	Element containing more than 12 cm solid brick or heavyweight concrete, or equivalent	250

In addition, the distribution of the specific capacity of the envelope element to the RC nodes, is achieved by another classification of the element, according to the specifications reported in Table 3-20.

Table 3-20. Classification of elements by mass distribution, according to EN 52016 [62].

Class	Specification
I	Element with external thermal insulation, characterised by mass concentrated in internal side
E	Element with internal thermal insulation, characterised by mass concentrated in external side
IE	Element with thermal insulation between two massive layers, characterised by mass divided over internal and external side
D	Uninsulated element characterised by mass equally distribute

As highlighted by Table 3-21, the capacities of each node of the RC model are set depending on the classification of the element. As reported in Table 3-21, the proposed RC network is composed by only one capacitive node, except for elements labelled IE and D, i.e. for elements characterised by insulation layer between two massive layers or uninsulated elements, respectively.

Table 3-21. Distribution of the element capacity to the RC network node, according to EN 52016.

Class	N <sub>1</sub>	N <sub>2</sub>	N <sub>3</sub>	N <sub>4</sub>	N <sub>5</sub>
I	0	0	0	0	C
E	C	0	0	0	0
IE	C/2	0	0	0	C/2
D	C/8	C/4	C/4	C/4	C/8

All these significant simplifications lead to a misleading evaluation of the dynamic response of the wall, and consequently of the energy loads required by a building, especially in heavyweight cases.

### 3.6 Conclusions

In this *Chapter*, the benchmark of ALMABuild has been performed following the BESTEST procedure, adopted for the validation of the main *Whole Building Software*. Following this procedure, analytical, empirical and comparative tests have been carried out, validating single elementary blocks of the ALMABuild library or globally the thermal zone sub-system.

Both the analytical validation, that consists in the comparison of the analytical solution of unsteady heat conduction through a multi-layered wall with numerical results, and the empirical test, conducted contrasting the measured indoor surface temperature of an external wall to the ALMABuild predictions, confirm the validity of the numerical procedure implemented in the ALMABuild *Building Massive Elements* block, as reported in Table 3-22.

Table 3-22. List of validation tests performed and ALMABuild blocks (recalling the section in which are described) involved for each test.

Validation	Considered block	Description link
<b>Analytical</b>	BME	2.6.2
<b>Empirical</b>	BME	2.6.2
<b>Comparative: solar contributions</b>	Solar Data and Solar Radiation Calculator	2.5.2 2.5.3
<b>Comparative: solar transmissions</b>	BCC	2.7.1
<b>Comparative: shading factors</b>	Shading model	2.8.1
<b>Comparative: energy need and power peaks</b>	Thermal zone subsystem; <i>simple model</i> BTB	2.4 2.9.2

Comparative tests, that represent the core of the BESTEST procedure, consist in the comparison of predictions obtained with the testing software with results achieved by a set of reference software, for a series of univocally defined cases. By means of comparative tests, the benchmark of the main ALMABuild blocks has been carried out using the list of reference software indicated by both the original BESTEST report and ASHRAE Standard 140. Since for all the cases analysed ALMABuild predictions are always within the maximum and minimum threshold values indicated by the BESTEST report or the ASHRAE Standard 140, it is possible to assess that the ALMABuild codes are validated.

Anyway, it should be remarked that, considering the ASHRAE Standard 140, for each test case, the discrepancy between the results obtained with the reference software is very large, going from 16% to 105%, with a mean value of 46%. This large interval is caused by the fact that the list of reference software contains obsolete codes (like SERIRES or S3PAS) and outdated version of still used tools, like ESP-r and TRNSYS. Proposing to periodically update the reference software list eliminating codes which use outdated models and by introducing new

software recognized as reliable and well diffused, ALMABuild has been compared to EnergyPlus and the new EN ISO 52016. The comparison with EnergyPlus showed a good agreement between the two software; in fact, a mean absolute discrepancy of the 15% and 10% is remarked for the annual heating and cooling load respectively, whilst referring to the power peaks, mean discrepancies of 2% and 7% are observed.

On the contrary, the comparison of ALMABuild predictions to those obtained with the new hourly method proposed by EN ISO 52016 evidenced very different results for heavyweight cases (with differences higher than 90%), due to the simplified way in which the thermal inertia of a thermal zone is computed by EN 52016



# Evaluation of the 3D temperature field of a zone

---

## Abstract

In this *Chapter* additional models for the description of the thermal balance of a zone in ALMABuild are described. In particular, starting from the GUIs developed for the implementation of these models in the Simulink desktop, the *radiative*, *convective* and *fully detailed* models are presented. The main features of the *radiative* and of the *convective models* is the possibility to evaluate the 3D spatial distribution in a room of the radiative and air temperature, respectively, based on a spatial discretization set by the user. In addition, the *fully detailed model* enables the calculation of the spatial distribution of the operative temperature, by coupling *radiative* and *convective* models.

Two case studies are explored with the aim to evidence the capabilities of these models. In the first case study, the *radiative model* is adopted for the evaluation of the effect of six different emitters (i.e. in-slab radiant floor, in-slab radiant ceiling, radiant suspended ceiling, hot water radiator, radiant wall and all-air system) and of two building thermal insulation levels on indoor local comfort conditions. This study is carried out performing annual dynamic simulations, evaluating the different transient behaviour of the emitters for different values of the thermal inertia of the system.

In the second case study, the *fully detailed model* is employed in order to analyse the impact of the position of the temperature sensor in a room on both local comfort conditions and dynamic response of the emitter. Three different positions of the indoor temperature sensor are considered: close to the corner opposite to the emitter, in the middle of the room and close to the emitter. Two radiators are taken into account: a small radiator, fed with hot water (80 °C), and an extended one, fed with water at a lower temperature (60 °C). Three control strategies are evaluated: constant inlet water temperature, weather compensation and fast restart control. Even in this case, several annual numerical simulations are carried out.

---

## 4.1 GUIs for detailed thermal zone models

In *Chapter 2*, analysing the main features of ALMABuild, the procedure for the implementation of the building model in the Simulink desktop has been described. More precisely, referring to the selection of the model by means of which simulating a thermal zone, only the GUI related to the data insertion for the *simple model* has been illustrated and only the associated *Building Thermal Balance* blocks have been examined. Anyway, three additional models for the description of the thermal zone are available in ALMABuild: the *radiative model*, the *convective model* and the *fully detailed model*.

Starting from the *Thermal zone* GUI represented in Figure 2.25, selecting one of the additional models, a GUI like the one represented in Figure 4.1a (which is related to the radiative model, but has the same structure of GUIs adopted for the other detailed models) will be used for the insertion of the geometry data of the room under analysis.

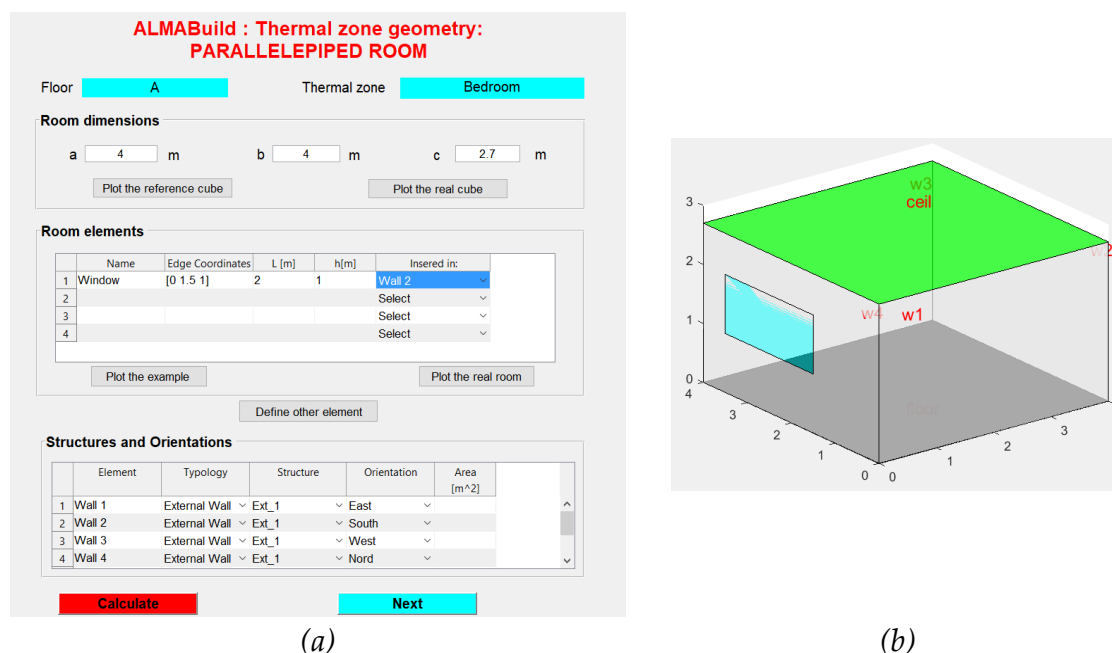


Figure 4.1. *Thermal zone properties* GUI for the data insertion for the BTB block *radiative model*.

As it can be seen in Figure 4.1a, the spatial coordinates of the four walls, the roof and the floor are evaluated only by defining width, depth and height of the thermal zone. Additional elements like windows, radiators, furniture or envelope elements characterised by different boundary conditions or thermal properties, can be introduced by defining the coordinates of the starting edge, their length and height and the surface in which they are inserted, since no element within the thermal zone are admitted. For helping the user in the definition of the thermal zone geometry, a graphical representation of the thermal zone, based on the data inserted by the user, is provided, as represented in Figure 4.1b.

Moreover, additional GUIs that help the user in the data insertion by means of examples are provided.

Then, the user has to associate to each element that composes the thermal zone the related label and its exposition. Finally, the area of each element is automatically evaluated as well as the view factors among the surfaces (i.e. in the case of the use of *radiative* or *fully detailed model*).

Since these detailed thermal zone models enable the evaluation of the spatial distribution of the radiative and/or air temperature, GUIs for the definition of the temperature sensor position and of the spatial discretization are provided (see Figure 4.2).

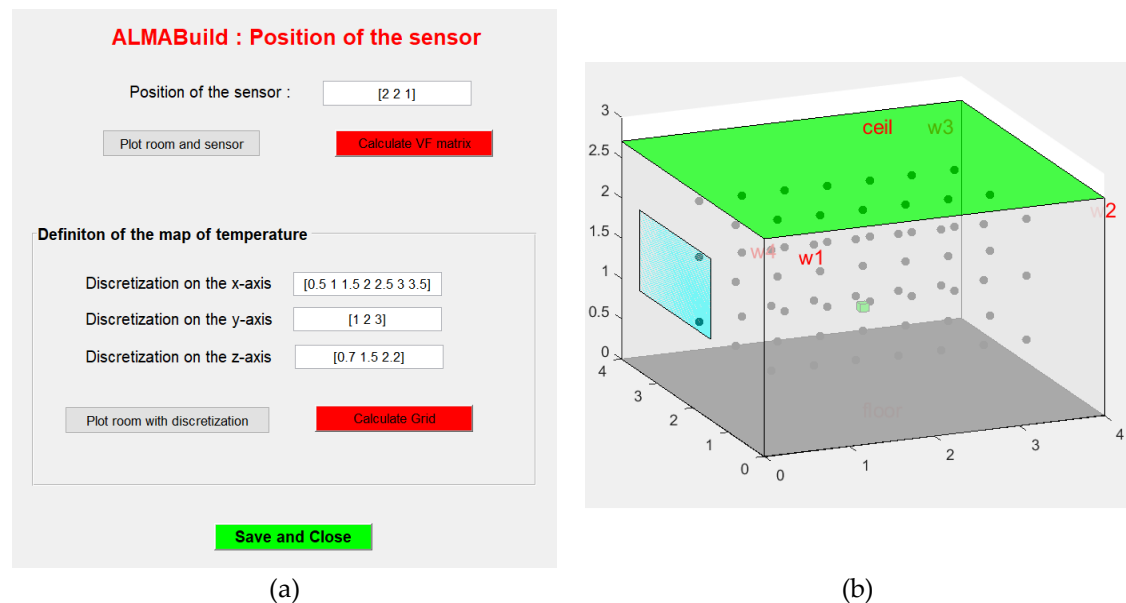


Figure 4.2. GUI for the definition of the temperature sensor position and of the spatial discretization, for the radiative model (a) and graphical representation of the inserted data (b). The sensor is represented as the green cube in (b), whilst the grid points are in grey.

## 4.2 Detailed BTB blocks

Contrary to the *simple model* (see Section 2.9.2), in which a single BTB block is used for solving the thermal balance of a zone, the *radiative*, the *convective* and the *fully detailed models* require customized blocks, that operate together with a BTB block, for a complete thermal balance of the zone. These additional customized blocks are based on the geometry of the zone and on the discretization mesh defined by the user. In this section, both the BTB blocks and these additional blocks used for solving the thermal balance of a zone by means of the *radiative*, the *convective* and the *fully detailed models* are described.

### 4.2.1 Radiative model

If the thermal zone is composed by active elements, like radiant floors or ceilings, the evaluation of the radiative heat transfer by means of the radiative star network is not adequate. In this case and in any case in which the exact calculation of the radiative heat transfer or the spatial distribution of the radiative temperature within the zone is required, the *radiative model* must be adopted for solving the thermal balance of the zone.

The evaluation of the radiative heat transfer between the internal surface of the envelope elements of the thermal zone is based on the net-radiation approach [106]. Three are the main hypothesis of this model: (i) each internal surface is isothermal; (ii) each surface behaves like a grey Lambert radiator with a uniform value of emissivity; (iii) reflected radiation is assumed to be purely diffuse.

Under these hypotheses, the radiosity ( $D_i$ ) of the  $i$ -th surface is defined as the total flux emitted by the surface:

$$D_i = \varepsilon_i \sigma_0 (T_{si,i} + 273)^4 + (1 - \varepsilon_i) \sum_j F_{ij} D_j \quad (4.1)$$

where  $\varepsilon_i$  and  $T_{si,i}$  are the infrared emissivity and the internal temperature of the  $i$ -th surface respectively,  $\sigma_0$  is the Stephan-Boltzmann constant and  $F_{ij}$  is the view factor between the  $i$ -th and the  $j$ -th surfaces.

From equation (4.1) it can be noted that the radiosity of a surface is given by the sum of the emissive power (i.e. first term of the equation) and of the reflected fraction of the radiation coming from all the other surfaces of the zone (i.e. the second term). The net radiative thermal flux of the  $i$ -th surface is given by the following balance equation:

$$Q_{ri} = A_i (D_i - \sum_j F_{ij} D_j) \quad (4.2)$$

where  $A_i$  is the area of the  $i$ -th surface. By combining (4.1) with (4.2), the radiative heat flux of the  $i$ -th surface can be written as follows:

$$Q_{ri} = \frac{A_i \varepsilon_i}{1 - \varepsilon_i} \left[ \sigma_0 (T_{si,i} + 273)^4 - D_i \right] \quad (4.3)$$

For each isothermal surface of the zone both (4.1) and (4.3) apply, meaning that  $2N$  equations, where  $N$  is the number of surfaces, can be written for the evaluation of the heat transfer between the internal surfaces of the zone. Since the number of equations depends on the number of surfaces, the internal radiative heat transfer is calculated within a customized Simulink sub-system. This sub-system, that is coupled to each indoor surface of the thermal zone, is composed by a *Radiosity calculation* block (in which equation (4.1) is implemented) and a



*Radiative calculation* block (which implements equation (4.3)). These customized blocks are automatically created if the building model is generated by means of the ALMABuild GUIs.

However, it has to be remarked that the evaluation of the radiative heat transfer among the internal surfaces of the zone by means of (4.1) and (4.3) requires as input data both the internal superficial temperature and the view factors ( $F_{ij}$ ). Moreover, view factors are required also for the evaluation of the radiative temperature in a given position within the room (grid point or sensor) which is calculated by means of the following relationship:

$$T_{rad} = \sqrt[4]{F_{ij} (T_{si,i} + 273)^4} - 273 \quad (4.4)$$

In ALMABuild, view factors among planar surfaces having any shape and orientation are automatically calculated during the insertion data procedure driven by GUI; for this purpose a Matlab script, based on the MATLAB Contour Double Integral Formula (CDIF) routine, following the procedure suggested by Lauzier and Rouse [107], has been developed. This approach is very robust and fast from a numerical point of view and there are no limitations on shape and number of involved surfaces; the only restriction is due to the shape of the zone, that must be a parallelepiped.

In Figure 4.3 the BTB block for the detailed radiative model is represented.

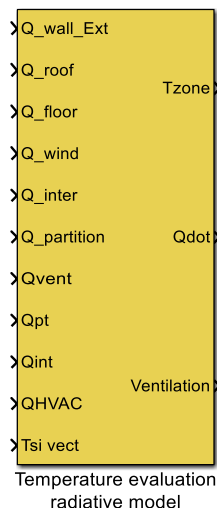


Figure 4.3. BTB block for detailed radiative model.

As for the simple model, the BTB block gives as output the *Temperature zone bus*, the *Power bus* and the *Ventilation bus*. However, comparing the BTB blocks for the temperature evaluation represented in Figure 2.28 and Figure 4.3, it can be noted that if the detailed radiative model is adopted, the BTB block requires an additional input. This input, labelled *Tsi vect*, is a vector composed by the inner

temperature of all the surface of the zone and is used for the evaluation of the local radiative temperature performed by means of equation (4.4).

The radiative temperature distribution in the thermal zone is calculated in the *Temperature map* sub-system, based on the spatial discretization grid defined by the user thanks to the related GUI (see Figure 4.2). As represented in Figure 4.4, the *Temperature map* subsystem requires as input the *Temperature zone* bus and the indoor superficial temperature of each surface of the zone, collected in the *Tsi vect* vector that is automatically created. Again, by using equation (4.4) the radiative temperature is evaluated for each grid point, together with a rough estimation of the operative temperature (based on the mean air temperature value calculated adopting the one-star model). Therefore, the sub-system gives as output the 3D spatial distribution of radiative and operative temperature within the thermal zone.

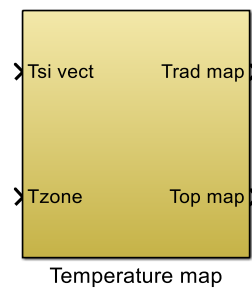


Figure 4.4. Temperature map sub-system. Inputs are the temperature of the inner surfaces of the zone in addition to the temperature zone bus, whereas the outputs are the map of mean radiant and operative temperature distribution within the zone.

Finally, it has to be highlighted that the choice of the detailed radiation model implies not only the use of a dedicated BTB block, but also the adoption of specific BME and BCC blocks. In Figure 4.5 a typical BME block, used together with the BTB *radiative model* block, is represented. It can be appreciated how this block differs from the BME block described in *Chapter 2*, based on a two-star node, since the BME block used in the *detailed radiative model* requires two additional inputs: (i) the internal radiative heat transfer of the element and (ii) the *Power bus* of the thermal zone. The first input replaces the radiative heat transfer evaluated in agreement with Standard EN 6946 [94], whilst the second input is used for the distribution of the radiative fraction of internal gains over all the surfaces of the thermal zone and it represents an additional heat gain of the internal node of the RC network.

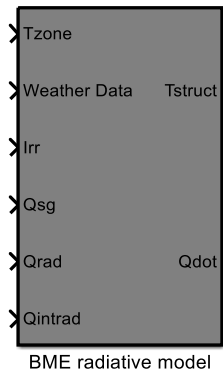


Figure 4.5. Building Massive Element block for thermal zone described by the radiative model.

### 4.2.2 Convective model

The *convective model* is adopted each time that the assumption of perfectly mixed air in the thermal zone does not apply or when stratification and planar distribution of the air temperature within the room is required. In these cases, one node model becomes inadequate.

Usually, problems related to the evaluation of the air flow pattern and air temperature fields are investigated by means of Computational Fluid Dynamics (CFD) analysis that consists in splitting the thermal zone in sub-volumes and in solving together the mass balance and the energy equations. CFD results are very detailed and give important information about the air flow distribution in a room; however the main drawback that limits the use of CFD in seasonal dynamic simulations for a whole building is that CFD simulations require a big amount of memory and the calculation can become very slow.

Zonal models are intermediate between CFD methods and one-node models; in this case, the thermal zone is divided in a limited number of sub-volumes (or air cells) having a parallelepiped shape, for which mass and heat balance equations are written [108]. Each cell can exchange with the adjacent cells mass and heat only by means of convection, since the air is transparent to radiation. Mass conservation applies both considering the total air mass or the diffusion of its components (like VOC, humidity, CO<sub>2</sub> ...). By solving the set of coupled balance equations, the air temperature distribution in a room and the air flow can be estimated. The most critical point of a zonal model consists in the evaluation of the air mass flow rate among the cells. A widely used approach (adopted by Daoud *et al.* [109], Haghghat *et al.* [110], Boukhris *et al.* [111] and Wurtz *et al.* [108] as examples) for the estimation of the air flow rate among adjacent cells consists in the adoption of power law equations, whose general formulation is the following:

$$m = C_d \rho_a A \Delta P^n \quad (4.5)$$

where  $A$  represents the contact area of two adjacent cells,  $\rho_a$  is the air density,  $\Delta P$  is the pressure difference between the cells,  $n$  is the flow exponent that depends on the air flow regime and  $C_d$  is the discharge coefficient, that Wurtz *et al.* [108] suggest to be a constant equal to  $0.83 \text{ m s}^{-1}\text{Pa}^{-n}$ . Teshome and Haghghat [112] propose for the estimation of  $C_d$  the use of a variable value, obtained by means of measurements or specific CFD analysis.

However, this pressure-based zonal model is not valid in presence of driving flows due to jets or plume, since the air velocity in a cell is not considered. A solution to this drawback has been proposed by Inard *et al.* [113]: pressure-based zonal model is used for the so called “current zones”, whilst specific flow laws (for air flows due jet, plume and thermal boundary layers) apply for cells characterised by the presence of driving flows, called “driving zones”. Musy *et al.* [114] improved this method defining a threshold for the air velocity: under the threshold in a driving zone the same equations of a current zone are adopted. Nevertheless, both the methods have important limitations; in fact, the most suitable correlation has to be selected, for each cell, before performing a simulation, requiring a prior knowledge of the air flow pattern. Moreover, correlations cannot be changed during the simulations, which represents a drawback when simulating intermittent operations of the heating system. In fact, a correlation that is adequate for the plume of a heater when this is switched on may not be suitable when the heater is off.

Even if the computational effort of a zonal model is much lower than that of a CFD simulation, up to day there is a lack of software able to evaluate the temperature distribution of a thermal zone and to simulate the behaviour of a HVAC system. These kinds of analyses can be done only by coupling different models implemented in different software, as described by Daoud *et al.* [109]. In fact, when Inard *et al.* [113], Wurtz *et al.* [115] and Megri et Yu [116] investigate the effects on the thermal conditions of the room of six different heater configurations, of an electric heater and of a fan coil (adopting the SIM\_ZONAL tool [117]), and of three different active surfaces configurations (by means of POMA+) respectively, the HVAC system is not taken into account or it is modelled in a very simple way.

For these reasons, with the aim to couple building models based on zonal approach with detailed HVAC system models, in ALMABuild a simplified zonal model is implemented.

The ALMABuild detailed convective model consists, as all the other zonal models, in the partitioning of a thermal zone into several cells in which air is assumed to be perfectly mixed. The air temperature of a cell ( $T_{cell}$ ) is determined by solving the following thermal balance:

$$\sum_k Q_k = \rho_a c_p \frac{dT_{cell}}{dt} \quad (4.6)$$

where  $Q_k$  is the convective heat transfer with adjacent cell or building element through the layer  $k$ . For each cell layer, the convective heat transfer is evaluated by means of a heat transfer coefficient that is calculated starting from a rough estimation of the mass flow across the cell layer that separates two adjacent cells. In fact, for layer  $k$  that separates cell  $i$  to  $j$ , the following equivalence can be written:

$$Q_k = m_k c_p (T_i - T_j) = h_k A_k (T_i - T_j) \quad (4.7)$$

where  $m_k$  is the air flow through the layer  $k$ ,  $c_p$  is the specific heat of air (J/(kg K)),  $T$  is the cell temperature (°C),  $h$  is the heat transfer coefficient (W/(m<sup>2</sup> K)) and  $A_k$  is the contact area between the two cells (m<sup>2</sup>). From equation (4.7) the heat transfer coefficient can be derived as:

$$h_k = \frac{m_k}{A_k} c_p \quad (4.8)$$

Since the specific heat capacity of air and the contact area between two adjacent cells are assumed to be known, the heat transfer coefficient is determined by evaluating the mass flow between the cells. The equations for the estimation of the mass flow depend on the typology of the layer (i.e. horizontal or vertical). However, the main hypothesis of this model is that the air flow is assumed to be driven only by buoyancy forces and the reference pressure of each cells is constant and assumed to be equal to the atmospheric pressure.

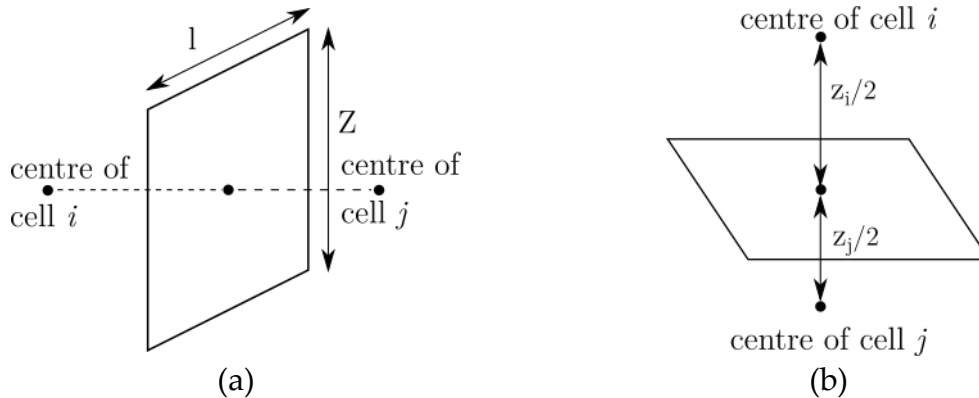


Figure 4.6. Layers between two cells: vertical (a) and horizontal (b).

The air flow across a vertical layer (Figure 4.6a) is estimated evaluating the position of the neutral point, that is the point where there is no pressure difference between the two sides of the layer. As represented in Figure 4.7, which shows the pressure difference between cell  $i$  and cell  $j$  as a function of the vertical

layer height, if only buoyancy forces are considered, the neutral point is located at the middle height of the layer (i.e. where the pressure difference is zero).

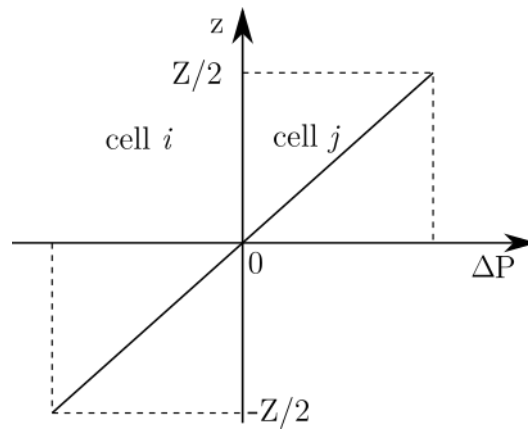


Figure 4.7. Pressure difference ( $\Delta P$ ) between cell  $i$  and cell  $j$  in a vertical layer, if only buoyancy forces are considered. The neutral point is located where  $\Delta P$  is zero.

Once defined the position of the neutral point, the mass flow among the vertical layer can be estimated adopting the equation reported in [108] as follows:

$$m_k = (\rho_i + \rho_j) C_d l |\Delta \rho g|^n \frac{Z^{n+1}}{2^{n+1}(n+1)} \quad (4.9)$$

where  $C_d$  is the discharge factor,  $l$  is the width of the layer (m),  $Z$  is the height of the layer (m),  $g$  is the gravitational acceleration ( $\text{m/s}^2$ ) and  $n$  is the flow exponent.

For horizontal layer (represented in Figure 4.6b) the pressure power law is used for estimating the air flow, evaluating the pressure difference adopting Bernoulli's equation:

$$m_k = C_d \rho_{ij} A \left| \left( \rho_i \frac{Z_i}{2} - \rho_j \frac{Z_j}{2} \right) g \right|^n \quad (4.10)$$

where  $\rho_{ij}$  is the mean density ( $\text{kg/m}^3$ ) of the air in cells  $i$  and  $j$ . The air density in each cell is evaluated according to the perfect gas law; as the reference pressure is assumed to be constant for each cell, the air density depends only on the cell temperature.

The air flow regime, i.e. laminar or turbulent flow, that determines the value of the flow exponent  $n$ , is estimated considering the Rayleigh number, which is equal to the product between the Grashof and Prandtl numbers. The flow exponent is equal to 0.5 for laminar flow (Rayleigh number lower than  $10^9$ ) and to 1 for turbulent flow, as suggested by Rajput [118].

The heat transfer between layers that separate air cells to building elements (e.g. walls, windows, floors, ceilings...) can be modelled in an accurate way adopting the boundary layer theory. For doing this, it would be required to subdivide the boundary cells in two sub-volumes, one representing the boundary layer and one the undisturbed air. The dimensions of these sub-cells are not fixed, because the boundary layer width depends on fluid dynamics conditions, that are variable during the simulation. With the aim of developing a simplified model, in ALMABuild the boundary layer theory is not implemented and the heat transfer between air cells and building elements is evaluated by means of the convective heat transfer coefficient reported in the European Standard EN ISO 6946 [94]. It has to be remarked that the Standard, when proposing the convective heat transfer coefficient, refers to the mean air temperature of the thermal zone. For this reason, the convective heat transfer between cells and building elements is estimated considering the inner surface temperature of the building element and the mean air temperature of the room.

As for the *radiative model*, the *convective model* of a thermal zone is not fully implemented in a static block, but it requires customized blocks in addition to the BTB block.

In Figure 4.8, the BTB block for the temperature evaluations with the *convective model* is represented. In this figure it can be noted that BTB inputs are linked to all the typology of thermal fluxes, as for the *simple* and *radiative models*, whilst the last input is a vector composed by the reduced air temperature of the air cells in which the thermal zone is divided. The reduced air temperature of the *i-th* cell is defined as:

$$T_{reduced} = T_{a,i} \frac{V_i}{V_{tot}} \quad (4.11)$$

where  $T_{a,i}$  is the air temperature in the middle of the *i-th* cell,  $V_i$  is the volume of the *i-th* cell, and  $V_{tot}$  is the total volume of the thermal zone. In this way, in the BTB block the mean air temperature of the thermal zone is evaluated as the sum of reduced temperature of all the cells of the thermal zone:

$$T_a = \sum_i T_{reduced,i} \quad (4.12)$$

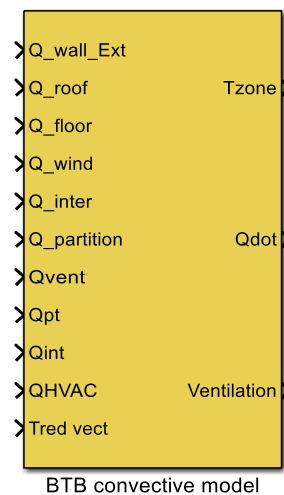


Figure 4.8. BTB block for detailed convective model.

The mean radiative temperature of the thermal zone is evaluated again with the radiative star network. The outputs of the BTB block are, as always, the *Temperature zone bus*, the *Power bus* and the *Ventilation bus*.

The detailed convective model is implemented in Simulink by means of a customized sub-system, represented in Figure 4.9, whose internal composition depends on the number of the air cells and on the zone geometry. This customized sub-system, which is automatically created if the building modelling is performed by means of the ALMABuild GUIs, requires as input a vector which contains the internal convective heat transfer per unit area of each envelope element of the thermal zone and the *Ventilation bus*.

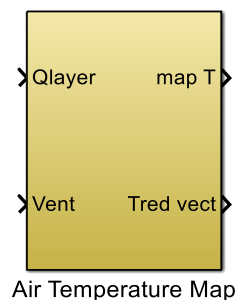


Figure 4.9. Customized Air Temperature Map block.

Within this sub-system, the heat transfer due to air infiltration is distributed over all the cells, in proportion to the ratio between the air cell volume and the net air volume of the zone. This sub-system is in turn composed by customized blocks (one for each air cell) in which the heat transfer across the layer and the air temperature of the cell are evaluated.

As output, the *Air Temperature Map* sub-system gives the air temperature distribution and the vector of reduced temperatures by means of which, in the related BTB block, the mean internal air temperature of the zone is evaluated.



### 4.2.3 Fully detailed model

In *radiative* and *convective* BTB blocks detailed models apply only to their related heat transfer mechanism, whereas the other mechanism is modelled by means of a star-node approach. Nevertheless, radiative and convective models can be coupled together, in order to investigate the spatial distribution of both the air and the mean radiant temperature, as required for comfort distribution assessments. In these cases, the evaluation of the thermal balance of the zone is performed by means of a fully detailed BTB block, represented in Figure 4.10.

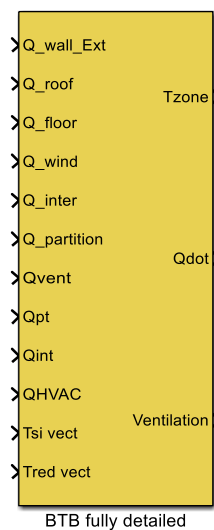


Figure 4.10. BTB block for *fully detailed model*.

In this figure it is possible to see that, in addition to the main thermal fluxes of a thermal zone, vectors of the inner surface temperature of envelope elements (input labelled *Tsi vect*) and of the reduced air temperature (*Tred vect* input) are required by the BTB block. The outputs of the BTB block are the *Temperature zone bus*, in which the mean air temperature of the thermal zone and the mean radiant temperature in a user defined point are evaluated by means of equations (4.12) and (4.4) respectively, the *Power bus* and the *Ventilation bus*. All the additional customized sub-systems described for both radiative and convective models are implemented in the Simulink desktop, enabling the calculation of the spatial distribution of the operative temperature in the zone.

## 4.3 Numerical performances of buildings models

In the previous sections, the different typologies of building models available in the ALMABuild library has been described in detail, putting in evidence the detail level of information on the thermal conditions of the thermal zone provided by the model. In particular, by adopting the *simple model*, described in *Chapter 2*, only average values of the air and mean radiant temperature of the

thermal zone can be obtained. The spatial distribution of the radiative and air temperature are predicted by using the *radiative* and the *convective* models respectively, whereas information on the 3D distribution of the operative temperature are given by the *fully detailed* model. Clearly, the specific kind of analysis available adopting a specific building model affects the numerical performance, intended as computing runtime, of a simulation. In Table 4-1 the computing runtime for annual dynamic simulations of buildings, adopting all the available building models present in ALMABuild, is reported. Simulations have been carried out with a desktop computer with a quad-core 3.40 GHz processor and 8 GB of RAM. In order to highlight the impact of each kind of building model on the computing runtime, thermal zones are considered in free-float conditions, i.e. HVAC systems are not taken into account.

Table 4-1. Computing runtime for annual dynamic simulations of buildings in free-float conditions, adopting different kind of models. Simulations are performed with a desktop computer with a quad-core 3.40 GHz processor and 8 GB of RAM. The multizone building is composed by four thermal zones.

<b>Model</b>	<b>Computing runtime</b>
<b>Simple</b>	10 s
<b>Simple, multizone</b>	40 s
<b>Radiative</b>	16 min
<b>Convective</b>	10 min
<b>Fully detailed</b>	29 min

As it can be seen in Table 4-1, the lowest computation runtime is obtained adopting the simple model. In this case, the annual simulation of thermal conditions within a single zone is carried out in around 10 s. It is interesting to note that the annual simulation of a multizone building composed by four zones requires around 40 s, i.e. four times the runtime needed for the simulation of a single zone. The adoption of a more complex building model determines longer computing runtime. The evaluation of the 3D radiative temperature distribution, based on 75 discretization points for a single thermal zone, requires around 16 minutes, whilst the estimation of the air temperature distribution, with the same spatial discretization, is faster. Finally, the slowest computing runtime is obtained by the most complex building. In fact, the annual simulation of a thermal zone with the *fully detailed model*, adopting a discretization grid composed by 75 points, takes around half an hour.

In conclusion, from the results reported in Table 4-1 it is possible to assess that the pre-calculation of weather-related data together with the adoption of computational lightweight models (based on RC networks) enable a fast and accurate annual simulations, which is a key feature for increasing the diffusion of these kinds of analysis among the designers.

#### 4.4 Verification of the view factor calculation procedure

In order to verify the reliability of the numerical procedure followed by ALMABuild for the calculation of the view factors among the inner surfaces, a room having a squared floor (5 m x 5 m), a height of 2.8 m and one window (2 m x 1 m) has been considered. View factors among the inner surfaces obtained by means of the Matlab script implemented in ALMABuild (based on CDIF [107]) are compared with those obtained for the same room by using two commercial software (TRISCO version 13.0 and COMSOL version 5.3). Figure 4.11 shows the room taken as a reference for the validation of the procedure followed for the evaluation of the view factors.

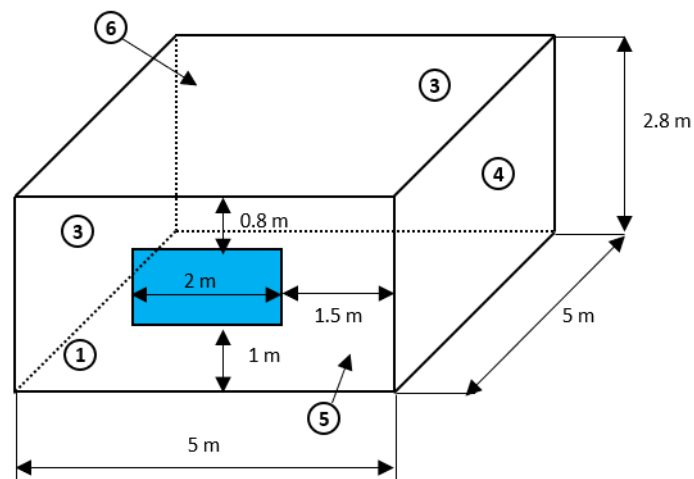


Figure 4.11. Reference room for the validation of the MATLAB routine for view factors calculation.

Table 4-2 reports the view factors calculated with COMSOL, TRISCO and ALMABuild for the test room represented in Figure 4.11; the maximum deviation between the view factors calculated with TRISCO is equal to 1.17% and with COMSOL is 2.32%. These results confirm that the numerical procedure followed in this work for the view factors evaluation can be considered as validated.

Table 4-2. View factors obtained with TRISCO, COMSOL and ALMABuild for the reference room, referring to surface labelled in Figure 4.11.

Surface #		1	2	3	4	5	6	7
1	TRISCO	0.000	0.139	0.108	0.139	0.133	0.131	0.000
	COMSOL	0.000	0.141	0.108	0.141	0.135	0.131	0.000
	ALMABuild	0.000	0.139	0.108	0.139	0.133	0.131	0.000
2	TRISCO	0.162	0.000	0.158	0.129	0.156	0.156	0.134
	COMSOL	0.164	0.000	0.160	0.129	0.158	0.158	0.132
	ALMABuild	0.162	0.000	0.158	0.129	0.156	0.156	0.132
3	TRISCO	0.126	0.158	0.000	0.158	0.156	0.156	0.144
	COMSOL	0.126	0.160	0.000	0.160	0.158	0.158	0.144
	ALMABuild	0.126	0.158	0.000	0.158	0.156	0.156	0.144
4	TRISCO	0.162	0.129	0.158	0.000	0.156	0.156	0.132
	COMSOL	0.164	0.129	0.160	0.000	0.158	0.158	0.132
	ALMABuild	0.162	0.129	0.158	0.000	0.156	0.156	0.132
5	TRISCO	0.277	0.278	0.278	0.278	0.000	0.377	0.284
	COMSOL	0.281	0.272	0.282	0.282	0.000	0.377	0.283
	ALMABuild	0.277	0.278	0.278	0.278	0.000	0.377	0.284
6	TRISCO	0.273	0.278	0.278	0.278	0.377	0.000	0.308
	COMSOL	0.277	0.282	0.282	0.282	0.377	0.000	0.308
	ALMABuild	0.273	0.278	0.278	0.278	0.377	0.000	0.308
7	TRISCO	0.000	0.019	0.021	0.019	0.023	0.025	0.000
	COMSOL	0.000	0.019	0.021	0.019	0.023	0.025	0.000
	ALMABuild	0.000	0.019	0.021	0.019	0.023	0.025	0.000

#### 4.5 Application of the radiative model: a case study

The ALMABuild *radiative model* for the description of a thermal zone has been used for the numerical investigation of the influence of heat emitters on the local thermal comfort in a room.

The evaluation of the local indoor thermal comfort due to different heaters has been investigated for long time by the scientific community with the aim to give an answer to the question if radiant heating systems are or not able to ensure better thermal comfort conditions than convective systems [119]. Nowadays it is evident that this question must be considered as “ill-posed” because the answer strongly depends by many boundary conditions, like the level of thermal insulation of the building, the sizing rules adopted for the emitters, the shape of the room, the position of emitters and control sensor and so on. By varying these conditions, the radiant systems can become better or worse than the convective ones in terms of guaranteed indoor conditions.

In particular, the adoption of a specific heat emitter is responsible of a different distribution of the operative temperature in a room. For example, heat emitters based on convection have higher risk of draught, are generally responsible of higher vertical temperature difference and temperature fluctuation and in presence of an erroneous direction of the air natural circulation (i.e. due to the position of the emitter in the room) they may provide local uncomfortable conditions close to the floor [120]. On the other side, with radiant floor or ceiling

heating systems there is higher risk that occupants feel cooler or hotter respectively the head or feet region [120]. Case by case the impact on the indoor comfort conditions of these systems must be evaluated in detail in order to select the best one in terms of comfort conditions. However, since the most diffuse commercial software used for energy dynamic simulations are generally able to associate to each room of a building only one convective and one radiant node, the information about the spatial variation of the comfort indoor conditions, due to the adoption of a specific heater in a room, is lost [121]. Therefore, the ALMABEST tool, which enables the evaluation of the spatial distribution of the operative temperature in a zone, represents a suitable tool for investigations on heater effects on the indoor comfort conditions.

In the following analysis, radiant (floor, ceiling or wall) or convective (radiators or all-air) heating systems are considered and the *radiative* BTB blocks are used. Thus, in this case the air temperature is assumed to be perfectly mixed since, as observed by Lin *et al.* [120], this assumption is acceptable in all the cases in which the air flow is low ( $<0.15$  m/s), as in the case of weak natural convection induced by small temperature gradients. Anyway, in the analysed cases the convective heat transfer coefficient between air and heated envelope element surfaces is evaluated as described by Awby *et al.* [122], modifying the related BME blocks.

### 4.5.1 The reference thermal zone

In order to show the potential of the numerical approach presented in the previous section, a typical room having a rectangular floor is considered. A complete description of the geometry of the room used as reference zone is reported in Figure 4.12a. The room is part of a one-story detached house located in Bologna (Italy). In the simulations, the heating system is switched on starting from September 1<sup>st</sup> until April 30<sup>th</sup>.

The floor is an insulated slab on grade and the roof is horizontal. The room height is 2.8 m and, as evidenced by Figure 4.12a, there are two external walls (with South and West orientation) and two internal walls. Internal walls separate the room from two heated rooms maintained at 20 °C during the whole heating season. The heat transfer across the internal walls is taken into account in the simulations. The window is placed on the West external wall and it is a double pane window for cases A while it is a triple pane window for case B. The infrared emissivity of the inner surfaces (active and passive) is imposed equal to 0.8. For sake of simplicity, shadings are not present and internal loads are considered equal to 0. Air infiltration is constant and equal to 0.3 Air Changes per Hour (ACH).

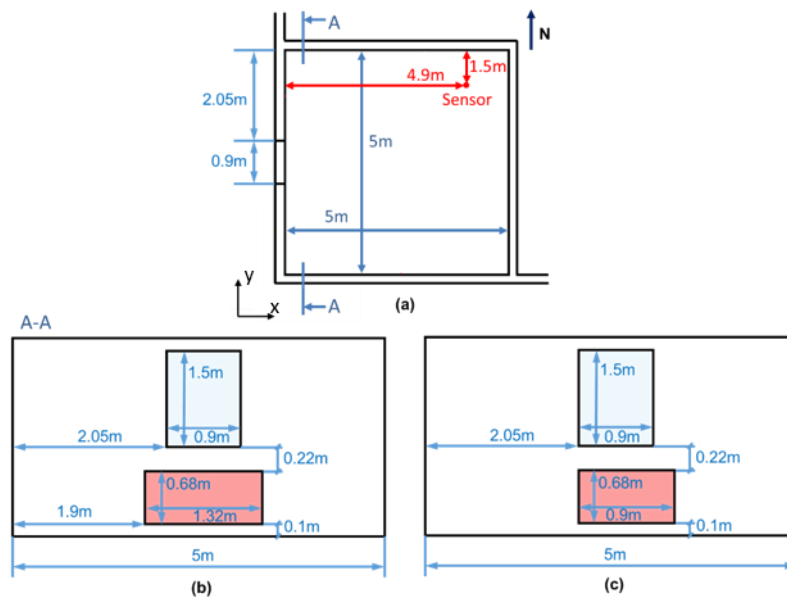


Figure 4.12. (a) Plan of the room with indication of the position of the sensor; (b) Position and size of window and radiator for case A; (c) Position and size of window and radiator for case B and C.

Two different insulation levels of the envelope are considered in this work (A, B). The roof is characterized by five layers (plaster, brick, screed, insulation, waterproofed); suspended ceiling is composed by two layers (insulation and drywall) placed 5 cm underneath the roof structure; slab on grade has four layers (tile, screed, insulation, light weight concrete); external walls consist of four layers (plaster, brick, insulation, plaster). Specific insulation thickness is adopted for the different cases (A, B) where each structure has different U-value (see Table 4-3). In all the cases the internal walls are characterized by a U-value of  $0.8 \text{ W}/(\text{m}^2\text{K})$ .

In Table 4-3 the values of thermal capacitance (C) refer to the whole structure. As an example, in case of suspended ceiling the thermal capacitance reported in Table 4-3 is the total thermal capacitance of the suspended panel and of the ceiling structure.

Table 4-3. Thermo-physical properties of the main envelope elements.

Case	A		B	
	U [ $\text{W}/(\text{m}^2\text{K})$ ]	C [ $\text{kJ}/(\text{m}^2\text{K})$ ]	U [ $\text{W}/(\text{m}^2\text{K})$ ]	C [ $\text{kJ}/(\text{m}^2\text{K})$ ]
External walls	0.89	218	0.20	232
Floor	0.21	175	0.14	231
Ceiling	0.46	240	0.21	252
Suspended- ceiling	0.24	251	0.15	262
Window	1.8	-	0.8	-

### 4.5.2 Heat emitter characteristics

Six different typologies of heat emitters are compared each to other:

- Emitter #1: classical underfloor heating system in which pipes are immersed in the floor screed (radiant floor);
- Emitter #2: heating system obtained by immersing pipes in the ceiling mass (radiant ceiling);
- Emitter #3: light suspended insulated panels made in drywall in which the pipes are immersed (radiant suspended ceiling);
- Emitter #4: classical hot water radiator;
- Emitter #5: vertical radiant surface installed on the external wall (radiant vertical wall);
- Emitter #6: ideal all-air heating system.

Emitters #1 and #2 are embedded surface systems characterized by a very large thermal inertia; they are able to reduce the peak consumption, which can determine significant energy savings if a proper control system is implemented [123]. Emitter #3 is based on a series of light suspended drywall panels attached to the inner side of the roof with an air cavity having a thickness of 5 cm. Emitter #4 is a classical hot water radiator placed under the window as indicated in Figure 4.12b,c. The radiator is made by cast iron elements with low water content (1.2 l/m<sup>3</sup>), characterised by a nominal power of 108 W per element and exponent equal to 1.325. The dimensions of the radiator change with the thermal insulation level of the external walls (case A and B, as indicated in Table 4-4). Emitter #5 covers the whole inner surface of the external wall without windows (see Figure 4.12), whilst Emitter #6 is an ideal all-air heating system based on the hypothesis of fully mixed air, which leads to a uniform air temperature distribution within the room. In Table 4-4 the area of the inner surfaces linked to the six heat emitter systems taken into account in this analysis for cases A and B is shown.

Table 4-4: List of radiant and convective heat emitters considered in numerical simulations.  $n_{el}$  is the number of element composing the radiator.

Emitter	1	2	3	4	5	6
Type	Radiant floor	Radiant ceiling	Radiant suspended ceiling	One radiator under the window	Radiant vertical wall	All air heating system
Area [m <sup>2</sup> ]	25	25	25	Case A: 0.898 ( $n_{el}=12$ ) Case B: 0.782 ( $n_{el}=10$ )	14	0

### 4.5.3 Heating system control

A room temperature control is adopted for the modulation of the heat delivered by the heaters. The heat flux delivered by the active inner surfaces is controlled by means of two hysteresis cycles based on the active surface

temperature and on the operative temperature calculated in the sensor position (Figure 4.12a). The sensor is placed 1.5 m above the floor.

The control system maintains the operative temperature in the point in which the room sensor temperature is placed within the band 19 °C - 20.5 °C. In meantime, the control system avoids that the surface temperature of the heaters becomes larger than: (i) 75 °C for the radiator (case 4); (ii) 29 °C for the radiant ceiling (case 2) and suspended ceiling (case 3); (iii) 28 °C for the radiant floor (case 1); (iv) 40 °C for the radiant wall (case 5). Between these two hysteresis cycles, the control of the active surface temperature has priority on the operative temperature sensed in the room for safety reasons.

### ***4.5.4 Inputs for the indoor thermal comfort analysis***

In order to associate to each point of the room a value of the predicted mean vote (PMV) a series of hypotheses are made on the typical occupant of the room; more in detail, the value of the metabolic rate of the occupant, the mechanical power, the partial vapour pressure in the room, the clothing area factor and the clothes surface temperature have to be fixed in order to obtain the PMV value.

In this work the local value assumed by PMV is calculated by assuming the metabolic rate of the occupants equal to 70 W/m<sup>2</sup>, their mechanical power equal 0 W/m<sup>2</sup>, the partial vapour pressure in the room equal to 1160 Pa (a uniform distribution of the relative humidity in the room is considered), the clothing area factor equal to 1.14 (typical of an occupant with trousers and long-sleeve shirt) and the clothes surface temperature equal to 25.5 °C.

### ***4.5.5 Discussion of the results***

A series of numerical dynamic simulations are made in order to study the effect of both building insulation (case A and B, see Table 4-3) and the typology of emitters (case 1,2,3,4,5,6, see Table 4-4) on the local thermal comfort conditions in the room. Each case is individuated by a code; as an example, the Case A1 refers to the room with non-insulated external walls (A, Table 4-3) in which a radiant floor (1, Table 4-4) is present.

All the results shown in this section are obtained by means of a yearly dynamic simulation which starts from day 212 (August 1<sup>st</sup>) and ends to day 211 of the following year. The weather data of the Typical Meteorological Year (TMY) of Bologna are taken by the CTI database [64]. Only the behaviour of the emitters during the winter season is here considered.



Radiative power share

In Table 4-5 the percentage of radiant heat power  $Q_r$  delivered by the heaters on the total power exchanged ( $Q_{tot}$ ) is shown for all the considered emitters, referring to the coldest winter day. In the cases of radiant floor, ceiling, suspended ceiling and radiant vertical wall this percentage is larger than 60% and it assumes its maximum value for radiant ceiling (92%) because natural convection is inhibited during winter. Hot water radiator has a limited percentage of radiant power (21%) due to strong natural convection generated around the radiator surface (in this case the radiator exponent is higher than 1.3).

Table 4-5. Radiative power share for the different heaters.

Emitters	1	2	3	4	5	6
$Q_r/Q_{tot}$ [%]	61%	92%	89%	21%	62%	0%

It is interesting to observe that the set point temperature of 20.5 °C is sensed by the room sensor with different combinations of convective and mean radiant temperature depending on the different radiative power share provided by the emitters. Table 4-6 shows the values of the convective and mean radiant temperature at the point in which the room sensor is placed (see Figure 4.12a) when the local operative temperature reaches the set point value of 20.5 °C, for case A. As expected, emitters characterized by higher radiant power share (see Table 4-5) are able to maintain the set point, in terms of operative temperature, with lower value of indoor air temperature; as an example, adopting the radiant floor (case A1) the set point is guaranteed with an indoor air temperature of 20.3 °C, whereas suspended ceiling (case A3) and hot water radiator (case A4) require indoor air temperature equal to 19.2 °C and 21.5 °C respectively. Radiant vertical wall (case A5) is the heater characterized by a more balanced radiant and convective power (see Table 4-5); in this case the set-point is reached with the same value of convective and mean radiant temperature.

Table 4-6. Convective ( $T_a$ ) and mean radiant temperature ( $T_{rad}$ ) when the room sensor measures an operative temperature of 20.5 °C, during the coldest day of the year, as a function of the adopted heat emitters with a low building thermal insulation level (case A).

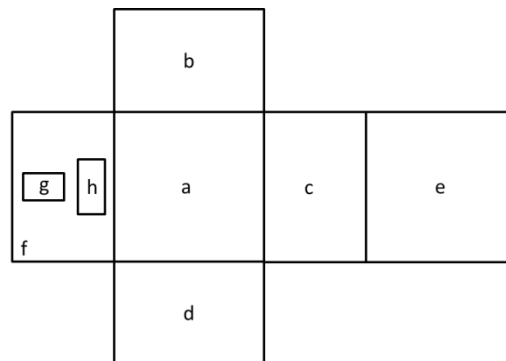
Case	A1	A2	A3	A4	A5	A6
$T_a$ [°C]	20.3	19.5	19.2	21.5	20.5	22.2
$T_{rad}$ [°C]	20.7	21.5	21.8	19.5	20.5	18.9

Inner surface temperature

Since each emitter is characterized by a specific radiative power share, the choice of the emitter affects, together with the building thermal insulation, the

temperature of the room inner surfaces. In Table 4-7 the distribution of the inner surface temperature ( $T_{si}$ ) as a function of emitter and of building insulation (case A and B) is shown by considering the coldest day of the year, when the emitters reach their maximum surface temperature ( $T_{em,max}$ ), indicated in bold in Table 4-7.

Table 4-7. Inner surface temperature (°C) distribution in the room when the emitters reach their maximum surface temperature ( $T_{em,max}$ ) during the coldest day of the year as a function of the thermal insulation level (A or B) and of the adopted emitter.



Surf.	A1	B1	A2	B2	A3	B3	A4	B4	A5	B5	A6	B6
a	<b>27.7</b>	<b>25.7</b>	20.1	20.4	20.0	19.9	19.1	20.0	20.1	19.9	18.5	19.3
b	19.9	19.9	20.2	20.3	20.2	20.1	19.6	20.1	20.1	20.0	19.3	19.8
c	19.9	19.9	20.2	20.3	20.2	20.1	19.6	20.1	20.3	20.0	19.3	19.8
d	16.9	19.2	17.2	19.6	18.2	19.5	16.9	19.5	<b>32.4</b>	<b>30.9</b>	17.2	19.1
e	18.8	19.4	<b>29.0</b>	<b>26.3</b>	<b>29.0</b>	<b>28.0</b>	18.7	19.7	19.0	19.4	18.6	19.4
f	16.9	19.2	17.2	19.6	18.0	19.5	16.7	19.4	17.5	19.3	17.0	19.1
g	14.1	17.9	15.0	18.3	15.3	18.3	13.4	17.5	14.4	18.1	13.9	17.2
h	-	-	-	-	-	-	<b>75.0</b>	<b>55.2</b>	-	-	-	-

From Table 4-7 it is evident that the surface temperature of external, non-heated envelope elements increases with the thermal insulation, whilst the temperature of the heated structures decreases. By observing the data reported in Table 4-7, it can be remarked that the temperature difference among the inner

surfaces is reduced in presence of thermally insulated walls, affecting the radiative heat transfer: radiation is progressively reduced in presence of a more uniform distribution of surface temperature among the elements of the room. In addition, Table 4-7 highlights how radiant emitters are able to work with a reduced surface temperature in thermally insulated rooms.

### Vertical temperature distribution

In Figure 4.13 the operative temperature ( $T_{op}$ ) profile at the centre of the room, as a function of the distance from the floor ( $Z$ ) obtained by adopting the different heaters is reported, considering the coldest day of the year and when heaters reach their maximum surface temperature. In addition, in Figure 4.13, surface temperature of the floor ( $Z=0$  m,  $T_{s, floor}$ ), and of the ceiling ( $Z=2.8$  m,  $T_{s, ceiling}$ ) are indicated. Two horizontal dashed lines highlight the heights suggested by ASHRAE 55 [124] for the evaluation of the comfort in a room for both seated ( $Z=0.6$  m) and standing ( $Z=1.1$  m) occupants.

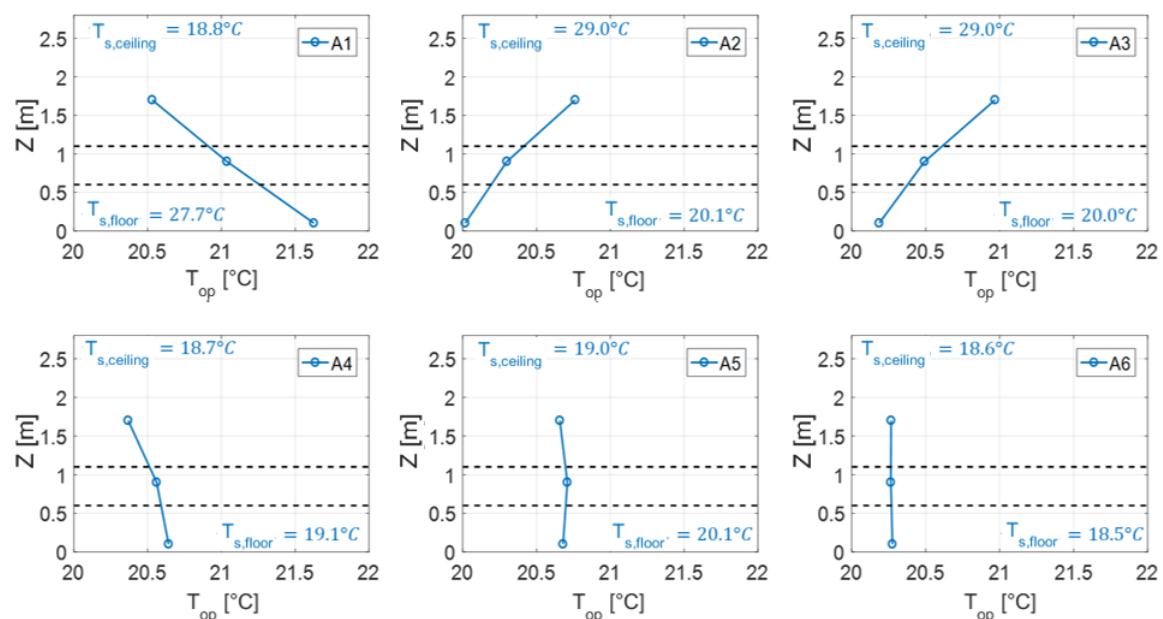


Figure 4.13. Vertical profile of the operative temperature at the centre of the room for the coldest day of the year when the heaters reach their maximum surface temperature.

Figure 4.13 shows that, for all the cases analysed, the temperature difference between 0.1 and 1.7 m levels is less than 3 K, as recommended by ASHRAE 55 [124]. In fact, the maximum temperature difference between these levels is 1.1 K (for the worst case A1). For cases A2 and A3 the temperature difference is 0.2 K (radiant ceiling) whereas for cases in which convection plays a more important role (A4, A5 and A6) this maximum difference is less than 0.1 K. Cases B, characterised by a larger thermal insulation of the room, are not reported in

Figure 4.13 for sake of simplicity, since it is expected that an increase of the thermal insulation will reduce the vertical temperature difference.

### Distribution of the operative temperature

The spatial distribution of the operative temperature within the zone, evaluated at 0.1, 0.9 and 1.7 m above the floor in the coldest day of the year, for buildings characterised by low thermal insulation (Case A), is represented in Figure 4.14, for each emitter. The reported spatial distribution refers to the time instant when the heaters reach their maximum surface temperature. In order to better highlight the differences existing among the cases, in Figure 4.14 a different scaling is used for the operative temperature plotted for each case.

The 3D spatial distribution of the operative temperature clearly demonstrates that radiator (Case A4) and radiant wall (Case A5) generate the larger variation of operative temperature within the room due to the presence of a hot spot close to the heated surface. As underlined by Table 4-7, Case A4 and A5 are characterized by the higher surface temperature of the heated surface that determines high operative temperature close to the emitter.

For the all-air system (Case A6), the operative temperature distribution is strongly influenced by the temperature difference existing among the inner surfaces (between the cold external walls and hot internal walls). It is important to highlight that the results obtained for Case A6 have to be considered as approximated because the adopted *radiative model* is not able to reconstruct the spatial distribution of the air temperature in a room in presence of significant air flows (air velocity larger than 0.1 m/s).

For the radiant floor, radiant ceiling and radiant suspended ceiling (A1, A2 and A3) the operative temperature has a more uniform horizontal distribution, even if the temperature vertical gradient is maximum with respect to the other emitters.

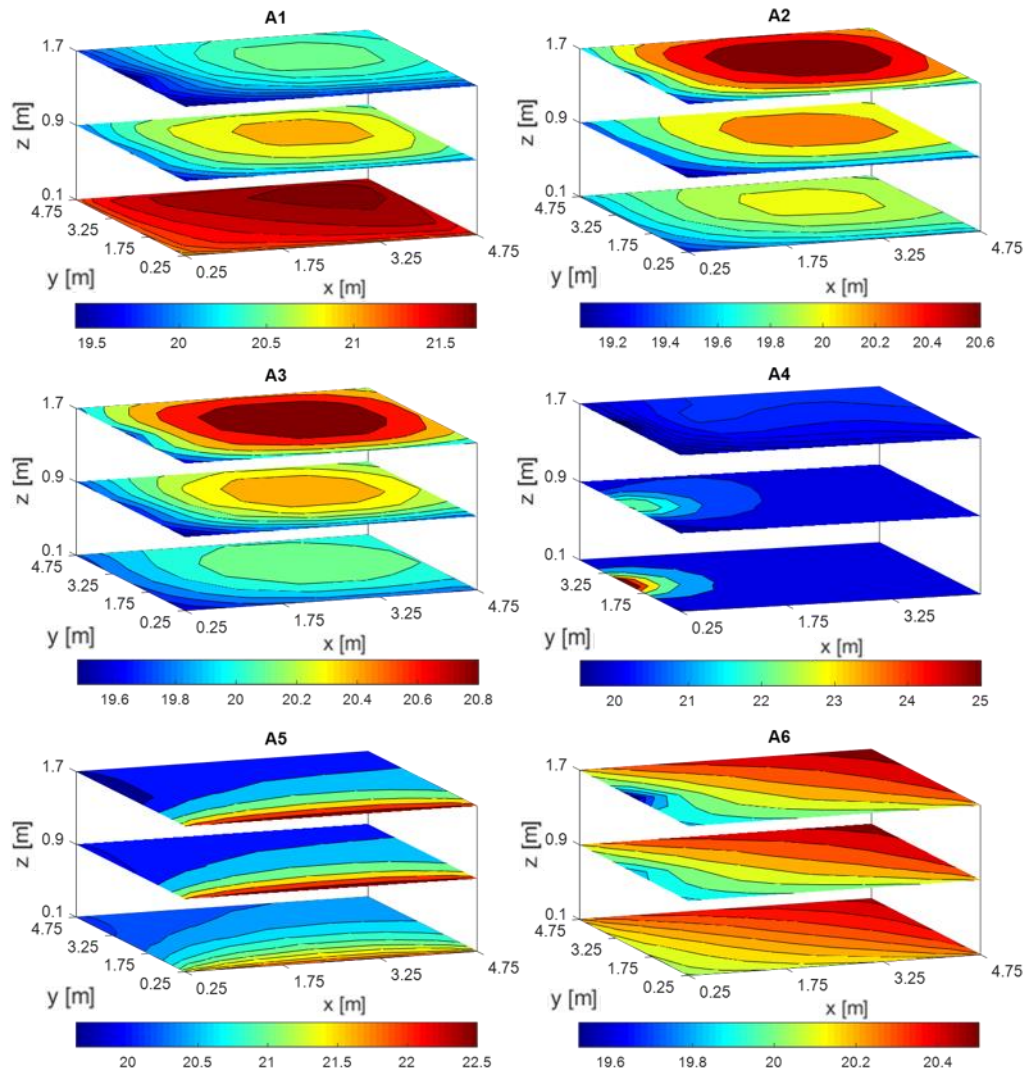


Figure 4.14. Room operative temperature distribution ( $^{\circ}\text{C}$ ) in the coldest day of the year when the heaters reach their maximum surface temperature, at three levels above the floor (0.1 m, 0.9 m and 1.7 m) in case of low thermal insulation (Case A).

#### Emitter dynamic behavior in presence of variable thermal loads

In presence of variable thermal loads, for evaluating the capability of the system to follow the thermal building demand, thermal inertia of heat emitters has to be taken into account. In order to highlight the performance of the different emitters in presence of variable thermal loads, the evolution of the operative temperature in the room during a day is analysed. Figure 4.15 shows the operative temperature ( $T_{op}$ ) at the point close to the inner walls in which the room sensor is placed (see Figure 4.12a), as a function of time during the coldest winter day from 12:00 to 21:00, when the external temperature goes from  $-6^{\circ}\text{C}$  up to  $1^{\circ}\text{C}$ , considering both low (Case A) and high thermal insulation buildings (Case B).

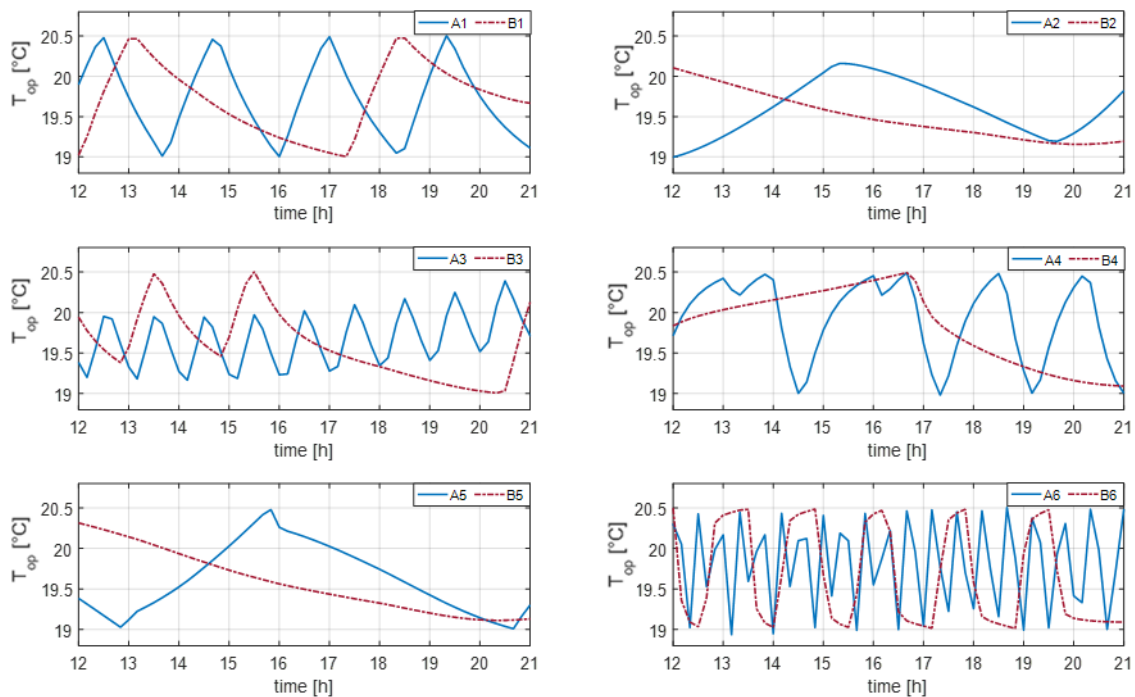


Figure 4.15. Operative temperature of the room measured in the coldest winter day by the room sensor in presence of different emitters and envelope thermal insulations.

By observing Figure 4.15, it can be remarked that the all-air heating system (Case A6, B6) is the fastest to vary the operative temperature in the room, due to the low thermal capacitance of the air node. The radiant floor (Cases A1, B1) is able to react faster than the radiant ceiling (Cases A2, B2) thanks to the higher convective exchange guaranteed during the winter. On the other side, the radiant floor (Cases A1, B1) and the radiant ceiling (Cases A2, B2) are both significantly slower than suspended ceiling heater (Cases A3, B3), because of the lower active mass of the suspended panel which is based on light elements (i.e. drywall).

In presence of low thermal insulation, the suspended ceiling heater (Case A3) is switched off before the room reaches the set point value of the operative temperature (20.5 °C) because the surface temperature reaches its maximum value (29 °C). This observation is still valid for Case A2. This result puts in evidence that for Case A (i.e. room with a low level of thermal insulation) suspended ceiling (3) and radiant ceiling (2) are not able to cover completely the maximum winter thermal load of the room due to the reduced contribution of the natural convection. In these cases, the operative set-point temperature in the room can be reached only by increasing the surface temperature of the radiant ceiling over 29 °C.

Moreover, Figure 4.15 underlines that all the heating systems here considered need more time to reach the set point (20.5 °C) when the building insulation level is increased. In fact, with higher thermal insulation level the thermal power delivered by the emitters is reduced, the temperature of the non-heated inner surfaces of the room increases and the surface temperature of the radiant emitters

decreases (see Table 4-7). This trend is confirmed by the results reported in Table 4-8, where the maximum thermal power emitted per square meter of floor, in presence of different thermal insulation of the envelope, are collected. However, high thermal insulation allows to increase the period in which the operative temperature can be maintained within the band 19-20.5 °C when the emitter is switched off.

Table 4-8. Maximum specific emitted thermal power as a function of emitter and of thermal insulation level.

$Q_{tot,max}$ [W/m <sup>2</sup> ]	1	2	3	4	5	6
<b>Case A</b>	67	48	53	57	55	60
<b>Case B</b>	45	30	43	26	46	31

It is interesting to calculate the time interval needed by the emitters to increase the local operative temperature of the point in which the temperature sensor is placed (see Figure 4.12a) from 19 °C to 20.5 °C ( $\Delta t_{on}$ ), as well as the time interval in which the operative temperature in the same point decreases from 20.5 °C to 19 °C when the heating system is switched off ( $\Delta t_{off}$ ). The sum of  $\Delta t_{on}$  and  $\Delta t_{off}$  can be linked to the hourly number of on-off cycles of the heating system.

Figure 4.16 shows the characteristic time  $\Delta t_{on}$  and  $\Delta t_{off}$  obtained with different emitters by considering a room with different levels of thermal insulation (Case A and B). The characteristic times are evaluated by considering all the on-off cycles done by the different emitters in the coldest month (January). The characteristic time  $\Delta t_{on}$  depends on many factors linked to building and emitters features (i.e. the emitter heating capacity, the instantaneous heating demand etc.), while the characteristic time  $\Delta t_{off}$  depends mainly on the heat losses factor and thermal capacity of the building.

Figure 4.16 underlines that heaters with higher thermal inertia (i.e. radiant floor (1), ceiling 2) and wall (5)) determine higher  $\Delta t_{on}$  and  $\Delta t_{off}$  values compared to the low capacity emitters; by increasing the building thermal insulation (from Case A to Case B) for all the emitters both  $\Delta t_{on}$  and  $\Delta t_{off}$  are increased.

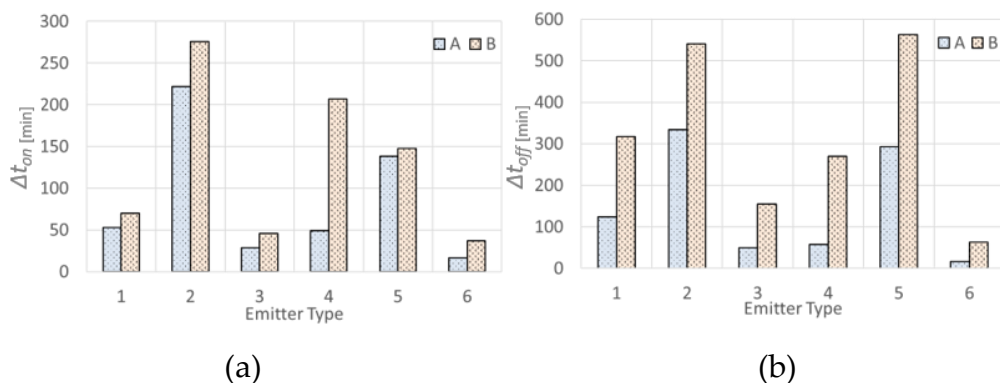


Figure 4.16. Characteristic time  $\Delta t_{on}$  (a) and  $\Delta t_{off}$  (b) for different emitters and for different building thermal insulation, by considering the control system dead band of 19-20.5 °C.

Local indoor thermal comfort conditions

By knowing the yearly local distribution of the operative temperature in the room, it is possible to derive detailed information about indoor thermal comfort conditions provided by the different emitters. The contour plots reported in Figure 4.17 and Figure 4.18 give information about the percentage of time during the whole winter in which a local value of PMV is within  $\pm 0.5$  ( $t_{\text{comf}}$ ). In Figure 4.17 the results obtained with radiant floor (1), ceilings (2) and suspended ceiling (3), for a control dead band equal to 19-20.5 °C and different thermal insulation levels (A and B) can be compared each to other, whilst Figure 4.18 concerns the hot water radiator (4), the radiant vertical wall (5) and the all-air system(6).

As a general observation, when external walls have a high thermal insulation (i.e. Cases B) the points of the room close to the external walls remain warmer, therefore the PMV distribution becomes more uniform with respect to Cases A, regardless the emitter. In fact, for all the emitters considered here, it can be observed that the minimum value of the percentage of time in which PMV is within  $\pm 0.5$  rises when the thermal insulation of the external walls is increased; this means that it becomes possible to maintain the room in optimal indoor comfort conditions farther during the year.

With a radiant floor (1) the temperature difference between the feet and the head region is large and therefore the risk that the occupants feel uncomfortable the head region is high, as observed in [120]. However, by comparing Case A1 with Case B1 reported in Figure 4.17 it can be remarked that the region within the room in which the occupants may feel the “cold head” effect is strongly reduced by increasing the thermal insulation of the room.

The radiant ceiling (cases 2 and 3) generate a lower vertical temperature difference with respect to the radiant floor (see Figure 4.15). By comparing the values of  $\tau_{\text{comf}}$  close to the floor ( $z=0.1$  m) for cases reported in Figure 4.17, it can be remarked that lower values are generally obtained in presence of radiant ceiling systems (“cold feet” effect), with suspended ceiling (cases A3, B3) characterised by the lowest  $\tau_{\text{comf}}$ . Also in this case,  $\tau_{\text{comf}}$  increase and is more uniformly spatially distributed in the room in presence of higher thermal insulation.



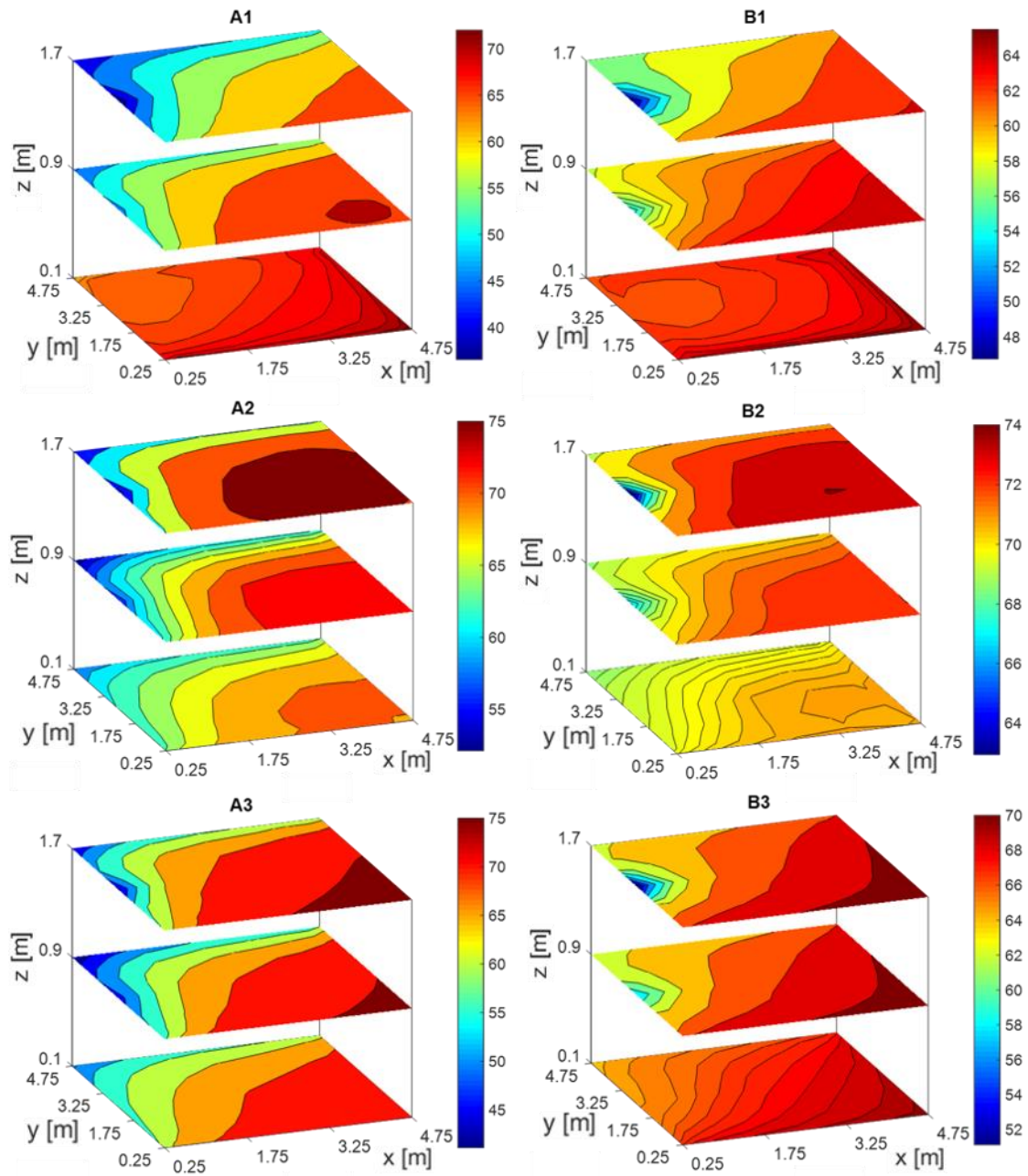


Figure 4.17.  $t_{comf}$  for emitters (1), (2) and (3), considering both low and high insulated buildings.

Window generates a cold spot close to the external wall which is more evident in presence of high thermal insulation. However, as it can be appreciated in Figure 4.18, the installation of a hot water radiator below the window mitigates the effect of the cold transparent envelope element. The radiator (cases A4, B4) is able to guarantee a uniform distribution of PMV, especially in presence of highly insulated external walls, even if close to the radiator a hot spot is present which determine large local PMV values. Anyway, since the present model uses a single convective node, the spatial distribution of the convective temperature in the room is approximated and, for this reason, the results shown in Figure 4.18 have

to be considered less accurate for emitters in which the radiative power share is lower (see Table 4-5).

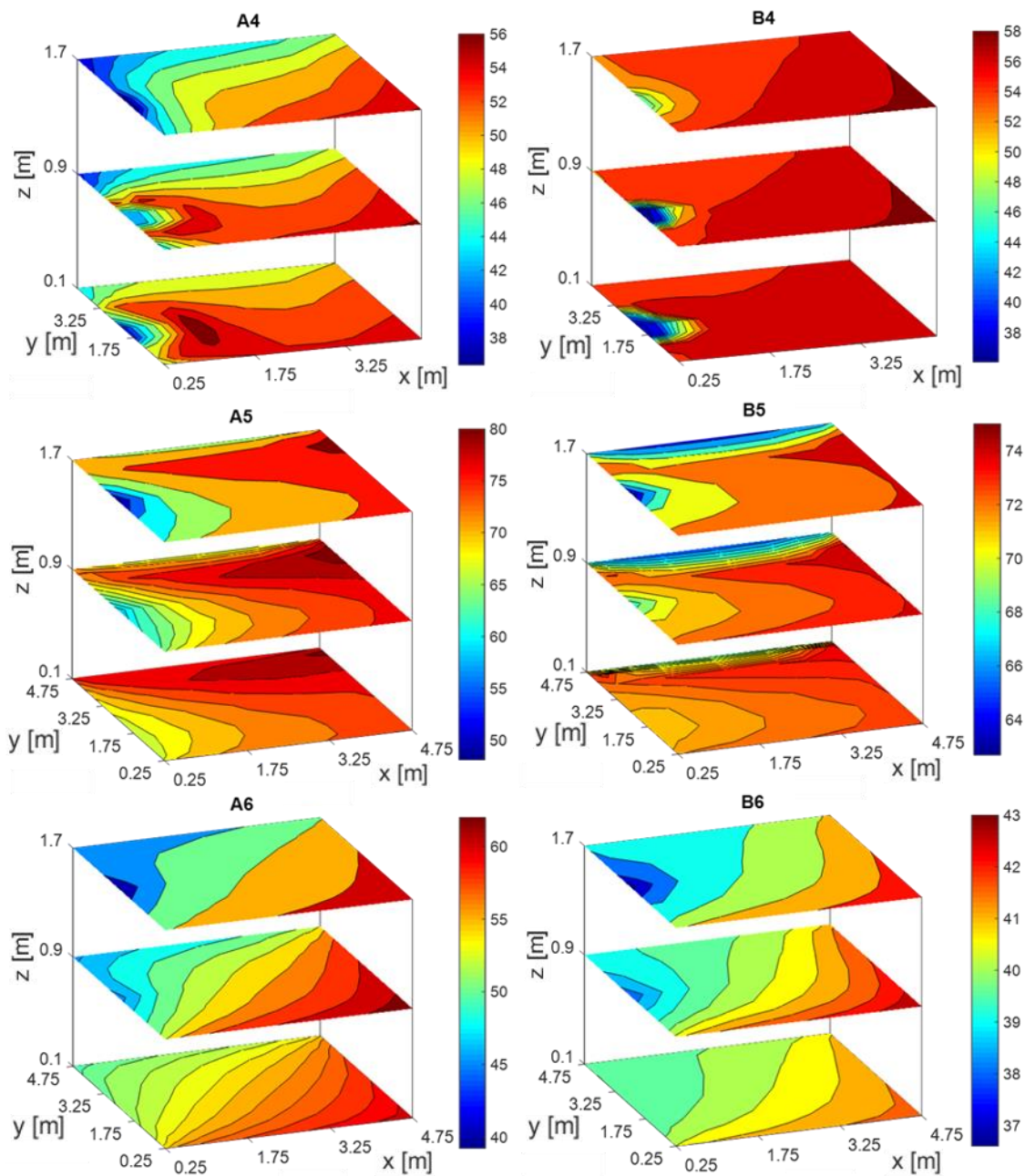


Figure 4.18.  $t_{comf}$  for emitters (4), (5) and (6), considering both low and high insulated building.

The same consideration can be done for all-air systems (cases A6, B6). In these cases, the air velocity and the local temperature fluctuations, linked to the fast reaction of these systems to the thermal load variation (see Figure 4.15) could play an important role on the distribution of the thermal indoor comfort conditions in a room. In fact, depending on the position of the inner warm air source, there would be a warmer zone and therefore a non-uniform air

temperature distribution in the room which is not accounted for in these simulations.

## 4.6 Application of the fully detailed model: a case study

In the previous case study, it has been observed that, referring to the evaluation of indoor comfort conditions achieved by means of hot water radiators, results have to be considered approximated since the *radiative model* has been adopted for describing the thermal zone, without taking into account the air flow in the room. For this reason, a new case study, that consists in the evaluation of the influence of the temperature sensor position on thermal comfort conditions and on the behaviour of a radiator in a room, is analysed using the *fully detailed model*.

The goal of this study is to find an answer to a practical issue: “Is there an optimal position for the indoor temperature sensor in a room, for maintaining adequate comfort conditions in a specific region of the room, achieving the lowest energy consumptions?”. In many practical cases, the temperature sensor is not located close to the area in which comfort conditions are required, thus the parameter of the control system has to be set by considering the position of the sensor with respect to the zone in which thermal comfort is required (sensor calibration).

### 4.6.1 Case study description

In this study, a multi-zone building located in Bologna (Italy), composed by three identical adjacent offices of 25 m<sup>2</sup> (5 x 5 m), is considered. Each office is 2.7 m height and has a double pane window of 1.35 m<sup>2</sup> in the South wall, as shown in Figure 4.19. The roof is horizontal with a thermal insulation layer ( $\lambda=0.039$  W/(m K)) of 6 cm. External walls present an insulation of 8 cm. No insulation is provided for the internal walls that separates the offices; on the contrary, the slab-on-grade floor contains 6 cm of insulation. The U-values of the office envelope elements are listed in Table 4-9.

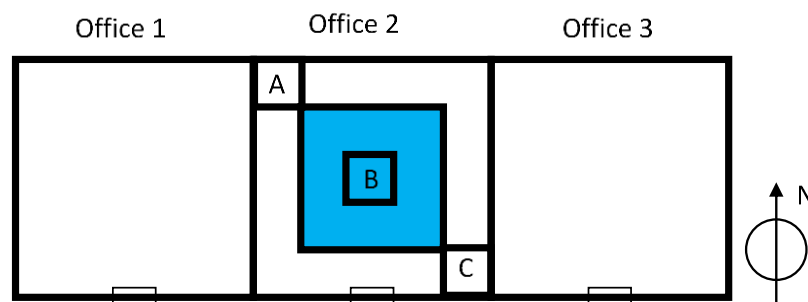


Figure 4.19. Plant view of offices. Comfort zone is evidenced in blue, whilst A, B and C refer to the position of the temperature sensor.

In this study, the analysis on energy consumptions and comfort assessment is focused on the central office, labelled *Office 2*. In Figure 4.19, the central zone of this office (highlighted in blue) represents the area, called comfort zone, in which comfort conditions are required. Labels *A*, *B* and *C* represent three different positions in which the indoor temperature sensor will be placed during the tests. In these cases the temperature sensor is not shaded, thus it is affected by both convective and radiative heat transfer and it measures the operative temperature in the position in which it is located.

Table 4-9. U-values of building elements.

	U [W/(m <sup>2</sup> K)]
<b>External wall</b>	0.31
<b>Internal wall</b>	0.99
<b>Floor</b>	0.27
<b>Roof</b>	0.42
<b>Window</b>	1.1

Figure 4.20 shows the thermal zone discretization on air cells having dimensions of 1 × 1 m in x-y plane and different heights, as shown in Figure 4.20b. The sensor is located in the middle of the corresponding air cell, that is 1 m above the floor. Clearly, only position *A* and *C* are “realistic”, since they are near to a wall, whilst sensor *B* represents an “ideal” sensor position, in the middle of the comfort zone. However, it has to be remarked that in practise, the temperature sensor is usually 1.5 m above the floor and rarely is placed close to external walls (i.e. position *A*).

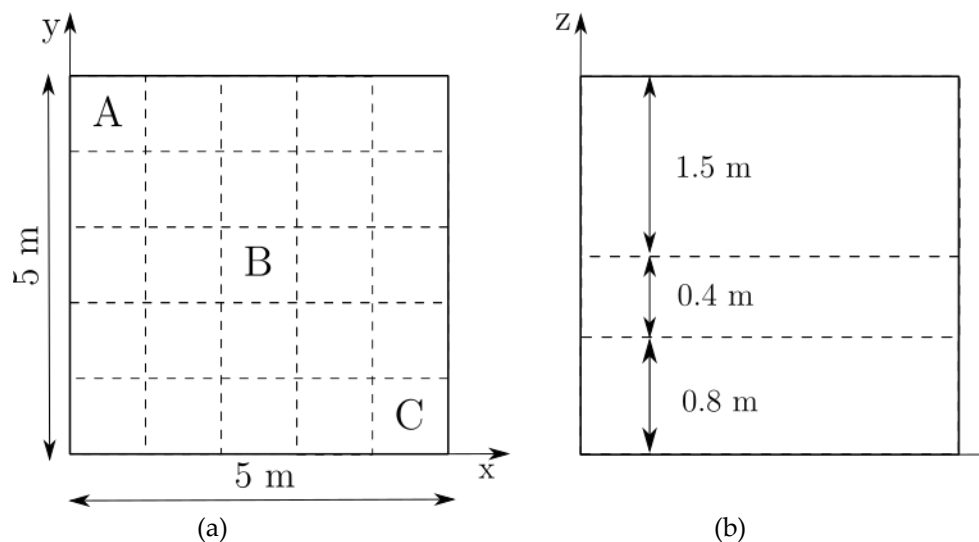


Figure 4.20. Room discretization in air cells, plant view (a) and height discretization (b).

Each office is heated by means of a radiator, characterised by a nominal power of 103 W/element, a water content of 1.44 l/element and an exponent equal to 1.32. Radiator is controlled by an on-off thermostat, which is on only from 6:00 to 20:00 each day; during the night the heating system is off. The heating system is

switched on one hour before people is assumed to start working, in order to reach comfort conditions after the night. For sake of simplicity, the hydraulic and the heat generation systems are not considered in this analysis; thus, the inlet water flow of the radiator is always set to the nominal value, when heating is required by the control system.

Simulations are performed considering the heating season starting from the 15<sup>th</sup> of October to the 15<sup>th</sup> of April. Comfort conditions reached in the comfort zone and the HVAC system behaviour are evaluated considering different HVAC configurations. Labels *R1* and *R2* refer to cases in which the radiator of *Office2* is sized imposing the inlet temperature to 80 °C and 60 °C respectively. In both the cases the same water flow, that determines a temperature difference of 10 K between radiator inlet and outlet, is considered. In case *R1* the radiator is composed by 12 elements, whilst in case *R2* the number of elements is 21. Labels *A*, *B* and *C* are used for referring to the sensor position. In all these cases, the temperature set-point is equal to 20 °C, with a dead band of 1 K. However, different set-point values are examined. Finally, three different control strategies of the radiator water inlet temperature are explored: (i) constant inlet temperature, (ii) weather compensation and (iii) fast restart.

### ***4.6.2 Constant water inlet temperature control strategy***

In these cases, the water inlet temperature is constant during the year and set to the nominal value, i.e. 80 °C for cases *R1* and 60 °C for cases labelled *R2*.

#### Cases *R1*

In this case, the smaller radiator, fed with water at 80 °C, is considered. Figure 4.21 represents the cumulative distribution of the mean operative temperature ( $T_{op}$ ) in the comfort zone, for the working time (7:00-20:00 each day), obtained locating the temperature sensor in different positions (*A*, *B* and *C*). The dashed lines represent the target band of the operative temperature required, in order to guarantee adequate comfort conditions (19.5-20.5 °C).

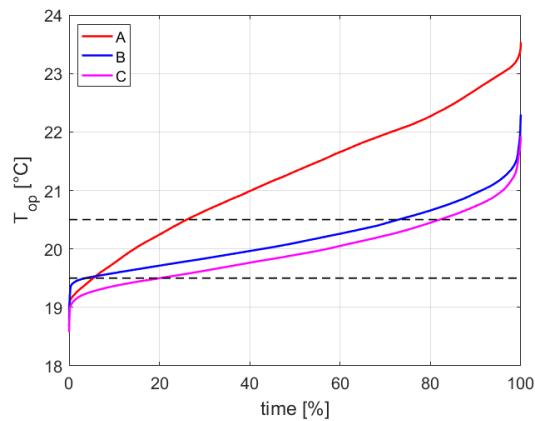


Figure 4.21. Cumulative distribution of the operative temperature of the comfort zone.

In Figure 4.21, it can be noted that if the sensor is located in position *A*, the curve is quite similar to a steep straight line, whilst case *B* and *C* exhibit flatter curves. In particular, it can be noted that curves *C* and *B* have the same shape and are only shifted. Since in Case *A* the cumulative operative temperature distribution in the comfort zone rapidly increase, the comfort time  $t_{conf}$ , i.e. the time percentage in which the mean operative temperature is between 19.5 and 20.5°C, is not very high (only 20.66% of the time). In fact, as reported also in Table 4-10, in this case the overheating time ( $t_{hot}$ ), that is the time percentage in which the mean operative temperature is greater than 20.5°C, is around 74%, revealing that the zone is often overheated. Sensor position *B* and *C*, on the contrary, guarantee comfort conditions for reasonable time interval, over the 60% of the working time, as represented by the flatter temperature distribution.

Table 4-10. Comfort and overheating time ( $t_{conf}$  and  $t_{hot}$ ) in the comfort zone for different position of the sensor.

Sensor position	$t_{conf}$ [%]	$t_{hot}$ [%]
<b>A</b>	20.7	74
<b>B</b>	69.2	27.1
<b>C</b>	61.9	18.0

The reason of the very different results obtained locating the sensor in position *A* instead of positions *B* and *C* could be explained analysing Figure 4.22, which represents the operative temperature distribution, at 1 m height from the floor, when the sensor (identified by the red dot) reaches the upper value of the control band (20.5 °C). In this figure it can be noted that, in each case, temperatures in position *B* and *C* do not differ significantly to those in the comfort zone (highlighted by the red rectangle), whilst the operative temperature in position *A* is the lowest in the room. This means that, as it can be seen in Figure 4.22 (a), when the sensor located in position *A* measures the operative temperature equal to 20.5 °C, the rest of the room is at a higher temperature, explaining the high overheating time observed for the comfort zone.



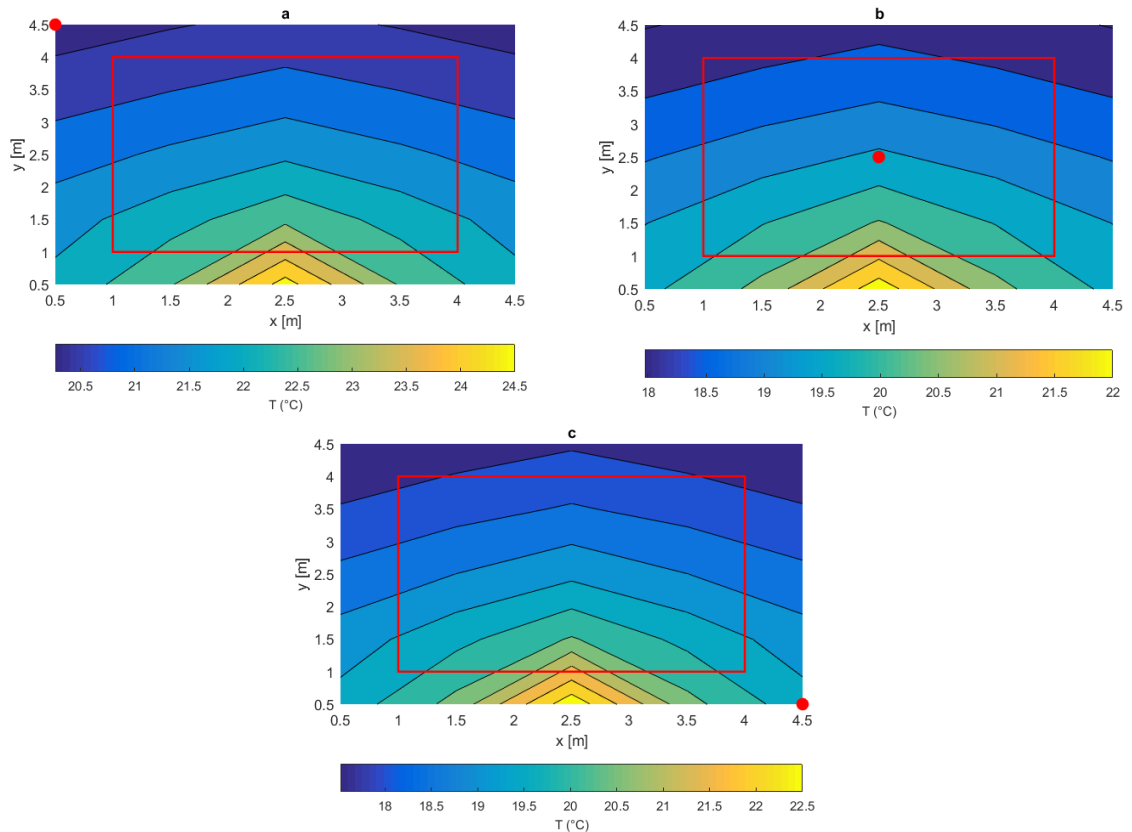


Figure 4.22. Operative temperature distribution at 1 m height from the floor, when the indoor temperature reaches the upper value of the control band (20.5 °C). a, b, c refers to the sensor position, highlighted with the red point. The red rectangle represents the comfort area.

Figure 4.23 shows the comparison between the trends of the operative temperature measured by the sensor and the mean operative temperature of the comfort zone, for two typical cold days. If the sensor is located in position A (Figure 4.23a), significant overheating can be observed. This is due to the fact that the mean operative temperature of the comfort zone rapidly increases when the heating system is turned on. On the contrary, the operative temperature in the room location in which the sensor is placed rises more slowly, as it can be appreciated comparing the slope of the red dotted line, that represents the operative temperature of the sensor in A (see Figure 4.19), to the blue solid line, that is approximately vertical during the restart of the heating system. This different behaviour represented in Figure 4.23a is due to the fact that the sensor is located far from the emitter and close to an external wall. In fact, the operative temperature in position A is strongly affected by the inner surface temperature of the external wall, that rises slowly due to the high thermal inertia; moreover as shown in Figure 4.22 the area close to the external wall in front of the emitter is colder than the inner areas of the room. For these reasons, in Figure 4.23a a time delay between the instants in which the sensor and the comfort zone reach the upper value of the target band could be appreciate. This delay is equal to 4 hours for the first day, and 8 hours for the second day.

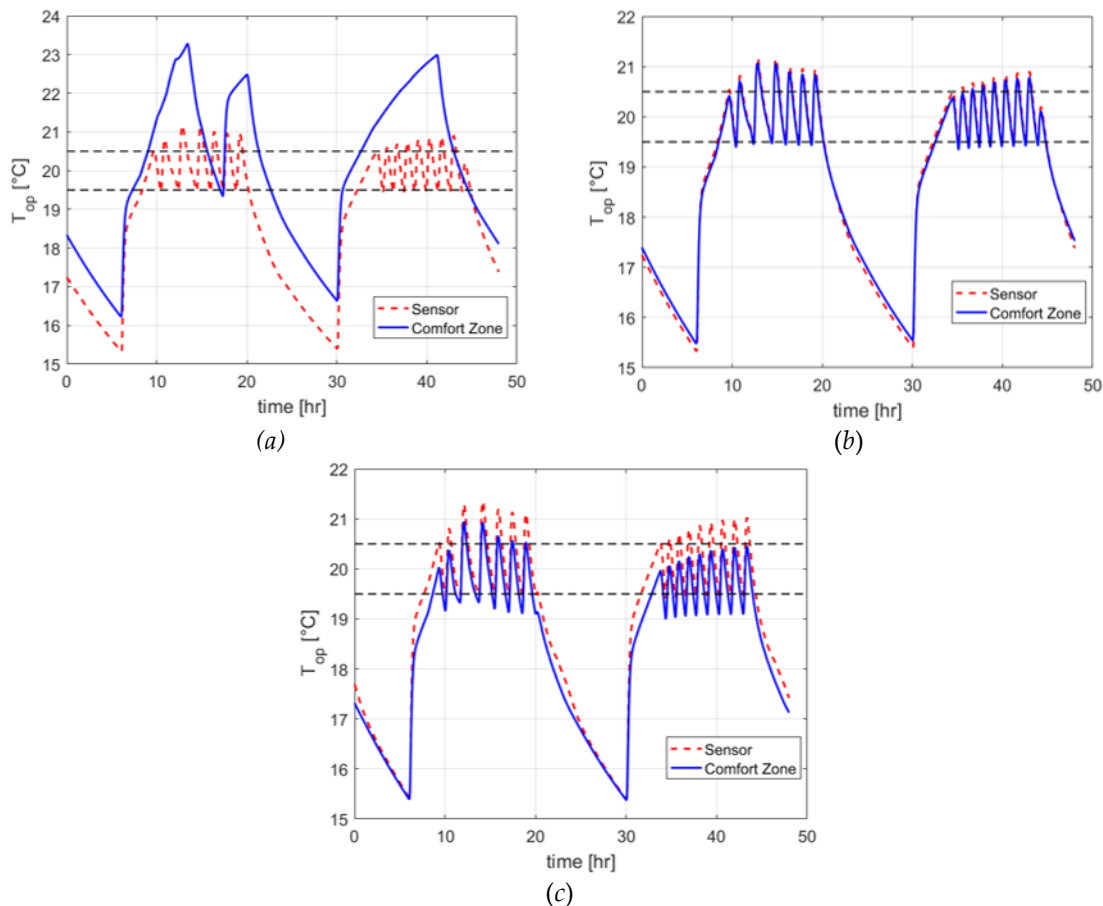


Figure 4.23. Comparison between the operative temperature of the sensor and in the comfort zone, for two typical days of the year. The sensor is in position A (a), B (b) and C (c).

On the contrary, if the sensor is located in *B* (Figure 4.23 b), the trends of the operative temperature of the sensor and of the comfort zone are very similar, that means that there is not an appreciable time delay during the sensor operations. Finally, with the sensor in position *C* (Figure 4.23c), slightly undercooling of the comfort zone is observed, but again no time delay in the reach of the upper value of the target band is observed.

The fact that in position *B* and *C* the operative temperature trends measured by the sensor are very similar to those obtained in the comfort zone (in position *C* the little undercooling can be reduced modifying the set-point value) enables to the control system to react to the variations of the operative temperature of the comfort zone with a limited time delay. On the contrary, if the sensor is placed in *A* the control system shows an evident time delay with respect to the operative temperature of the comfort zone.

In Table 4-11 the following averaged parameters, by means of which the controls system behaviour is evaluated, are listed for each sensor position:

- the average heating time (interval in which the radiator is turned on) between two consecutive shutdowns of the radiator ( $t_{on}$ );
- the average shutdown time (night is not considered) ( $t_{off}$ );



- the seasonal operating time (i.e. the seasonal time in which radiators are on) ( $t_{on,y}$ );
- the seasonal energy released by the radiator to the thermal zone ( $E$ ).

From the results collected in Table 4-11, it can be seen that if the sensor is located in position A, the average heating time  $t_{on}$  is around 235 minutes, whilst if the sensor is in position B and C,  $t_{on}$  falls down of approximately the 90%.

Table 4-11. Control system dynamics and energy demand with different sensor position (A, B, C).

Sensor position	$t_{on}$ [min]	$t_{off}$ [min]	$t_{on,y}$ [hr]	E [kWh]
A	235	780	1061	1631
B	27	161	461	1422
C	22	151	401	1370

The analysis of the average shutdown time ( $t_{off}$ ) reveals that since the sensor in position A leads to significant overheating, the time required for the temperature to decrease down to 19.5 °C is more than 12 hours; on the contrary in case B and C  $t_{off}$  is around 2.5 hours.

Considering the seasonal operating time  $t_{on,y}$ , it can be remarked that locating the temperature sensor in A determines the highest value, that is more than twice the value obtained for Case B and C. However, the heating demand in Case A is only 15% higher than Case B, whereas Case C is characterised by energy savings of 3.6% with respect to Case B.

Related to the control parameters mentioned above, Figure 4.24 shows the cumulative distribution of the daily number of on-off cycle of the thermal plant. In this figure it can be seen that if the sensor is located in A, the radiator switches on only once a day for about the 60% of the heating season, that means that radiator operates for a long time a day. On the contrary, Case B and C have similar cumulative distribution, characterised by a maximum of 10 daily on-off cycles. It can be appreciated that if the sensor is located near the radiator (Case C) the number of on-off cycle is slightly higher than if the sensor is positioned in the middle of the room.

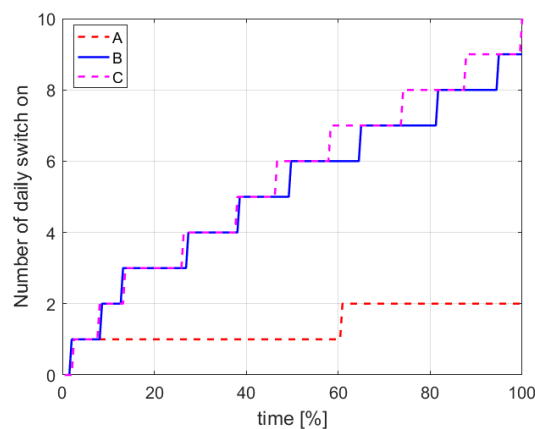


Figure 4.24. Cumulative distribution of the number of daily on-off cycles of the radiator.

Cases R1 with different control settings

By means of Figure 4.21 it has been observed that the best indoor comfort conditions are achieved locating the thermostat sensor in *B*, i.e. in the middle of the comfort zone. However, this location is “ideal” and positions *A* and *C* are more realistic ones. Therefore, in order to improve comfort conditions obtained with the sensor located in more realistic positions, the temperature set-point and dead-band are modified.

Since in Case A significant overheating is evidenced, in case labelled *Abis* the temperature set point is moved down from 20 °C to 19 °C, whilst in case *Atris* the set point is 19.25 °C and the dead band is reduced to 0.5 K, so that the radiator is on between 19° C and 19.5 °C.

In Figure 4.25, the comparison between the cumulative distribution of the mean operative temperature of the comfort zone obtained with the sensor located in position *A*, with different settings is shown.

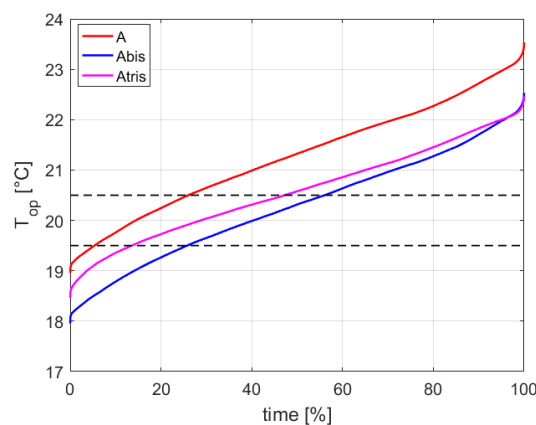


Figure 4.25. Cumulative distribution of the mean operative temperature of the comfort zone, sensor in position A.

In Figure 4.25 it can be noted that, moving down the set-point, the cumulative distribution of temperature is shifted down and the overheating time is significantly reduced. However the temperature distribution is not very flat and the comfort time improves but it is still too low, as reported in Table 4-12.

The change of the dead band width determines a different profile of the cumulative temperature distribution, which is a little bit flatter compared to the other cases, but again comfort time is not adequate. A further reduction of the set-point temperature does not represent a good solution, because the undercooling time will be higher and consequently the comfort time will still not be adequate.

Table 4-12. Comfort and overheating time ( $t_{comf}$  and  $t_{hot}$ ) in the comfort zone, with sensor in position A.

Case	$t_{comf}$ [%]	$t_{hot}$ [%]
<b>A</b>	20.7	74.0
<b>Abis</b>	30.2	44.0
<b>Atris</b>	33.7	52.0

In conclusion, it can be assessed that position *A* for temperature sensor, due to the distance from the emitter and its proximity to external wall, can introduce energy losses during the heating season due to the non-optimal work of the control system. In fact, sensors located close to external walls far from the emitters determine a slowest reaction of the thermal plant, due to the high thermal inertia of the external wall that, by means of its internal surface temperature, strongly affects the operative temperature. This leads to an increase of the time delay in the operations of the thermal plant, as highlighted by  $t_{on}$  and  $t_{off}$  parameters (see Table 4-11), that must be taken into account for a good behaviour of a control system based on a closed loop logic.

#### Sensor in position C

In the first simulations, it has been highlighted that the performances of the control system with the temperature sensor located in position *B* and *C* are quite similar and it has been noted that the cumulative temperature distribution seems to have the same shape (see Figure 4.21). Analysing the effect of different control set-point values for a sensor placed in position *A*, it has been shown that a change of set-point leads to a shift of the cumulative temperature distribution. This means that, in principle, is possible to “tune” the results obtained with the sensor placed in *C* by varying the set-point. A numerical test is made with the setpoint set to 20.2 °C for the sensor in position *C*.

In Figure 4.26, the new (labelled *Cbis*) set-point is compared to the distribution obtained by sensor in position *B*. It is possible to appreciate that the red dashed line (referring to case *Cbis*) is superimposed to the blue line, that refers to case *B*. Therefore, numerical results demonstrate that it is always possible to “tune” the sensor placed near to the radiator, as in the case of thermostatic valves, in order to obtain the same results that can be reached by the sensor in position *B*.

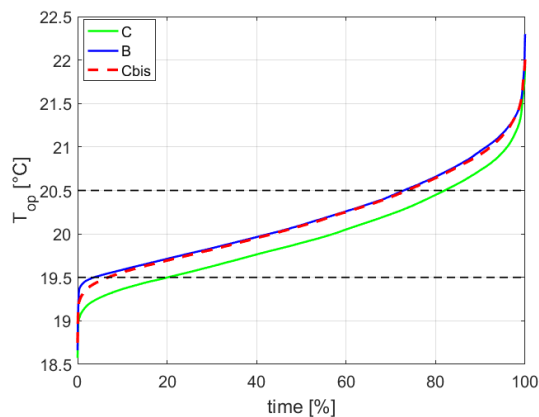


Figure 4.26. Comparison of the cumulative distribution of the mean operative temperature in the comfort zone, for sensors in position *C*, with different settings, and Case *B*.

### Cases R2

Cases labelled *R2*, as previously stated, are characterised by a bigger radiator compared to case *R1*; the same nominal water flow is considered, but the inlet water temperature is set to 60 °C. Thus, the goal of the following analysis is to investigate if the cumulative mean operative temperature of the comfort zone and the control system dynamics are affected by the emitter size.

Figure 4.27 shows the cumulative distribution of the mean operative temperature in the comfort zone obtained locating the temperature sensor in different positions. Comparing these trends to the one represented in Figure 4.21, referring to case *R1*, no big differences can be observed: sensor in position *A* leads to important overheating, whilst with sensor in position *B* and *C* curves are flat, similarly to case *R1*.

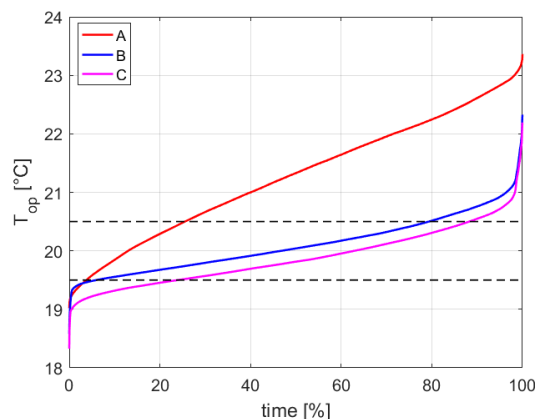


Figure 4.27. Cumulative distribution of the mean operative temperature in the comfort zone, for cases *R2*, for different thermostat sensor position (*A*, *B* and *C*).

In order to better investigate the effect of the radiator size on comfort conditions, the comparison of the cumulative distribution of the operative temperature in the comfort zone obtained with radiator *R1* and *R2*, with the sensor in *B*, is represented in Figure 4.28. In this figure, it can be observed that

with lower inlet water temperature (60 °C, Case *R2*), the operative temperature overcomes 20.5 °C for less time during the heating season if compared to Case *R1*.

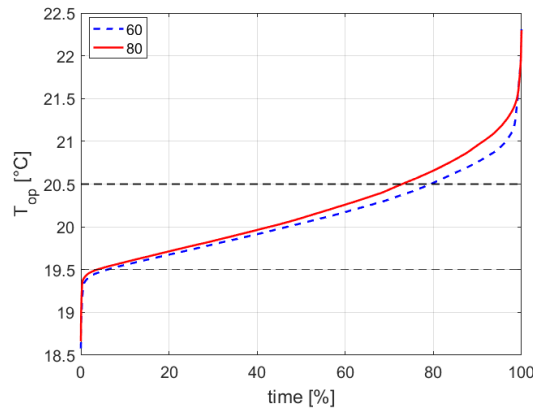


Figure 4.28 Comparison between cumulative mean operative temperature for case *B*, with inlet water temperature of 80 °C (red solid line) and 60 °C (blue dotted line).

Trends similar to those reported in Figure 4.28 are observed for each sensor position. This is confirmed also by the results reported in Table 4-13, where comfort and overheating time obtained for the three sensor positions are reported together with their difference ( $\Delta$ ) with the results concerning Case *R1*.

From this Table it is possible to appreciate that, for each sensor position, the adoption of a bigger radiator (fed with water at a lower temperature) determines an increment of the comfort time. However, it can be noted that the increase of the comfort time depends on the sensor position; in fact, the highest difference is observed for sensor in *B* (+4.3%) whilst in Case *A* the difference of comfort time is only 1%. In addition, Table 4-13 shows that the adoption of large radiators (*R2*) implies a reduction of the overheating time around 6% for Case *B* and *C*; on the contrary, if the sensor is in *A*, overheating slightly increased (+0.5%).

Table 4-13. Comfort parameters for cases with radiator water inlet temperature of 60 °C.

Sensor position	$t_{conf}$ [%]	$\Delta$ [%]	$t_{hot}$ [%]	$\Delta$ [%]
<b>A</b>	21.7	+1	74.5	+0.5
<b>B</b>	73.5	+4.3	20.5	-6.6
<b>C</b>	64.3	+2.4	11.7	-6.3

The different size of the radiator affects also the control system dynamics, as it can be inferred from the results collected in Table 4-14. In fact, the biggest is the radiator and the greater is its thermal capacity. The increment of the thermal inertia of the radiator influences the average heating time ( $t_{on}$ ), that rises of about 15% for cases *B* and *C*, since surface temperature of the radiator rises slower than for case *R1*. As a consequence, also the seasonal operating time of the heating system ( $t_{on,y}$ ) increases: increments of 4%, 8% and 9% are observed for Case *A*, *B* and *C*, respectively. The higher thermal inertia of the radiator affects also the

average shutdown time ( $t_{off}$ ); increments of 2%, 7% and 4% for case A, B and C are obtained, respectively. These increments are due to the fact that the radiator continue to release energy to the zone, after it has been turned off, until a thermal equilibrium with the zone is achieved: the more is the thermal capacity of the radiator, the higher is the time required by the radiator to achieve a thermal equilibrium.

Table 4-14. Control parameters for cases with radiator water inlet temperature of 60 °C, and comparison ( $\Delta$ ) with case R1.

Sensor position	$t_{on}$ [min]	$\Delta$ [%]	$t_{off}$ [min]	$\Delta$ [%]	$t_{on,y}$ [hr]	$\Delta$ [%]	E [kWh]	$\Delta$ [%]
A	235	0	796	+2.1	1107	+4.3	1592	-2.4
B	31	+15	173	+7.5	500	+8.5	1372	-3.5
C	25	+14	157	+4	439	+9.5	1320	-3.6

Finally, even if the seasonal and the average heating time increase adopting a bigger radiator. The energy demand decreases of about 3% with respect to cases labelled R1, due to the lower inlet water temperature. It has to be underlined that this energy demand does not take into account the heat generation system, thus the potential energy consumption reduction could be greater if heat pumps and condensing boilers are adopted, since these heat generators are characterised by better performances whit lower inlet and return water temperature respectively.

### 4.6.3 Use of weather compensation

In the previous sections it has been shown that even putting the sensor in the “ideal” position, the maximum comfort time is about 70%. This is due to the fact that the radiator operates with a constant water flow at a constant temperature, releasing to the office the same amount of power independently by the instantaneous thermal load, which varies continuously during the season. In fact, the heat losses of the office are not constant, according to variable external conditions. For these reasons, the comfort time in the comfort zone can be improved by adding a weather compensation to the control logic. Following this logic, the radiator inlet water temperature is changed according to the curves represented in Figure 4.29. The temperature sensor is still located in position A, B and C.

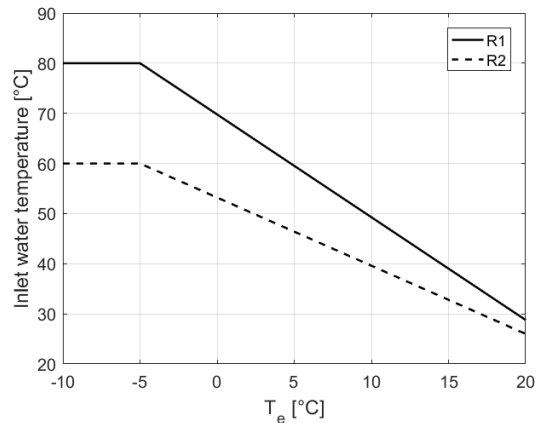


Figure 4.29. Weather compensation curves for Case R1 and R2.

Cases R1

Referring to Figure 4.29, it can be noted that, adopting the weather compensation curve, the radiator inlet water temperature is set to its nominal value if the external air temperature is lower than  $-5\text{ }^{\circ}\text{C}$ , whilst for higher outdoor temperatures the inlet water temperature is reduced up to  $35\text{ }^{\circ}\text{C}$  (if the external temperature is  $17\text{ }^{\circ}\text{C}$ ).

In Figure 4.30 the cumulative distribution of the mean operative temperature of the comfort zone obtained locating the sensor in different positions is reported. It can be noted that, if the sensor is in B or C, the temperature distribution is almost all contained between the target comfort conditions. Comparing the temperature profiles obtained adopting the weather compensation (see Figure 4.30) to the ones obtained without it (see Figure 4.21), an important reduction of the overheating is highlighted for Case B and C. On the contrary, the sensor in A still determines significant overheating.

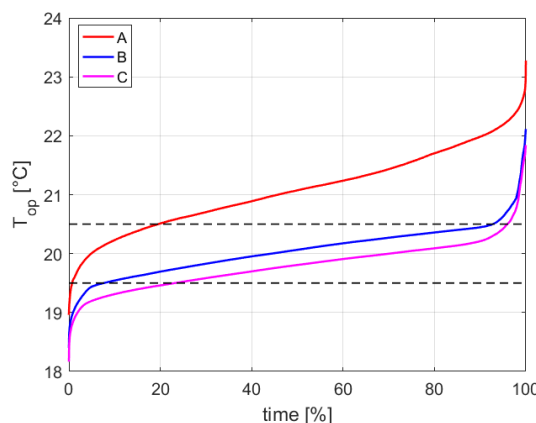


Figure 4.30. Cumulative distribution of the mean operative temperature of the comfort zone.

Analysing the parameters collected in Table 4-15, it is possible to appreciate that by means of weather compensation, that permits to modulate the heating power released by the radiator to the room, the overheating time in the comfort

zone is drastically reduced (less than 10%) if the sensor is located in *B* and *C*. The reduction of the overheating time determines an increase of the comfort time, that is over 85% if the sensor is in its “ideal” position. The comparison of the results obtained adopting the weather compensation to the respective Case in which the weather compensation is not used, evidences increments ( $\Delta$ ) of 16% and 11% of the comfort time, for Case *B* and *C*, whereas if the sensor is placed in *A*, comfort conditions are reduced (-1.9%). In addition, for Case *A*, a 6% increment of the overheating time, that now is around 80%, is observed. On the contrary, for both Case *B* and *C* overheating is drastically reduced by the adoption of the weather compensation: reduction of 20% and 14% are observed for Case *B* and *C* respectively.

Table 4-15. Comfort and overheating time ( $t_{comf}$  and  $t_{hot}$ ) in comfort zone adopting the weather compensation.

Sensor position	$t_{comf}$ [%]	$\Delta$ [%]	$t_{hot}$ [%]	$\Delta$ [%]
<b>A</b>	18.8	-1.9	80	+6
<b>B</b>	85.1	+16	7.3	-20
<b>C</b>	72.7	+11	4.1	-14

The different effect of the weather compensation on the comfort conditions depending on the sensor position can be explained keeping in mind that the sensor in position *B* and *C* reacts as it is measuring the mean operative temperature of the comfort zone (see Figure 4.23). On the contrary, the temperature sensor in position *A* is characterized by a great time delay, that is amplified by the modulation of the power released by the radiator to the room, causing a rise of the overheating if the weather compensation is adopted.

In Table 4-16, the characteristic parameters describing the control system behaviour, obtained adopting the weather compensation, are reported. These parameters are greatly affected by the weather compensation: the mean heating time ( $t_{on}$ ) is more than two (sensor in position *A*) and three (sensor in *B* and *C*) times the respective values obtained without the weather compensation. Consequently, also the seasonal heating time ( $t_{on,y}$ ) is increased: +123%, +215% and 216% for Cases *A*, *B* and *C*.

Table 4-16. Control parameters for cases with weather compensation.

Sensor position	$t_{on}$ [min]	$t_{off}$ [min]	$t_{on,y}$ [hr]	$E$ [kWh]
<b>A</b>	725	800	2369	1635
<b>B</b>	132	263	1456	1378
<b>C</b>	94	215	1265	1318

In addition, also the average shutdown time ( $t_{off}$ ) is increased by the adoption of the weather compensation: increments of 3%, 64% and 42% are observed. These results can be explained considering that massive elements (like walls), can store more heat if the weather compensation is adopted, due to the long time in



which the heating system is on. In this way, when the heating system is off, massive elements can release additional energy to room, slowing the indoor air temperature decrease.

Finally, it would be expected that, as the mean and the seasonal heating time have greatly increased, the total energy demand have increased too. This is true if the sensor is located in *A*, but it has to be highlighted that even if the seasonal heating time has increased more than twice, the energy demand has growth of only the 0.3% with respect to the case without the weather compensation. Moreover, in Cases *B* and *C*, adopting the weather compensation, the energy demand is reduced of 3% and 4% respectively.

In Figure 4.31 the cumulative distribution of the number of daily on-off cycle of the heating system is represented. In agreement with the control parameters reported in Table 4-16, if the sensor is in *A*, the heating system performs for almost the heating season only one on-off cycle per day. A reduction of the number of on-off cycle can be appreciate also for sensor located in *B* and *C*, by comparing Figure 4.31 to Figure 4.24. In fact, without weather compensation, for case *B*, for 50% of the heating season the number of daily on-off cycle is 5; whilst adopting the weather compensation, the heating system performs only 3 on-off cycle.

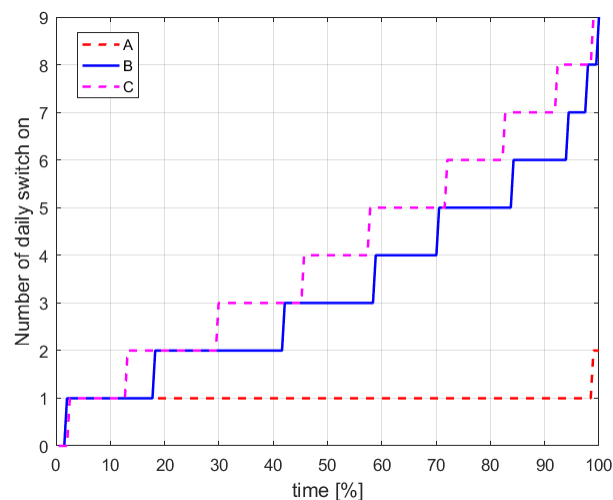


Figure 4.31. Cumulative distribution of the number of daily on-off cycles of the heating system adopting the weather compensation.

In conclusion, it can be assessed that if the indoor temperature sensor is located in position *B* and *C*, the weather compensation increases the performances of the control system and of the comfort time in the comfort zone and leads to a reduction of the total energy demand. On the contrary, when the sensor is located in *A*, the weather compensation is responsible of an increase of the overheating and consequently of a worsening of indoor comfort conditions.

Cases R2

According to Figure 4.29, the water inlet temperature for radiator *R2*, adopting the weather compensation, is set to 60 °C for external air temperatures lower than -5 °C, otherwise the it is reduced up to 26 °C (when the outdoor temperature is 20 °C). The cumulative distribution of the mean operative temperature of the comfort zone is represented in Figure 4.32. The profiles reported in Figure 4.32 are very similar to those represented in Figure 4.30 concerning the adoption of radiator *R1*: if the sensor is in *B* and *C*, the operative temperature is almost all contained in the target band; whilst the sensor located in position *A* is responsible of important overheating and guarantees target comfort conditions for a short time.

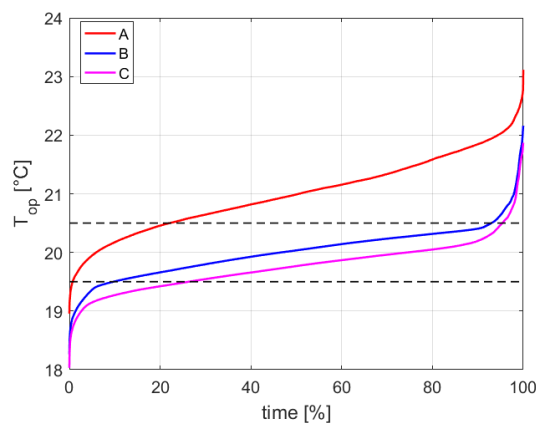


Figure 4.32. Cumulative distribution of the mean operative temperature of the comfort zone in cases *R2* adopting the weather compensation, for different sensor position.

In Table 4-17, the results related to the comfort conditions in the comfort zone are reported. Again, it can be remarked that locating the sensor in *A*, comfort conditions are maintained only for 21.4% of the working time, whilst for around 78% of the total time overheating conditions appears. If the sensor is in *B*, comfort time is 83%, whilst in position *C* it is reduced to 69%. In addition, in Table 4-17 are reported also the differences of comfort conditions obtained with radiator *R2* and *R1*, considering the adoption of the weather compensation.

Table 4-17. Comfort parameters for cases *R2* with weather compensation, for different sensor position, and comparison ( $\Delta$ ) with results obtained for radiator *R1*.

Sensor position	$t_{comf}$ [%]	$\Delta$ [%]	$t_{hot}$ [%]	$\Delta$ [%]
<b>A</b>	21.4	+2.6	77.9	-2.1
<b>B</b>	83.2	-1.9	7.0	-0.3
<b>C</b>	69.0	-3.7	4.6	+0.5

The results evidence that when the sensor is located in *A*, the comfort time is slightly increased (+2.6%) by adopting radiator *R2*, whereas in the other case

radiator *R2* determines a comfort time reduction (-1.9% and -3.7% for Case *B* and *C*, respectively).

The parameters by means of which the control system behaviour is described are reported in Table 4-18 together with the percentage difference with the case *R1*, considering the weather compensation. From this Table, it can be observed that the mean heating time increases of around 8% if the sensor is in *B* or *C*, whilst in case *A* the difference between the two radiators is reduced to 2%. The increment of the mean heating time enables to store more energy in the massive elements, thus also the mean shutdown time ( $t_{off}$ ) increases with the adoption of the bigger radiator, except if the sensor is located in *A*: in this case an 8% reduction of  $t_{off}$  is obtained. However, the seasonal heating time ( $t_{on,y}$ ) seems not to be affected by the radiator size, since differences are around than 1% for each sensor position, except the case in which the sensor is in the “ideal” position (*B*), for which the discrepancy due to the radiator is only 0.1%.

Finally, as evidenced for the constant inlet temperature cases, the adoption of a bigger radiator, fed with water at lower temperature, determines a reduction of the energy demand of around 3%, slightly depending on the sensor position.

Table 4-18. Control parameters for cases *R2*, for different sensor position, and comparison ( $\Delta$ ) with cases *R1*, considering the weather compensation.

Sensor position	$t_{on}$ [min]	$\Delta$ [%]	$t_{off}$ [min]	$\Delta$ [%]	$t_{on,y}$ [hr]	$\Delta$ [%]	E [kWh]	$\Delta$ [%]
<b>A</b>	741	+2.2	736	-8.0	2395	+1.1	1583	-3.2
<b>B</b>	143	+8.3	292	+11	1457	+0.1	1342	-2.6
<b>C</b>	101	+7.5	234	+8.8	1255	-0.8	1280	-2.9

#### 4.6.4 Fast restart strategy

For all the cases analysed in the previous sections, it can be remarked that the sum between comfort and overheating time is lower than unity, revealing the presence of undercooling conditions. Except cases characterised by the temperature sensor located in *A*, for which undercooling is close to zero, the undercooling time is higher than 10%. Undercooling conditions appear in the first hours of the day, due to a slow rise of the air temperature after the night. In fact, in critical conditions, one hour of preheating (from 6:00 to 7:00) is not able to guarantee adequate comfort conditions at the beginning of the working time. This problem reveals that the emitter, in Case *R1*, can be considered as slightly undersized.

In cases in which radiators are sized for low inlet water temperature (Case *R2*), this inconvenient can be overcome imposing a high inlet water temperature during the restarts. This is possible if the radiators are coupled to gas boilers for which water temperature of 80 °C are possible. On the contrary, this is not

possible with conventional heat pumps able to guarantee a maximum water temperature of 55/62 °C. In the following simulations, during the preheating hour, the radiator inlet water temperature is set to 80 °C if the operative temperature measured by the sensor is below the lower value of the control band of the thermostat (19.5 °C), otherwise the inlet water temperature is set according to the weather compensation curve (see Figure 4.29).

In comparison with all the previous cases, the adoption of the fast restart strategy leads to the highest overheating of the comfort zone, for sensor in position *A*, as represented in Figure 4.33. In fact, in this case, the overheating time is more than 90% and consequently comfort conditions are guaranteed only for 7% of the total working time, as reported in Table 4-19.

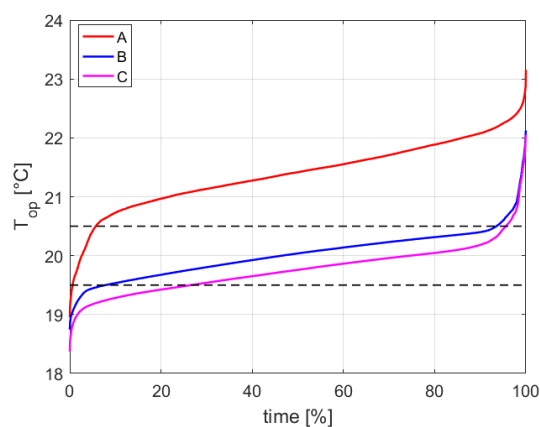


Figure 4.33. Cumulative distribution of the mean operative temperature in the comfort zone, for fast restart cases.

On the contrary, if the sensor is located in *B*, the cumulative distribution is almost all contained in the target band, in fact comfort conditions are guaranteed for 86.3% of the working time, which represents the maximum value obtained among all the considered cases. Moreover, the overheating time is around 6% of the working time. Comparing these results to the ones obtained adopting the weather compensation without the fast restart strategy, an increment of 3.2 % in the comfort time and a reduction of 0.5% of the overheating time can be observed.

Table 4-19. Comfort and overheating time for fast restart cases, and comparison to cases without fast restart strategy, Case *R2*.

Sensor position	$t_{comf}$ [%]	$\Delta$ [%]	$t_{hot}$ [%]	$\Delta$ [%]
<b>A</b>	6.9	-15	92.7	14.8
<b>B</b>	86.3	3.2	6.5	-0.5
<b>C</b>	69.4	0.4	4.6	0

Finally, if the sensor is located in *C*, the overheating time is the lowest compared to the other cases, but the comfort time is lower than the one obtained with the sensor in position *B* because of significant undercooling conditions.

The adoption of the fast restart strategy affects the heating system performances, whose parameters are reported in Table 4-20. Since during the restart the emitter releases an “extra” power, due to the high temperature of the inlet water, the mean heating time ( $t_{on}$ ) decreases in all the cases: for case *A* the decrease is of 7.8% (from 741 to 683 minutes), whilst for cases *B* and *C* the decrement is around 30%, with a mean heating time lower than two hours.

Due to the high overheating that characterises cases with the sensor in position *A*, the mean shutdown time ( $t_{off}$ ) in this case is greater than 13 hours, with an increment of 7.5% with respect the case without the fast restart strategy. On the contrary, if the sensor is in position *B* and *C*, shutdown time decreases of around 18%. The adoption of the fast restart strategy determines also the reduction of the seasonal heating time ( $t_{on,y}$ ) which decreases of 8% , 15% and 18% for sensors located in *A*, *B* and *C*, respectively.

Table 4-20. Control parameters for fast restart cases, sensor in different positions, and comparison to cases without the adoption of the fast restart strategy, Case R2.

Sensor position	$t_{on}$ [min]	$\Delta$ [%]	$t_{off}$ [min]	$\Delta$ [%]	$t_{on,y}$ [hr]	$\Delta$ [%]	E [kWh]	$\Delta$ [%]
A	683	-7.8	791	7.5	2197	-8.3	1646	4
B	102	-29	238	-19	1232	-15	1345	0.2
C	70	-31	192	-18	1024	-18	1282	0.2

Finally, it would be expected that the adoption of the fast restart strategy, with the aim to increment the comfort conditions reducing the undercooling, would lead to an increment of the total energy demand. Comparing the results collected in Table 4-20 with those reported in Table 4-18, it is possible to appreciate that if the sensor is in position *B* and *C*, the energy demand increases only 0.2%. On the contrary, when the sensor is located in *A*, the increment of the energy demand is more relevant, around 60 kWh (+4%).

In conclusion, it is possible to assess that the adoption of the fast restart strategy in addition to the weather compensation in presence of sensor in position *B* and *C* could be a highly recommended action in order to improve the performances of the heating system. In fact, it leads to an increment of the comfort conditions of about the 3% with the same energy demand (only +0.2%). On the contrary, if the sensor is in *A*, due to the non-optimal behaviour of the control system caused by the position of the sensor, the adoption of the fast restart control leads to an increment of indoor uncomfortable conditions with an increase of the energy demand and for these reasons this strategy cannot be recommended in this case.

## 4.7 Conclusions

In this *Chapter*, additional models for the solution of the thermal balance of a zone have been described, together with the GUIs that drive the user to the implementation of these models. More in detail, by means of the *radiative model*, the radiative heat transfer between the internal surfaces of a thermal zone are exactly evaluated, enabling the evaluation of the spatial distribution of the radiative temperature in a room. On the contrary, the *convective model*, based on a zonal-model, allows the determination of an approximated spatial distribution of the air temperature in a room, by splitting the room in several air-cell and evaluating the convective air flow pattern. Finally, the *radiative* and the *convective models* are coupled in the *fully detailed model*, by means of which the spatial distribution of the operative temperature can be estimated.

The calculation procedure adopted in ALMABuild for the evaluation of the view factors required by the *radiative model*, based on the MATLAB Contour Double Integral Formula (CDIF), has been validated comparing the obtained view factors for a reference room with those of commercial software (i.e. Comsol and Trisco).

Then, the *radiative model* has been used in a case-study related to the evaluation of the thermal comfort conditions in a room, obtained by considering six different emitters (i.e. in-slab radiant floor, in-slab radiant ceiling, radiant suspended ceiling, hot water radiator, radiant wall and all-air system) and two building thermal insulations levels. The numerical results demonstrate that in-slab ceiling is characterized by the highest radiative power share (92%) and therefore the highest difference between radiative and convective temperature is remarked. The vertical distribution of the operative temperature has been calculated as a function of the emitter. About the behaviour of the emitters in presence of dynamic thermal loads, the numerical results demonstrate that all-air heating system is faster than radiant systems. The suspended radiant ceiling is 80% faster with respect to the in-slab radiant ceiling to raise the temperature of the room from 19 to 20.5 °C in presence of low thermal insulation of the walls. However, due to the reduced contribution of the convective heat transfer component in winter, radiant ceiling can have problems to provide enough thermal power to the thermal zone, in particular for rooms having a low thermal insulation. It has been shown that an increase of the envelope thermal insulation is able to reduce the maximum surface temperature of the emitters and it is responsible of a more uniform distribution of the inner surface temperature in the room. In order to study the local indoor thermal condition distribution in the room during the whole winter, the percentage of time in which the local PMV is within  $\pm 0.5$  (optimal comfort conditions) has been calculated in a series of dynamic simulations by varying the emitter and the room thermal insulation. The results show that radiant floor is able to guarantee good performances both

in thermally insulated and in non-thermally insulated rooms. On the contrary, radiant ceiling and radiant vertical walls have to be used only in rooms having a good thermal insulation level in order to optimize their performances. As a general conclusion, the detailed numerical results presented in this section demonstrate that in buildings with very low transmission losses the differences existing among the selected emitters are strongly attenuated. In fact, a more uniform distribution of the temperature of the inner surfaces of the room is able to reduce the differences between convective and radiant emitters in terms of capability to obtain uniform indoor thermal comfort conditions. On the contrary, in presence of low thermal insulation levels a proper selection of the heat emitter can drastically reduce the local thermal uncomfortable conditions in a thermal zone.

Finally, the *fully detailed model* has been used in order to study the influence of the position of the indoor temperature sensor on the reached comfort conditions in the room and on the behaviour of the heating system, based on radiators.

In this study, three different sensor positions have been considered by placing the sensor of the wall faced to the radiator (*A*), in the middle of the comfort zone (*B*) and close to the radiator (*C*). Moreover, two different sizing rules for the emitters have been considered: radiator sized assuming an inlet water temperature of 80 °C (*R1*), radiator sized setting the inlet water temperature at 60 °C (*R2*). In addition, three different control strategies have been studied (constant inlet water temperature, weather compensation and fast restart strategy).

The results show that position *A* is not a good position for the temperature sensor, since it is too far from the emitter and strongly affected by the thermal inertia of the external walls. For these reasons, the temperature sensor in *A* is not able to adequately regulate the heat released by the emitter to the thermal zone. In fact, important overheating (more than 70% of the working time) are observed in the comfort zone for these cases. Even modifying the temperature set-point and dead-band or changing the radiator sizing, comfort conditions obtained locating the sensor in *A* cannot be significantly improved. On the contrary, when the sensor is placed in *B* the comfort zone is able to maintain the correct comfort condition for long time. If the sensor is placed in *C* the results are similar to those obtained with sensor in *B*; it has been demonstrated that the sensor can be tuned by modifying the set-point in order to align the results to those obtained placing the sensor in *B*.

Analysing the heating system behaviour, it is possible to see that, if the sensor is in placed in *A*, the heating system reacts with an important (more than 3 hours) time delay to the change of indoor conditions, contrary to cases in which the sensor is placed in *B* and *C*. The seasonal energy demand is strongly related to the comfort conditions: Case *A* is the most energy consuming because the position of the sensor is responsible of important overheating. The sizing of the radiator influences the seasonal heating time, that is greater for the biggest

radiator (*R2*). Larger radiators and lower inlet temperature (60 °C) determine a reduction of energy consumption compared to a small radiator (*R1*) fed with water at 80 °C.

The adoption of a weather compensation, that reduces the inlet water temperature according to the value of the external air temperature, determines an increase of comfort conditions in all the cases coupled to a reduction of the energy demand, except when the sensor is placed in *A*.

Finally, the fast restart strategy, that can be adopted for large radiators (*R2*) in addition to the weather compensation with the aim to reduce the undercooling conditions during the first hours of the working time, determines an improvement of comfort conditions coupled to a slight increment of energy consumptions.

In conclusion, the analysis of the case studies presented in this *Chapter* evidences the capability of ALMABEST to give detailed information about the optimal coupling of the emitter and thermal zones by taking into account the dynamic behaviour of the envelope elements. In addition, ALMABEST can be proficiently used in order to study the effect of the control strategies on energy consumptions and comfort conditions of a thermal zone.



# Optimizations in building design

---

## Abstract

The enhancement of the energy efficiency of buildings requires to designers the evaluation of several building layouts and energy consumptions. Optimization algorithms can help designers to find a detailed evaluation of the best solution, among different configurations, which allows to achieve this goal. In this *Chapter*, after a brief overview on the main concepts of optimization problems and on examples of the integration of optimization algorithms into simulation-based design processes, the coupling of Matlab Optimization Toolbox with ALMABuild is explored by means of five case-studies.

The first four cases are related to single-objective optimization problems, in which it is required to minimize the total (heating and cooling) annual energy demand of a building by finding the optimal configuration of different combinations of the three design parameters considered: the insulation thickness of the external opaque envelope elements, the total clear area and the overhang length. For each case study the same methodology has been adopted: firstly, few numerical simulations are carried out with the aim to determine the dependencies of the objective function (the energy demand) to the input parameters. Then, by means of the direct search Matlab optimization algorithm the local minimum curve and the global minimum of the objective function is found, refining the discretization of the input parameters.

Finally, in the fifth case study, a multi-objective optimization is performed. More in detail, windows exposition, insulation thickness and position within the envelope element stratigraphy and total clear area are varied with the aim to minimize the heating energy demand maximizing the indoor comfort conditions. It has been demonstrated as a pre-calculation of the sensitivity of the objective functions to the design parameters can be very useful in order to reduce the dimension of the design space, by obtaining a significant reduction of the calculation time needed to find the optimal solution of the problem.

---

## 5.1 Introduction

Optimization is a powerful process that can be applied to every discipline (mathematics, engineering, economy...) that is aimed to find the set of variables that determines the best (whatever is the criterion) solution of a problem, eventually under some constraints. Thus, optimization problems are characterised by three main features:

- Input parameters: they are the variables that affect the optimization problem;
- Objective function: it is the function, that represents a performance measure, that has to be maximized or minimized;
- Constraints: they can involve both the input parameters and the objective functions, and they consist of lower/upper bounds or they are described by means of equations or inequalities.

Optimization problems can deal with one or more objective functions: if a unique objective function is present, the optimization is defined as *single objective optimization*, otherwise we speak about *multi-objective optimization*. The simplest method that can be used for solving both single or multi-objective optimization problems is the *Brute force* approach. This approach consists in the evaluation of the objective function for each set of variables defined in the input parameter space. This method is clearly inefficient and can be used only if the evaluation of the objective function does not require a high computational cost (CPU time) and the input parameter space is limited.

Single and multi-objective optimizations are performed by means of different algorithms. Deterministic algorithms, i.e. methods developed by the classical branch of mathematic algorithms [125], can be applied for solving single objective optimizations. These methods are generally the fastest ones, since they use mathematical rules for moving toward the best solution. Depending on the features of the objective function and of the optimization problem, different approaches and algorithms can be used. As an example, if no constraints are provided to the optimization problem, the *Newton Method*, the first gradient-based approach proposed, can be adopted. Anyway, when the objective function is quadratic, the Newton method does not perform well and the *Simplex Method*, introduced by Spendley *et al.* [126] and upgraded by Nelder and Mead [127], should be used. On the contrary, if optimization problems are constrained, other approaches have been proposed: as an example, *linear* [128], *quadratic* [129] and *non-linear* [130] techniques are applied when the objective function is linear, quadratic or smooth.

Stochastic or random approach is applied for both single or multi-objective optimizations. Contrary to the deterministic approach, in this kind of algorithms randomness is added in different way, in order to mimic the typical evolution path toward the optimum observed in nature. As an example, *Genetic algorithms*

[131] are a class of stochastic methods that estimate the optimal solution of the objective function by the mimic of the evolution of species; the *Particle Swarm Optimization* [132] is another family of stochastic methods that aims to emulate the social behaviour of birds flocking whilst the *Simulated Annealing* [133] emulates the annealing heat treatment that is used in metallurgy for increasing the size of crystal and consequently reducing their defects.

Single-objective optimizations can deal with problems in which more than one output parameter is required to be maximized (or minimized). In this case, the multi-criteria approach is adopted and a single objective function is built up normalizing and summing different objectives. Therefore, the optimization problem, given  $n$  objectives to be optimized, can be written as follows:

$$\min f(w_1 f_1 + \dots + w_n f_n) \quad (5.1)$$

where the coefficients  $w_i$  represent appropriate weight coefficients for the specific problem. This kind of approach is more efficient and easier to implement compared to multi-objective optimizations; anyway, as it can be observed from (5.1), this approach requires the prior knowledge of the weights  $w_i$  that determine the compromise between the objective. Since generally values of weights are not known, multi-objective optimizations can start by assigning unitary weights to each objective. Contrary to single-objective optimizations in which the result is a single set of input parameters, multi-objective optimizations are characterised by several "optimal" configurations, that compose the so-called *Pareto frontier*. Once the Pareto frontier has been determined, the designer can select, among the set of "optimal" configurations, the one that fulfil the best trade-off among the objective functions within the designer needs.

The Pareto frontier concept requires the introduction of a new definition of optimality: the *Pareto optimality*. A certain input parameter configuration,  $\mathbf{x}_i$ , is said to be Pareto optimal if its objective functions are *non-dominated*. A solution, which is the vector of objective functions  $\mathbf{F}(\mathbf{x}_1)$ , composed by  $n$  objective functions  $f_i$ , dominates another solution, namely  $\mathbf{F}(\mathbf{x}_2)$  if:

$$\begin{cases} f_i(\mathbf{x}_1) \leq f_i(\mathbf{x}_2) & \forall i \\ \exists j : f_j(\mathbf{x}_1) < f_j(\mathbf{x}_2) \end{cases} \quad (5.2)$$

In order to clarify these aspects, consider Figure 5.1, in which values of two objective functions  $f_1$  and  $f_2$  are represented for three different configurations  $A$ ,  $B$  and  $C$ .  $A$  is dominated by  $B$  since, as represented in Figure 5.1,  $f_1(\mathbf{x}_A) > f_1(\mathbf{x}_B)$  and  $f_2(\mathbf{x}_A) > f_2(\mathbf{x}_B)$ , therefore  $A$  is not on the Pareto frontier. On the contrary,  $B$  and  $C$  compose the Pareto frontier, as they are non-dominated solutions. In fact,

it can be observed that  $f_1(\mathbf{x}_B) < f_1(\mathbf{x}_C)$  but  $f_2(\mathbf{x}_B) > f_2(\mathbf{x}_C)$ , meaning that the optimization of an objective function leads to a worsening of the other function.

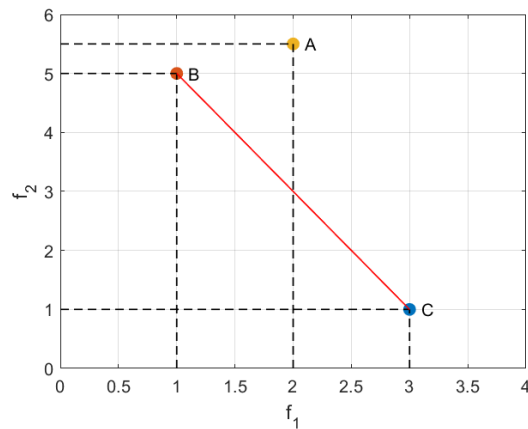


Figure 5.1. Example of Pareto Frontier. In red is highlighted the Pareto frontier, composed by points  $B$  and  $C$ , whilst  $A$  represent a dominated solution.

Optimization algorithms can be successfully adopted in design process of NZEB, giving to the designer important feedback for the selection of envelope material and HVAC components. In this kind of optimization problems, example of input parameters are: (i) the envelope materials; (ii) windows typology, dimensions and expositions; (iii) dimensions of shadings devices and (iv) sizing of the HVAC components. Constraints of the project can be represented by minimum building volume, minimum windows area and maximum investment costs. Finally, goals to be achieved can be the minimization of energy demand, the maximization of indoor thermal comfort, the maximization of the renewable energy exploitation and the minimization of the total costs.

In literature, several examples of use of optimizations algorithm in building design can be found. Jie *et al.* [134] adopt a single-objective optimization algorithm for the estimation of the insulation thickness of walls and roof in existing buildings that optimizes the objective function composed by three different criteria (primary energy saving ratio, global cost saving ratio and pollutant emission reduction ratio). Multi-objective optimization algorithms have been used in several applications in building design process: Torres-Rivas *et al.* [135] solved a multi-objective optimization problem for finding the insulation type and thickness for reducing the economic and environmental impact of the enhancement of building insulation, taking into account the condensation risk in the envelope materials. Moreover, Schito *et al.* [136] coupled TRNSYS with Matlab for the evaluation of the optimal hygrothermal set-points for HVAC systems in an historic building museum that minimize energy needs, artwork preservation risks and thermal visitors' discomfort. Starke *et al.* [137] used multi-objective optimization technique for the determination of the optimal configuration of a heat pump assisted by a solar collector for swimming pool;

whereas Perez *et al.* [138] performed optimizations at urban scale in the design of an energy district and Penna *et al.* [139] analysed the impact of incentives on the determination of the optimal retrofits solutions, considering energy, costs and indoor thermal comfort aspects. Finally, Manzan and Clarich [140] coupled Daysim (a tool used for the computation of internal illuminance and electrical energy required for lighting), ESP-r (that performs the building energy simulations) and modeFRONTIER (software that drives the optimization process) for the optimization of the fixed inclined shading devices, taking into account energy consumptions and the number of hours in which venetian blinds are deployed in an intermediate position.

However, even if it is well recognised that optimization algorithms are attractive techniques that can help designers in the realization of high energy efficient buildings, up to now they are rarely applied by the building design community [141]. One of the limiting factors is that the designers prefer to have a single tool able to perform both building energy simulations and optimizations, whilst generally two separates software packages have to be coupled: in fact, in [136], [137] and [139] TRNSYS has been used for performing energy simulations and Matlab for solving the optimization problems. For this reason, Yigit and Ozorhon [142] developed a tailored-made thermal simulations model in Matlab for searching optimal design of typical buildings in Turkey, since they recognize that carrying out both the energy simulations and the optimization processes on a single computational platform eliminates compatibility issues and increase the flexibility and user-friendliness of the procedure.

In agreement with Yigit and Ozorhon [142], in this *Chapter*, four single-objective and one multi-objective optimizations are performed coupling ALMABEST with the Matlab Optimization Toolbox, in order to demonstrate the capabilities of this approach.

## 5.2 Case study 1

In the first case study analysed, the building described in the BESTEST report for Case 900 is considered. As represented in Figure 5.2, the building is composed by two windows in the South wall, a horizontal roof, four external walls, no internal partitions and by an insulated slab-on-grade.

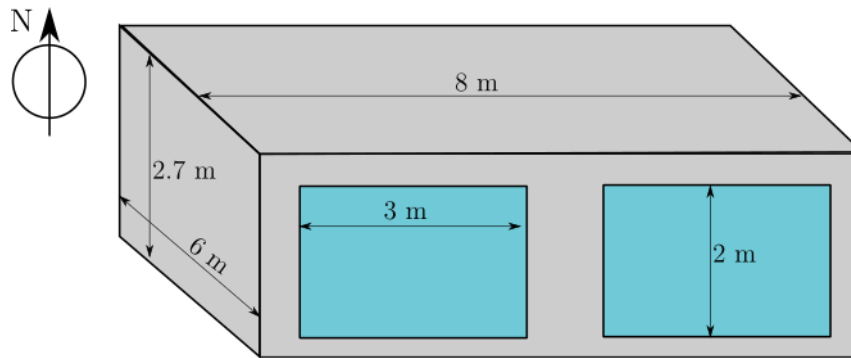


Figure 5.2. Geometry of the reference building.

The stratigraphy of the envelope element is the one described as *heavyweight* in the BESTEST report, with little modifications: the same insulation thickness, set to 7 cm, is adopted for both the external walls and the roof; in Table 5-1 the thermal transmittance values of each element are collected. The window area is 12 m<sup>2</sup>, the slab-on-grade is 48 m<sup>2</sup> and the internal volume is 129.6 m<sup>3</sup>. Air change rate due to infiltrations is 0.41 h<sup>-1</sup>, constant internal gains are accounted for 200 W (60% radiative, 40% convective).

Table 5-1. Thermal transmittance values of the envelope elements in the reference case.

	External wall	Roof	Window	Slab-on-grade
U [W/(m <sup>2</sup> K)]	0.46	0.47	3	0.04

The ideal HVAC system described in the BESTEST report is considered: if the indoor air temperature is less than 20 °C, the heating system is on whilst the cooling system is on when the indoor air temperature is higher than 27 °C.

In this case study, the goal to achieve is the reduction of the total energy demand, modifying two parameters: the thickness of the insulation layer of walls and roof and the total clear area. Firstly, in order to describe the dependency of the total energy demand on these parameters, several simulations are performed adopting the *Brute force* approach. Adopting this approach, the insulation thickness is varied from 0 to 30 cm and the total clear area from 6 (minimum value that guarantees an acceptable illuminance in the building) to 21 m<sup>2</sup>.

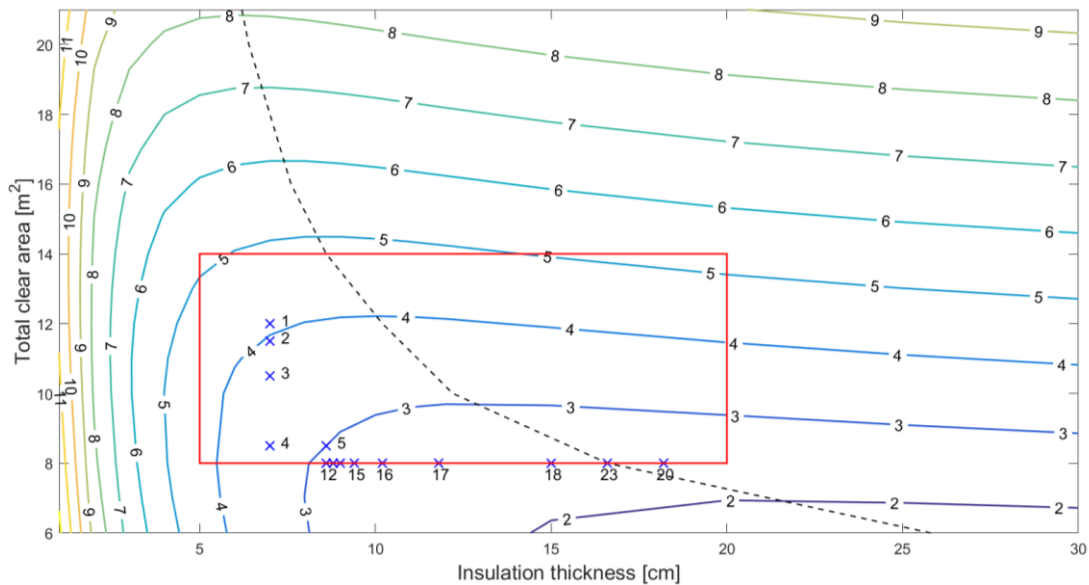


Figure 5.3. Total annual energy demand [MWh] as a function of the insulation thickness of the external walls and roof and of the total clear area.

The results are reported in Figure 5.3 where the level curves, that represent the total energy demand expressed in MWh, are plotted as a function of the insulation thickness and the total clear area. In this figure it is possible to appreciate that high clear areas determine high total energy demand, whereas the minimum energy demand is achieved with the minimum clear area and large thermal insulation.

Moreover, in Figure 5.3 three different regions can be noted:

- in the first one (insulation thickness lower than 5 cm), the total energy demand weakly depends on the clear area; in fact, in this region, the level curves are near vertical;
- in the second region (insulation thickness higher than 20 cm), the total energy demand strictly depends on the clear area, whilst it is slightly influenced by the insulation thickness.
- in the third region (insulation thickness within 5 and 20 cm), the total energy demand depends on both the parameters and local minimum of the total energy demand can be found as a combination of the two parameters.

Selecting a value of clear area, it can be noted that the same total energy demand is reached adopting two different values of insulation thicknesses. As an example, setting the clear area to 14 m<sup>2</sup>, the same total energy demand (5 MWh) is reached adopting 6 or 15 cm of insulation thickness. This fact clearly reveals that, for each value of total clear area, there is a value of insulation thickness that guarantees the local minimum of the total energy demand. The position of these local minimum, evaluated by means of the Matlab Optimisation Toolbox (*patternsearch* command), is represented in Figure 5.3 by the dotted line. It can be seen that the biggest is the clear area the lower is the insulation thickness that

guarantees the minimum energy demand. This is due to the fact that the higher is the clear area, the higher are the solar heat gains and high thermal insulations thicknesses reduce the dissipation of heat gains outside the thermal zone, by increasing the energy consumptions during the summer season.

The direct use of the Optimization Matlab functions, like the *patternsearch*, for solving optimization problems in building design becomes natural using ALMABEST, which shares with Matlab the same working space. In this way, the definition of the objective function, the starting point, eventual constraints and lower and upper bounds for input parameters becomes easy. The objective function is defined by means of an own-developed Matlab function, in which:

- the input data of the Simulink building model to optimize are uploaded;
- the variables of the optimization problem (i.e. the insulation thickness and the total clear area in this case) are changed within the space design;
- the simulation of the model is recalled and performed;
- the objective function is defined based on the outputs of the simulation.

Then, after having defined all the input required by the optimization function, the optimization problem is solved performing several times the simulation of the building model automatically.

With the aim to see how the direct search optimization method works, let us suppose to find the best combination of clear area and thermal insulation of the external opaque elements (walls and roof) that minimize the total energy demand. As represented by the rectangle in Figure 5.3, the range in which the two parameters are contained goes from 5 to 20 cm for insulation thickness and from 8 to 14 m<sup>2</sup> for the clear area. Limits of this range have been supposed assuming architectural and economic aspects. In Figure 5.3, the cross points represent the path that the direct search algorithm, recalled by the *patternsearch* command, performs to reach the optimal combination of the two parameters. The starting point, evidenced by cross labelled 1, is the reference building configuration described above. As indicated by the numbers next to each cross point, the optimisation algorithm performs only 23 iterations to reach the minimum and 30 iterations to assess that it is really the combination of parameters that guarantees the minimum total energy demand. As it can be seen, the local minimum drops exactly the local minimum curve. By means of this optimisation algorithm, only 64 combinations over 988 (76 different values of insulation thickness, 13 different clear areas) have been considered, with a time saving of 94%. In fact, at each iteration, the algorithm evaluates the objective function in a set of points (mesh) around the current point (i.e. the initial point or the point where the minimum has been reached in the previous iteration). If the algorithm finds a direction in which it is possible that the minimum is situated, the mesh expands, as it can be appreciated considering iterations 1 to 5, whilst when a possible minimum is reached, the mesh is contracted until a lower value



in the objective function is found or the mesh dimensions are less than the mesh tolerances.

The significance of optimization on the design phase of energy efficient buildings that can be observed in Figure 5.4, where the ratio between the total energy consumptions, for each building configuration, and the energy demand of the reference case is represented as a function of the non-dimensional insulation thickness and clear area.

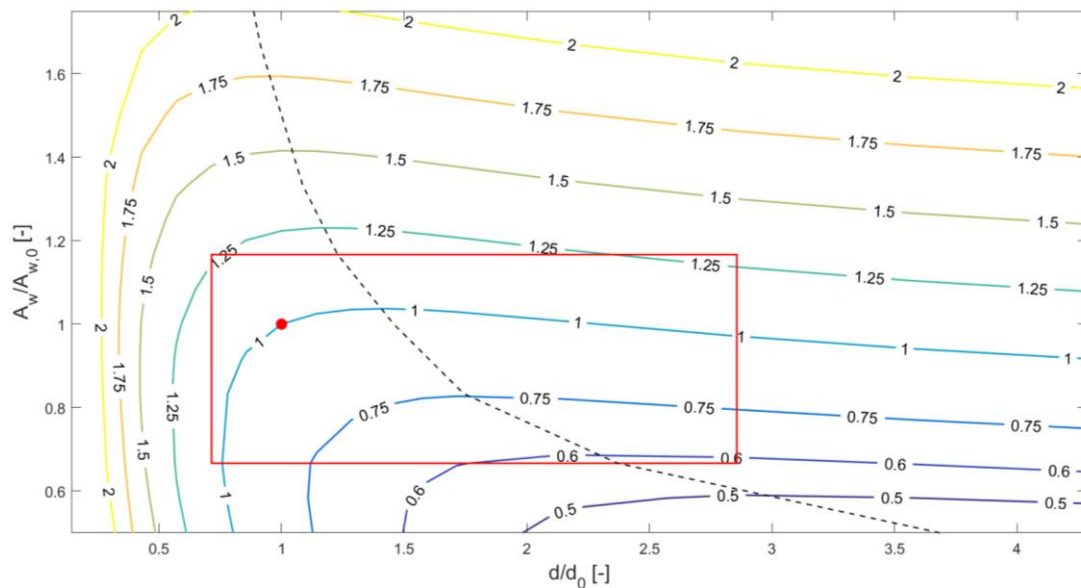


Figure 5.4. Ratio between the total energy consumptions and the total energy consumptions for the reference case, as a function of non-dimensional insulation thickness and clear area. The red point indicates the reference case.

The reference case is defined in terms of adopted clear area  $A_{w,0}$  of 12 m<sup>2</sup> and insulation thickness  $d_0$  equal to 7 cm. Unitary level curve identifies building configurations characterised by the same energy demand of the reference case (evidenced by the red point), whilst values lower than unity indicates lower energy consumptions than the reference case. In Figure 5.4, it can be appreciated that reducing the clear area ( $A_w/A_{w,0}$  lower than one) and increasing the insulation thickness ( $d/d_0$  higher than unity) the total energy demand can be halved. Referring to the constraints represented by the red rectangle in Figure 5.4, adopting the optimal configuration determined by the optimization algorithm, energy savings for 43.5% can be achieved, reducing energy needs from 4.17 MWh for the reference case to 2.36 MWh for the optimised one.

### 5.3 Case study 2

In the second case study, the reference building is the same described in the previous case and, as for Case 910 of BESTEST (see Figure 3.6a), a horizontal

overhang above the windows is added. The goal of this case study is to find the optimal overhang length that minimize the annual energy demand for heating and cooling. In this case, the lighting energy demand is neglected, even if also this contribution should be considered in the design of energy efficient shadings devices, as remarked by Manzan [143]. Before adopting an optimization algorithm, few annual numerical simulations are performed with different overhang lengths with the aim to observe the dependency of the total energy demand to this input parameter and limit the variable space in which the optimization algorithm will search the best solution.

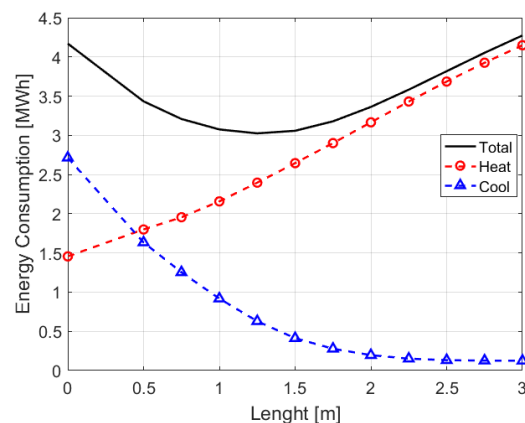


Figure 5.5. Total, heating and cooling annual energy demand as a function of the overhang length.

As represented in Figure 5.5, the heating demand increases with the overhang length. In fact, the higher are the shadings due to the overhang, the lower are the solar gains. On the contrary, the cooling energy demand rapidly decreases and it can be observed that it is slightly affected by the overhang length for values higher than 2 m. It can be noted that for low overhang lengths the cooling demand represents the main fraction of the total energy needs and vice versa for high overhang lengths the heating demand is the dominant energy need. Moreover, it should be remarked that heating and cooling demand are affected in an opposite way by the overhang length. As a consequence, a minimum for the total energy demand occurs, as evidenced in Figure 5.5 for overhang lengths between 1 and 1.5 m.

Now, having defined the design space (overhang length between 1 and 1.5 m), the optimization problem has been solved by adopting the *patternsearch* Matlab algorithm. The optimal overhang length found by the optimization algorithm is 1.3 m. The total energy demand obtained with the optimized overhang length is 3.03 MWh, that determines a reduction of 27.4% of the total energy need compared to the case without any overhang.

## 5.4 Case study 3

The same reference building adopted in the previous cases is considered also in the third case study. This time, the objective of optimization is the reduction of the total energy demand finding the best configuration of insulation thickness of opaque envelope elements (roof and vertical walls) and the overhang length above the windows. Again, in order to observe the dependency of the heating, cooling and total energy consumptions to those parameters, numerical simulations are carried out varying the insulation thickness from 0 to 30 cm and the overhang length from 0 to 3 m.

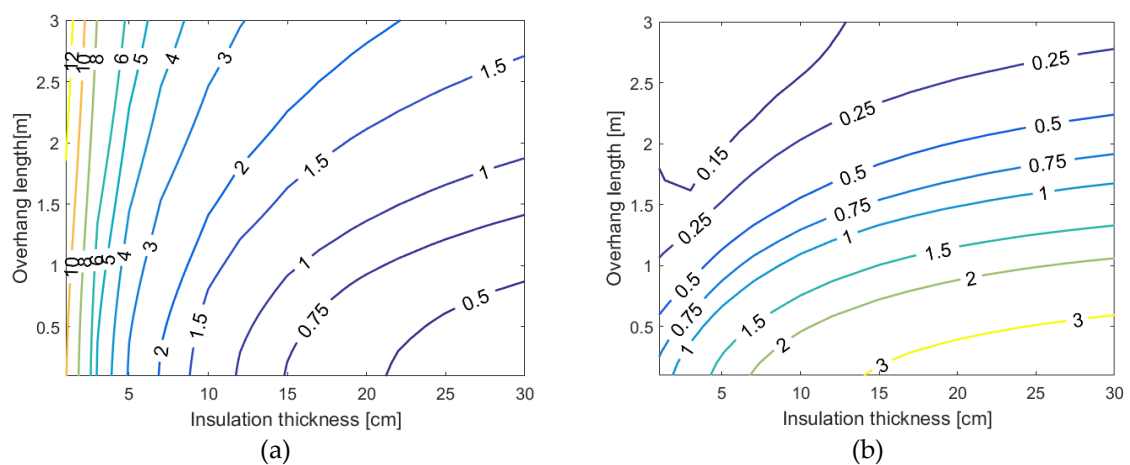


Figure 5.6. Annual heating (a) and cooling (b) energy demand [MWh], as a function of insulation thickness and overhang length.

Considering the annual heating demand (see Figure 5.6a), it can be observed that for insulation thicknesses lower than 5 cm the energy consumption is slightly affected by the overhang length. Anyway, a clear dependence of the heating demand to the input parameters is remarked: the higher is the insulation thickness as well as the lower is the overhang length, the lower is the heating energy consumption.

On the contrary, the cooling energy demand, represented in Figure 5.6b, evidences the opposite trend described for the heating energy consumptions. In fact, in Figure 5.6b it can be observed that high insulation thicknesses and low overhang lengths determine the highest cooling demand, whilst the minimum values are obtained by low insulations and high overhangs, that reduce the solar gains. Thus, the minimum total energy need is obtained by the optimal trade-off between heating and cooling energy consumptions.

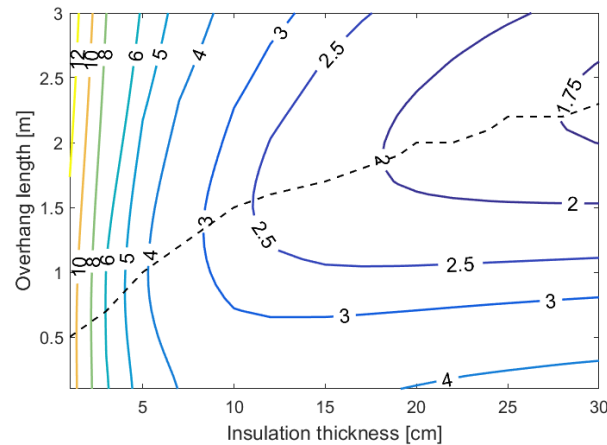


Figure 5.7. Total annual energy demand as a function of insulation thickness of opaque envelope elements and overhang length. The dotted line is the local minimum curve.

In Figure 5.7 it can be appreciated that lower total energy demand is obtained for buildings characterised by high insulation and medium-high (from 2 to 2.5 m) overhang length, which is a different building configuration compared to those that minimize separately the heating or cooling energy consumptions. Moreover, in Figure 5.7 the curve of the local minimum of the total energy demand is represented with a dotted line. From this curve, it can be remarked that overhangs are always needed in order to minimize the total energy demand and the higher is the insulation thickness, the higher is the overhang length (up to 2.3 m).

Comparing the total energy needs obtained in the optimal building configuration (overhang length of 2.3 m and 30 cm of insulation) to that of the reference building, a reduction of around 60% is observed, from 4.17 to 1.74 MWh.

## 5.5 Case study 4

The last case study dealing with single-objective optimizations starts from the same reference building defined in Case study 1; the total energy demand is minimized modifying three input parameters: insulation thickness of external opaque envelope elements, total clear area and overhang length. The design space goes from 5 to 20 cm for insulation thickness, from 8 to 14 m<sup>2</sup> for the total clear area and from 0 to 2.1 m as overhang length.

Dependencies of the total energy demand to the input parameters can be analysed considering Figure 5.8 in which the level curves of the energy consumptions, expressed in MWh, are reported for different clear areas.

For fixed total clear area, it is possible to observe that the minimum energy consumption is achieved with the highest insulation thicknesses and high overhang lengths, whereas low insulations determine the highest energy needs. Considering also the total clear area, Figure 5.8 clearly evidences that the

minimum energy demand is obtained with the lowest windows area. In fact, for buildings with 8 m<sup>2</sup> of clear area (see Figure 5.8a) the level curve of 1.5 MWh is observed, whilst for buildings with 10 or 12 m<sup>2</sup> (Figure 5.8 b-c) covered by windows the lowest level curve is 2 MWh, that increases to 2.5 MWh if the clear area is of 14 m<sup>2</sup> (Figure 5.8d).

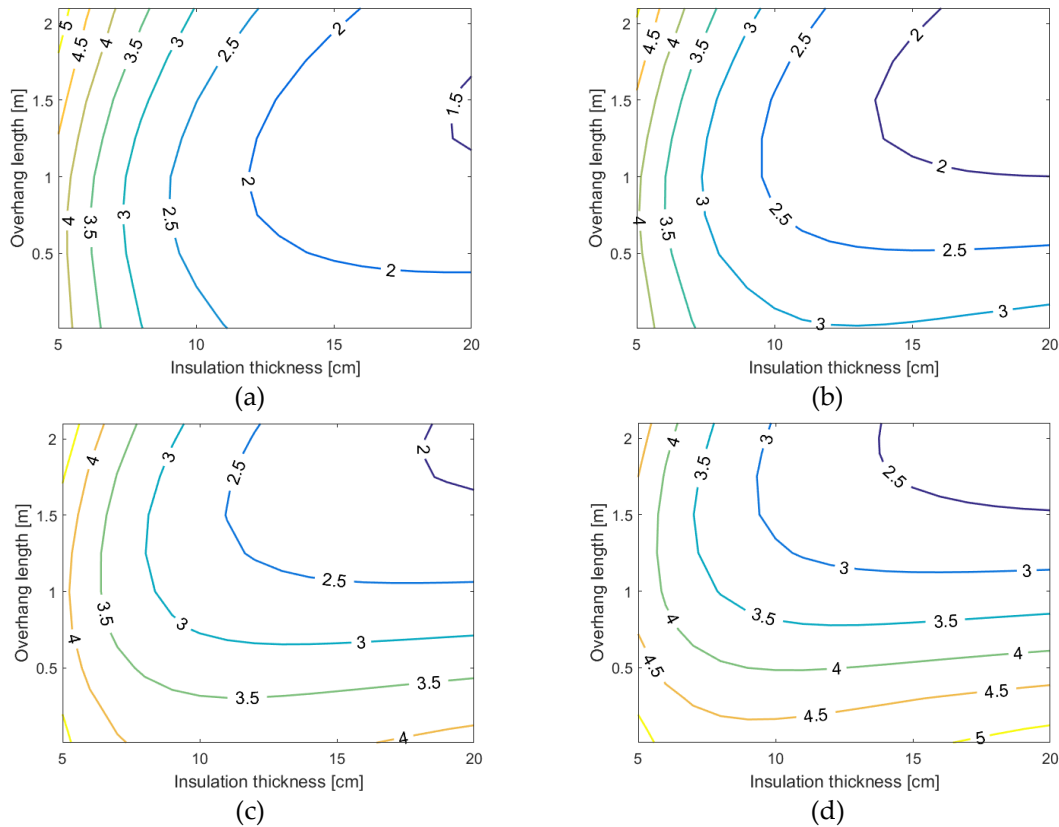


Figure 5.8. Total energy demand [MWh] as a function of insulation thickness and overhang length for total clear area of 8 (a), 10 (b), 12 (c) and 14 (d) m<sup>2</sup>.

Since in Figure 5.8 it has been observed that the lower energy consumptions are achieved maximizing the insulation thickness, the *patternsearch* optimization algorithm has been used for searching the curve that, for each windows area, determines the best overhang length, considering building with the highest insulation.

As represented in Figure 5.9, overhangs are always required for optimizing the total energy needs; in fact, the lowest value of the overhang length is around 1.45 m. Moreover, it can be observed that the highest is the clear area, the highest is the overhang length that determines the minimum energy consumption. For clear area higher than 12 m<sup>2</sup> the optimal overhang length is always 2.1 m, because this has been fixed as upper boundary for this parameter in the optimization problem.

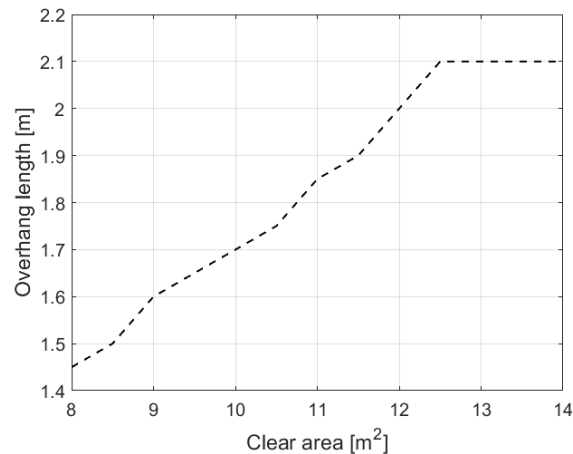


Figure 5.9. Local minimum curve: the optimal overhang length is expressed as a function of the total clear area, considering the maximum insulation thickness.

Finally, a Matlab optimization algorithm has been used for finding the lowest energy demand, considering all the design space. The selected optimization algorithm takes only 17 iterations, with 43 evaluations of the objective functions to find the optimal solutions, whilst the *Brute force* method would require 4576 (16 different values of insulation thickness, 13 different clear areas and 22 different overhang lengths) numerical simulations. Therefore, the optimization algorithm takes less than 1% of the time that would be used adopting the *Brute force* approach is necessary. The optimal input parameter configuration (30 cm of insulation thickness, 8 m<sup>2</sup> of total clear area and overhang length of 1.45 m) determines energy demand around 1.46 MWh, with a reduction of 65% compared to the reference case.

## 5.6 Multi-objective optimization case study

In this case study, contrary to the previous ones, two opposite goals are optimized modifying the design parameters, starting from the reference building used in the previous case studies (see Case 1). More in detail, two different building configurations are analysed: in the first, the two windows are both inserted in the South wall (as represented in Figure 5.2), whilst the second configuration consists in building with a window on both East and West walls. In addition, three input parameters are considered: (i) the total clear area, whose range is between 8 and 12 m<sup>2</sup>; (ii) the insulation thickness, from 1 to 30 cm and (iii) the position of the insulation layer, on the external or internal side of the envelope element.

In this case, the building is provided with a heating system composed by radiators, whose characteristics are collected in Table 5-2. The inlet water temperature is constant and set to 70 °C and radiators are sized imposing a temperature difference between inlet and outlet of 20 K. The heating system is controlled by an on-off thermostat, whose operative set-point temperature is 21

°C and the dead-band is  $\pm 1$  K. For sake of simplicity, distribution and heat generation systems are neglected.

The building, an office, is assumed to be occupied from 7:00 to 20:00; in these hours convective and radiative internal gains (120 and 80 W, respectively) are presents. The heating system is on from the 15 of October to the 1<sup>st</sup> of May, from 5:00 to 19:00.

Table 5-2. Main characteristics of a radiator element.

Nominal power [W]	115
Exponent [-]	1.33
Water content [l]	0.44
Weight [kg]	1.31

Instantaneous comfort conditions are evaluated by means of the Predicted Mean Vote and the Predicted Percentage of Dissatisfied, as described in Standard EN ISO 7730 [13], considering constant values of humidity ratio (since in ALMABuild the evaluation of the indoor air humidity ratio is not available), air velocity and metabolic rate and a different thermal insulation due to clothing: 1 clo in winter and 0.5 clo in summer (see Table 5-3).

Table 5-3. Constant parameters for the evaluation of indoor comfort conditions.

	Winter	Summer
Humidity ratio [%]	60	60
Air velocity [m/s]	0.1	0.1
Metabolic rate [met]	1.2	1.2
Clothing [clo]	1	0.5

The two objective functions that have to be minimized are the annual heating energy demand, calculated as the energy provided by radiators to the office, and the mean annual (for the occupied hours) PPD.

### ***5.6.1 Analysis of the sensitivity of the objective functions to different building configurations***

Before performing the multi-objective optimization taking into account all the input parameters, the sensitivity of the objective functions to the different building configurations (windows on the South or East-West walls, insulation on the internal or external side of envelope elements) is investigated by means of numerical simulations.

Firstly, the dependence of heating energy demand and of the mean annual PPD to the position of the insulation layers in the envelope elements has been analysed considering building with a total clear area of 9 m<sup>2</sup>, with windows on both the East and West walls, and different insulation thicknesses.

The results, represented in Figure 5.10, show that both the positions of the insulation layer determine a trade-off between energy consumptions and comfort conditions. Since same conclusions can be assessed modifying the total clear area or the position of the windows, both the positions of the insulation layer in the external opaque envelope elements have to be considered as input parameters in the optimization.

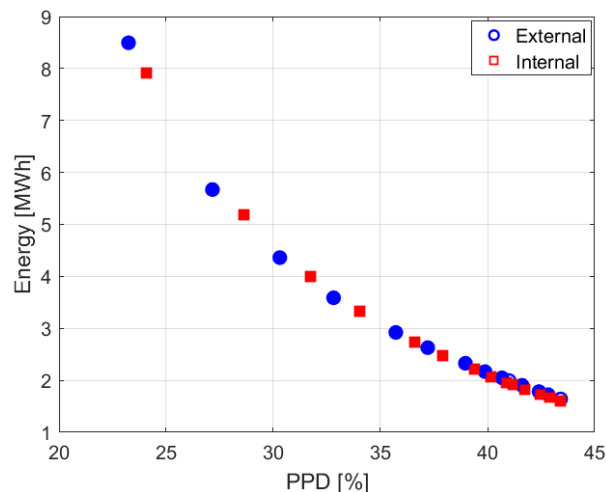


Figure 5.10. Heating energy demand and mean annual PPD for buildings with windows in both East and West walls (total clear area of 9 m<sup>2</sup>) considering different insulation levels, both in the external and internal layers. The filled markers refer to solutions that compose the Pareto frontier.

The same procedure is adopted focusing on the position of the windows: both on the South wall or one in both the East and West walls. From the results depicted in Figure 5.11, concerning buildings with 8 m<sup>2</sup> of clear area and different insulation thicknesses, it can be observed that if windows are on both the East and West walls, buildings are characterised by higher energy consumptions and higher mean annual PPD than buildings with windows only on the South wall. This fact is highlighted in Figure 5.11, by remarking that all the solutions related to buildings characterised by windows on the South wall compose the Pareto frontier.



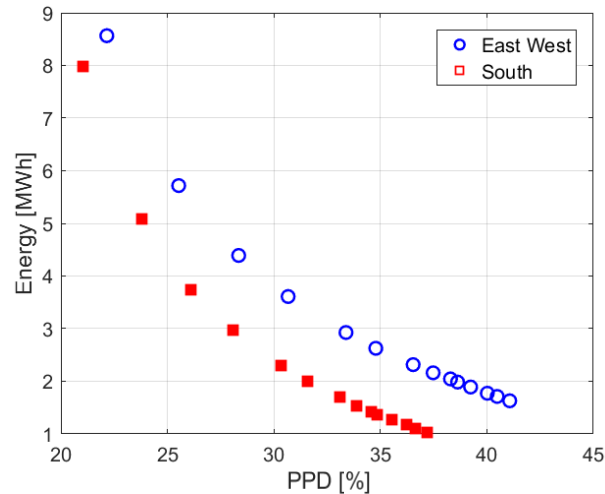


Figure 5.11. Heating energy demand and mean annual PPD for buildings characterised by total clear area of 8 m<sup>2</sup>, considering different insulation thicknesses (on the external side of the elements) and various windows exposition. Filled markers concern solution of the Pareto frontier.

The reasons of the higher energy consumptions and mean annual PPD that characterise building configurations with windows on the East-West walls can be inferred analysing the trend of the operative temperature on a typical winter and summer day, as represented in Figure 5.12. Referring to a typical winter day (see Figure 5.12a), it can be observed that the increasing temperature rate is the same for both the windows expositions, since this rate depends on the heat delivered by the same radiators. Anyway, if windows are in South wall, during the central hours of a day, the solar heat gains are enough to prevent the use of radiators, contrary to cases in which windows are in the East-West walls: in that case radiators have always to be on. This is confirmed considering, in Figure 5.12a, the indoor operative temperature from 10:00 to 16:00: if the windows are in the East-West walls, the heating system is switched on three times, whilst when windows are exposed to South the heating system is always off since the solar gains are enough for maintaining the operative temperature at around 20.5°C.

On the contrary, in a typical summer day (see Figure 5.12b) it can be observed that the operative indoor temperature is always higher if windows are in both the East and West walls, increasing the hot feelings of the occupant and reducing the comfort conditions. Again, the reason of this trend is related to solar gains: contrary to winter, in summer the higher solar gains are obtained with the East-West exposition.

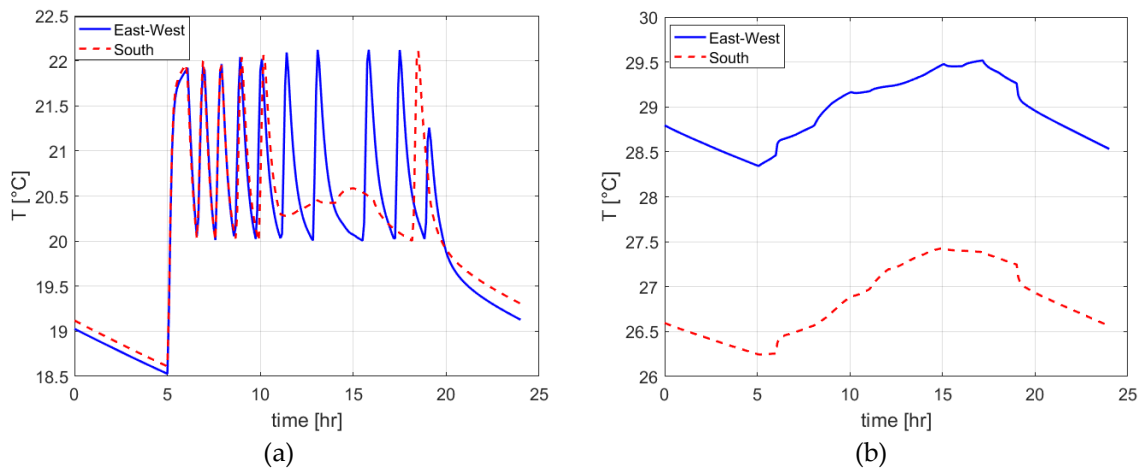


Figure 5.12. Indoor operative temperature for a typical winter (a) or summer (b) day, for buildings with two window expositions: East-West (blue solid line) or South (red dashed line).

In conclusion, solar gains (lower in winter and higher in summer for East-West exposition compared to South exposition) have been recognized as the cause of the higher energy consumptions and the higher mean annual PPD that characterise buildings with windows on both the East and West walls compared to the buildings with windows exposed to South. Since solar gains are not affected by the other design parameters, it can be assessed that the East-West building configuration can be neglected in the multi-objective optimization. Clearly, in this case we are referring to situations in which windows can be inserted in the South wall.

### 5.6.2 Results of the multi-objective optimization

After the sensitivity analysis of different design configurations on the objective functions, by means of which the dimension of the design space has been halved excluding buildings characterised by windows on East-West walls, the multi-objective optimization of heating energy demand and mean annual PPD is performed by means of the Matlab Optimization Toolbox.

The Pareto frontier which collects the optimal building configurations and determine the best trade-offs between energy needs and comfort conditions is represented in Figure 5.13. In this way, the designer can select among the optimal building configurations the one that satisfy custom requirements related to the designer needs (e.g. preference on high comfort conditions instead of very energy efficient building).

In this figure it can be observed that the Pareto frontier is mainly composed by buildings characterised by envelope elements with thermal insulation on the external side. Insulation on the internal side represents an optimal building configuration only with low total clear area and low insulation thickness (mainly 1 cm).

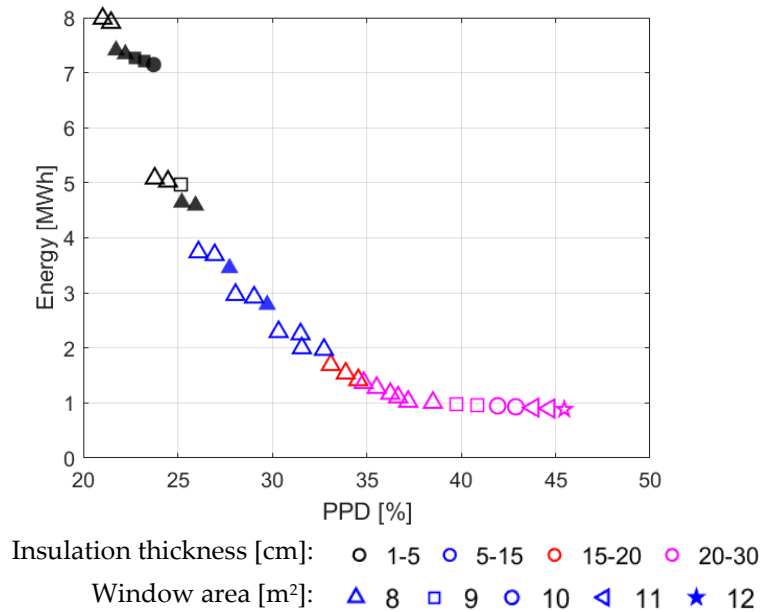


Figure 5.13. Pareto frontier for the optimization of mean annual PPD and of heating energy demand. Results concern buildings composed by windows on the South wall; filled markers refer to internal insulation of opaque elements.

Referring to buildings with insulation on the external side, in Figure 5.13 it can be observed that the higher the insulation thickness and the total clear area are, the lower is the energy consumptions and the higher is mean annual PPD. On the contrary, reducing both the insulation thickness and the total clear area the energy consumptions greatly increase but the mean annual PPD values are reduced. Anyway, the minimum value of the mean annual PPD is around 20%, revealing that indoor discomfort periods are never eliminated.

## 5.7 Conclusions

In this *Chapter*, single and multi-objective optimizations problems, related to the maximization of the building performance by finding its optimal configuration, have been solved coupling the Matlab Optimization Toolbox to ALMABEST. Contrary to other *whole building software* that require the co-simulation, ALMABEST enables the solution of optimization problems in a single computational environment. In fact, the Matlab Optimization Toolbox can be easily adopted within ALMABEST, by defining the Simulink file in which the building model is implemented in the objective function required by the optimization command. In this way, by means of ALMABEST optimizations can be carried out without dealing with any compatibility issue.

By performing four single-objective optimizations, searching the best building configuration that minimize the total annual energy demand, performances of the Matlab direct search algorithm have been investigate. Moreover, the *Brute force* approach has been adopted for verifying that that the optimal solution

found by the optimisation algorithm is really the optimal one. The improvements on the building energy performance obtained by optimizing the building configuration are remarkable: energy savings from 27.4% to 65% with respect to the reference case are achieved in the four case studies.

In addition, in the last case study, that concerns a multi-objective optimization, it has been demonstrated that a pre-analysis of the sensitivity of the objective functions to the input parameters can help in the reduction of the dimension of the design parameter space. In other words, by performing few numerical simulations it is possible to make less wide the design space in which the optimization algorithm will search the optimal configuration. As an example, in this case, the sensitivity analysis allowed to halve the design space dimension, accelerating the whole procedure for the optimal searching.

# Occupant behaviour

---

## Abstract

In this *Chapter*, the effects due to the occupant interactions with the building elements on the total energy demand and on indoor comfort conditions are investigated by means of a series of annual numerical simulations. More in detail, the focus is set on the effects of the window openings performed by the occupant for adjusting the indoor comfort conditions during the year. The occupant behaviour has been modelled by means of the stochastic *Humphreys Adaptive Algorithm* [144]. Referring to a single-zone office without any cooling system and heated by radiators, energy demand and comfort conditions have been predicted for several building configurations in which thermal insulation thickness, window typology (double and triple pane, high and low SHGC) and shadings are modified, both considering and neglecting the occupant behaviour. The comparison of the results evidences that the occupant behaviour determines an increment of both energy demand and comfort conditions if buildings are characterised by high solar gains (no shadings, high SHGC windows and high insulations), whereas buildings with reduced solar gains (high shadings and low SHGC windows) are not affected by the user behaviour.

Moreover, as a result of a sensitivity analysis of energy demand and indoor conditions (performance indicators) to the design parameters carried out both considering and neglecting the occupant behaviour, it is remarked that occupants, by means of their actions, make performance indicators less sensitive to the design parameters.

In addition, performing multi-objective optimizations with the aim to find the building configurations that maximize the indoor comfort conditions and minimize the energy demand, it is observed that also the Pareto frontier is affected by the occupant behaviour: if occupants can open the windows, the Pareto frontier is characterised by a reduced spread between the solutions and by few optimal building configurations, compared to the optimizations performed neglecting the user behaviour. Finally, the robustness of the optimal building configurations, individuated by the Pareto frontiers, to the occupant behaviour is evaluated introducing a new sensitivity parameter.

---

## 6.1 Introduction

Nowadays, it is well recognised that energy consumptions of buildings are strongly affected by the envelope elements characteristics, as well as the building geometry and the design of the HVAC system. As stated in *Chapter 1*, in the past decades several researchers worked on the development of computational models for the building energy performance assessment, leading to very accurate thermal models of buildings. Usually, in the energy models of a building the occupant behaviour is neglected or taken into account by means of simple deterministic rules [145]. Anyway, both building energy performance and indoor comfort conditions are affected by occupants, able to release sensible and latent heat and interact with building and HVAC systems [146].

If the occupant behaviour is ignored, a discrepancy between measured and predicted energy consumptions of buildings is expected. As an example, Haas *et al.* [147] found that the actual energy savings obtained by the refurbishment of Austrian residential buildings were lower than the predicted ones due to the occupant behaviour; whereas the comparison of actual and predicted (by means of dynamic simulations performed in the design phase) energy consumptions of 62 Leadership in Energy Environmental Design (LEED) buildings evidenced normalized root-mean-squared differences of 18% [148].

Moreover, occupant behaviour is intrinsically affected by uncertainty. In fact, occupant behaviour patterns not only vary between each other, but each occupant does not behave in a deterministic way. In fact, the analysis conducted by Brager *et al.* [149] in a naturally ventilated building in which occupants can interact with windows showed that occupants, with the same activity level and clothing, had different thermal response, even if they experienced the same indoor conditions. Therefore, it has been noted that identical thermal conditions lead to different windows operations (opening and closing). Different occupant behaviour patterns have been observed also by Al-Mumin *et al.* [150], who analysed the cooling energy demand of 30 residences in Kuwait and found that the inner temperature set-point was moved by the occupants within the range below 19 °C to above 25 °C under similar conditions. In addition, occupants behave differently if they share a common space or are in private space, due to psychological and social issues. For example, Haldi and Robinson [151] showed that in common spaces occupants tend to limit their actions (blinds operations) with respect to occupants in private spaces. This uncertainty in occupant behaviour leads to a wide spread of results in the evaluation of the energy building performances: Clevenger and Haymaker [152], by means of a series of numerical simulations of a primary school in which occupancy schedules (lighting, equipment, people and hot water schedules) and environmental preferences of occupants (air change ratio, set point temperature, occupancy density...) were varied, found that the spread in the predicted energy

consumption can overcome 150% of the reference case. On the contrary, Li *et al.* [153] measuring the cooling energy need in 25 household of a residential building in Beijing in summer, found that energy consumptions of identical buildings varied from 0 to 14 kWh/m<sup>2</sup>, with an average of 2.3 kWh/m<sup>2</sup>, due to the difference of time activation of air conditioning systems and the number of rooms in which cooling was activated by the occupants (all the rooms of building or only some of them). In the same way, Guerra-Santin *et al.* [154], analysing the energy consumption for heating and hot water production of the Dutch housing stock, found that 4.2% of the differences of the total energy needs depends on the occupant behaviour, whilst 42% is due to difference in insulation level and types of dwelling or HVAC system. More recently, Gill *et al.* [155] compared the energy consumptions of 26 low-energy buildings and they found that the occupant behaviour is responsible of an increase of 51%, 37% and 11% in terms of heat, electricity and hot water consumptions compared similar buildings.

Since the occupant behaviour has been recognised to play an important role in the building energy consumptions, in the last two decades researchers started to develop models for mimic the occupant behaviour patterns. As stated by Parys *et al.* [156], six are the main research fields on behavioural model of occupants in offices: (i) occupancy pattern (arrival and departure time); (ii) occupant control of shading devices; (iii) occupant control of windows; (iv) occupant control of artificial lighting; (v) occupant control of appliances and (vi) occupant control of thermal environment (e.g. air change ratio, thermostat set-point..).

For each of these research fields, several models have been proposed without achieving a unique wide accepted model. Referring to the occupancy model, the starting point is represented by the *Lightswitch* model, introduced by Newsham *et al.* [157]. This model consists in the definition of the state of a cell office (occupied or vacant) based on the probability of transitions, evaluated by empirical data. Later, this model has been improved by Reinhart [158], who proposed to use more deterministic occupancy profiles, and by Page *et al.* [159], who included long vacations, due to holidays. More recently, Mahdavi and Tahmasebi [160] proposed a new non-probabilistic occupancy model whose predictive accuracy has been demonstrated to be quite higher than other probabilistic models, but yet not satisfactory.

For the occupant control of shading devices, many field researches have been performed, with the aim to find the driving forces that induce the occupant to deploy blinds. Visual comfort (i.e. glare avoidance) has been recognised as the main stimulus for occupant actions [161] - [162], followed by the high internal temperature [163] - [164]. However, only few models have been developed, with the *Lightswitch-2002* as the first model to be proposed [165].

The occupant control of windows consists in its opening and closing. In fully conditioned buildings, windows are not operable and the occupant cannot open them; in this case no behavioural models are required. On the other hand, in

buildings not provided by cooling systems, opening the windows is the only solution for summer free cooling. The first model that has been proposed, introduced by Warren and Parkins [166], consists of two different probability functions, one for small and the other for large openings. Several models have been developed later and the stochastic *Humphreys Adaptive Algorithm* [144] represents one of the most important ones. This model, valid for natural ventilated building, assumes the indoor and outdoor temperature as the driving factors for the windows opening. Two years later, Yun *et al.* [167] proposed a model in which different probabilities of window openings are defined depending on the typology of user, that has been classified as active, medium and passive.

Occupant control of artificial lighting is the only occupant behavioural field where similar patterns have been proposed by researchers. In fact, as stated by Parys *et al.* [156], probability functions of switch on the lighting as a function of the indoor illuminance described by the model introduced by Reinhart and Voss [168] have similar trends to the ones obtained by other proposed models [169] – [170].

Appliance operations clearly are not induced by external or internal environmental conditions. For this reason, it is quite difficult to find a model for the occupant control of appliances; some models try to define the percentage of the nominal power of appliances that is actually used in office during the working time and during the night [171] - [172], but the profiles obtained depend on the activity that is performed in the office and on the geographical area.

Finally, the occupant control of the thermal environment has not been deeply investigated and few models have been proposed. Nicol and Humphreys [173] introduced a model in which the probability functions of switching on the heating or cooling system depends on the outdoor and indoor temperature, whereas Fabi *et al.* [174] developed a model that provides the set-point temperature for heating system as a function of indoor and outdoor conditions (temperature, humidity, solar radiation, wind speed).

The development of occupant behavioural models enables to take into account the occupant behaviour in dynamic building energy simulations and to evaluate its influence on the total energy consumption. Since generally occupants are modelled by means of stochastic models and users can be classified as passive, medium or active, the main energy parameters are affected by variability. As an example, Parys *et al.* [156], proposing their comprehensive modular behavioural model, found that, for a precise building design, the standard deviations of heating and cooling energy, at building level, were 9% and 10% respectively. Hoes *et al.* [175] proposed three different resolution levels of the occupant behaviour, from standard user profiles to more complex algorithms, like the Sub-Hourly Occupancy Control (SHOCC) [176] and the User Simulation of Space Utilization (USSU) [177]. The adequate resolution level



depends on the sensitivity of the performance indicator (e.g. heating/cooling energy demand, maximum/minimum indoor air temperature) to the occupant behavioural model: the more is the sensitivity the more is the complexity of the behavioural model. Finally, Karjalainen [178] stated that, in order to have robust solutions, i.e. solutions that are characterised by low sensitivity to variations on the input data, buildings should be designed in a way that makes them less sensitive to occupant behaviour. Examples of robust design of buildings are non-operable windows and occupant detection for the control of lighting. In its work, Karjalainen compared the energy consumptions for heating, cooling and electricity considering three different user behaviours (careless, normal and conscious) and two design strategies (ordinary and robust). Results shows that the adoption of robust design limits the sensitivity of the total energy consumption to the occupant behaviour. In fact, in the case described in [178], in ordinary design the difference in terms of annual energy consumptions between careless and conscious occupant behaviour is around 5 MWh/y (82% of the careless total energy consumption), whilst, in the robust design this difference is reduced to 0.48 MWh/y (36% of the careless total energy consumption).

In this *Chapter*, the different sensitivity of both energy consumption and indoor comfort conditions to different design parameters, both considering and ignoring the occupant behaviour related only to the window opening, is investigated by means of numerical simulations. Moreover, multi-objective optimizations are performed with the aim to obtain the best combinations of the design parameters and implications related to the adoption of the occupant behaviour are examined.

## 6.2 Occupant behaviour model

In this case study, the occupant behaviour related to the windows opening is taken into account, neglecting the occupant control of blinds, thermal environment, appliances, artificial lighting and considering a fixed occupancy schedule for sake of simplicity. For the windows opening due to the occupant behaviour, the stochastic *Humphreys Adaptive Algorithm* [144] has been implemented in ALMABuild.

This algorithm has been developed from field surveys conducted in 15 UK offices. The starting point of this algorithm is the evaluation of the comfort conditions sensed by the occupant. Comfort temperature ( $T_{conf}$ ) is estimated as a function of the running mean outdoor temperature ( $T_{rmo}$ ), as follows:

$$\begin{cases} T_{conf} = 0.33T_{rmo} + 18.8 & \text{if } T_{rmo} > 10^{\circ}\text{C} \\ T_{conf} = 0.09T_{rmo} + 22.6 & \text{if } T_{rmo} \leq 10^{\circ}\text{C} \end{cases} \quad (6.1)$$

The occupant is stated to sense comfort conditions if the operative temperature is within the range  $\pm 2$  K around the comfort temperature; otherwise the occupant state is *hot* (operative temperature higher than 2 K to the comfort temperature) or *cold* (temperature under the range). If uncomfortable indoor conditions are sensed by the occupant, the window opening probability ( $Prob_w$ ) is evaluated by means of a logit function, derived from field surveys:

$$\text{logit}(Prob_w) = 0.171T_{op} + 0.166T_e - 6.4 \quad (6.2)$$

$$Prob_w = \frac{\exp(\text{logit}(Prob_w))}{1 + \exp(\text{logit}(Prob_w))} \quad (6.3)$$

Then, the window opening probability is compared to a random number within the range 0-1. If the occupant state is *hot*, the window is closed and the window opening probability is greater than the random number then the window is opened by the occupant. On the contrary, if the occupant state is *cold*, the window is open and the random number is greater than the window opening probability, the occupant closes the window. It has to be remarked that, in the *Humphreys Adaptive Algorithm* comfort conditions are evaluated only as a function of the indoor operative temperature, neglecting the effects of air humidity ratio on occupant feelings. In our simulations, contrary to the Rijal *et al.* [144], the *Humphreys Adaptive Algorithm* is run every 10 minutes, instead of every hour.

### 6.3 Reference building

The building considered for this case study is a single zone office, located in Bologna, Italy. The geometry of the reference building is the same of the BESTEST Case 900. As represented in Figure 5.2, the building is composed by two windows inserted in the South Wall and has a horizontal roof. All the walls are exposed to the outdoor environment. The floor is a slab-on-grade of 48 m<sup>2</sup> and the internal air volume is of 129.6 m<sup>3</sup>. Infiltrations are responsible of a constant air-change rate of 0.41 h<sup>-1</sup>. In this case study, the building is heated by radiators, whose characteristics are listed in Table 6-1.

Table 6-1. Main characteristics of a radiator element.

Nominal power [W]	91.1
Exponent [-]	1.31
Water content [l]	0.74
Weight [kg]	5.4

The inlet water temperature is 80 °C and radiators are sized in order to obtain a water temperature difference between inlet and outlet of 10 K. The control

system of the heating system is composed by a thermostat with a dead band of  $\pm 1$  K and a set-point temperature of 21 °C or 23 °C. For sake of simplicity, the distribution and heat generation systems are not taken into account.

In the office no cooling systems are provided, so natural ventilation, through windows openings, is the only cooling mechanism available. Therefore the building is in free-float conditions. The air change rate due to the window opening is modelled as a function of the absolute temperature difference between indoor and outdoor. This air change rate function is based on the results obtained by the surveys of Larsen and Heiselberg [179], considering mean values of the wind speed. The air change rate profile for single-sided natural ventilation implemented in ALMABuild is represented in Figure 6.1.

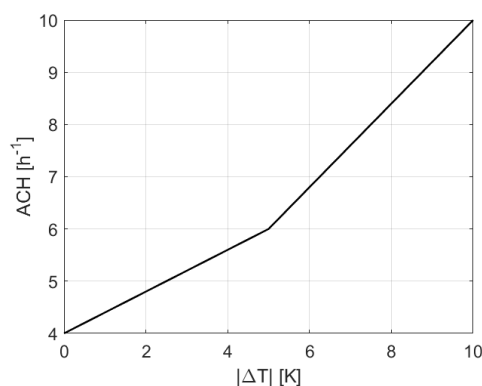


Figure 6.1. Air change rate (ACH) as a function of the absolute temperature difference between indoor and outdoor.

Occupancy is modelled by means of fixed schedule: occupants work from 7:00 to 20:00; for the same hours convective and radiative constant internal gains equal to 120 and 80 W respectively are added. On the contrary, the heating system is on from 5:00 to 19:00, each day from the 15 of October to the 1<sup>st</sup> of May.

Heating energy consumptions are evaluated as the energy provided by radiators to the office, whereas occupant comfort conditions are estimated by means of the adaptive comfort temperature, as described in the previous section.

## 6.4 Case Study

As stated in the introduction, numerical simulations are performed with the aim to investigate the sensitivity of the heating energy demand and the indoor thermal conditions to various design parameters, both considering and ignoring the occupant behaviour. In addition, multi-objective optimizations are performed and implications of the occupant behaviour on the Pareto frontier and on the solutions that optimise the energy demands and the indoor comfort conditions are examined.

### 6.4.1 Input data

In this case, various combinations of thermal insulations of the external opaque elements, windows and shadings are considered. As reported in Table 6-2, five different levels of thermal insulation of external walls and roof (labelled  $In_0$ ,  $In_5$ ,  $In_{10}$ ,  $In_{15}$  and  $In_{20}$ ) are considered. The thermal insulation layer is always at the external side of the envelope element.

Table 6-2. Thermal transmittance of external opaque envelope elements for different thermal insulation thicknesses.

Label	Insulation thickness [cm]	$U_{WALL}$ [W/(m <sup>2</sup> K)]	$U_{ROOF}$ [W/(m <sup>2</sup> K)]
<b>In<sub>0</sub></b>	0	2.04	1.53
<b>In<sub>5</sub></b>	5	0.58	0.53
<b>In<sub>10</sub></b>	10	0.33	0.32
<b>In<sub>15</sub></b>	15	0.24	0.23
<b>In<sub>20</sub></b>	20	0.18	0.18

Four different kinds of window, characterised by different thermal and optical properties (see Table 6-3), are analysed. Double pane windows are labelled  $D$ , whilst  $T$  refers to triple pane window. Window  $D1$  is a double pane window filled with air;  $D2$  is a low-emissivity double pane window filled with Krypton;  $D3$  is a double pane window with low SHGC and filled with Argon and  $T1$  is a low-emissivity triple pane window filled with Xenon.

Table 6-3. Characteristics of the analysed windows.

Window	$U_w$ [W/(m <sup>2</sup> K)]	SHGC [-]
<b>D1</b>	1.6	0.596
<b>D2</b>	0.86	0.598
<b>D3</b>	1.26	0.397
<b>T1</b>	0.4	0.408

Finally, shadings due to a horizontal overhang above the windows are considered. The overhang geometry is similar to the one represented in Figure 3.6a for BESTEST cases with windows in the South wall; five different lengths of the overhang are considered. In Table 6-4, for each overhang length the annual mean shading factor, i.e. the reduction of the incident solar radiation, is reported.  $Sh_0$  refers to the absence of overhang, thus the shading factor is unitary, since there are no shadings. On the contrary, in the other cases (from  $Sh_1$  to  $Sh_4$ ) the overhang has an increasing length, from 0.5 m to 2 m, that reduces the incident solar radiation on the windows up to the 62%.

Table 6-4. Shading factor for different overhang geometries.

Overhang configuration	Sh <sub>0</sub>	Sh <sub>1</sub>	Sh <sub>2</sub>	Sh <sub>3</sub>	Sh <sub>4</sub>
Shading factor [-]	1	0.88	0.75	0.67	0.62

### 6.4.2 Results ignoring the occupant behaviour

In this paragraph, results of annual numerical simulations performed with ALMABuild considering different combinations of thermal insulation thickness, shadings and windows, neglecting the user behaviour and setting the temperature set-point to 21 °C are analysed.

Table 6-5. Annual heating energy consumptions [MWh/y], for cases with set-point temperature equal to 21 °C, for different shadings, insulation thicknesses and windows. For each window, minimum energy demand is highlighted on bold.

Shading\insulation	In <sub>0</sub>	In <sub>5</sub>	In <sub>10</sub>	In <sub>15</sub>	In <sub>20</sub>
<b>Window D1</b>					
Sh <sub>0</sub>	10.23	3.30	1.99	1.47	<b>1.18</b>
Sh <sub>1</sub>	10.30	3.37	2.05	1.51	1.22
Sh <sub>2</sub>	10.42	3.48	2.14	1.59	1.29
Sh <sub>3</sub>	10.58	3.62	2.29	1.72	1.43
Sh <sub>4</sub>	10.73	3.78	2.43	1.86	1.56
<b>Window D2</b>					
Sh <sub>0</sub>	9.60	2.70	1.46	0.95	<b>0.70</b>
Sh <sub>1</sub>	9.69	2.77	1.50	0.99	0.73
Sh <sub>2</sub>	9.81	2.88	1.58	1.04	0.76
Sh <sub>3</sub>	9.98	3.03	1.70	1.15	0.85
Sh <sub>4</sub>	10.14	3.17	1.84	1.29	0.98
<b>Window D3</b>					
Sh <sub>0</sub>	10.22	3.20	1.85	1.29	<b>1.00</b>
Sh <sub>1</sub>	10.28	3.26	1.90	1.33	1.03
Sh <sub>2</sub>	10.36	3.34	1.97	1.40	1.08
Sh <sub>3</sub>	10.47	3.44	2.07	1.49	1.18
Sh <sub>4</sub>	10.57	3.54	2.18	1.59	1.27
<b>Window T1</b>					
Sh <sub>0</sub>	9.96	2.96	1.64	1.09	<b>0.82</b>
Sh <sub>1</sub>	10.03	3.04	1.69	1.14	0.85
Sh <sub>2</sub>	10.14	3.13	1.78	1.21	0.91
Sh <sub>3</sub>	10.27	3.24	1.88	1.31	1.00
Sh <sub>4</sub>	10.37	3.37	1.99	1.41	1.11

Heating energy consumptions obtained in all the analysed cases are collected in Table 6-5. Results concerning window *D1* show that, for each shading level, no thermal insulation implies the highest energy consumption. Increasing the thermal insulation thickness and consequently reducing heat losses, the heating energy demand strongly decreases: heating demand without insulation is from 6 to 14 times higher than cases characterised by 20 cm of insulation. On the other hand, the results highlight also that increasing the shading, thus reducing the

solar gains, the heating energy demand rises: increments between 5% (for no insulated buildings) and 40% (for buildings with the maximum insulation thickness) are observed for buildings characterised by high shadings with respect to cases without shadings. Therefore, the lowest heating energy demand is obtained by the office design that contemplates the highest insulation level and no shadings, as evidenced in Table 6-5. The same trend is observed for each typology of window. Comparing the lowest energy demand obtained for each window typology, it is interesting to note that the lowest value is achieved with window *D2*; in fact, *D2* is characterized by low thermal transmittance, assuring low heat losses, and by high SHGC that is responsible of high solar gains that help to reduce the heating energy demand. On the contrary, the low heat losses obtained by the triple pane window *T1* do not compensate the low solar gains due to the low SHGC of the glazed system; an increment of 16% is evidenced.

In Figure 6.2 the percentage of annual working time in which the occupant feels comfort conditions (i.e. comfort time), as a function of insulation thickness and shadings, is reported for each window. More in detail, Figure 6.2a shows the comfort time obtained with window labelled *D1*. Considering the cases with no shadings (solid blue line), in Figure 6.2a it can be noted that the increase of the insulation thickness determines lower comfort conditions. In fact, it can be observed that without insulation comfort conditions are guaranteed for 48.6% of the working time, whereas if opaque elements have 20 cm of thermal insulation, comfort time is reduced to 35.6%. The reason of this behaviour is that, increasing the insulation thickness, the incoming solar radiation becomes the main thermal flux of the thermal balance of the office, leading to a frequent overheating condition (i.e. the occupant comfort state is *hot*). In fact, in the case with 20 cm of thermal insulation overheating conditions are evidenced for the 41.4% of the working time. On the contrary, in case of shadings, maximum comfort conditions are obtained considering an optimal thermal insulation thickness. In particular, the more are the shadings the higher is the optimal insulation thickness: 5 cm for shadings configurations *Sh*<sub>1</sub> to *Sh*<sub>3</sub> and 10 cm for *Sh*<sub>4</sub> configuration (overhang length of 2 m). If the insulation thickness is higher than the optimal one, the increasing of overheating conditions is no more compensate by the reduction of undercooling conditions.

If windows are of typology *D2* (Figure 6.2b), some differences with the trends observed for *D1* windows can be found. In particular, high thermal insulation thicknesses are responsible of the worst comfort conditions, for all the shadings considered. In fact, window *D2* is characterised by the same SHGC of window *D1* and by a lower thermal transmittance. Therefore, the incoming solar radiation is the same considering both window *D1* or window *D2*, but window thermal losses are reduced. In this way, adopting windows *D2* the solar radiation is even more important in the thermal balance of the zone and it determines frequent overheating conditions (up to 53% for no shading case). For this reason, optimal

comfort conditions are obtained with low thermal insulation thickness (5 cm for all the cases) except for the case of no shading. In this last case the best solution is obtained for no thermal insulation.

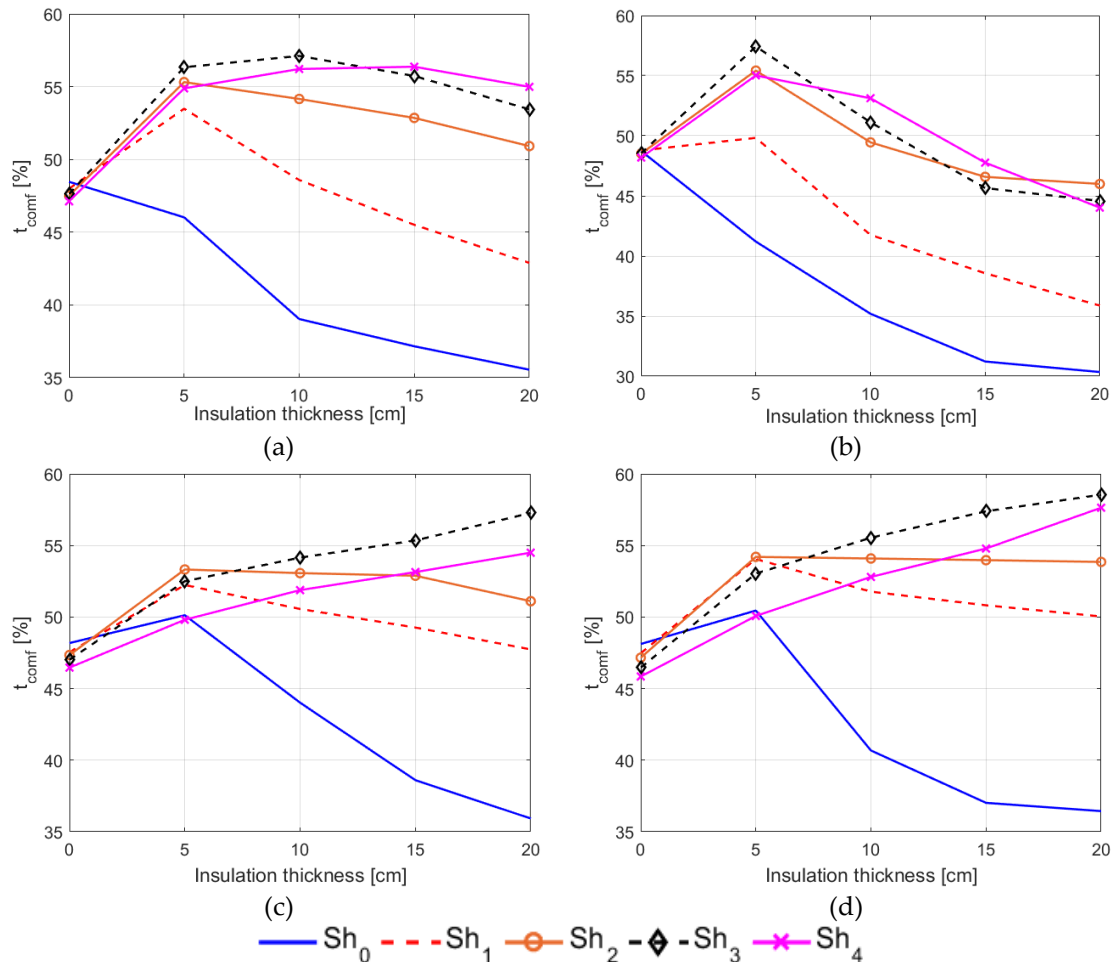


Figure 6.2. Annual comfort time ( $t_{\text{comf}}$ ) for different insulation thickness, shadings and windows for cases with set point temperature equal to 21 °C, neglecting the occupant behaviour. (a) refers to window *D1*, (b) to window *D2*, (c) to window *D3* and (d) to *T1*.

Window *D3* has a thermal transmittance similar to window *D1*, but a reduced SGHC factor, meaning that window *D3* transmits lower incident solar radiation. As represented in Figure 6.2c, the reduced transmitted solar radiation implies a shift of the optimal insulation thickness: for high shadings ( $Sh_3$  and  $Sh_4$  in the figure) the best comfort conditions are obtained with 20 cm of insulation of the opaque elements, whilst in the other cases 5 cm is the optimal insulation thickness. It has to be underlined that, for high shadings, overheating conditions disappear.

Finally, Figure 6.2d shows the comfort time trends for cases in which triple pane window (typology *T1*) are considered. This window, as reported in Table 6-3, is characterised by low SHGC and low thermal transmittance. In Figure 6.2d trends similar to the ones observed for window *D3* can be noted. In fact, high

insulation thickness guarantees the highest comfort time, for cases with significant shadings. Moreover, comparing Figure 6.2d with Figure 6.2c and Figure 6.2b it can be appreciated that the highest comfort times are obtained adopting the triple pane window, revealing that high thermal performances of windows must be coupled to low SHGC in order to reduce both undercooling and overheating conditions. This is confirmed by observing Figure 6.3, where overheating and undercooling times are represented for the building configuration that guarantees the highest comfort time, for each window typology. In this figure it can be appreciated that, low SHGC window determines small overheating time (lower than 2%) but frequent undercooling (around 40%), whereas high SHGC windows determines an increment of overheating and a consequent drop of undercooling.

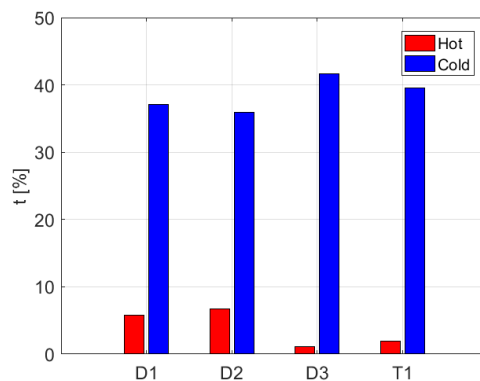


Figure 6.3. Overheating (*hot*) and undercooling (*cold*) times for the optimal (highest comfort time) configuration for each window typology.

In addition, in Figure 6.3 it can be inferred that the use of high thermal performance window (*D2*) with high SHGC lead to a reduction of undercooling increasing overheating and, vice versa, low SHGC with medium thermal performance windows reduce overheating increasing undercooling conditions.

In Figure 6.2 it can be remarked that the highest comfort time is slightly above 55%, because of frequent undercooling conditions, as evidenced by Figure 6.3. Therefore, new numerical simulations have been carried out increasing the thermostat set-point temperature from 21 °C to 23 °C, with the aim to improve comfort conditions by reducing undercooling.

Looking at the results represented in Figure 6.4, related to the comfort time achieved with the new indoor temperature set-up, it can be noted that, generally, comfort conditions are improved reaching, in particular design parameter combinations, values of comfort time close to 100%. In addition, it can be observed that shadings are very important to prevent summer overheating; in fact, the lowest comfort times are obtained if there are no shadings.

More in detail, comparing Figure 6.4a to Figure 6.2a, increments of comfort time from 21% to 37%, due to the higher set-point temperature, are observed. As in the previous cases, if no shadings are provided, the higher is the insulation



thickness, the lower is the comfort time. On the contrary, the presence of shadings coupled to adequate thermal insulation implies comfort times higher than 90%. In general, optimal insulation thickness are higher compared to the respective shading level with a low set-point temperature.

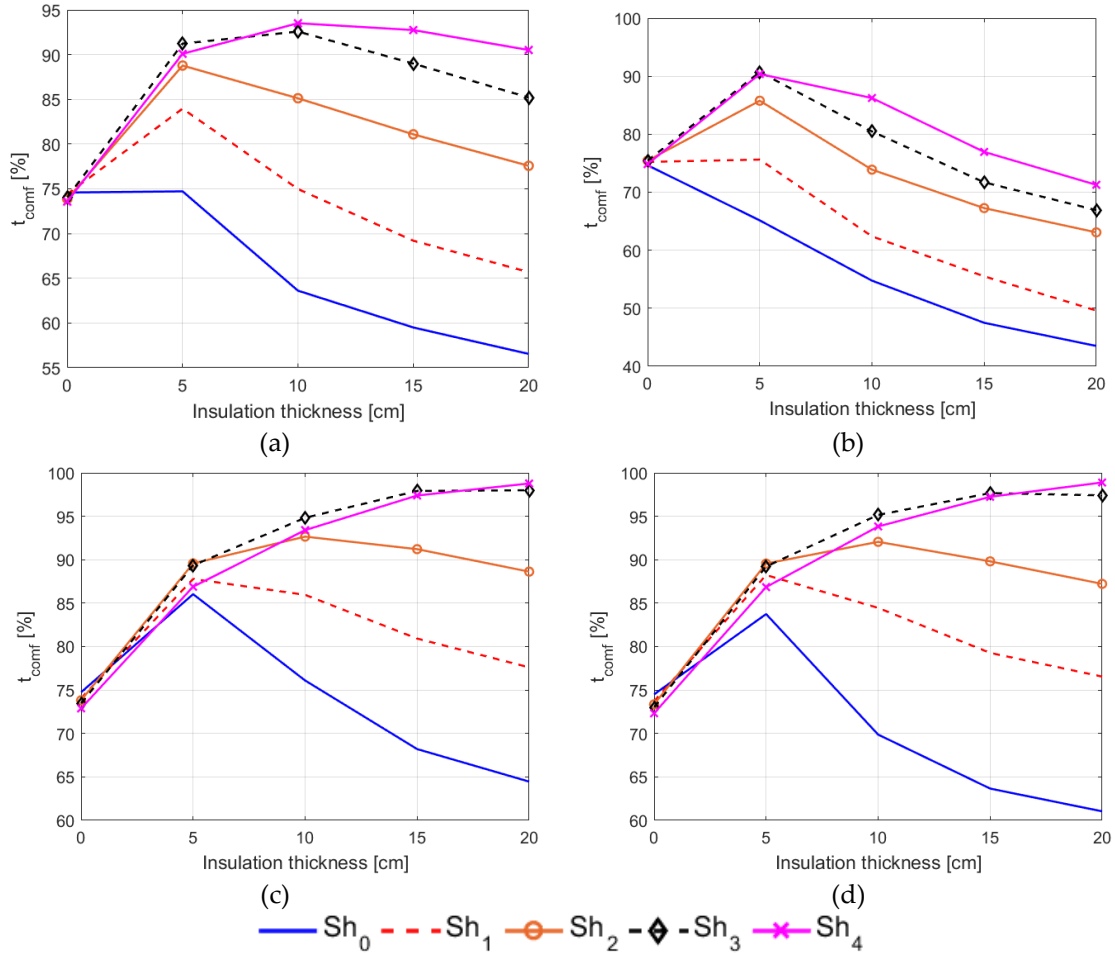


Figure 6.4 Annual comfort time for different insulation thickness, shadings and windows for cases with set point temperature equal to 23 °C, neglecting the occupant behaviour. (a) refers to window *D1*, (b) to window *D2*, (c) to window *D3* and (d) to *T1*.

Comfort conditions guaranteed by the high SHGC double pane window with low thermal transmittance (*D2*), represented in Figure 6.4b, are the worst compared to the other window typology. In fact, the highest comfort time is around 90%. Due to the high solar gains and the low window heat losses, if the thermal insulation thickness is higher than 5 cm, overheating time rises to more than 20% (see Figure 6.5), strongly reducing comfort time.

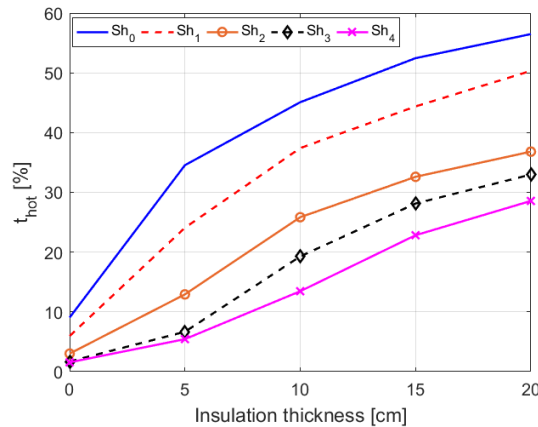


Figure 6.5. Overheating time ( $t_{hot}$ ) for window  $D2$ , as a function of insulation thickness and shadings, indoor set-point temperature of 23 °C.

On the contrary, low SHGC windows ( $D3$  and  $T1$ , whose performance are represented in Figure 6.4c-d, respectively) are able to guarantee high comfort times. In particular, for window  $D3$ , comfort time is higher than 90% when shadings are provided (from  $Sh_2$  to  $Sh_4$ ). Adopting window  $D3$  the optimal insulation thickness varies from 10 to 20 cm, with higher values for high shadings. On the other hand, adopting the triple pane window and the highest values of insulation thickness and shadings, comfort conditions are almost always achieved: in this case the comfort time is 99%.

In Table 6-6, the heating energy consumptions related to the cases with the highest temperature set-point are collected. As the results reported in Table 6-5 for the case with low set-point, it can be observed that the lower energy consumptions are obtained increasing the thermal insulation thickness and reducing the shadings. Again, the minimum energy needs are obtained adopting the high SHGC window with high thermal performances, window  $D2$ . Anyway, higher heat losses correspond to the increment of the set-point and, consequently, greater heating energy needs: increments of about 40-50% are observed for minimum energy consumptions.

Table 6-6. Heating energy demand [MWh/y], for cases with high set-point, varying shadings, insulation and windows, neglecting the occupant behaviour. For each window, minimum energy demand is highlighted on bold.

Shading\insulation	In <sub>0</sub>	In <sub>5</sub>	In <sub>10</sub>	In <sub>15</sub>	In <sub>20</sub>
<b>Window D1</b>					
<b>Sh<sub>0</sub></b>	11.93	4.19	2.67	2.03	<b>1.69</b>
<b>Sh<sub>1</sub></b>	12.02	4.29	2.75	2.10	1.75
<b>Sh<sub>2</sub></b>	12.15	4.41	2.87	2.22	1.85
<b>Sh<sub>3</sub></b>	12.30	4.57	3.02	2.37	2.00
<b>Sh<sub>4</sub></b>	12.43	4.74	3.19	2.53	2.16
<b>Window D2</b>					
<b>Sh<sub>0</sub></b>	11.26	3.48	1.99	1.37	<b>1.06</b>
<b>Sh<sub>1</sub></b>	11.34	3.56	2.05	1.43	1.10
<b>Sh<sub>2</sub></b>	11.51	3.69	2.16	1.53	1.17
<b>Sh<sub>3</sub></b>	11.67	3.85	2.32	1.68	1.32
<b>Sh<sub>4</sub></b>	11.82	4.02	2.49	1.84	1.47
<b>Window D3</b>					
<b>Sh<sub>0</sub></b>	11.90	4.02	2.45	1.80	<b>1.45</b>
<b>Sh<sub>1</sub></b>	11.95	4.09	2.51	1.85	1.49
<b>Sh<sub>2</sub></b>	12.04	4.19	2.60	1.93	1.57
<b>Sh<sub>3</sub></b>	12.15	4.30	2.71	2.04	1.68
<b>Sh<sub>4</sub></b>	12.24	4.42	2.81	2.15	1.78
<b>Window T1</b>					
<b>Sh<sub>0</sub></b>	11.60	3.77	2.22	1.57	<b>1.22</b>
<b>Sh<sub>1</sub></b>	11.67	3.85	2.29	1.63	1.27
<b>Sh<sub>2</sub></b>	11.78	3.95	2.39	1.73	1.37
<b>Sh<sub>3</sub></b>	11.89	4.08	2.50	1.83	1.48
<b>Sh<sub>4</sub></b>	12.00	4.20	2.62	1.96	1.59

### 6.4.3 Results considering the occupant behaviour

After the analysis of the effects of different design solutions on energy consumptions and indoor comfort conditions neglecting the occupant behaviour, new numerical simulations are carried out with the aim to investigate the impact of occupant control of window openings. Since the *Humphreys Adaptive Algorithm*, used for modelling the occupant behaviour, is a stochastic pattern, five numerical simulations are performed for each design combination. Therefore, for each building configuration, the relative standard deviation ( $\sigma_i^*$ ) for both energy consumptions and comfort time has been evaluated by means of the following relationship:

$$\sigma_i^* = 100 \frac{\sigma_i}{|\mu_i|} \quad (6.4)$$

where  $\sigma_i$  is the standard deviation of the *i*-th output parameter (i.e. comfort time and annual heating energy demand) and  $\mu_i$  is the mean value of the *i*-th output, obtained for the same building configuration. As it can be seen in Figure 6.6, the

relative standard deviations are very low: maximum values are lower than 0.15% for the comfort time (Figure 6.6a), whilst for the energy consumptions in almost all the cases the relative standard deviation is lower than 0.5% (Figure 6.6b). Therefore, in the followings, results obtained considering the mean occupant behaviour are reported.

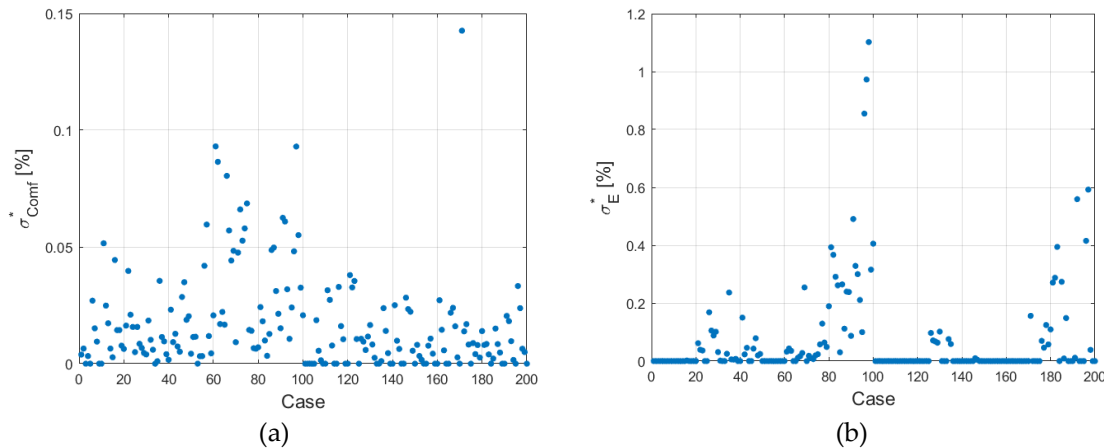


Figure 6.6. Relative standard deviation for comfort time (a) and heating energy consumptions (b), for each building configuration, due to the stochastic user behaviour model.

Results collected in Table 6-7 are referred to the cases characterised by indoor temperature set-point equal to 21 °C. From these results, it can be observed that high thermal insulation thickness (that reduces heat losses to the outdoor environment) and the absence of shadings (maximizing the solar gains) determine the lower heating energy demand. This assessment is valid for each windows typology. Minimum heating energy demand is achieved by adopting the high SHGC double pane window with low thermal transmittance (*D2*): in fact, this window is able to minimize the transmission heat losses and to maximize the solar gains. On the contrary, the triple pane window determines an increment of 14% of the energy needs, followed by the double pane window *D3* (+39%) and window *D1* (+65%).

In Figure 6.7, results related to comfort conditions achieved in the working time for different combinations of insulation thickness, shadings and windows are represented. Figure 6.7a reports the trends of the comfort time obtained adopting windows labelled *D1*. In this figure it can be observed that, except in cases without shadings, the higher the insulation, the greater the comfort time. In fact, if no shadings are considered, the comfort time slightly depends on insulation thickness for values higher than 5 cm. This particular trend reveals that the reduction of undercooling conditions is compensated by the increase of overheating. On the contrary, in case of shadings, the reduction of the frequency of undercooling conditions is higher than the increase of overheating. Anyway, in Figure 6.7a it can be noted that the highest comfort time is obtained adopting

the shading configuration  $Sh_2$ , meaning that, for achieving optimal comfort conditions, the incident solar radiation should not be reduced too much.

Table 6-7. Heating energy consumptions [MWh/y], for cases with set-point temperature equal to 21 °C, for different shadings, insulation thickness and windows, considering the occupant behaviour. For each window, minimum energy demand is highlighted on bold.

Shading\insulation	In <sub>0</sub>	In <sub>5</sub>	In <sub>10</sub>	In <sub>15</sub>	In <sub>20</sub>
<b>Window D1</b>					
<b>Sh<sub>0</sub></b>	10.22	3.30	1.99	1.47	<b>1.19</b>
<b>Sh<sub>1</sub></b>	10.29	3.37	2.05	1.51	1.22
<b>Sh<sub>2</sub></b>	10.41	3.48	2.13	1.59	1.30
<b>Sh<sub>3</sub></b>	10.57	3.62	2.28	1.72	1.43
<b>Sh<sub>4</sub></b>	10.72	3.77	2.43	1.86	1.56
<b>Window D2</b>					
<b>Sh<sub>0</sub></b>	9.60	2.70	1.47	0.97	<b>0.72</b>
<b>Sh<sub>1</sub></b>	9.69	2.77	1.51	1.01	0.74
<b>Sh<sub>2</sub></b>	9.81	2.88	1.58	1.05	0.78
<b>Sh<sub>3</sub></b>	9.98	3.03	1.70	1.16	0.86
<b>Sh<sub>4</sub></b>	10.13	3.17	1.84	1.29	0.98
<b>Window D3</b>					
<b>Sh<sub>0</sub></b>	10.22	3.20	1.85	1.30	<b>1.00</b>
<b>Sh<sub>1</sub></b>	10.27	3.26	1.90	1.34	1.03
<b>Sh<sub>2</sub></b>	10.35	3.34	1.97	1.40	1.08
<b>Sh<sub>3</sub></b>	10.47	3.44	2.06	1.49	1.17
<b>Sh<sub>4</sub></b>	10.56	3.54	2.18	1.59	1.27
<b>Window T1</b>					
<b>Sh<sub>0</sub></b>	9.96	2.96	1.64	1.09	<b>0.82</b>
<b>Sh<sub>1</sub></b>	10.04	3.04	1.69	1.13	0.85
<b>Sh<sub>2</sub></b>	10.14	3.13	1.78	1.21	0.91
<b>Sh<sub>3</sub></b>	10.27	3.24	1.88	1.31	1.00
<b>Sh<sub>4</sub></b>	10.36	3.37	1.99	1.42	1.11

$Sh_2$  is the optimal shadings configuration also for building characterised by window  $D2$ , as inferred by Figure 6.7b. Contrary to window  $D1$ , in these cases, for each shading configuration the highest the thermal insulation thickness, the highest the comfort time. This trend is observed also for buildings defined by low SHGC window; anyway for windows  $D3$  or  $T1$  the highest comfort time is achieved adopting the  $Sh_1$  shadings configuration, as it can be observed in Figure 6.7c and Figure 6.7d. In fact, overheating conditions are already prevented by both the windows openings and the reduced solar gains due to the low SHGC of the windows. Thus, an excessive reduction of the incident solar radiation, due to high shadings configurations, lead to frequently undercooling conditions.

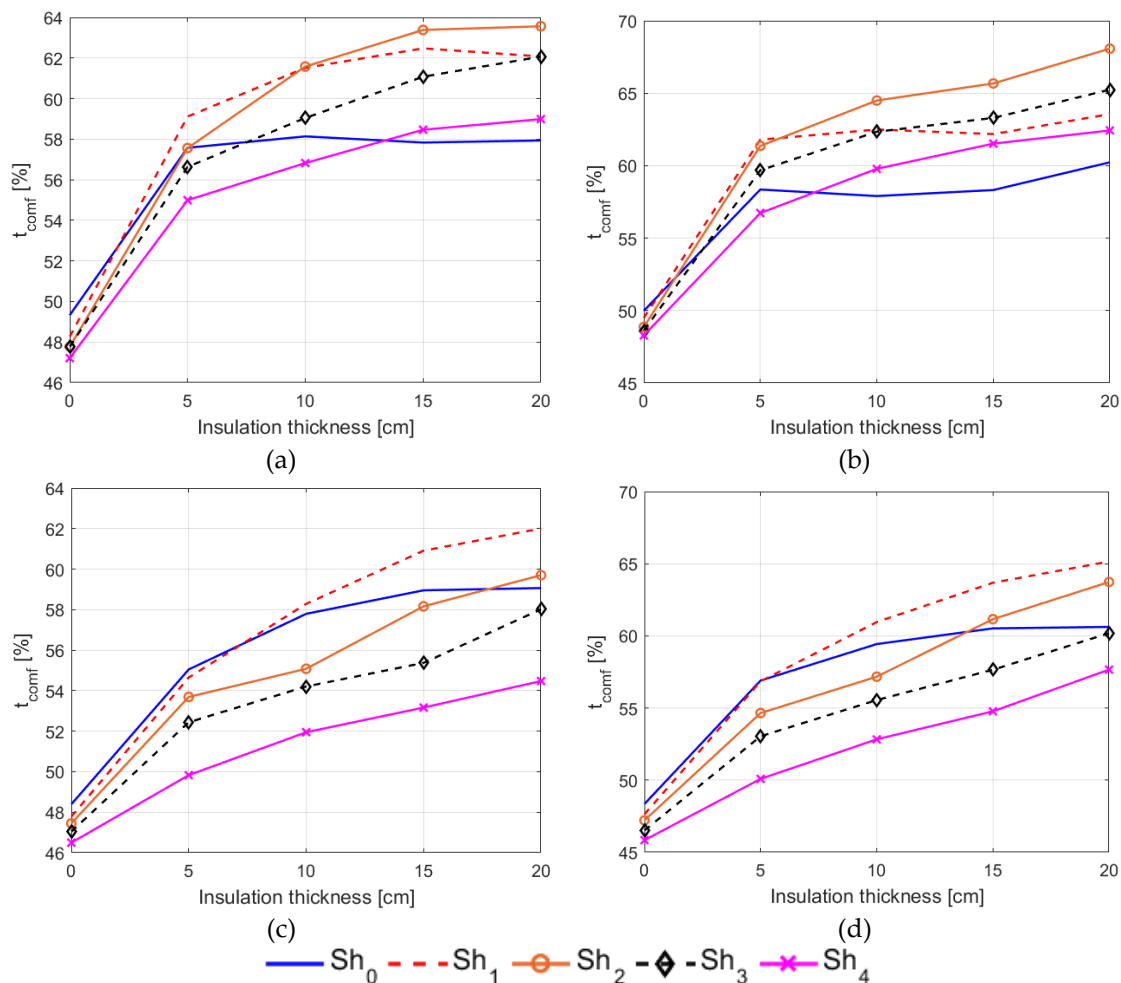


Figure 6.7. Annual comfort time ( $t_{\text{comf}}$ ) for different insulation thickness, shadings and windows in cases with set point temperature equal to 21 °C, considering the occupant behaviour. (a) refers to window  $D1$ , (b) to window  $D2$ , (c) to window  $D3$  and (d) to  $T1$ .

Comparing the comfort time for each window typology, obtained both neglecting (Figure 6.2) and accounting for (Figure 6.7) the occupant behaviour, it can be remarked that the optimal building configurations are characterised by lower shadings and higher insulation thickness, if the occupant is considered. This leads to a reduction of the frequency of undercooling conditions that, as represented in Figure 6.8, are lower than 30%; however, an increment of overheating conditions is observed.

Since even considering the occupant behaviour frequent undercooling conditions are evidenced, indoor comfort can be improved increasing the set point temperature.

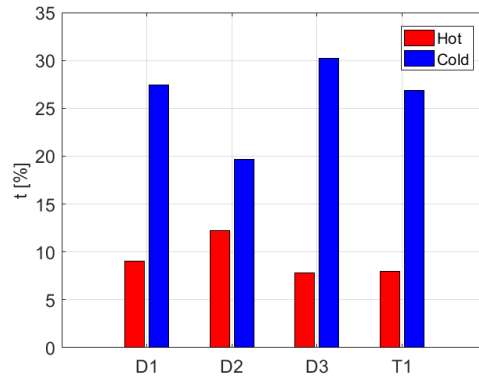


Figure 6.8. Overheating (*hot*) and undercooling (*cold*) times for the optimal (highest comfort time) configuration for each window typology, considering occupant behaviour.

In Figure 6.9 trends of the comfort time are reported when the set point temperature is 23 °C. Again, similar trends are observed for each window typology. The highest comfort times are achieved adopting the shadings configuration  $Sh_4$ , that is characterised by the lowest shading factor (see Table 6-4), whereas the lower are the shadings the lower is the comfort time.

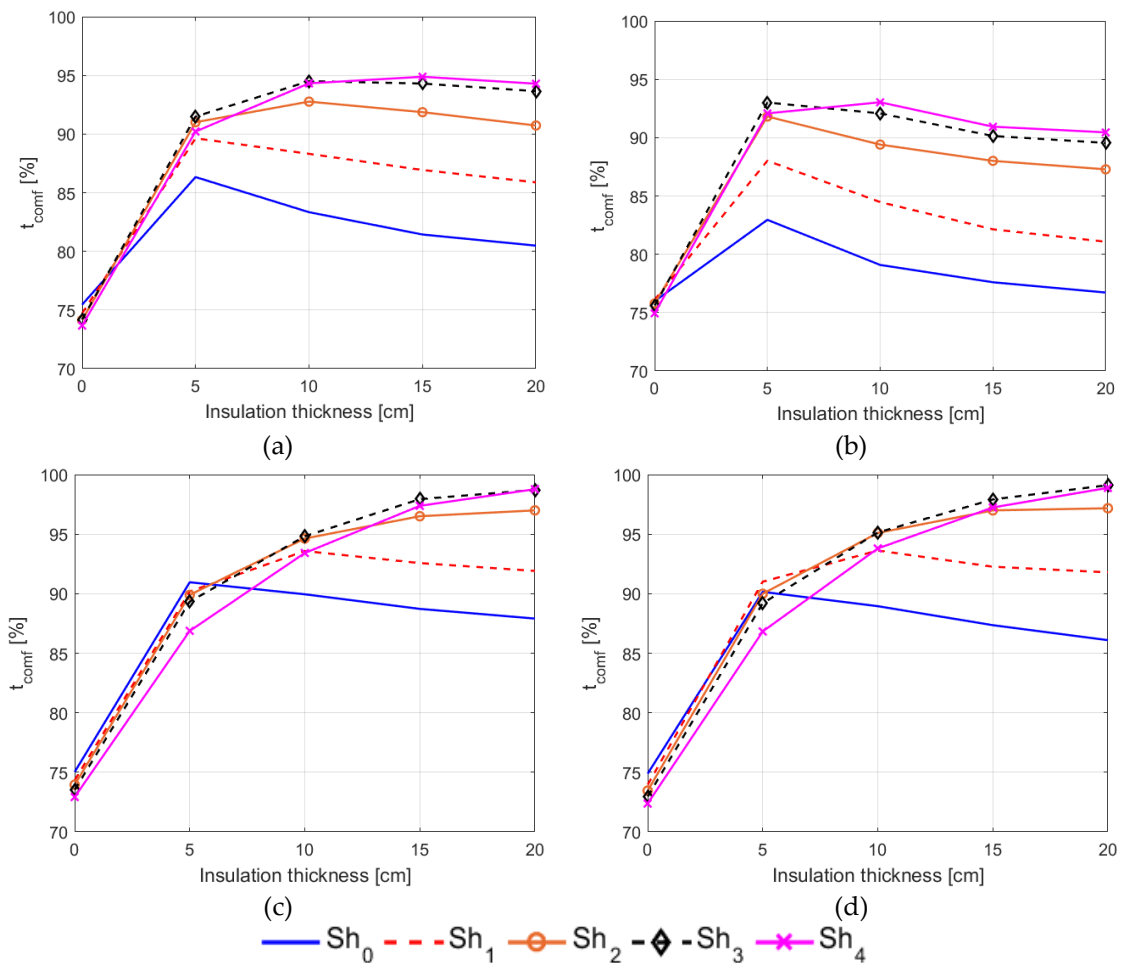


Figure 6.9. Annual comfort time ( $t_{comf}$ ) for different insulation thickness, shadings and windows in cases with set point temperature equal to 23 °C, considering the occupant behaviour. (a) refers to window D1, (b) to window D2, (c) to window D3 and (d) to T1.

Comfort time values greater than 95% are obtained by low SHGC windows, as highlighted in Figure 6.9c and Figure 6.9d. In these cases, for shading configurations  $Sh_2$  to  $Sh_4$ , high thermal insulation thicknesses imply high comfort times. The highest comfort time is 99% and is achieved by the triple pane window.

As highlighted in Table 6-8, for each window typology the lowest energy demand is achieved reducing the solar gains (high shadings) and maximizing the thermal insulation. Contrary to the cases in which the temperature set-point is 21 °C, the minimum heating demand is achieved by the triple pane window instead of the double pane window  $D2$ . In fact, adopting a higher temperature set-point, buildings characterised by windows  $D2$  require 11% more energy than buildings in which window  $T1$  is installed; whereas the adoption of windows  $D1$  and  $D3$  requires 39% and 15% more energy, respectively. Improvements on comfort conditions due to the increment of set-point temperature determine higher heating energy demand: comparing the results collected in Table 6-7 and in Table 6-8 increments between 40% to 100% are observed.

Table 6-8. Heating energy consumptions [MWh/y], for cases with set-point temperature equal to 23 °C, for different shadings, insulation thickness and windows, considering the occupant behaviour. For each window, minimum energy demand is highlighted on bold.

Shading\insulation	In <sub>0</sub>	In <sub>5</sub>	In <sub>10</sub>	In <sub>15</sub>	In <sub>20</sub>
<b>Window D1</b>					
<b>Sh<sub>0</sub></b>	12.03	4.20	2.69	2.07	<b>1.76</b>
<b>Sh<sub>1</sub></b>	12.09	4.29	2.77	2.14	1.82
<b>Sh<sub>2</sub></b>	12.23	4.41	2.88	2.26	1.91
<b>Sh<sub>3</sub></b>	12.35	4.57	3.02	2.37	2.01
<b>Sh<sub>4</sub></b>	12.48	4.76	3.19	2.53	2.16
<b>Window D2</b>					
<b>Sh<sub>0</sub></b>	11.33	3.53	2.15	1.67	<b>1.40</b>
<b>Sh<sub>1</sub></b>	11.42	3.59	2.20	1.69	1.42
<b>Sh<sub>2</sub></b>	11.58	3.70	2.30	1.72	1.43
<b>Sh<sub>3</sub></b>	11.73	3.85	2.41	1.82	1.49
<b>Sh<sub>4</sub></b>	11.87	4.02	2.50	1.91	1.57
<b>Window D3</b>					
<b>Sh<sub>0</sub></b>	11.98	4.02	2.45	1.80	<b>1.45</b>
<b>Sh<sub>1</sub></b>	12.04	4.09	2.51	1.85	1.50
<b>Sh<sub>2</sub></b>	12.10	4.18	2.60	1.93	1.57
<b>Sh<sub>3</sub></b>	12.22	4.31	2.71	2.04	1.68
<b>Sh<sub>4</sub></b>	12.29	4.43	2.82	2.15	1.78
<b>Window T1</b>					
<b>Sh<sub>0</sub></b>	11.68	3.77	2.22	1.59	<b>1.26</b>
<b>Sh<sub>1</sub></b>	11.75	3.85	2.29	1.67	1.31
<b>Sh<sub>2</sub></b>	11.83	3.95	2.38	1.73	1.39
<b>Sh<sub>3</sub></b>	11.95	4.08	2.50	1.84	1.48
<b>Sh<sub>4</sub></b>	12.05	4.22	2.62	1.96	1.59



### 6.4.4 Comparison of results

The adoption of the occupant behaviour model in numerical simulations determines remarkable implications on both energy consumptions and comfort indoor conditions. More in detail, comparing the heating energy demand for cases characterised by low set-point values (see Table 6-5 and Table 6-7), it can be observed that the adoption of occupant behaviour model in numerical simulations determines increments lower than 0.5% of the energy consumption, except cases characterised by double pane window *D2* (in this case increments are lower than 3%). Moreover, both considering or neglecting the occupant control of windows, the minimum energy demand is achieved adopting the double pane window *D2*, the highest insulation thickness without any shading.

On the contrary, the occupant behaviour strongly affects comfort conditions. In fact, different comfort time trends are observed for each window typology without shadings: if windows are not operable (see Figure 6.2a), the higher the insulation, the less the comfort time. When the occupant can control the window openings (see Figure 6.7a) higher thermal insulations determine increments of the comfort time. In fact, as it can be appreciated in Figure 6.10, if windows are operable, the occupant can reduce overheating by increasing the air change rate by opening the windows.

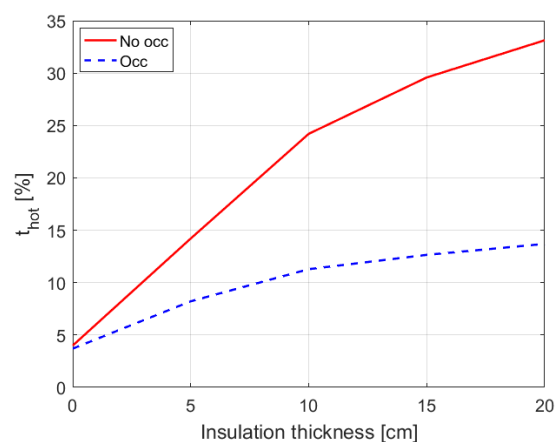


Figure 6.10. Overheating time ( $t_{hot}$ ) for buildings characterised by window *D1*, shading *Sh2* and set-point of 21 °C as a function of insulation thickness, both considering and neglecting the occupant behaviour.

Overheating reductions driven by occupant behaviour are observed in all the cases, determining an increment of the comfort time from less than 1% (for cases with low SHGC windows and high shadings) to 30% (for cases without shadings, high thermal insulation thickness and high SHGC windows).

Analysing the heating demand concerning cases characterised by a set point temperature of 23 °C, low increments are observed for buildings with operable windows: if the window *D1* is considered, increments are less than 5%, whereas referring to low SHGC windows cases discrepancies are less than the 3% and no

differences are remarked for high shadings cases. On the contrary, referring to buildings in which windows  $D2$  are installed, high increments of energy needs are due to the occupant windows openings: for high insulation and no shading, the heating demand is 34% higher than the respective case without window opening.

On the other hand, as for cases characterised by a low set-point temperature, the occupant control of windows determines remarkable increments (up to 33%) of the comfort time for buildings without shadings, high thermal insulation and high SHGC window. Referring to buildings with high shadings and low SHGC windows differences due to the adoption of the occupant behaviour model are not remarked. However, it has to be highlighted that, with the higher set-point, similar trends of comfort time are observed both considering or neglecting the occupant behaviour: the only difference that can be appreciated is related to the insulation thickness that determines the maximum comfort time, that is higher if the occupant can open the window.

In conclusion, it can be stated that the occupant behaviour determines a slight increment of the heating energy demand, except for cases characterised by high set-point temperature and the adoption of windows  $D2$ . Moreover, accounting for the occupant behaviour more remarkable increase of comfort conditions, due to the reduction of overheating conditions, are evidenced.

#### ***6.4.5 Implications of the occupant behaviour on energy consumptions and indoor comfort conditions sensitivity to design parameters***

The robustness of a design configuration can be assessed performing a sensitivity analysis of the results to the design parameters. In this case, a sensitivity analysis of heating energy demand and of comfort time is carried out comparing the results obtained for different building configurations, both considering and neglecting the occupant behaviour. Since the same conclusions can be stated for both the temperature set-points considered, only the results related to cases characterised by a set point of 23 °C are analysed.

In Figure 6.11 the sensitivity of comfort conditions to the insulation thickness, ( $S_{conf,i}$ ), neglecting and considering the occupant behaviour, is represented for different shadings and windows. The  $S_{conf,i}$  parameter depicted in Figure 6.11 is defined as:

$$S_{conf,i} = \left| \max t_{conf,i} - \min t_{conf,i} \right|_{w,sh} \quad (6.5)$$

where the subscripts  $w$  and  $sh$  indicate that the difference between the maximum and minimum comfort time ( $t_{comf}$ ) is evaluated for constant window typology and shadings, thus varying only the insulation thickness,  $i$ .

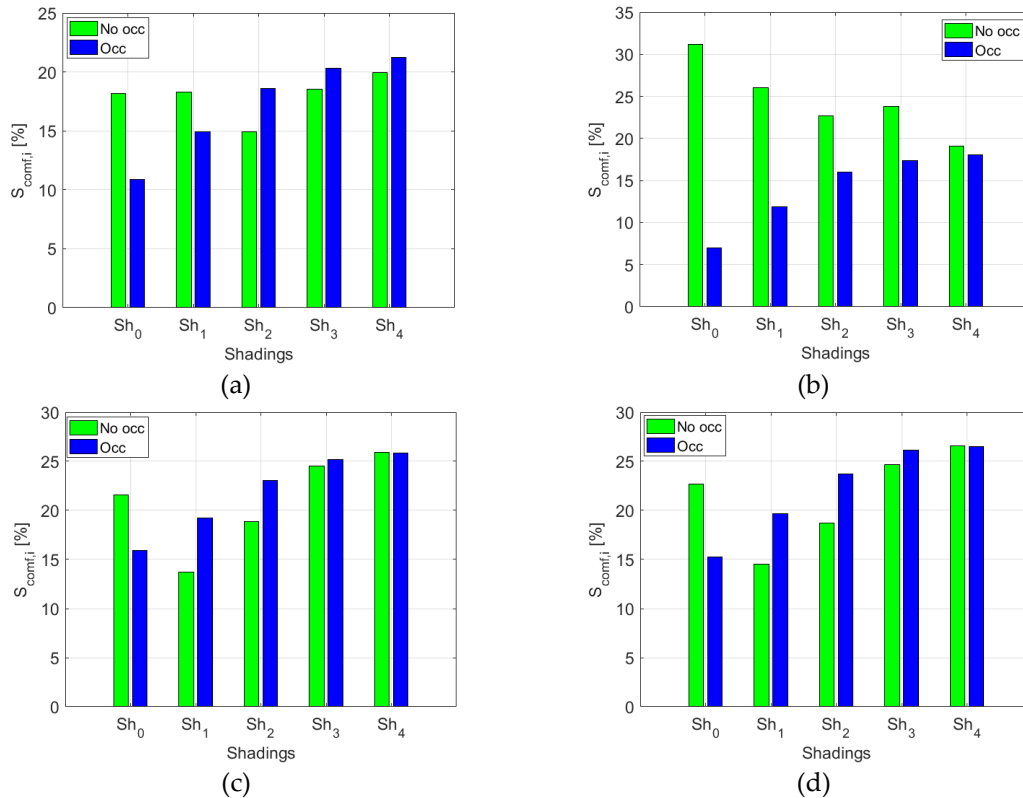


Figure 6.11. Comfort time sensitivity to insulation ( $S_{comf,i}$ ) considering (blue bars) or neglecting (green bars) the occupant behaviour, for different shadings and windows: (a), (b), (c) and (d) refer to window  $D1$ ,  $D2$ ,  $D3$  and  $T1$ , respectively.

The comparison of the sensitivity of the comfort time to the insulation of the external envelope elements highlight that buildings without shadings are more sensitive to insulations if the occupant behaviour is neglected, regardless the window typology. However, differences between the cases in which the occupant behaviour is neglected (green bars in Figure 6.11) and cases in which it is considered (blue bars) are reduced by increasing the shadings: in fact, for each window typology, it can be remarked that for shadings  $Sh_3$  and  $Sh_4$  green and blue bars define almost the same sensitivity. Moreover, in Figure 6.11 it can be appreciated that low SGHC windows determine the highest sensitivity to the insulation level if the occupant behaviour is taken into account.

The sensitivity of comfort conditions to shadings ( $S_{comf,sh}$ ), reported in Figure 6.12, is evaluated similarly to the sensitivity to insulation thickness:

$$S_{comf,sh} = \left| \max t_{comf,sh} - \min t_{comf,sh} \right|_{w,i} \quad (6.6)$$

thus, as the difference between the maximum and minimum comfort time evaluated fixing window typology and insulation thickness.

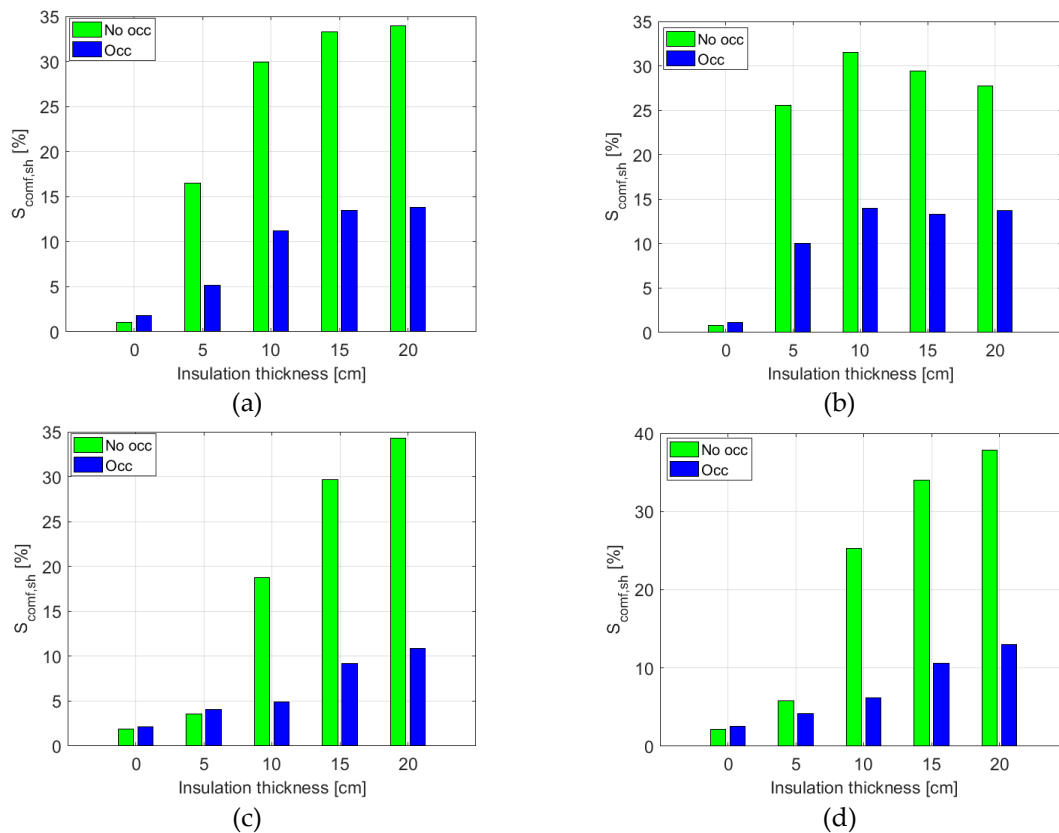


Figure 6.12. Comfort time sensitivity to shadings ( $S_{conf,sh}$ ) considering (blue bars) or neglecting (green bars) the occupant behaviour, for different insulations and window: (a), (b), (c) and (d) refer to window  $D1$ ,  $D2$ ,  $D3$  and  $T1$ , respectively.

The results reported in Figure 6.12 emphasize that the occupant behaviour strongly affects the sensitivity of comfort conditions to the shadings. In fact, it can be observed that the comfort time sensitivity to the shadings is less than 15% if the occupant can open the windows, whereas if windows are not operable the sensitivity rises up to 35%. Moreover, it can be remarked that, concerning the cases in which the occupant behaviour is considered, low SHGC window determines the lower sensitivity to shadings.

Analysing both the results reported in Figure 6.11 and Figure 6.12, it can be assessed that the possibility of the occupant to interact with the building by opening the windows, in order to modify the indoor comfort conditions, determines a reduction of the sensitivity of comfort conditions to the design parameters.

Similar conclusions can be stated considering the sensitivity of the energy demand to the design parameters, represented in Figure 6.13 and Figure 6.14. In particular, in Figure 6.13 the sensitivity ( $S_{E,i}$ ) to insulation of external envelope elements is evaluated as:

$$S_{E,i} = \left| \frac{\max E_i - \min E_i}{\max E_i} \right|_{w,sh} \quad (6.7)$$

where  $E$  is the annual heating energy demand.

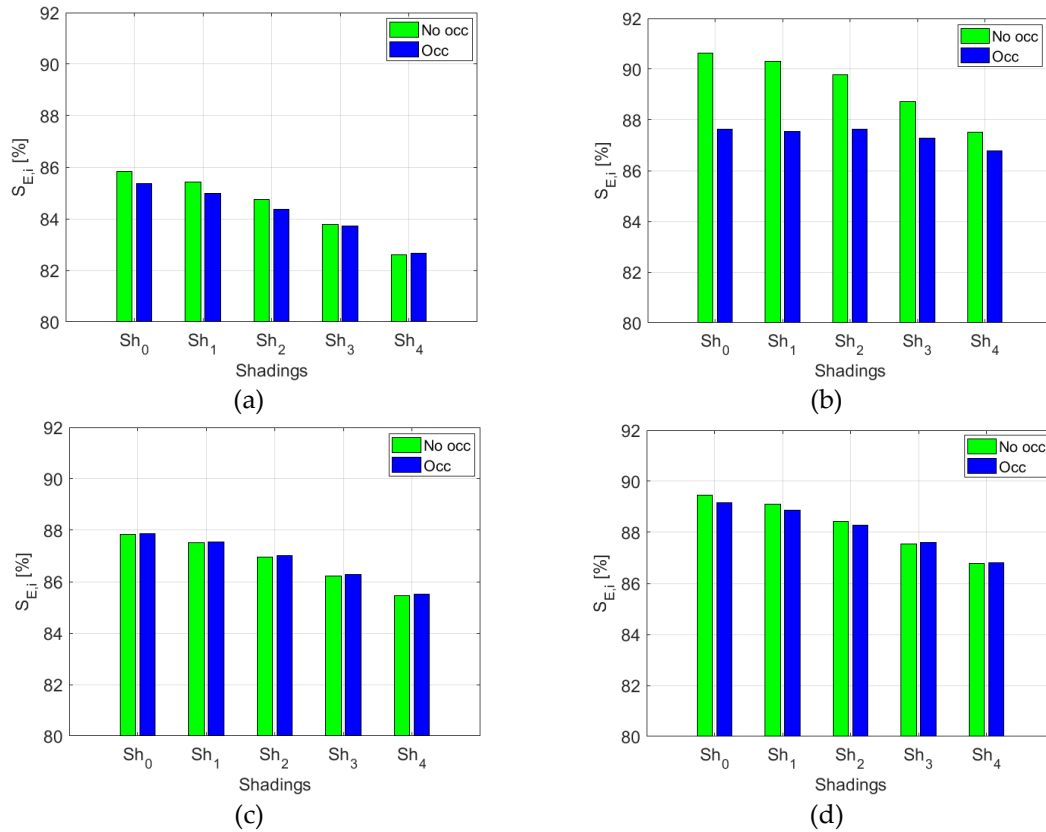


Figure 6.13. Comparison of  $S_{E,i}$  for different shadings and windows: (a), (b), (c), (d) refers to windows  $D1$ ,  $D2$ ,  $D3$  and  $T1$ , respectively.

Comparing the results represented in Figure 6.13 for different windows, it can be observed that the highest sensitivities of the energy demand to insulation thickness are obtained by adopting windows  $D2$  and  $T1$  (see Figure 6.13b-d), that are characterised by high thermal performances (i.e. low thermal transmittance). Moreover, except for window  $D2$ , the occupant behaviour does not significantly affect the sensitivity of the energy demand to the insulation thickness.

Finally, the sensitivity of the energy demand to shadings, reported in Figure 6.14, is evaluated as:

$$S_{E,sh} = \left| \frac{\max E_{sh} - \min E_{sh}}{\max E_{sh}} \right|_{w,i} \quad (6.8)$$

Again, Figure 6.14 highlights that the occupant behaviour determines low sensibility of the energy demand to the shadings. Moreover, it is observed that,

the higher is the insulation thickness, and thus the higher is the weight of solar gains on the global heat balance of the office, the higher is the sensitivity to shadings. However, buildings which have windows  $D2$ , if the occupant behaviour is considered, the highest sensitivity of the energy demand to shadings is achieved by a medium insulation thickness.

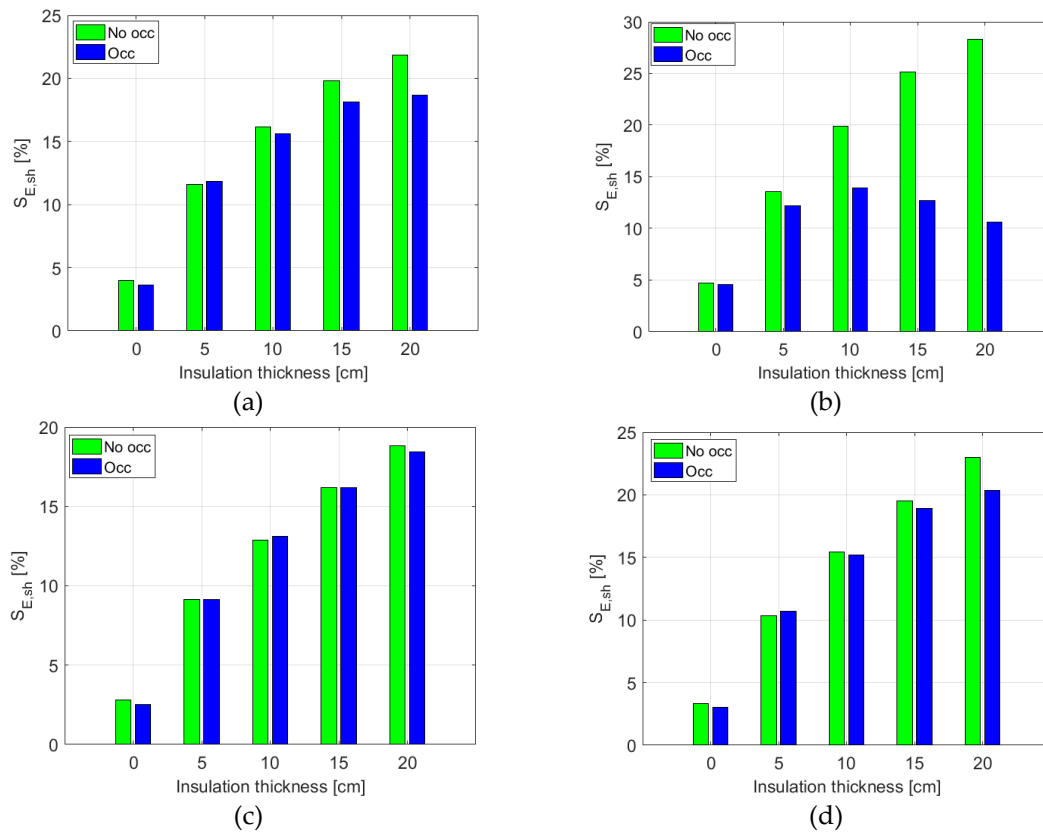


Figure 6.14. Sensitivity of energy demand on shadings  $S_{E,sh}$ , both considering (blue bars) and neglecting (green bars) the occupant behaviour, for different insulations and windows  $D1$  (a),  $D2$  (b),  $D3$  (c) and  $T1$  (d).

#### 6.4.6 Multi-objective optimizations

In section 6.4.4 it has been highlighted that the occupant control of window openings determines different dependencies of the comfort time to the building design parameters compared to the cases in which windows are not operable. Observing Figure 6.2 to Figure 6.9 it can be noted that the maximum comfort time is obtained by different combinations of shadings, insulation level and windows if the occupant behaviour is considered or neglected. As an example, referring to the cases characterised by the lower thermostat settings it can be remarked that, if the occupant can open the window the best comfort conditions are achieved with the highest insulation thickness, regardless the window typology. On the

contrary, if windows are not operable, the maximum comfort time is reached adopting lower insulations.

Although the same dependencies of heating energy demand to shadings and insulation are evidenced, it can be observed that the typology of windows that determines the minimum energy consumptions is different if the occupant behaviour is neglected or considered. In fact, concerning cases characterised by a temperature set-point of 23 °C, the minimum energy demand is achieved by window *D2* if windows are not operable, whereas window *T1* determines the lowest energy needs when the occupant behaviour is taken into account.

Therefore, it can be stated that the optimal design parameters combination is affected by the occupant behaviour. However, since optimal energy demand (i.e. the lowest) and best comfort conditions (i.e. the highest) are usually contrasting goals and are achieved by different building configurations, the optimal building design is carried out solving multi-objective optimization problems. Since it is expected that the user behaviour affects also the Pareto frontier, this approach is adopted both considering and neglecting the occupant behaviour.

For these reasons, multi-objective optimizations of both energy demand and comfort conditions are carried out. Numerical simulations are performed constantly increasing: (i) the thermal insulation thickness of 2.5 cm from 0 to 20 cm and (ii) the overhang length of 0.25 m from 0 to 2 m. Again, the four window typologies are considered together with both the set-points (21 °C or 23 °C). The two objective functions that have to be minimized are: (i) the annual heating demand ( $E$ ) and (ii) the annual discomfort time ( $t_{disc}$ ) evaluated as the complement to unity of the comfort time.

In Figure 6.15a, the Pareto frontier related to buildings with windows *D1* and a set-point 21 °C is represented. In this figure it can be observed that if the occupant behaviour is neglected (empty markers), nondominated solutions, i.e. the optimal ones, are obtained for large insulations (thickness greater than 15 cm, represented by diamond markers) and any shadings. Additional non-dominated configurations are characterised by low medium insulation (5-10 cm, triangle marker) and shadings (overhang length between 1 and 1.5 m, highlighted by magenta colour). The first configurations guarantee the lowest energy demands, whilst the second ones determine the lowest discomfort time.

As evidenced by Figure 6.15a, a good trade-off between heating energy demand and comfort conditions is achieved by buildings characterised by high thermal insulations and medium shadings. However, when the occupant behaviour is considered (filled markers), the Pareto frontier is composed only by solutions related to high insulations and low or absent shadings (blue and red markers, respectively). Moreover, in Figure 6.15a it can be appreciated that the occupant behaviour determines better values for both the energy demand and comfort time compared to buildings in which windows are non-operable.

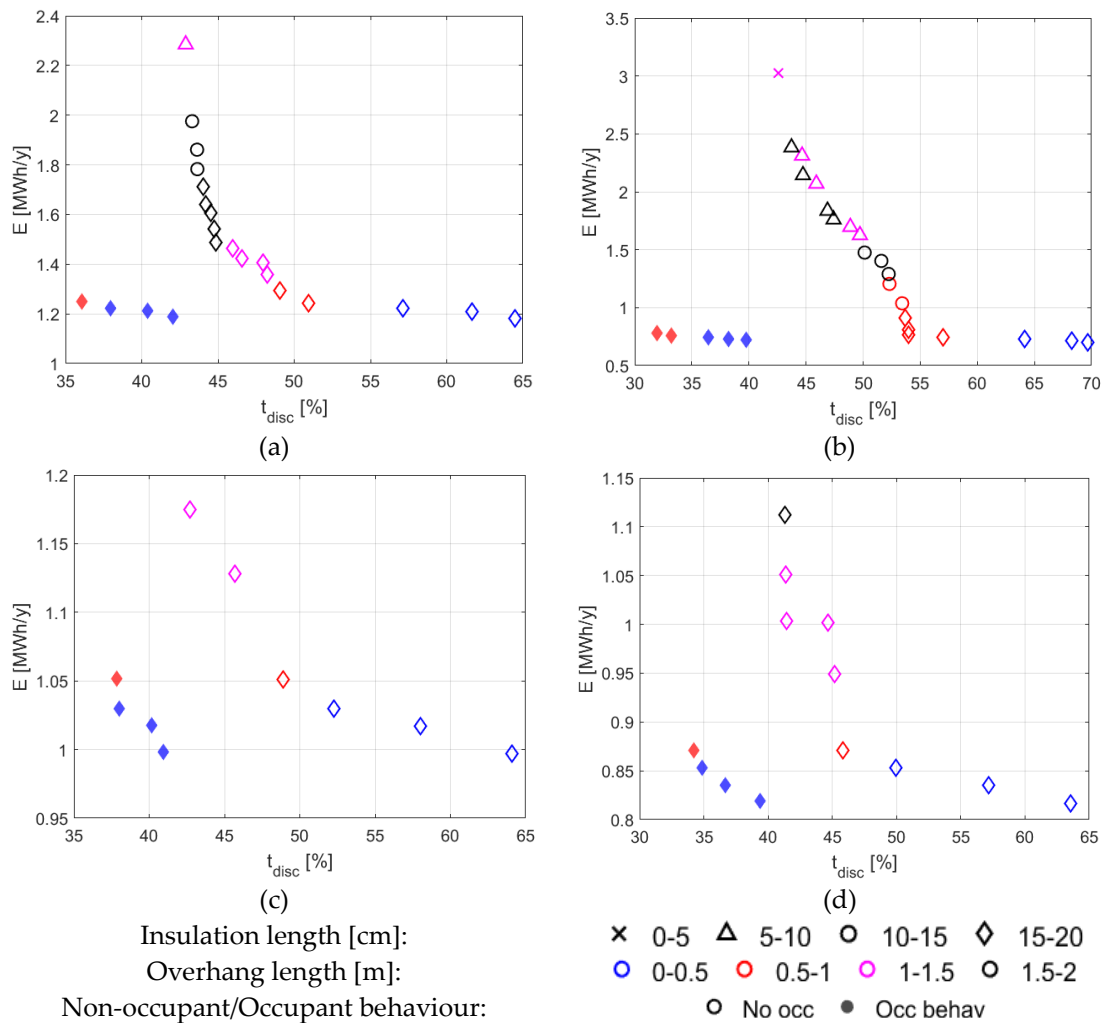


Figure 6.15. Pareto frontiers of multi-objective optimizations for different window typologies, referring to buildings with set point of 21 °C. (a) refers to buildings composed by window *D1*, (b) to buildings with windows *D2*, (c) to cases with window *D3* and (d) to window *T1* cases.

Referring to buildings composed by windows *D2* (see Figure 6.15b), if windows are non-operable, the Pareto frontier is composed by several building configurations: those characterised by high insulation and low shadings guarantee the lowest energy demand, whilst moving towards lower insulation and higher shadings the heating demand rises and the discomfort time decreases. As remarked for windows *D1*, also in these cases optimal building configurations are characterised by high insulations and low shadings if the occupant behaviour is taken into account.

Buildings characterised by both double and triple pane low SHGC windows show similar Pareto frontiers (see Figure 6.15c-d). In fact, not accounting the occupant behaviour, optimal solutions are obtained for high insulations and from absent to medium shadings: the higher the shadings, the higher the heating demand and the comfort time. On the contrary, referring to cases in which the occupant behaviour is considered, optimal solutions are obtained by buildings defined by high insulations and very low shadings.



In conclusion, the analysis of the results reported in Figure 6.15 put in evidence three important aspects related to the adoption of the occupant behaviour in numerical simulations:

- Solutions obtained neglecting the occupant behaviour are characterised by higher values of both energy demand and discomfort time compared to the solutions concerning the occupant behaviour;
- The spread between the results, if the occupant behaviour is considered, is very low compared to the Pareto frontier for cases in which the occupant behaviour is neglected;
- If the occupant behaviour is neglected, the Pareto frontier is described by several building configurations (up to 21), whereas if the occupant behaviour is accounted the building configurations composing the Pareto frontier are no more than 5.

It has to be remarked that the Adaptive Humphreys Algorithm considers the probability associated to the window opening correlated to the indoor thermal conditions; in fact, following this model, the window is opened only if the occupant considers the indoor temperature too high. That means that, in this model, random window openings (contrary to the indoor comfort conditions) are not considered. In this last case (random window opening not correlated to the indoor thermal conditions) larger deviations of the energy consumptions are expected with respect to the cases described in this thesis. Of course, if the window opening is considered as a function not only of the indoor temperature but of other comfort parameters (e.g. CO<sub>2</sub> concentration, indoor air humidity ratio) occupant can open the window despite feeling cold conditions, leading to a rise of uncomfortable conditions and higher energy consumptions.

If the set-point temperature is shifted from 21 °C to 23 °C, different assessments can be inferred. More in detail, as represented in Figure 6.16a, the Pareto frontier of buildings with non-operable windows is composed by lots of configurations, starting from high insulated buildings without shadings (that guarantee the lowest energy demand) moving to medium and low insulations coupled to high shadings, that determine the lowest discomfort time. Similarly, if the occupant can open the windows, it can be observed that optimal configurations are described by high insulations and any level of shadings: moving from absent to high shadings, the heating demand rises and the discomfort time is reduced. However, the lowest discomfort time and the highest energy consumption are achieved by building characterised by medium insulation (15 cm) and high shadings (overhang length of 2 m).

If buildings are composed by high SHGC double pane window (*D2*), almost the same building configurations compose the Pareto frontier, both if the occupant behaviour is neglected or considered. In fact, in Figure 6.16b it can be seen that the lowest energy consumptions are achieved by high insulated buildings without shadings, whereas moving to higher shadings and lower

insulated buildings the heating demand rises and the discomfort time drops. It can be remarked that if the occupant behaviour is neglected, the lowest discomfort time is achieved for very low insulations (thickness lower than 5 cm) and high shadings configuration.

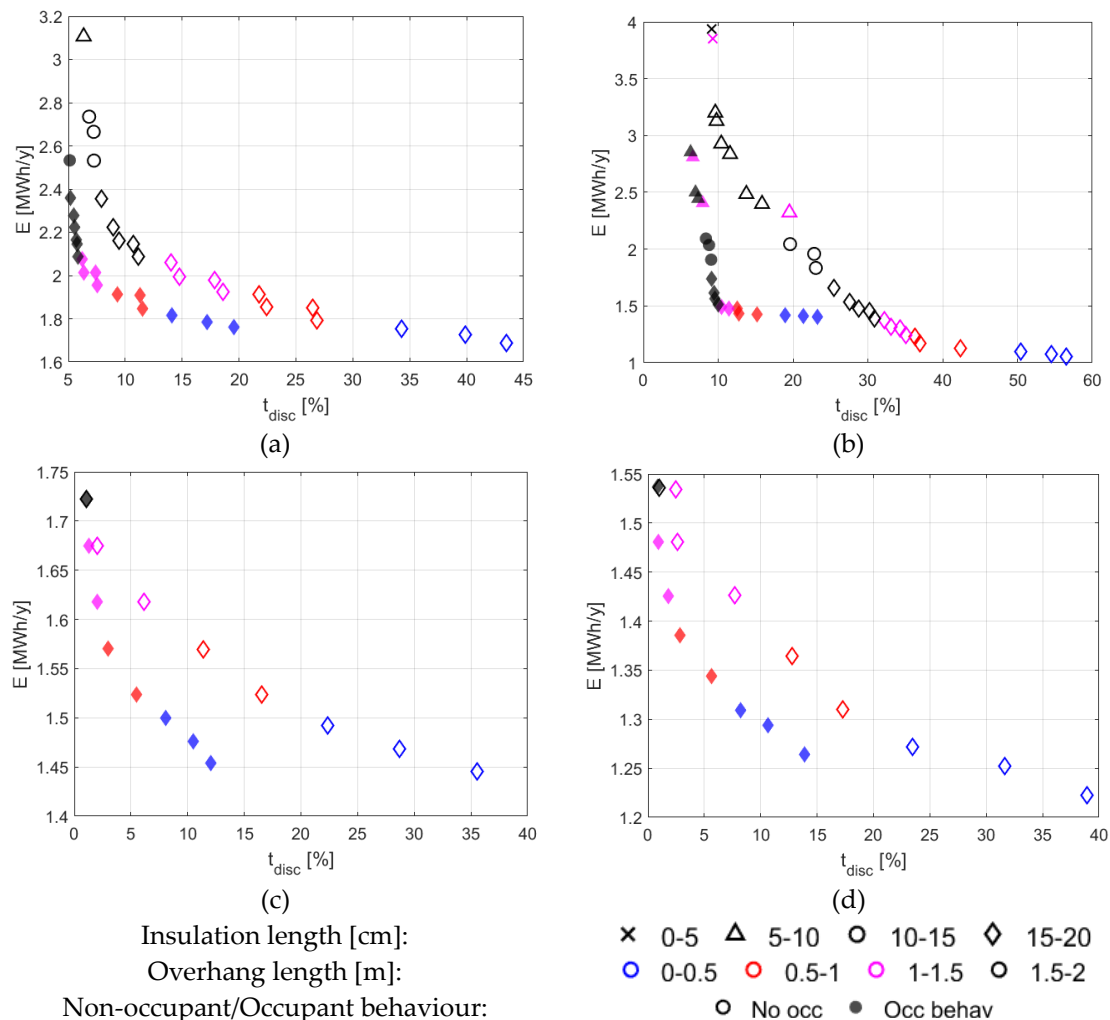


Figure 6.16. Pareto frontiers of multi-objective optimizations for different windows typology, referring to buildings with thermostat set point equals to 23 °C. (a) refers to buildings composed by window  $D1$ , (b) to buildings with windows  $D2$ , (c) to cases with window  $D3$  and (d) to window  $T1$  cases.

Anyway, the two Pareto frontiers have different shapes and if the occupant behaviour is taken into account, a good trade-off between energy demand and comfort time can be observed: buildings defined by high insulations and medium/high shadings are characterised by discomfort time and energy demand not so higher than the lowest ones (around +6% and +0.2 MWh, respectively).

As represented in Figure 6.16c-d, high insulated buildings are the only building configurations that compose the Pareto frontiers for buildings defined by low SHGC window, both considering and neglecting the occupant behaviour. More in detail, the higher the shadings, the higher the energy consumption and

the lower the discomfort time. However, it should be noted that only one configuration described by the highest shadings composes the Pareto frontier. Moreover, it can be remarked that for high shading configurations, results concerning the occupant behaviour are very close to the ones obtained neglecting it. In fact, in these cases, as analysed in the previous sections, the frequency of overheating is close to zero and, consequently, the occupant does not interact with windows.

Again, the comparison of the Pareto frontiers obtained with different windows typologies both neglecting and considering the occupant behaviour put in evidence that the spread between the results is higher if the occupant behaviour is neglected. However, in these cases, the difference among the results due to the adoption or not of the occupant behaviour is reduced and, for some building configurations, energy demand and discomfort time are the identical. Anyway, generally, it can be assessed that the occupant behaviour determines solutions with lower discomfort time and energy consumptions.

Finally, multi-objective optimizations of energy consumptions and discomfort time have been carried out for the two temperature set-points, adding to the design parameters (i.e. insulation thickness and shadings) the windows typology. Since this is the only insulation level that composes the Pareto frontier, results represented in Figure 6.17 are related only to building with high insulations (thickness greater than 15 cm).

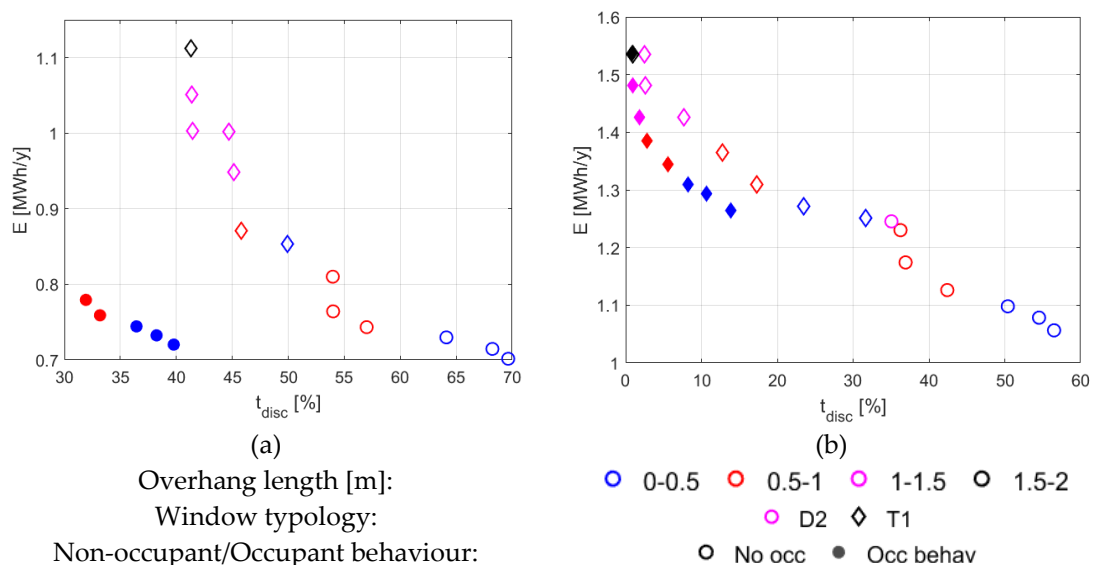


Figure 6.17. Pareto frontiers of multi-objective optimizations referring to buildings with thermostat set point equals to 21 °C (a) and 23 °C (b).

When the heating set-point temperature is 21 °C (Figure 6.17a), it can be remarked that if the occupant behaviour is neglected, the lowest energy consumptions are achieved by buildings with windows *D2* and low shadings, whereas adopting the triple pane window (*T1*) and increasing the shadings the

discomfort time is reduced. On the contrary, if the occupant behaviour is taken into account, the Pareto frontier is composed only by buildings defined by windows  $D2$ , with low shadings (overhang length lower than 1 m). Again, the Pareto frontier concerning the occupant behaviour is defined by a reduced spread between the results and between the building configurations; moreover, it can be observed that the occupant behaviour determines lower discomfort time and, generally, lower heating demand.

The Pareto frontiers observed when the heating temperature set-point is fixed at 23 °C (see Figure 6.17b) are similar to the ones described for the lower thermostat settings, both considering or neglecting the occupant behaviour. Anyway, adopting the higher temperature set-point, it can be noted that if the occupant behaviour is considered, the Pareto frontier is composed only by buildings characterised by triple pane windows. Moreover, it can be remarked that the lowest energy needs are obtained if the occupant behaviour is neglected: the difference between the lowest values achieved neglecting or considering the occupant behaviour is around 0.2 MWh/y. This difference is strongly reduced if the discomfort time is lower than 20%. In fact, in this region, the two Pareto frontiers tend to converge. Again, the spread of the Pareto frontier is higher if the occupant behaviour is neglected.

### 6.5 User-free solutions

The analysis of the Pareto frontiers defining the optimal building configurations for each window typology, represented in Figure 6.16, put in evidence that some configurations compose the Pareto frontiers related to both the cases in which the occupant behaviour is neglected or considered. Anyway, as it can be observed in Figure 6.16 and how assessed in the previous sections, the occupant behaviour affects energy consumptions and comfort conditions depending on the building configuration. It has to be remarked that, in the design phase of a building, in addition to energy performances and comfort conditions also the robustness of a solution has to be accounted. In fact, as in real applications design parameters are affected by some variability, if a solution is very sensitive to an input parameter (i.e. it is not robust), high discrepancies between simulations and real data can occur; thus, a robust solution can be preferable.

Since occupant behaviour is intrinsically affected by variability, buildings should be designed with low sensitivity to it. Karjalainen [178] proposed examples of robust building designs that consists in limiting the occupant operations adopting, as an example adopting non-operable windows. However, it should be noted that occupant prefers to have the possibility to interact with building, thus trying to limit this operation should be counter-productive.

Therefore, the occupant interactions with the building should be limited reducing the conditions that lead to occupant interactions.

In general, the sensitivity of a solution to the  $j$ -th design parameter can be evaluated introducing the parameter  $\zeta_j$ , defined as:

$$\zeta_j = \sum_i w_i \left| \frac{\delta F_i}{\delta x_j} \frac{\delta x_j}{F_i} \right| \quad (6.9)$$

where  $F_i$  is the  $i$ -th function composing the objective functions vector  $F$ ,  $x_j$  is the  $j$ -th design parameter for which the robustness of the solution is evaluated and  $w_i$  is the weight coefficient of the  $i$ -th function. By means of the weight factors, it is possible to give more significance to the sensitivity of a specific output with respect to the others. The highest is  $\zeta_j$ , the highest is the sensitivity of the solutions to the parameter  $j$ ; consequently, robust solutions are individuated by low values of  $\zeta_j$ .

From equation (6.9), the sensitivity of the design configurations described in the previous sections to the occupant behaviour,  $\zeta_{occ}$  is evaluated by the following relationship:

$$\zeta_{occ} = w_E \left| \frac{E_{occ} - E_0}{E_0} \right| + w_t \left| \frac{t_{disc,occ} - t_{disc,0}}{t_{disc,0}} \right| \quad (6.10)$$

where  $E$  is the annual heating energy demand and  $t_{disc}$  is the discomfort time; subscript  $occ$  refers to cases in which the occupant behaviour is considered and  $0$  to cases in which occupant behaviour is neglected,  $w_E$  and  $w_t$  are the weight factor related to energy and comfort parameters. In this analysis, the same significance has been considered for each objective, so that weight factors are unitary.

In Figure 6.18, referring to the optimal building configurations that compose the Pareto frontiers both considering and neglecting the occupant behaviour for each window typology represented in Figure 6.16, the sensitivity of the solutions is shown.

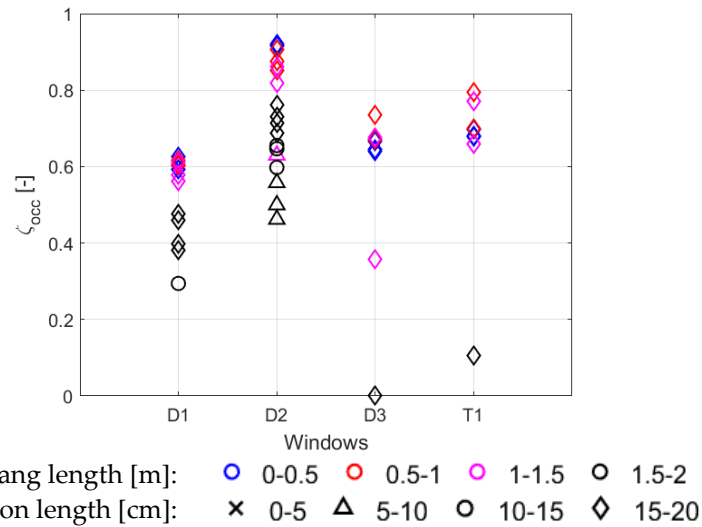


Figure 6.18. Sensitivity to the occupant behaviour of optimal building configurations for each window typology.

In Figure 6.18 it can be appreciated that low SHGC windows (i.e. *D3* and *T1*) are characterised by the lowest values of sensitivity, revealing very robust solutions. In particular, it can be noted that for window *D3*, the building configuration characterised by insulation thickness of 20 cm and high shadings has a sensitivity to the occupant behaviour near to zero, meaning that the solution is not significantly affected by the occupant behaviour. This aspect is highlighted in Figure 6.19, where the maximum number of yearly window openings (*Wop*) for specific window typology and shading configuration is shown. In fact, in this figure it is evident that occupants rarely interact with the windows if windows and shadings determine low solar gains.

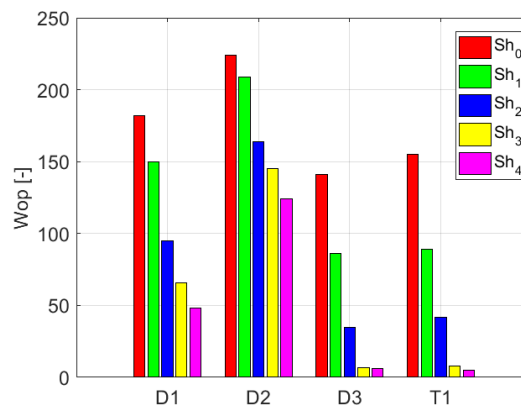


Figure 6.19. Maximum number of window openings for specific window and shading configurations.

Finally, by comparing Figure 6.16 to Figure 6.18, it can be remarked that if the occupant behaviour is considered, the more robust buildings configurations determine the higher energy consumptions. Therefore, a trade-off between

energy performance, indoor comfort conditions and robustness of the solution have to be found depending on the design needs.

## 6.6 Conclusions

In this *Chapter* implications of the occupant behaviour, related to the window openings, on the evaluation of the optimal building design have been evidenced. In particular, referring to a single-zone office in which only the heating system is provided, the sensitivity of annual heating energy demand and adaptive comfort conditions to insulations thickness of opaque elements, windows typology (double and triple pane, high and low SHGC and thermal transmittance) and shadings, both considering and neglecting the occupant behaviour, have been analysed by means of annual numerical simulations. The evaluation of the adaptive comfort conditions is based only on the indoor operative temperature and neglecting the effect of air humidity ratio on occupant feelings. Two different set-points of the indoor temperature are considered: 21 °C and 23 °C. The results show that, in all the cases, comfort conditions are guaranteed for acceptable percentage of the working time only adopting the highest set-point value. Moreover, it is observed that the occupant interaction with the building determines an increment of comfort conditions compared to the cases in which the occupant behaviour is neglected.

More in detail, the highest differences related to the occupant behaviour are evidenced for buildings without shadings and characterised by high insulations and high SHGC windows. On the contrary, buildings designed with low SHGC windows and high shadings are not influenced by the occupant behaviour, revealing that these are the most robust configurations. Similar conclusions can be assessed referring to the energy demand. Anyway, the analysis of the results evidenced a different sensitivity of both energy demand and indoor comfort conditions to the design parameters, depending on whether the occupant behaviour is considered or not. More precisely, it is remarked that the occupant behaviour tends to reduce the sensitivity to the design parameters. This fact has implications on the optimizations of both the energy demand and comfort conditions: it is observed that, if the occupant behaviour is considered, the Pareto frontier is characterised by a reduced spread between the results and it is composed by few building configurations, contrary to cases in which the occupant behaviour is neglected. In addition, it is evidenced that optimal building configurations depend on the occupant behaviour.

Finally, for the optimal building configurations individuated by the Pareto frontiers, the sensitivity of the energy consumptions and comfort conditions to the occupant has been evaluated, proposing a new parameter that enable to estimate the robustness of a solution.

By means of this case study, it has been highlighted the need of taking into account the occupant behaviour in a realistic way, in order to find optimal design solutions, since they are strongly affected by the occupant interactions with the building.



---

# CLOSURE

---

In this Thesis, a new Whole Building Energy Simulation tool (ALMABEST) has been presented. This tool has been developed in Matlab with the aim to use all the specific features of Simulink for the analysis of dynamic systems. The reasons that justify the development of this new tool have been discussed in detail in this dissertation.

It has been demonstrated that a first important goal achieved by ALMABEST is the simplification of the creation of the building modelling in Simulink: the adoption of specific GUIs for the data insertion and the automatic creation of the building modelling, thanks to a series of *m-files*, enable to overcome the main drawback which is responsible of the limited diffusion of similar Simulink-based tools (see SIMBAD, HAMBASE, CARNOT and IBPT among others).

The use of ALMABEST in a series of case studies demonstrate that the choice of Matlab as working frame can reduce the use of complex co-simulations for the detailed evaluation of indoor comfort conditions and for solving multi-objective optimization problems. This aspect can enlarge the number of users having the skills for the management of the sophisticated dynamic simulations required by the NZEB design since only the use of a unique tool operating in Matlab is needed.

Moreover, ALMABuild forced the author to a deep and critical investigation of all the mechanisms which are involved in building physics. This investigation was not possible by using commercial codes because in these cases the user is able to understand only partially in which way the tool is able to model a specific aspect of the building physics.

Since the development of ALMABEST started only three years ago, many improvements can still be obtained. For this reason, a collaboration with the CARNOT research group is in progress for making available a link between ALMABEST and CARNOT by enlarging the availability of blocks related to HVAC components.

On the other hand, additional improvements related to building physics aspect can be achieved in ALMABuild. In particular, as remarked in many points of this dissertation, the mass transfer modelling across the envelope elements needs to be further developed thanks to introduction of additional RC networks. In this way, the analysis of the water condensation risk on envelope elements and the evaluation of the indoor air humidity ratio in a thermal zone can be accurately studied, especially in summer and in presence of high occupancy density. The adoption of the air humidity ratio modelling in ALMABuild will

make available a more accurate calculation of the cooling thermal loads, taking into account also latent heat loads.

Moreover, models for the diffusion within the thermal zone of contaminants, like CO<sub>2</sub>, have to be implemented in ALMABuild. In this way, the evaluation of the indoor air quality becomes available for the designers.

Furthermore, pressure-based models for the estimation of the air flow pattern within a zone, in presence of driving flows is another expected improvement for ALMABuild. In this way, the performance of mechanical cooling devices and the air change rate due to the natural ventilation (i.e. window openings) can be estimated more accurately.

Finally, another important improvement of ALMABuild is linked to the implementation of the luminance models for the evaluation of the natural daylight in a thermal zone, enabling the estimation of the lighting energy demand.

For these reasons, this Thesis must be considered as the first step toward the development of a complete Simulink library for the energy dynamic simulations of buildings and HVAC systems. But a good first step is important for a successful travel.

---

# REFERENCE

---

- [1] UNFCCC. The Kyoto Protocol to the United Nations Convention on Climate Change, New York, 1997.
- [2] UNFCCC. "Paris Agreement," 2015. [Online]. Available: [https://unfccc.int/sites/default/files/english\\_paris\\_agreement.pdf](https://unfccc.int/sites/default/files/english_paris_agreement.pdf). [Accessed 2018 10 29].
- [3] EU. Directive 2009/29/EC of the European Parliament and of the Council of 23 April 2009 amending Directive 2003/87/EC so as to improve and extend the greenhouse gas emission allowance trading scheme of the Community, Bruxelles, 2009.
- [4] EC. A Roadmap for Moving to a Competitive Low Carbon Economy in 2050, vol. 112, Brussels, 2011.
- [5] European-Council. 2030 Climate and Energy Policy Framework, Brussels, 2014.
- [6] World Energy Council. Resource 2016, London: World Energy Council, 2016.
- [7] Eurostat. "Eurostat Database," 2018. [Online]. Available: <http://ec.europa.eu/eurostat/web/energy/data/database>.
- [8] EU. Directive 2010/31/EU OF THE European Parliament and of the Council of 19 May 2010 on the Energy Performance of Buildings, Bruxelles, 2010.
- [9] EU. Directive 2012/27/EU of the European Parliament and of the Council of 25 October 2012 on Energy Efficiency, amending Directives 2009/125/EC, Bruxelles, 2012.
- [10] B. P. I. Europe. Europe's Building under the Microscope, Bruxelles, 2011.
- [11] Building Performance Institute Europe. 97% of Buildings in the EU need to be upgraded. 2017. [Online]. Available: [http://bpie.eu/wp-content/uploads/2017/12/State-of-the-building-stock-briefing\\_Dic6.pdf](http://bpie.eu/wp-content/uploads/2017/12/State-of-the-building-stock-briefing_Dic6.pdf).
- [12] CTI. Assunzioni di base, condizioni al contorno, profili dei carichi per la corretta applicazione e per la validazione di metodi per il calcolo delle prestazioni energetiche e dei carichi termici di progetto in regime dinamico. 2015. [Online]. Available: <https://www.cti2000.it/index.php?controller=documenti&action=showDocuments&argid=48&tabid=0&subtab=7&s=&fd=&order=5&omode=1>.

Accessed 2018]

- [13] EN. EN ISO 7730: Ergonomics of the thermal environment –Analytical determination and interpretation of thermal comfort using calculation of the PMV and PPD indices and local thermal comfort criteria, Bruxelles, 2005.
- [14] IBPSA. Building Energy Simulation Tools directory. June 2018. [Online]. Available: <http://www.buildingenergysoftwaretools.com/about-us>. [Accessed 01 08 2018].
- [15] S. S. Parashar and N. Fateh. Multi-objective MDO solution strategy for multidisciplinary design using modeFRONTIER. In *Inverse problems, Design and Optimization Symposium*, Miami, Florida (USA), 2007.
- [16] D. B. Crawley, J. W. Hand, M. Kummert and B. T. Griffith. Contrasting the capabilities of building energy performance simulation programs. *Building and Environment*, 43.4, 661-673, 2008.
- [17] D. McLean. The simulation of solar energy systems. PhD Thesis, University of Strathclyde, 1982.
- [18] E. O. Aasem. Practical simulation of buildings and air-conditioning systems in the transient domain. PhD Thesis, University of Strathclyde, 1993.
- [19] T. Chow. Atomic modelling in air-conditioning simulation. PhD Thesis, University of Strathclyde, 1995.
- [20] I. Beausoleil-Morrison, D. Cuthbert, G. Deuchars and G. McAlary. The simulation of fuel cell cogeneration systems in residential buildings. In *Proceedings eSim*, 2002.
- [21] A. Ferguson and N. J. Kelly. Modelling of building-integrated Stirling CHP systems. In *Proceedings eSIM*, 2006.
- [22] J. Clarke. Domain integration in building simulation. *Energy and Buildings*, 33: 303-308, 2001.
- [23] R. Padovan and M. Manzan. Genetic optimization of a PCM enhanced storage tank for Solar Domestic Hot Water Systems. *Solar Energy*, 103: 563-573, 2014.
- [24] D. B. Crawley, L. K. Lawrey, F. C. Winkelmann, W. Buhl, Y. Joe Huang, C. O. Pedersen, R. K. Strand, R. J. Liesen, D. E. Fisher, M. J. Witte and J. Glazer. EnergyPlus: creating a new-generation building energy simulation program. *Energy and Buildings*, 33. 4: 319-331, 2001.
- [25] T. Nouidui, M. Wetter and W. Zuo. Functional mock-up unit for co-simulation import in EnergyPlus. *Journal of Building Performance Simulation*, 7.3: 192-202, 2014.

- [26] S. W. Dols, S. E. Emmerich and B. J. Polidoro. Coupling the multizone airflow and contaminant transport software CONTAM with EnergyPlus using co-simulation. *Building Simulation*, 9.4: 469-479, 2016.
- [27] Soares N., A. Gaspar , P. Santos and J. Costa. Multi-dimensional optimization of the incorporation of PCM-drywalls in lightweight steel-framed residential buildings in different climates. *Energy and Buildings*, 70: 411-421, 2014.
- [28] G. Mitalas and J. Arseneault. Fortran IV program to calculate z-transfer functions for the calculation of transient heat transfer through walls and roofs. Ottawa: National Research Council of CANADA, Division of Building Research, 1970.
- [29] S. Klein, W. Beckman, J. Mitchell, J. Duffie , N. Duffie and T. Freeman. TRNSYS 17: A Transient System Simulation Program. Madison,USA: Solar Energy Laboratory, University of Wisconsin. 2010. [Online]. Available: <http://sel.me.wisc.edu/trnsys>. [Accessed 2016].
- [30] M. Y. Ferroukhi, R. Djedjig, K. Limam and R. Belarbi. Hygrothermal behavior modeling of the hygroscopic envelopes of buildings: A dynamic co-simulation approach. *Building Simulation*, 9.5: 501-512, 2016.
- [31] Y. Fan, T. Hayashi and K. Ito. Coupled simulation of BES-CFD and performance assessment of energy recovery ventilation system for office model. *Journal of Central South University*, 19.3: 633-638, 2012.
- [32] M. Ferrara, E. Sirombo and E. Fabrizio. Energy-optimized versus cost-optimized design of high-performing dwellings: The case of multifamily buildings. *Science and Technology for the Built Environment*, 24.5: 513-528, 2018.
- [33] P. Potočnik, B. Vidrih, A. Kitanovsky and E. Govekar. Analysis and optimization of thermal comfort in residential buildings by means of a weather-controlled air-to-water heat pump. *Building and Environment*, 140: 68-79, 2018.
- [34] J. Hirvonen and K. Sirén. A novel fully electrified solar heating system with a high renewable fraction - Optimal designs for a high latitude community. *Renewable Energy*, 127: 298-309, 2018.
- [35] M. Wetter. Multizone building model for thermal building simulation in modelica. In *Modelica Conference 2006*, 2006.
- [36] S. Attia, M. Hamdy, W. O'Brien and S. Carlucci. Assessing gaps and needs for integrating building performance optimization tools in net zero energy buildings design. *Energy and Buildings*, 60: 110-124, 2013.
- [37] A. Prada, A. Gasparella and P. Baggio. On the performance of meta-models in building design optimization. *Applied Energy*, 225: 814-826, 2018.

- [38] G. L. Morini and S. Piva. The simulation of transients in thermal plant. Part I: Mathematical model. *Applied Thermal Engineering*, 27.11-12: 2138-2144, 2007.
- [39] G. L. Morini and S. Piva. The simulation of transients in thermal plant. Part II: Applications. *Applied Thermal Engineering*, 28.2-3: 244-251, 2008.
- [40] M. W. Ahmad, M. Mourshed, B. Yuce and Y. Rezgui. Computational intelligence techniques for HVAC systems: A review. *Building Simulation*, 9. 4: 359-398, 2016.
- [41] T. R. Nielsen, R. H. Peuhkuri, P. Weitzmann and C. Gudum. Modeling Building Physics in Simulink. Department of Civil Engineering, Technical University of Denmark, 2002.
- [42] V. M. Nik, A. S. Kalagasidis and E. Kjellström. Assessment of hygrothermal performance and mould growth risk in ventilated attics in respect to possible climate changes in Sweden. *Building and Environment*, 55: 96-109, 2012.
- [43] A. S. Kalagasidis. A multi-level modelling and evaluation of thermal performance of phase change materials in buildings. *Journal of Building Performance Simulation*, 7.4: 289-308, 2013.
- [44] V. Muresan, B. Radu, D. Radu and L. Pacurar. A Detached House Simulation using the International Building Physics. *Applied Mechanics and Materials*, 162: 567-574, 2012.
- [45] A. S. Kalagasidis, P. Weitzmann, T. R. Nielsen, R. Peuhkuri, C.-E. Hagentoft and C. Rode. The International Building Physics Toolbox in Simulink. *Energy and Buildings*, 39: 665-674, 2007.
- [46] C. Wemhöner, B. Hafner and K. Schwarzer. Simulation of solar thermal systems with CARNOT blockset in the environment Matlab Simulink. In *Proceedings Eurosun 2000*, 2000.
- [47] Delahaye A., B. Hoffschmidt , F. Späte, U. Stuckmann, S. Warerkar, W. Fryn, H. Kinast and B. Bonnema. Solar air collector development and optimization of existings elements for facades. In *Proceedings of the Solar World Congress 2005*, 2005.
- [48] F. Ochs, G. Dermentzis and W. Feist. Investigation of new concepts of ground heat exchangers and building integrated heat exchangers for passive houses by means of dynamic building and system simulation. In *13th Conference of International Building Performance Simulation Association (IBPSA)*, Chambéry, 2013.
- [49] G. Dermentzis, F. Ochs, D. Siegele and W. Feist. Façade integrated micro-heat pump -Energy performance simulations. In *Fifth German-Austrian IBPSA Conference - Bausim*, 2014.

- [50] M. de Wit, H. Driessen and M. van der Velden. ELAN, a Computermodel for Building Energy Design: Theory and Validation. Faculteit der Bouwkunde, Technische Universiteit, 1987.
- [51] M. de Wit and G. Donze. A model for the prediction of indoor air humidity. In *Proceedings of the International Symposium on Energy, Moisture and Climate in Buildings*, Rotterdam, 1990.
- [52] A. Van Schijndel and M. de Wit. Advanced simulation of building systems and control with SIMULINK. In *Proceedings of the 8th International IBPSA Conference*, Eindhoven, 2003.
- [53] M. de Wit. Heat air and moisture model for building and systems evaluation. Eindhoven: Technische Universiteit, 2006.
- [54] H. Schellen and A. Van Schijndel. Setpoint control for air heating in a church to minimize moisture related mechanical stress in wooden interior parts. *Building Simulation*, 4.1: 79-86, 2011.
- [55] A. Fratean and P. Dobra. Control strategies for decreasing energy costs and increasing self-consumption in nearly zero-energy buildings. *Sustainable Cities and Society*, 39: 459-475, 2018.
- [56] A. Husaunndee, R. Lahrech, H. Vaezi-Nejad and J. C. Visier. SIMBAD: a simulation toolbox for the design and test of HVAC control systems. In *Proceedings of the 5th international IBPSA conference*, Prague, 1997.
- [57] P. Riederer, D. Marchio and J. C. Visier. Influence of sensor position in building thermal control: criteria for zone models. *Energy and Buildings*, 34: 785-798, 2002.
- [58] Z. El Khoury, P. Riederer, N. Couillaud, J. Simon and M. Raguin. A multizone building model for a Matlab/Simulink environment. In *Proceedings of the ninth International IBPSA Conference*, Montréal, 2005.
- [59] P. Riederer, W. Keilholz and V. Ducreux. Coupling of TRNSYS with Simulink – a method to automatically export and use TRNSYS models within Simulink and vice versa. In *Proceedings of the 11th International IBPSA Conference*, Glasgow, 2009.
- [60] O. Ahmed, L. Hocine, M. Boubekur, F. Siham and G. Hervé. Supervisory control of a building heating system based on radial basis function neural networks. In *Electrical Engineering-Boumerdes (ICEE-B), 2017 5th International Conference*, 2017.
- [61] R. Missaoui, H. Joumaa, S. Ploix and S. Bacha. Managing energy Smart Homes according to energy prices: Analysis of a Building Energy Management System. *Energy and Buildings*, 71: 155-167, 2014.
- [62] CEN. EN ISO 52016-1:Energy performance of buildings – Energy needs for heating and cooling, internal temperatures and sensible and latent

- heat loads. Part 1: Calculation procedure. Bruxelles, 2017.
- [63] METEONORM. Global Meteorological Database for Solar Energy and Applied Climatology, Version 5. [Online]. Available: <http://www.meteonorm.com>. [Accessed 20 09 2017].
- [64] Comitato Termotecnico Italiano. «Test Reference Year» [Online]. Available: <https://try.cti2000.it/>. [Consultato il giorno 20 01 2017].
- [65] UNI. UNI TS 11300-1, Energy performance of buildings- Part 1: Evaluation of energy needs for space heating and cooling, Milano, 2014.
- [66] P. Cooper. The absorption of radiation in solar stills. *Solar Energy*, 12.3: 333-346, 1969.
- [67] J. Spencer. Fourier series representation of the position of the sun. *Search*, 2.5: 171-172, 1971.
- [68] R. Perez, P. Ineichen, R. Seals, J. Michalsky and R. Stewart. Modeling daylight availability and irradiance components from direct and global irradiance. *Solar Energy*, 44.5: 271-289, 1990.
- [69] K. A. Pickering. The southern limits of the Ancient Star Catalog and the Commentary of Hipparchos. *DIO*, 12: 3-27, 2002.
- [70] J. A. Duffie and W. A. Beckman. *Solar Engineering of Thermal Processes*. John Wiley & Sons, 2013.
- [71] P. Koronakis. On the choice of the angle of tilt for south facing solar collectors in the Athens basin area. *Solar Energy*, 36.3: 217-225, 1986.
- [72] B. Liu and R. Jordan. Daily insolation on surfaces tilted towards the equator. *Transaction ASHRAE*, 67: 526-541, 1962.
- [73] V. Badescu. 3D isotropic approximation for solar diffuse irradiance on tilted surfaces. *Renewable energy*, 26.2: 221-233, 2002.
- [74] J. E. Hay and J. Davies. Calculation of the Solar Radiation Incident on an Inclined Surface. In *Proceedings of the First Canadian Solar Radiation Data Workshop*, Toronto, 1980.
- [75] D. Reindl, W. A. Beckman and J. Duffie. Evaluation of hourly tilted surface radiation models. *Solar Energy*, 45.1: 9-17, 1990.
- [76] N. Igawa, Y. Koga, T. Matsuzawa and H. Nakamura. Models of sky radiance distribution and sky luminance distribution. *Solar Energy*, 77: 137-157, 2004.
- [77] P. Loutzenhiser, H. Manz, C. Felmann, P. Strachan, T. Frank and G. Maxwell. Empirical validation of models to compute solar irradiance on inclined surfaces for building energy simulation. *Solar Energy*, 81: 254-267, 2007.
- [78] CEN. EN ISO 13370: Thermal performance of buildings - Heat transfer via the ground - Calculation methods. Bruxelles, 2017.



- [79] M. Leung, C. Tse Norman, L. Lai and T. Chow. The use of occupancy space electrical power demand in building cooling load prediction. *Energy and Buildings*, 55: 151-163, 2012.
- [80] A. Paniagua-Tineo, S. Salcedo-Sanz, C. Casanova-Mateo, E. Ortiz-Garcia, M. Cony and E. Hernandez-Martin. Prediction of daily maximum temperature using a support vector regression algorithm. *Renewable Energy*, 36.11: 3054-3060, 2011.
- [81] E. Krüger and B. Givoni. Predicting thermal performance in occupied dwellings. *Energy and Buildings*, 36.3: 301-307, 2004.
- [82] J. Crabb, N. Murdoch and J. Penman. A simplified thermal response model. *Building Services Engineering Research and Technology*, 8.1: 13-19, 1987.
- [83] A. Tindale. Third-order-lumped-parameter simulation method. *Building Services Engineering Research and Technology*, 14.3: 87-97, 1993.
- [84] T. R. Nielsen. Simple tool to evaluate energy demand and indoor environment in the early stages of building design. *Solar Energy*, 78: 73-83, 2005.
- [85] CEN. EN ISO 13790: Energy performance of buildings – Calculation of energy use for space heating and cooling. Bruxelles, 2008.
- [86] M. J. Oliveira Panão, C. A. Santos, N. M. Mateus and G. C. da Graça. Validation of a lumped RC model for thermal simulation of a double skin natural and mechanical ventilated test cell. *Energy and Buildings*, 121: 92-103, 2016.
- [87] G. Kokogiannakis, P. Strachan and J. Clarke. Comparison of the simplified methods of the ISO 13790 standard and detailed modelling programs in a regulatory context. *Journal of Building Performance Simulation*, 1.4: 209-219, 2008.
- [88] M. Atamaca, E. Kalaycioglu and Z. Yilmaz. Evaluation of the heating & cooling energy demand of a case residential building by comparing the national calculation methodology of Turkey and EnergyPlus through thermal capacity calculations. Energy Systems Laboratory, Texas A&M University, 2011.
- [89] F. Lorenz and G. Masy. Méthode d'évaluation de l'économie d'énergie apportée par l'intermittence de chauffage dans les bâtiments. Traitement par différences finies d'un modèle à deux constantes de temps. Faculté de Sciences Appliquées, Université de Liège, Belgium (in French), 1982.
- [90] M. Gouda, S. Danaher and C. Underwood. Building thermal model reduction using nonlinear constrained optimization. *Building and Environment*, 37: 1255 – 1265, 2002.

- [91] T. A. Mara, F. Garde, H. Boyer and M. Mamode. Empirical validation of the thermal model of a passive solar cell test. *Energy and Buildings*, 33: 598-599, 2001.
- [92] G. Fraisse, C. Viardot, O. Lafabrie and G. Achard. Development of a simplified and accurate building model based on electrical analogy. *Energy and Buildings*, 34: 1017-1031, 2002.
- [93] C. Underwood. An improved lumped parameter method for building thermal modelling. *Energy and Buildings*, 79: 191-201, 2014.
- [94] CEN. EN ISO 6946: Building components and building elements. Thermal resistance and thermal transmittance. Calculation methods. Bruxelles, 2017.
- [95] Berkeley Laboratories. WINDOW v7.4. 2016. [Online]. Available: <https://windows.lbl.gov/tools/window/documentation>. [Accessed 20 09 2016].
- [96] S. M. Elsherbiny, G. Raithby and K. Hollands. Heat transfer by natural convection across vertical and inclined air layers. *Journal of Heat Transfer*, 104.1: 96-102, 1982.
- [97] M. Rubin. Calculating heat transfer through windows. *International Journal of Energy Research*, 6.4: 341-349, 1982.
- [98] R. Judkoff and J. Neymark. International Energy Agency building energy simulation test (BESTEST) and diagnostic method. No. NREL/TP--472-6231, Golden, CO (US): National Renewable Energy Laboratory, 1995.
- [99] A. P. Brunger and F. C. Hooper. Anisotropic sky radiance model based on narrow field of view measurements of shortwave radiance. *Solar Energy*, 5.1: 53-64, 1993.
- [100] M. G. Davies. Building heat transfer. John Wiley & Sons, 2004.
- [101] ASHRAE 140. Standard Method of Test for the Evaluation of Building Energy Analysis Computer Programs, Atlanta, 2011.
- [102] D. Zhu, T. Hong, D. Yan and C. Wang. A detailed loads comparison of three building energy modelling programs: EnergyPlus, DeST and DOE-2.1E. *Building Simulation*, 6.3: 323-335, 2013.
- [103] CEN. EN ISO 13791: Thermal performance of buildings. Calculation of internal temperatures of a room in summer without mechanical cooling. General criteria and validation procedures. Bruxelles, 2012.
- [104] R. J. Moffat. Describing the uncertainties in experimental results. *Experimental thermal and fluid science*, 1.1: 3-17, 1988.
- [105] EnergyPlus Testing. EnergyPlus 8.3. Testing with Thermal Envelope and Fabric Load tests from ANSI/ASHRAE Standard 140-2011. [Online]. Available:

[https://energyplus.net/sites/all/modules/custom/nrel\\_custom/eplus\\_files/current\\_testing\\_reports/ASHRAE140-Envelope-8.3.0-b45b06b780.pdf..](https://energyplus.net/sites/all/modules/custom/nrel_custom/eplus_files/current_testing_reports/ASHRAE140-Envelope-8.3.0-b45b06b780.pdf..)

[Consultato il giorno 27 11 2017].

- [106] H. Baehr and K. Stephan. Heat and Mass Transfer. Berlin: Springer, 2006.
- [107] N. R. D. Lauzier. MATLAB function that calculates view factors between two planar surfaces. 2003. [Online]. Available: <https://it.mathworks.com/matlabcentral/fileexchange/5664-view-factors..> [Accessed 22 September 2017].
- [108] E. Wurtz, M. Musy and L. Mora. Introduction of specific laws in zonal model to describe temperature fields and air flow patterns in mixed ventilated buildings. *Journal of the Human-Environment System*, 3.1: 43-59, 1999.
- [109] A. Daoud, N. Galanis and O. Bellache. Calculation of refrigeration loads by convection, radiation and condensation in ice rinks using a transient 3D zonal model. *Applied Thermal Engineering*, 28.14: 1782-1790, 2008.
- [110] F. Haghghat, Y. Li and A. C. Megri. Development and validation of a zonal model – POMA. *Building and Environment*, 36.9: 1039-1047, 2001.
- [111] Y. Boukhris, L. Gharbi and N. Ghrab-Morcos. Modeling coupled heat transfer and air flow in a partitioned building with a zonal model: Application to the winter thermal comfort. *Building Simulation*, 2.1: 67-74, 2009.
- [112] E. J. Teshome and F. Haghghat. A new generation of zonal models. *ASHRAE Transactions*, 112 (Part 2): 163-174, 2006.
- [113] C. Inard, H. Bouia and P. Dalicieux. Prediction of air temperature distribution in buildings with a zonal model. *Energy and Buildings*, 24.2: 125-132, 1996.
- [114] M. Musy, F. Winkelmann, E. Wurtz and A. Sergent. Automatically generated zonal models for building air flow simulation: principles and applications. *Building and Environment*, 37. 8-9: 873-881, 2002.
- [115] E. Wurtz, L. Mora and C. Inard. An equation-based simulation environment to investigate fast building simulation. *Building and Environment*, 41.11: 1571-1583, 2006.
- [116] A. C. Megri and Y. Yu. New calibrated zonal model (POMA+) for temperature and airflow predictions. *Building and Environment*, 94.1: 109-121, 2015.
- [117] E. Wurtz, F. Deque, L. Mora, E. Bozonnet and S. Trompezinsky. SIM\_ZONAL: a software to evaluate the risk of discomfort: coupling with an energy engine, comparison with CFD codes and experimental measurements. In *Proceedings Building Simulation*, Eindhoven, 2003.

- [118] R. K. Rajput. Heat and Mass Transfer. Tata McGrawhill, 1999.
- [119] C. Karmann, S. Schiavon and F. Bauman. Thermal comfort in buildings using radiant vs. all-air systems: A critical literature review. *Building and Environment*, 111: 123-131, 2017.
- [120] B. Lin, Z. Wang, H. Sun, Y. Zhu and Q. Ouyang. Evaluation and comparison of thermal comfort of convective and radiant heating terminals in office buildings. *Building and Environment*, 106: 91-102, 2016.
- [121] F. Ochs, M. Magni, M. Bianchi and D. Siegele. Steady state and transient simulation of a radiant heating system. In *Proceedings of Building Simulation Applications (BSA2017)*, Bolzano, 2017.
- [122] H. B. Awby and A. Hatton. Natural convection from heated room surfaces. *Energy and Buildings*, 30: 233-244, 1999.
- [123] D. Olsthoorn, F. Haghighat, A. Moreau and G. Lacroix. Abilities and limitations of thermal mass activation for thermal comfort, peak shifting and shaving: A review. *Building and Environment*, 118: 113-127, 2017.
- [124] ASHRAE 55. Thermal Environmental Conditions for Human Occupancy. Atlanta, 2013.
- [125] M. Cavazzuti. Optimization methods: from theory to design. Modena: Springer, 2013.
- [126] W. Spendley, G. R. Hext and F. R. Himsworth. Sequential application of simplex design in optimization and evolutionary operation. *Technometrics*, 4: 441-461, 1962.
- [127] J. A. Nelder and R. Mead. A simplex method for function minimization. *Computer Journal*, 7. 4: 308-313, 1965.
- [128] N. Karmarkar. A new polynomial-time algorithm for linear programming. In *Proceedings of the sixteenth annual ACM symposium on Theory of computing*, 1984.
- [129] H. J. Ferrau, C. Kirches, A. Potechka, H. G. Bock and M. Diehl. qpOASES: A parametric active-set algorithm for quadratic programming. *Mathematical Programming Computation*, 6.4: 327-363, 2014.
- [130] K. Schittkowski. NLPQL: A Fortran subroutine solving constrained nonlinear programming problems. *Annals of Operations Research*, 5.2: 485-500, 1986.
- [131] J. H. Holland. Adaptation in natural and artificial systems: An introductory analysis with applications to biology, control, and artificial intelligence. University of Michigan, 1975.
- [132] S. Mostaghim, J. Branke and H. Schmeck. Multi-objective particle swarm. In *Proceedings of the 9th annual conference on genetic and*, London, 2006.
- [133] S. Kirkpatrick, C. D. Gelatt and M. P. Vecchi. Optimization by simulated

- annealing," *Science*, 220.4598: 671-680, 1983.
- [134] P. Jie, F. Zhang, Z. Fang, H. Wang and Y. Zhao. Optimizing the insulation thickness of walls and roofs of existing buildings based on primary energy consumption, global cost and pollutant emissions. *Energy*, 159: 1132-1147, 2018.
- [135] A. Torres-Rivas, M. Palumbo, A. Haddad, L. F. Cabeza, L. Jiménez and D. Boer. Multi-objective optimization of bio-based thermal insulation materials in building envelopes considering condensation risk. *Applied Energy*, 224: 602-614, 2018.
- [136] E. Schito, P. Conti and D. Testi. Multi-objective optimization of microclimate in museum for concurrent reduction of energy needs, visitors' discomfort and artwork preservation risks. *Applied Energy*, 224: 147-159, 2018.
- [137] A. R. Starke, J. M. Cardemil and S. Colle. Multi-objective optimization of a solar assisted heat pump for swimming pool heating using genetic algorithm. *Applied Thermal Engineering*, 142: 118-126, 2018.
- [138] N. Perez, P. Riederer and C. Inard. Development of a multiobjective optimization procedure dedicated to the design of district energy concept. *Energy and Buildings*, 178: 11-25, 2018.
- [139] P. Penna, A. Prada, F. Cappelletti and A. Gasparella. Multi-objective optimization for existing buildings retrofitting under government subsidization. *Science and Technology for the Built Environment*, 21: 847-861, 2015.
- [140] M. Manzan and A. Clarich. FAST energy and daylight optimization of an office with fixed and movable shading devices. *Building and Environment*, 113: 175-184, 2017.
- [141] Z. Tian, X. Zhang, X. Jin, X. Zhou, B. Si and X. Shi. Towards adoption of building energy simulation and optimization for passive building design: A survey and a review. *Energy and Buildings*, 158: 1306-1316, 2018.
- [142] S. Yigit and B. Ozorhon. A simulation-based optimization method for designing energy efficient buildings. *Energy and Buildings*, 178: 216-227, 2018.
- [143] M. Manzan. Genetic optimization of external fixed shading devices. *Energy and Buildings*, 72: 431-440, 2014.
- [144] H. Rijal, P. Tuohy, M. Humphreys, J. Nicol, A. Samuel and J. Clarke. Using results from field surveys to predict the effect of open windows on thermal comfort and energy use in buildings. *Energy and Buildings*, 39: 823-836, 2007.
- [145] L. Degelman. A model for simulation of daylighting and occupancy

- sensor as an energy control strategy for office building. In *Proceedings of Building Simulation 99*, Kyoto, Japan, 1999.
- [146] A. Mahdavi. People in building performance simulation. *Building Performance Simulation for Design and Operation*, pp. 56-83, 2011.
- [147] R. Haas, H. Auer and P. Biermayr. The impact of consumer behavior on residential energy demand for space heating. *Energy and Buildings*, 27.2: 195-205, 1998.
- [148] C. Turner and M. Frankel. Energy performance of LEED for new construction buildings. *New Buildings Institute*, 4: 1-42, 2008.
- [149] G. Brager, G. Paliaga and R. de Dear. Operable windows, personal control and occupant comfort. *ASHRAE Transactions*, 110: 17-35, 2004.
- [150] A. Al-Mumin, O. Khattab and G. Sridhar. Occupants' behavior and activity patterns influencing the energy consumption in the Kuwaiti residences. *Energy and Buildings*, 35.6: 549-559, 2003.
- [151] F. Haldi and D. Robinson. Adaptive actions on shading devices in response to local visual stimuli. *Journal of Building Performance Simulation*, 3.2: 135-153, 2010.
- [152] C. M. Clevenger and J. Haymaker. The impact of the building occupant on energy modeling simulations. In *Joint International Conference on Computing and Decision Making in Civil and Building Engineering*, Montreal, Canada, 2006.
- [153] Z.-J. Li, Y. Jiang and Q.-P. Wei. Survey on energy consumption of air conditioning in summer in a residential building in Beijing. *Journal of heating ventilation and air conditioning*, 37.4: 46-51, 2007.
- [154] O. Guerra Santin, L. Itard and H. Visscher. The effect of occupancy and building characteristic on energy use for space and water heating in Dutch residential stock. *Energy and Building*, 41.11: 1223-1232, 2009.
- [155] Z. M. Gill, M. J. Tierney, I. M. Pegg and N. Allan. Low-energy dwellings: the contribution of behaviours to actual performance. *Building Research & Information*, 38.5: 491-508, 2010.
- [156] W. Parys, D. Saelens and H. Hens. Coupling of dynamic building simulation with stochastic modelling of occupant behaviour in offices -a review-based integrated methodology. *Journal of Building Performance Simulation*, 4.4: 339-358, 2011.
- [157] G. Newsham, A. Mahdavi and I. Beausoleil-Morrison. Lightswitch a stochastic model for predicting office lighting energy consumption. In *Proceedings of the third European Conference on Energy Efficiency Lighting*, Newcastle-upon-Thyne, 1995.
- [158] C. Reinhart. Daylight availability and manual lighting control in office

- buildings - simulation studies and analysis of measurements. Karlsruhe, Germany: University of Karlsruhe, 2001.
- [159] J. Page, D. Robinson, N. Morel and J. Scartezzini. A generalized stochastic model for simulation of occupant presence. *Energy and Buildings*, 40.2: 83-98, 2008.
  - [160] A. Mahdavi and F. Tahmasebi. Predicting people's presence in buildings: An empirically based model performance analysis. *Energy and Buildings*, 86: 349-355, 2015.
  - [161] I. Raja, J. Nicol, K. McCartney and M. Humphreys. Thermal comfort use of control in naturally ventilated buildings. *Energy and Buildings*, 33.3: 235-244, 2001.
  - [162] V. Inkarojrit. Balancing comfort: occupants' control of window blinds in private office. Berkeley, California: Univeristy of California, 2005.
  - [163] F. Haldi and D. Robinson. On the behaviour and adaptation of office occupants. *Building and Environment*, 43.12: 2163-2177, 2008.
  - [164] Y. Sutter, D. Dumortier and M. Fontoynt. The use of shading systems in VDU task offices: a pilot study. *Energy and Buildings* 38.7: 780-789, 2006.
  - [165] C. Reinhart. Lightswitch-2002: a model for manual and automated control of electric lighting and blinds. *Solar Energy*, 77.1: 121-126, 2004.
  - [166] P. Warren and L. Parkins. Window-opening behavior in office buildings. *ASHRAE Transactions*, 90: 1056-1076, 1984.
  - [167] G. Yun, P. Tuohy and K. Steemers. Thermal performance of naturally ventilated building using a combined algorithm of probabilistic occupant behaviour and deterministic heat and mass balance models. *Energy and Buildings*, 41.5: 489-499, 2009.
  - [168] C. Reinhart and K. Voss. Monitoring manual control of electric lighting and blinds. *Lighting Research and Technology*, 35.3: 243-260, 2003.
  - [169] D. Lindelöf and N. Morel. A field investigation of the intermediate light switching by users. *Energy and Buildings*, 38.7: 790-801, 2006.
  - [170] A. Mahdavi and C. Pröglhöf. Toward empirically-based models of people's presence and actions in buildings. In *Proceedings of building simulation*, Glasgow, 2009.
  - [171] B. Abushakra, A. Sreshthaputra, J. Haberl e D. Claridge. Compilation of diversity factors and schedules for energy and cooling load calculations. *ASHRAE Research Project 1093-RP*, 2001.
  - [172] K. Kawamoto, Y. Shimoda and M. Mizuno. Energy saving potential of office equipent power management. *Energy and Buildings*, 36.9: 915-923, 2004.
  - [173] J. Nicol and M. Humphreys. A stochastic approach to thermal comfort -

- occupant behavior and energy use in buildings. *ASHRAE Transactions*, vol. 110, pp. 554-568, 2004.
- [174] V. Fabi, R. V. Andersen and S. P. Corgnati. Influence of occupant's heating set-point preferences on indoor environmental quality and heating demand in residential buildings. *HVAC&R Research*, 19.5: 635-645, 2013.
- [175] P. Hoes, J. Hensen, M. Loomans, B. de Vries and D. Bourgeois. User behavior in whole building simulation. *Energy and Buildings*, 41.2: 295-302, 2009.
- [176] D. Bourgeois. Detailed occupancy prediction, occupancy-sensing control and advanced behavioural modelling within whole-building energy simulation. Québec: Université Laval, 2005.
- [177] V. Tabak, B. de Vries, J. Dijkstra and J. Jessurun. Interaction in activity location scheduling. In *Proceedings of the 11th International Conference on Travel Behavior Research*, Kyoto, Japan, 2006.
- [178] S. Karjalainen. Should we design buildings that are less sensitive to occupant behaviour? A simulation study of effects of behaviour and design on office energy consumption. *Energy Efficiency*, 9: 1257-1270, 2016.
- [179] T. S. Larsen and P. Heiselberg. Single-sided natural ventilation driven by wind pressure and temperature difference. *Energy and Buildings*, 40.6: 1031-1400, 2008.



In this Appendix are collected the tools reported in the Building Energy Simulation Tools (BEST) directory, except tools dedicated to training and support services. Referring to the BEST directory, for each tool there is a brief and non-exhaustive description and its major capabilities are listed. The listed capabilities of a software are:

- Whole Building Energy Simulation (WBES);
- Load Calculations (LC);
- HVAC system selection and sizing (HS);
- Parametrics and Optimisation (PO);
- Energy Conservation Measures (ECM);
- Code Compliance (CC);
- Ratings and Certificates (RC);
- Utility Bill and Meter Data Analysis (UBMDA);
- Weather Data and Climate Analysis (WDCA);
- Building Energy Auditing (BEA);
- Building Energy Benchmarking (BEB);
- Lighting Simulation (LS);
- Air Flow Simulation (AFS);
- Life-Cycle Analysis (LCA);
- Detailed Component Simulation (DCS);
- Solar and Photovoltaic Analysis (SPA);
- Other (O).

Table A-6-9. List of tools from the BEST directory [14].

<b>Tool name</b>	<b>Description</b>	<b>Capabilities</b>
<b>Accelerad</b>	Suite of programs for daylight analysis	LS
<b>AcousticCalc</b>	Prediction of the sound levels in a room of HVAC systems	HS, PO
<b>Adtek AccuComm</b>	Calculation of heating and cooling loads for commercial buildings	LC, HS
<b>Adtek AccuDuct</b>	Design of Air ducts	HS
<b>Adtek AccuLoad</b>	Calculation of heating and cooling loads for residential buildings	LC
<b>Adtek Energy Analyzer</b>	Energy comparison of different HVAC systems	WBES
<b>AET</b>	Simplified and quick simulations for the evaluation of energy use of commercial and residential building	WBES, BEB
<b>AGi32</b>	3D lighting design software	LS
<b>AnTherm</b>	Calculates temperature distribution in building structures with thermal bridges	WBES, PO, RC
<b>Assembly U-factor Calculator</b>	Calculation of thermal conductance of an envelope element	LC, LCA
<b>Autodesk Green Building Studio</b>	It uses the DOE-2.2 simulation engine for the calculation of building energy performance. Design at conceptual stage	WBES, PO, ECM
<b>Autodesk Insight</b>	For the creation and management of input files for DOE-2.2 and EnergyPlus simulation engine	WBES, LS, SPA
<b>AWDABPT Buildings</b>	Dynamic simulation of power plant failure and restoration	LC
<b>AWDABPT Underground Enclosures</b>	Simulations of heating/cooling plant failure and restoration for underground rooms	LC
<b>BACnet Device Simulator</b>	Simulation of devices in large networks	WBES, LS
<b>BACnet Explorer</b>	Module of the BACnet library for visualization of devices properties	HS, BEA, LS
<b>BACnet Stack</b>	Module of the BACnet library for database integration	HS, BEA, LS
<b>BEAVER</b>	Based on constant hourly time step	WBES, CC
<b>Benchmark my building</b>	Compare energy efficiency of a building to other in the same location	BEB
<b>Berkeley Lab WINDOW</b>	Calculation of the thermal performance of fenestration	CC, RC, DCS
<b>BlueSol</b>	Design of photovoltaic systems	SPA
<b>Bsim</b>	Analysis of the indoor thermal climate in complex buildings	WBES, AFS
<b>BSIMAC</b>	Hourly time step, fast simulation of annual energy needs, HVAC peak power, indoor temperature	WBES, LC, HS
<b>Building Energy Asset Score</b>	Provides an energy efficiency evaluation of building envelope and energy systems	ECM, RC, BEA

<b>Building Modeling for Energy Conservation</b>	Bin-weather modelling software	ECM, UBMDA, WDCA, BEA
<b>Building Performance Database</b>	American database of energy-related characteristics of residential and commercial buildings	ECM, BEA, BEB
<b>BuildingOS</b>	Collections and visualization of building data and utility bills for analysis	CC, UBMDA
<b>CAMEL</b>	Air-conditioning load estimation	LC, HS
<b>CAN-QUEST</b>	Canadian adaptation of eQUEST	WBES, CC
<b>Cepenergy Management Software</b>	Software for evaluation the Energy Efficiency	UBMDA, BEA, BEB
<b>CLIMATE 1</b>	Global weather database	WDCA
<b>Climate Consultant</b>	Visualization of weather data	WDCA
<b>Cold Room Calc</b>	Calculation of refrigeration load calculation for cold rooms (e.g. food storage...)	LC
<b>COMFEN India Version</b>	Simple single-zone facade analysis tool for commercial building based on EnergyPlus and Radiance simulation engine	PO, CC
<b>COMFIE</b>	Use sub-hourly time steps, finite volume method,	WBES, LC, RC
<b>Comfort and Weather Analysis</b>	Generation of urban comfort chart based on ASHRAE 55	WDCA, AFS
<b>Commercial Building Energy Saver</b>	For retrofitting of small and medium office	WBES, ECM
<b>CONTAM</b>	Multizone airflow and contaminant transport software	WBES, AFS
<b>Cool Room Calc</b>	Calculation of air-conditioned room cooling loads.	LC
<b>cove.tool</b>	Find the optimal design of a building based on big data analysis	PO, ECM, LCA
<b>CYPETHERM Suite</b>	It complies with several Standard ISO, thermal load calculation based on the Radiant Time Series Method	WBES, LC, CC
<b>Daylight Performance of Laser Cut Panels</b>	Provides input data of daylight availability for EnergyPlus considering complex glazing systems	LS
<b>DEKSOFT</b>	Web applications for thermal, energy and acoustics analysis of a building	LC, BEA, SPA
<b>Demand Response Quick Assessment Tool</b>	It predicts the energy savings of several demand responsive strategies	WBES, ECM, CC
<b>DesignBuilder</b>	Use of different simulation engines (EnergyPlus, Radiance, CFD)	WBES, LC, PO
<b>DEXCell Energy Manager</b>	Management software for the verification of energy savings	UBMDA, BEA, SPA
<b>DIAL+ Cooling</b>	Calculation of heating and cooling loads, energy consumption for lighting	LC, BEB, WDCA
<b>DIAL+ Lighting</b>	Lighting simulation based on the RADIANCE simulation engine	PO, WDCA, LS

<b>DIVA-for-Rhino</b>	Plugin for Rhinoceros for the evaluation of daylight and energy consumptions for single thermal zone	LS, SPA
<b>DL-Light</b>	Evaluation of distribution of natural light in buildings	LS
<b>e!Sankey pro</b>	Depiction of Sankey diagrams	BEA
<b>Easy Accountax</b>	It provides the accounting data, TAX filing process and VAT Returns.	O
<b>ECBC App</b>	It displays the Energy Conservation Building Code compliance value of the envelope elements	HS, ECM, CC
<b>ECOCITIES</b>	Addressed for the optimisation of energy saving measures for buildings groups	WBES, PO
<b>EcoDesigner Star</b>	BIM models coupled with hourly energy simulation	WBES, HS
<b>eCurv</b>	Provider of demand management software services	ECM, UBMDA, BEA
<b>EDAPT</b>	It is a design-assistance project and program management software based on OpenStudio. Addressed to ESCOs	WBES, ECM
<b>EDGE</b>	Calculation of carbon footprint of the building and comparison with different scenarios	WBES, RC
<b>EE4 CBIP</b>	Determination of the compliance of a building to the Canadian Commercial Building Incentive Program performance requirements	CC
<b>EE4 CODE</b>	Determination of the compliance of a building to Canada's Model National Energy Code for Buildings	CC
<b>EFEN</b>	Prediction of the size of HVAC equipment based on dynamic simulations performed adopting the EnergyPlus engine	HS
<b>Elements</b>	Editing of custom weather files for building energy modelling	WDCA
<b>EnerCAD</b>	Addressed for the predesign stage and the optimisation of building projects	ECM, BEA
<b>Energinet Energy Management Software</b>	Administrative system for Energy, Waste and Environment Management	UBMDA, WDCA
<b>Energy Cost Calculator</b>	Calculates the energy cost from the energy demand of simple buildings	WBES, LC, PO
<b>Energy Grader</b>	Online calculator of energy performance of a building based on energy consumption data	LC, BEA, BEB
<b>Energy Model Quality Check Tool</b>	Based on input and output files of energy simulation software, it generates reports on energy model quality of the building as per ASHRAE 90.1 Appendix G standards.	WBES
<b>Energy Profile Tool</b>	Simple building energy analysis tool, for ASHRAE Level 1 and 2 audits	ECM, BEA, BEB
<b>EnergyCAP Enetrprise</b>	Energy Information software	UBMDA, BEB
<b>EnergyCap Professional</b>	Software for utility bill tracking of public-school districts	UBMDA, BEB
<b>EnergyElephant</b>	Determines the building energy benchmark from	WBES, BEA

	energy bills	
<b>Energyperiscope</b>	Generation of sales proposal of solar and renewable energy systems based on custom bills	UBMDA, WDCA, SPA
<b>EnergyPlus</b>	One of the most popular BES tools	WBES, HS, CC
<b>ENERWIN</b>	Hourly time step	WBES, LC, CC
<b>EnExPlan</b>	Used for calculating energy savings due to suggestions made by the software	WBES, LC, ECM
<b>Engineerign Toolbox</b>	Evaluation of physical properties of air, refrigerant...	O
<b>EP-Quick</b>	Creates input file for EnergyPlus	WBES
<b>epwmap</b>	Shows the available free EPW weather files required by EnergyPlus	WDCA
<b>eQuest</b>	Based on DOE-2.2 simulation engine for the calculation of building energy performance.	WBES
<b>ESBO</b>	Simulation tool bases on IDA simulation engine	WBES, LC, PO
<b>ESP-r</b>	Proper simulation engine	WBES
<b>EVAP-COND</b>	Software package for the simulation of finned-tube evaporator and condenser, tube by tube simulations	HS
<b>FineGREEN</b>	BIM simulation environment coupled with EnergyPlus	WBES; LC, HS
<b>FineHVAC</b>	BIM application for calculation of HVAC loads	LC, HS
<b>FloorspaceJS</b>	Creation of simple building geometry for Building Energy models	O
<b>gEnergy</b>	Based on EnergyPlus simulation engine, it performs simulation on the cloud	WBES
<b>GenOpt</b>	Multiparameter optimization program, that can be coupled with all text-based BES tools, like EnergyPlus and TRNSYS	PO
<b>GLHEPRO</b>	Design software focused on vertical borehole-type ground loop heat exchangers; it provides input for the simulation of ground heat exchanger in EnergyPlus	HS, DCS
<b>Ground Loop Design</b>	Optimisation of ground source heat pump system design	HS, ECM, DCS
<b>Groundhog</b>	Radiance based software for lighting analysis	LS
<b>Hancock Energy Efficiency Cloud</b>	Suite of apps for collecting and managing information for ASHRAE level 1 and 2 energy audits	ECM, CC, BEA
<b>Hancock Energy Management</b>	Energy information system	ECM, UBMDA, BEB
<b>Hancock Software HEAT Energy Audit HAP</b>	Tool for the energy auditing of single family and manufactured homes	WBES, ECM, BEA
<b>Hear Map Generator Tool - Type 1</b>	It adopts a constant hourly time step	WBES
<b>Hear Map Generator Tool - Type 2</b>	Visualisation of one BES output at a time	PO, RC
<b>Heat Pump Design Model</b>	Visualisation of many BES outputs at the same time	PO, RC
	Research tool, steady state simulation of heat pump	PO, DCS

APPENDIX B

<b>HEED</b>	Easy simulation software for comparison of different building designs	WBES, ECM, SPA
<b>Hippo CMMS</b>	Maintenance management solution	HS, LCA
<b>Home Energy Score</b>	DOE's program for rating home characteristics (envelope, HVAC, control system...)	ECM, RC, BEA
<b>Honeybee</b>	It connects the visual programming environment of Grasshopper to four validated simulation engines (EnergyPlus, Radiance, Daysim and OpenStudio) enabling parametric analysis	WBES, PO, LS
<b>HOT2000</b>	design software for low-rise residential buildings.	WBES, LC, ECM
<b>HVAC ResLoad-J</b>	Evaluation of peak cooling and heating loads for residential and commercial buildings	LC, HS, CC
<b>HVAC Solution Pro Software</b>	HVAC system design	HS
<b>HVACSIM+</b>	Based on a modular approach, it performs dynamic simulations of building/HVAC/control systems with variable time steps	HS
<b>IDA ICE</b>	Proper simulation engine	WBES, HS, CC
<b>IES</b>	In agreement with the global rating systems like LEED, GreenStar and more	WBES, HS, CC
<b>IMAC Assistant</b>	Evaluation of the neutral temperatures for Indian buildings based on adaptive thermal comfort models	WDCA, AFS
<b>jEPlus</b>	Perform parametric analysis using EnergyPlus	PO
<b>Kalkener</b>	Online simulation software for solar thermal water heating systems	PO, LCA, SPA
<b>kW Psychrometric Functions</b>	Enables psychrometric analysis of HVAC process in a spreadsheet	LC, BEA
<b>Ladybug</b>	Plugin for Grasshopper, it performs weather data analysis and then test initial design options	PO, WDCA
<b>LESOSAI</b>	Provides the calculation of heating power, and creates official reports on heating energy use	LC, CC, BEA
<b>Life Cycle Analysis Tool</b>	Calculation of the life cycle costs in a building energy project, based on the EnergyPlus outputs	LCA, SPA
<b>LightStanza</b>	Optimisation of daylight strategies	WDCA, LS
<b>LoopDA 3.0</b>	Used for the sizing of natural ventilation openings	WBES, ECM
<b>LoopLink Pro</b>	Design of ground source heat pump system for commercial buildings	HS
<b>LoopLink RLC</b>	Design of ground source heat pump system for residential and light commercial buildings	HS
<b>Measurabl</b>	Reporting software	ECM, UBMDA, BEA
<b>METEONORM 7</b>	Climatic database of Typical Meteorological Years	WDCA
<b>MHEA</b>	Tool of the Weatherization Assistant, for energy audit and retrofit of mobile homes	WBES, ECM, BEA
<b>Micropas6</b>	Evaluation of building energy consumption based on hourly calculations	O

<b>Modelica Buildings library</b>	Open source library for fast modelling of building energy and control systems	WBES, AFS, DCS
<b>MODEN</b>	It is able to simulate heterogeneous energy system	WBES, BEA
<b>Multi-city Comfort and Weather Comparison</b>	Generation and comparison of urban comfort chart for Indian cities	WDCA, AFS
<b>N++</b>	Building energy modelling interface, based on EnergyPlus simulation engine	WBES, HS, PO
<b>NEAT</b>	Tool of the Weatherization Assistant, for energy audit and retrofit of single-family houses	WBES, ECM, BEA
<b>novaEquer</b>	Evaluation of environmental impact of buildings by means of yearly simulations. It uses the energy simulation tool COMFIE	RC, LCA
<b>OnGrid Tool</b>	Design of PV systems based on electric bills	UBMDA
<b>OpenStudio</b>	It contains the energy simulation engine EnergyPlus, Esp-r, CEN/ISO 13790 and the airflow engine CONTAM	WBES, EC, LS
<b>OptiMiser</b>	For building energy audit	WBES, SPA
<b>OptiMiser Commercial</b>	Audit software, that includes several energy conservation measures for the analysis of retrofit	LC, ECM, BEA
<b>Physibel</b>	Set of 1D/2D/3D simulations program	WBES, LC
<b>Pilio Building Energy Management</b>	Evaluate energy efficiency performance of building by means of weather analytics and comparison benchmarking based on energy bills	UBMDA, WDCA, BEA
<b>Pilio Degree Days Data Subscription</b>	Collection of weather data	UBMDA, WDCA, BEB
<b>Pipe Flow Expert</b>	Design of pumping and piping systems	HS
<b>PLEIADES</b>	It computes the indoor natural lighting by means of the RADIANCE engine	WBES, LC, PO, CC, LCA
<b>PowerCalc</b>	Design of the electrical power distribution of a building	LC, ECM, CC
<b>Primero Comfort</b>	Based on EnergyPlus simulation engine, it evaluates and optimises the thermal comfort and the cooling energy demand	PO, RC, WDCA
<b>PsyCalc</b>	Calculation of psychrometric properties	WDCA
<b>Psychrometric Analysis Design Suite</b>	It performs psychrometric analysis of HVAC process	HS, WDCA, AFS
<b>QwickLoad</b>	Calculation of HVAC loads for commercial and residential buildings based on the Transfer Function Method	LC
<b>Radiance</b>	Suite of programs for determination of lighting	LS
<b>REM/Design</b>	Building energy modelling for the design phase	WBES, ECM, CC
<b>REM/Rate</b>	Home energy rating tool	WBES, CC, RC
<b>SEED</b>	Sharing and managing of energy performance data of buildings	BEB
<b>Sefaira Architecture</b>	SketchUp and Revit real time plugins	WBES, PO, LS
<b>Sefaira Systems</b>	Used for rigorous analysis of HVAC system size and design	WBES, LC, HS
<b>SEMERGY</b>	Determination of building energy demand and	BEA, BEB

	optimisation of the combinations of refurbishment measures	
<b>SimScale</b>	Design and simulation of products	AFS, DCS
<b>SimulationX Green Building</b>	Simulation tool for building and district energy systems	WBES, HS, PO
<b>Snugg Pro</b>	Cloud-based auditing tool for residential buildings	LC, ECM, BEA
<b>SPOT Pro</b>	Optimisation of photosensor-based electric control system for energy savings	LS
<b>StruBim</b>	Create analysis models from structural models	O
<b>Tas Ambiens</b>	CFD program for airflow evaluation in buildings	O
<b>Tas Engineering</b>	tool for concept development	WBES, HS, CC
<b>TOP-Energy</b>	Based on a modular approach, it simulates various types of energy systems and compares different variants	PO, BEA, DCS
<b>TRACE 700 Chiller Plant Analyzer</b>	Evaluation of energy consumption of different chiller plant configurations based on predetermined load profiles	LCA
<b>TRACE 700 Load Design</b>	Module of TRACE 700, for the calculation of loads according to algorithms recommended by the ASHRAE	LC, AFS
<b>TRACE Load Express</b>	Calculation of detailed HVAC load reports for heating, cooling and airflow capacities	LC
<b>Trace700</b>	Adopted for the energy and economic analysis of HVAC system configurations.	WBES, AFS, LCA
<b>Trane Acoustics Program</b>	Estimation of sound level in a room	O
<b>Trane Pipe Design</b>	Detailed calculation for piping design	O
<b>TRANSOL</b>	Design and optimization of solar thermal system based on the TRNSYS simulation engine	DCS, SPA
<b>TREAT</b>	Energy audit software approved by the DOE for all residential housing types, hourly time steps	WBES, ECM
<b>TRNSYS</b>	Component based, it follows a modular approach	WBES, DC, PO
<b>UrbaSun</b>	Computation of solar radiation in urban areas, for solar energy and photovoltaic panels layout optimisation	WDCA, SPA
<b>urbawind</b>	Computation of wind effects in urban areas	WDCA, AFS
<b>VariTrane Duct Designer</b>	Calculation for the design of air ducts	O
<b>w2bill Smart</b>	Management software for data from the Internet of Things	UBMDA
<b>XienceSim</b>	FEM simulator, multi-physics analysis buildings with parametrized geometry	PO, SPA
<b>Xinpas Daylight Ratio Evaluator</b>	Plugin of Revit, it performs daylight calculations	PO, LS



In this *Appendix*, all the seven bus signals adopted in ALMABuild for the transfer of information among different blocks are described. All the variables that compose each bus are defined together their physical meaning and their unit of measure.

The first bus signal is the *Weather Data Bus*, that is created in the *Weather Data Reader* block (see 2.5.1) and contains the main information related to weather data used for the description of the ambient conditions. The height variables composing this bus are listed and described in Table B- 1. The *Weather Data Bus* can be recalled in the Simulink desktop by means of the *Goto* block, tagged *Weather\_Data*.

Table B- 1. Components of the Weather Data bus.

Label	Description	Unit measure
<i>Te</i>	Ambient air temperature	°C
<i>Hbh</i>	Hourly beam solar radiation on horizontal plane	W/m <sup>2</sup>
<i>Hdh</i>	Hourly global solar radiation on horizontal plane	W/m <sup>2</sup>
<i>Pvoap</i>	Outdoor water vapour pressure	Pa
<i>Tsky</i>	Fictive temperature of the sky	°C
<i>H.R.</i>	Outdoor air humidity ratio	%
<i>Wind</i>	Outdoor mean wind speed	m/s
<i>Tmonth</i>	Mean monthly ambient air temperature	°C

The description of the sun position in the sky and other information related to the sun, like the sunrise hour angle are collected in the *Sun bus* that is created in the *Solar Data* block (see 2.5.2). This bus, whose components are reported in Table B- 2, is used for the evaluation of the components of the incident solar radiation on a surface. As for the *Weather Data Bus*, the *Sun bus* is recalled by means of a *Goto* block tagged *Sun*.

Based on both the *Weather Data bus* and the *Sun bus*, the *Solar Radiation bus* is created in both the *Solar Radiation Calculator* and *Solar Radiation Reader* blocks. This bus is composed by the three components of the instantaneous incident solar radiation for a given exposition, labelled *Beam*, *Diffuse* and *Reflected*, expressed in W/m<sup>2</sup>.

Table B- 2. Component of the Sun bus.

Label	Description	Unit measure
<i>Solar azimuth</i>	Azimuth angle of the sun that defines it direction in the sky	Rad
<i>Solar elevation</i>	Angle that defines the high of the sun in the sky	Rad
<i>F1</i>	F <sub>1</sub> coefficient of the Perez model	-
<i>F2</i>	F <sub>2</sub> coefficient of the Perez model	-
<i>Omega</i>	Solar hour angle	Rad
<i>Day-night</i>	Define the day and the night: it is equal to 1 From the astronomic sunrise to the sunset, otherwise is zero	-
<i>Omega_s</i>	Sunrise hour angle	Rad
<i>Solar declination</i>	Angle that defines the position of the sun on the celestial Sphere in the equatorial coordinate system	Rad

The fourth bus signal is the *Temperature zone bus* that the first output of a Building Thermal Balance block and contains the information about the convective and radiative temperature of the thermal zone, expressed in °C:

- $T_a$ , that is the mean air temperature of the thermal zone;
- $T_{rad}$ , that is the mean radiative temperature of the thermal zone.

Also the *Temperature zone bus* is recalled in the Simulink desktop by a *Goto* block tagged  $T_{\{thermal\ zone\ name\}}$ .

The *Superficial temperature bus*, like the *Temperature zone bus*, is an output of both Building Massive Elements and Building Clear Components blocks, and it contains information about the superficial temperature of the envelope element modelled by beams of the BME or BCC block. Again, the components of this bus are expressed in °C:

- $T_{se}$ , it represents the temperature of the envelope element surface that is not pointed towards the considered thermal zone;
- $T_{si}$ , is the temperature of the internal surface of an envelope element.

The *Power bus*, whose components are listed in Table B- 3, is an output of BME, BCC and BTB blocks, and contains information about the different thermal fluxes that affect both envelope elements and globally the thermal zone. Positive values of powers are related to powers entering into the thermal zone. Since this bus is used for both envelope elements and the thermal zone, if it is the output of a block used for the modelling of a wall, as an example, the  $Q_{ci}$  component represents the power exchanged by the envelope element for convection with the internal surroundings. On the contrary, if the *Power bus* is the output of a *Thermal zone* block this bus represents the total power exchanged for internal convection by all the envelope elements of the thermal zone. The *Power bus* is also the output of each emitter of the HVAC system, by means of which HVAC and building models are coupled.

Table B- 3. Components of the Power Bus.

Label	Description	Unit measure
$Q_{ce}$	Power related to convective heat transfer of the External surface of envelope element	W
$Q_{re}$	Power related to radiative heat transfer of the external surface of the envelope element of the zone with the external surroundings	W
$Q_{sky}$	Long-wave radiative heat transfer of the external surface of the envelope element with the sky	W
$Q_{sop}$	Solar radiation absorbed by external surface of opaque elements (also frame for windows)	W
$Q_{stv}$	Solar radiation absorbed by glasses of windows	W
$Q_g$	Thermal flux due to the heat transfer with the ground	W
$Q_{ci}$	Convective heat transfer of the internal surface of the envelope element with indoor	W
$Q_{ri}$	Radiative heat transfer of the internal surface of the envelope element with indoor	W
$Q_{sg}$	Solar gains due to the solar radiation transmitted by all clear components of the thermal zone and absorbed by the internal surface of envelope elements	W
$Q_{c,int}$	Convective component of the internal heat gains of the zone	W
$Q_{r,int}$	Radiative component of the internal heat gains of the zone	W
$Q_{c,HVAC}$	Convective component of the power delivered by the HVAC system to the zone	W
$Q_{r,HVAC}$	Radiative component of the power delivered by the HVAC system to the zone	W
$Q_{vent}$	Power exchanged by the thermal zone for infiltrations and all kinds of ventilation (natural, mechanical, with other thermal zones)	W

Finally, the last bus signal is the *Ventilation bus*, that collects information on the heat and mass transfer due to ventilation phenomena. This vector is composed by the both the thermal flux and the massive air flow due to different causes: infiltrations, natural or mechanical ventilation and airflow to adjacent thermal zones. For all these components, positive values are used for fluxes (thermal or massive) entering in the considered thermal zone.

Table B- 4. Components of the Ventilation bus.

Label	Description	Unit measure
$Q_{infiltration}$	Power related to air infiltrations	W
$Q_{natural}$	Power related to natural ventilation	W
$Q_{mechanical}$	Power related to mechanical ventilation	W
$Q_{inter}$	Power related to airflow to adjacent thermal zones	W
$m_{infiltration}$	Airflow due to infiltrations	kg/s
$m_{natural}$	Airflow due to natural ventilation	kg/s
$m_{mechanical}$	Airflow due to mechanical ventilation	kg/s
$m_{inter}$	Airflow to adjacent thermal zones.	kg/s







In this Appendix all the blocks of the ALMABuild library are briefly described defining, for each block, input, output and the parameter required.

Firstly, blocks collected in the Climatic Data sub-system, adopted for managing with weather related data are listed in Table C- 1.

In Table C- 2 the Building Massive Element blocks that are used if the thermal balance of the zone is solved according to the *simple model* are reported. On the contrary, in Table C- 3 BME blocks required if the *radiative model* is adopted, are collected. From Table C- 3 a huge number of intersection blocks, i.e. ceilings and internal walls, can be found. In fact, specific blocks have been developed in order to couple thermal zone modelled with a specific detail level. That means that, by means of the proper intersection element, a thermal zone can be modelled according to the *simple model* and the adjacent zone can be described by adopting the *radiative model*. In addition, in Table C- 3 a specific block focused on the modelling of a radiator installed on external walls can be found.

In Table C- 4, BME blocks related to active envelope elements, like radiant floor, ceilings or walls, are described. Even in this case, intersection elements can couple thermal zone modelled according to different detail level.

Building Clear Component blocks used for the description of window, either if the *simple* or the *radiative model* is adopted for solving the thermal balance of the zone, are collected in Table C- 5.

In Table C- 6 all the Building Thermal Balance blocks available in the ALMABuild library are listed.

Finally, additional blocks used in the building modelling are listed and described in Table C- 7.

Table C- 1. List of blocks of the Climatic Data blockset.

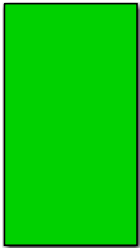
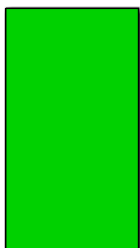
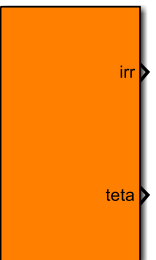
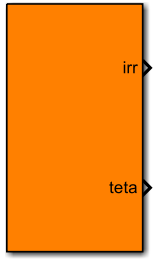
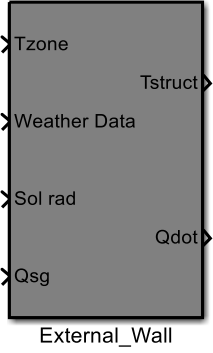
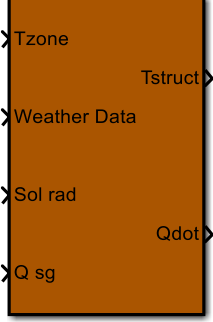
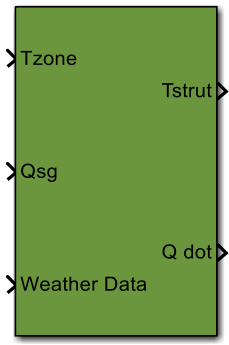
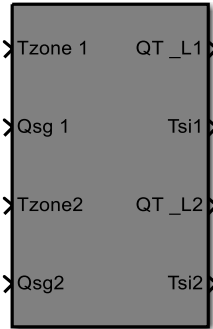
 <p style="text-align: center;">Weather Data Reader</p>	<p><b>Input:</b></p> <ul style="list-style-type: none"> <li>• Climatic_Data structure defined in the workspace.</li> </ul> <p><b>Output:</b></p> <ul style="list-style-type: none"> <li>• Weather Data bus, that is connected to the <i>Goto</i> block tagged <i>Weather_Data</i>.</li> </ul> <p><b>Parameters:</b> none</p>
<p><b>Description:</b> this block is used for importing in SIMULINK the weather data defined in the base workspace</p>	
 <p style="text-align: center;">Solar Data</p>	<p><b>Input:</b></p> <ul style="list-style-type: none"> <li>• Weather Data bus, recalled by a <i>From</i> block</li> </ul> <p><b>Output:</b></p> <ul style="list-style-type: none"> <li>• Sun bus, connected to the <i>Goto</i> block tagged <i>Sun</i>.</li> </ul> <p><b>Parameters:</b> none</p>
<p><b>Description:</b> this block is used for the evaluation of the parameters related to the sun position in the sky.</p>	
 <p style="text-align: center;">Solar Radiation Calculator</p>	<p><b>Input:</b></p> <ul style="list-style-type: none"> <li>• Weather Data bus;</li> <li>• Sun bus.</li> </ul> <p><b>Output:</b></p> <ul style="list-style-type: none"> <li>• Solar radiation bus;</li> <li>• Angle of incidence of the beam solar radiation.</li> </ul> <p><b>Parameters:</b></p> <ul style="list-style-type: none"> <li>• Latitude;</li> <li>• Slope of the surface;</li> <li>• Exposition of the surface;</li> <li>• Albedo.</li> </ul>
<p><b>Description:</b> this block is used for the evaluation of the angle of incidence (teta) and beam, diffuse and reflected fractions of the incident solar radiation of a surface.</p>	
 <p style="text-align: center;">Solar Radiation Reader</p>	<p><b>Input:</b> none</p> <p><b>Output:</b></p> <ul style="list-style-type: none"> <li>• Solar radiation bus;</li> <li>• Angle of incidence of the beam solar radiation.</li> </ul> <p><b>Parameters:</b></p> <ul style="list-style-type: none"> <li>• Beam, diffuse and reflected solar radiation over the surface;</li> <li>• Angle of incidence of beam solar radiation.</li> </ul>
<p><b>Description:</b> this block recalls data about the incident solar radiation on a surface and the angle of incidence, collected in the <i>Ambient_Data</i> structure.</p>	



Table C- 2. List of Building Massive Element blocks, for thermal zone described by means of the *simple model*.

 <p style="text-align: center;">External_Wall</p>	<p><b>Input:</b></p> <ul style="list-style-type: none"> <li>• Temperature zone bus;</li> <li>• Weather Data bus;</li> <li>• Solar radiation bus, accounting the incident radiation on external surface;</li> <li>• Internal Solar gains.</li> </ul> <p><b>Output:</b></p> <ul style="list-style-type: none"> <li>• Superficial temperature bus;</li> <li>• Power bus of the building element.</li> </ul>
<p><b>Description:</b> in this block the 3R4C network is implemented for simulating the dynamic behaviour of external walls.</p> <p><b>Parameters:</b></p> <ul style="list-style-type: none"> <li>• Wall stratigraphy (thickness, thermal conductivity, density and thermal capacity of each layer);</li> <li>• Surface properties (area, outdoor and indoor solar absorbance and infrared emissivity).</li> </ul>	<p><b>Input:</b></p> <ul style="list-style-type: none"> <li>• Temperature zone bus;</li> <li>• Weather Data bus;</li> <li>• Solar radiation bus for the surface;</li> <li>• Internal solar gains.</li> </ul> <p><b>Output:</b></p> <ul style="list-style-type: none"> <li>• Superficial temperature bus;</li> <li>• Power bus of the building element.</li> </ul>
 <p style="text-align: center;">Roof</p>	<p><b>Input:</b></p> <ul style="list-style-type: none"> <li>• Temperature zone bus;</li> <li>• Weather Data bus;</li> <li>• Solar radiation bus for the surface;</li> <li>• Internal solar gains.</li> </ul> <p><b>Output:</b></p> <ul style="list-style-type: none"> <li>• Superficial temperature bus;</li> <li>• Power bus of the building element.</li> </ul>
<p><b>Description:</b> in this block the 3R4C network is implemented for simulating the dynamic behaviour of roof or non-vertical external massive elements.</p> <p><b>Parameters:</b></p> <ul style="list-style-type: none"> <li>• Element stratigraphy (thickness, thermal conductivity, density and thermal capacity of each layer);</li> <li>• Surface properties (area, outdoor and indoor solar absorbance and infrared emissivity);</li> <li>• Slope of the roof.</li> </ul>	<p><b>Input:</b></p> <ul style="list-style-type: none"> <li>• Temperature zone bus;</li> <li>• Weather Data bus;</li> <li>• Solar radiation bus for the surface;</li> <li>• Internal solar gains.</li> </ul> <p><b>Output:</b></p> <ul style="list-style-type: none"> <li>• Superficial temperature bus;</li> <li>• Power bus of the building element.</li> </ul>

 <p style="text-align: center;">Floor</p>	<p><b>Input:</b></p> <ul style="list-style-type: none"> <li>• Temperature zone bus;</li> <li>• Solar gains;</li> <li>• Weather Data bus.</li> </ul>
<p><b>Description:</b> this block is used for simulating the dynamic behaviour of a slab-on-grade floor.</p> <p><b>Parameters:</b></p> <ul style="list-style-type: none"> <li>• Floor stratigraphy (thickness, thermal conductivity, density and thermal capacity of each layer);</li> <li>• Ground data (as required by EN ISO 13370);</li> <li>• Floor data (exposed perimeter and other data required by EN 13370);</li> <li>• Surface properties.</li> </ul>	<p><b>Output:</b></p> <ul style="list-style-type: none"> <li>• Superficial temperature bus;</li> <li>• Power bus of the building element.</li> </ul>
 <p style="text-align: center;">Internal Wall</p>	<p><b>Input:</b></p> <ul style="list-style-type: none"> <li>• Temperature zone bus of zone 1;</li> <li>• Solar gains from zone 1;</li> <li>• Temperature zone bus of zone 2;</li> <li>• Solar gains from zone 2.</li> </ul>
<p><b>Description:</b> this block is used for the simulation of a wall that separates two adjacent thermal zones (1 and 2).</p> <p><b>Parameters:</b></p> <ul style="list-style-type: none"> <li>• Wall stratigraphy (thickness, thermal conductivity, density and thermal capacity of each layer);</li> <li>• Surface properties (area, solar absorbance and infrared emissivity of each side of the wall).</li> </ul>	<p><b>Output:</b></p> <ul style="list-style-type: none"> <li>• Power bus to zone 1;</li> <li>• Temperature of the surface facing zone 1;</li> <li>• Power bus to zone 2;</li> <li>• Temperature of the surface facing zone 2.</li> </ul>


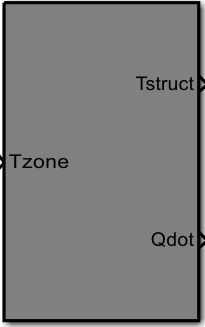
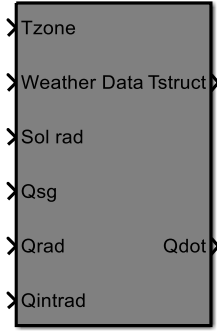
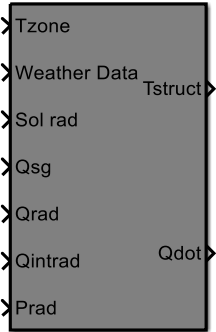
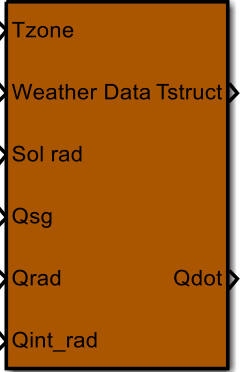
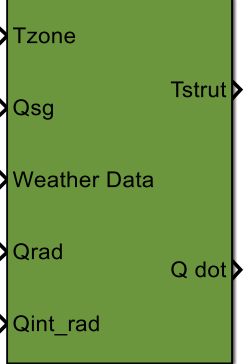
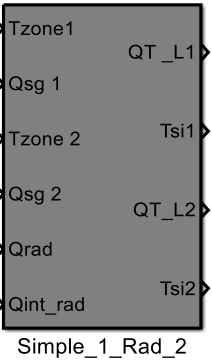
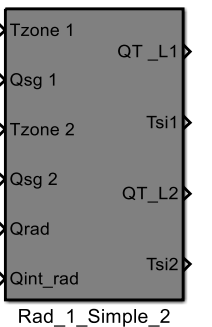
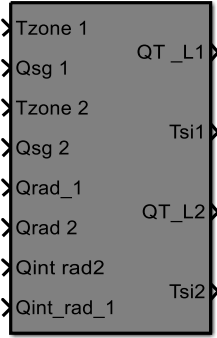
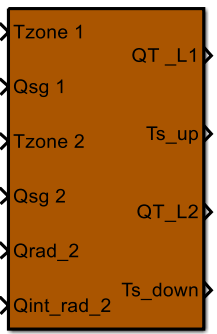
	<p><b>Input:</b></p> <ul style="list-style-type: none"> <li>• Temperature zone bus of the upper zone (labelled 1);</li> <li>• Solar gains from the upper zone (labelled 1);</li> <li>• Temperature zone bus of the lower zone (labelled 2);</li> <li>• Solar gains from the lower zone (labelled 2).</li> </ul>
<p><b>Description:</b> this block is used for simulating the behaviour of a ceiling. The required stratigraphy has to be defined from the lower to the upper zone;</p> <p><b>Parameters:</b></p> <ul style="list-style-type: none"> <li>• Ceiling stratigraphy (thickness, thermal conductivity, density and thermal capacity of each layer);</li> <li>• Surface properties (area, solar absorbance and infrared emissivity).</li> </ul>	<p><b>Output:</b></p> <ul style="list-style-type: none"> <li>• Power bus to zone 1;</li> <li>• Temperature of the surface facing the upper zone;</li> <li>• Power bus to the lower zone;</li> <li>• Temperature of the surface facing the lower zone 2.</li> </ul>
	<p><b>Input:</b></p> <ul style="list-style-type: none"> <li>• Temperature zone bus of the zone in which the wall is contained.</li> </ul>
<p><b>Description:</b> this block is used for simulating an internal partition, i.e. a wall all contained within the thermal zone.</p> <p><b>Parameters:</b></p> <ul style="list-style-type: none"> <li>• Wall stratigraphy (thickness, thermal conductivity, density and thermal capacity of each layer);</li> <li>• Area and infrared emissivity.</li> </ul>	<p><b>Output:</b></p> <ul style="list-style-type: none"> <li>• Superficial temperature bus;</li> <li>• Power bus of the building element.</li> </ul>

Table C- 3. List of Building Massive Element blocks adopted if the *radiative model* is used for the description of the thermal zone, for non-active envelope elements.

 <p style="text-align: center;">No Element</p>	<p><b>Input:</b></p> <ul style="list-style-type: none"> <li>• Temperature zone bus;</li> <li>• Weather Data bus;</li> <li>• Solar radiation bus, accounting the incident radiation on external surface;</li> <li>• Internal Solar gains;</li> <li>• Radiative heat flux involving the internal surface of the element;</li> <li>• Radiative component of internal gains.</li> </ul>
<p><b>Description:</b> this block contains the radiative model of an external wall.</p> <p><b>Parameters:</b></p> <ul style="list-style-type: none"> <li>• Wall stratigraphy;</li> <li>• Surface properties (area, outdoor and indoor solar absorbance and infrared emissivity);</li> <li>• Total area of internal surface of the zone.</li> </ul>	<p><b>Output:</b></p> <ul style="list-style-type: none"> <li>• Superficial temperature bus;</li> <li>• Power bus of the building element.</li> </ul>
 <p style="text-align: center;">With Radiator</p>	<p><b>Input:</b></p> <ul style="list-style-type: none"> <li>• Temperature zone bus;</li> <li>• Weather Data bus;</li> <li>• Solar radiation bus, accounting the incident radiation on external surface;</li> <li>• Internal Solar gains;</li> <li>• Radiative heat flux involving the internal surface of the element;</li> <li>• Radiative component of internal gains.</li> <li>• Power released by the hot water flowing across the radiator.</li> </ul>
<p><b>Description:</b> this block is used for simulating an external wall in which a radiator is installed.</p> <p><b>Parameters:</b></p> <ul style="list-style-type: none"> <li>• Wall stratigraphy;</li> <li>• Surface properties;</li> <li>• Total area of internal surface of the zone;</li> <li>• Radiator properties.</li> </ul>	<p><b>Output:</b></p> <ul style="list-style-type: none"> <li>• Superficial temperature bus of the radiator;</li> <li>• Power bus of the element.</li> </ul>

 <p>The diagram shows a brown rectangular block labeled "Roof Rad". On the left side, there are six input ports with chevron symbols: Tzone, Weather Data Tstruct, Sol rad, Qsg, Qrad, and Qint_rad. On the right side, there are two output ports with chevron symbols: Qdot and Qrad.</p>	<p><b>Input:</b></p> <ul style="list-style-type: none"> <li>• Temperature zone bus;</li> <li>• Weather Data bus;</li> <li>• Solar radiation bus, accounting the incident radiation on external surface;</li> <li>• Internal Solar gains;</li> <li>• Radiative heat flux involving the internal surface of the element;</li> <li>• Radiative component of internal gains.</li> </ul>
<p><b>Description:</b> this block is used for the radiative modelling of roof or non-vertical external massive elements.</p> <p><b>Parameters:</b></p> <ul style="list-style-type: none"> <li>• Wall stratigraphy;</li> <li>• Surface properties;</li> <li>• Slope of the element;</li> <li>• Total area of internal surface of the zone.</li> </ul>	<p><b>Output:</b></p> <ul style="list-style-type: none"> <li>• Superficial temperature bus;</li> <li>• Power bus of the building element.</li> </ul>
 <p>The diagram shows a green rectangular block labeled "No Elements". On the left side, there are five input ports with chevron symbols: Tzone, Qsg, Weather Data, Qrad, and Qint_rad. On the right side, there are two output ports with chevron symbols: Tstrut and Q dot.</p>	<p><b>Input:</b></p> <ul style="list-style-type: none"> <li>• Temperature zone bus;</li> <li>• Internal Solar gains;</li> <li>• Weather Data bus;</li> <li>• Radiative heat flux involving the internal surface of the element;</li> <li>• Radiative component of internal gains.</li> </ul>
<p><b>Description:</b> block composed by the radiative model of a passive slab-on-grade floor.</p> <p><b>Parameters:</b></p> <ul style="list-style-type: none"> <li>• Floor stratigraphy;</li> <li>• Ground data (EN 13370);</li> <li>• Additional floor data (EN 13370);</li> <li>• Surface properties;</li> <li>• Total area of internal surface of the zone.</li> </ul>	<p><b>Output:</b></p> <ul style="list-style-type: none"> <li>• Superficial temperature bus;</li> <li>• Power bus of the building element.</li> </ul>

	<p><b>Input:</b></p> <ul style="list-style-type: none"> <li>• Temperature zone bus of zone 1;</li> <li>• Solar gains from zone 1;</li> <li>• Temperature zone bus of zone 2;</li> <li>• Solar gains from zone 2.</li> <li>• Radiative heat flux involving the internal surface of the element, facing zone 2;</li> <li>• Radiative component of internal gains of zone 2.</li> </ul>
<p><b>Description:</b> this block is used for the modelling of an internal wall that divides zone (1), described by the <i>simple model</i>, from a zone (2), in which the <i>radiative model</i> is used.</p> <p><b>Parameters:</b></p> <ul style="list-style-type: none"> <li>• Wall stratigraphy;</li> <li>• Surface properties (area, solar absorbance and infrared emissivity of each side of the wall).</li> <li>• Total area of internal surface of the zone 2.</li> </ul>	<p><b>Output:</b></p> <ul style="list-style-type: none"> <li>• Power bus to zone 1;</li> <li>• Temperature of the surface facing zone 1;</li> <li>• Power bus to zone 2;</li> <li>• Temperature of the surface facing zone 2.</li> </ul>
	<p><b>Input:</b></p> <ul style="list-style-type: none"> <li>• Temperature zone bus of zone 1;</li> <li>• Solar gains from zone 1;</li> <li>• Temperature zone bus of zone 2;</li> <li>• Solar gains from zone 2.</li> <li>• Radiative heat flux involving the internal surface of the element, facing zone 1;</li> <li>• Radiative component of internal gains of zone 1.</li> </ul>
<p><b>Description:</b> this block is used for the modelling of an internal wall that divides zone (1), in which the <i>radiative model</i>, is used from zone (2), described by the <i>simple model</i>.</p> <p><b>Parameters:</b></p> <ul style="list-style-type: none"> <li>• Wall stratigraphy;</li> <li>• Surface properties (area, solar absorbance and infrared emissivity of each side of the wall).</li> <li>• Total area of internal surface of zone 1.</li> </ul>	<p><b>Output:</b></p> <ul style="list-style-type: none"> <li>• Power bus to zone 1;</li> <li>• Temperature of the surface facing zone 1;</li> <li>• Power bus to zone 2;</li> <li>• Temperature of the surface facing zone 2.</li> </ul>

 <p style="text-align: center;">Rad_1_Rad_2</p>	<p><b>Input:</b></p> <ul style="list-style-type: none"> <li>• Temperature zone bus of zone 1;</li> <li>• Solar gains from zone 1;</li> <li>• Temperature zone bus of zone 2;</li> <li>• Solar gains from zone 2.</li> <li>• Radiative heat flux involving the internal wall surface (to zone 1);</li> <li>• Radiative heat flux involving the internal wall surface (to zone 2);</li> <li>• Radiative component of internal gains of zone 1.</li> <li>• Radiative component of internal gains of zone 2.</li> </ul> <p><b>Output:</b></p> <ul style="list-style-type: none"> <li>• Power bus to zone 1;</li> <li>• Temperature of the surface facing zone 1;</li> <li>• Power bus to zone 2;</li> <li>• Temperature of the surface facing zone 2.</li> </ul>
<p><b>Description:</b> this block is used for the modelling of an internal wall that divides two adjacent thermal zones, both described by the <i>radiative model</i>.</p> <p><b>Parameters:</b></p> <ul style="list-style-type: none"> <li>• Wall stratigraphy;</li> <li>• Surface properties (area, solar absorbance and infrared emissivity of each side of the wall).</li> <li>• Total area of internal surface of both the zones.</li> </ul>	<p><b>Input:</b></p> <ul style="list-style-type: none"> <li>• Temperature zone bus of the upper zone (labelled 1);</li> <li>• Solar gains from the upper zone (labelled 1);</li> <li>• Temperature zone bus of the lower zone (labelled 2);</li> <li>• Solar gains from the lower zone (labelled 2);</li> <li>• Radiative heat flux involving the internal surface of the element, facing zone 2;</li> <li>• Radiative component of internal gains of zone 2.</li> </ul> <p><b>Output:</b></p> <ul style="list-style-type: none"> <li>• Power bus to zone 1;</li> <li>• Temperature of the surface facing the upper zone;</li> <li>• Power bus to the lower zone;</li> <li>• Temperature of the surface facing the lower zone 2.</li> </ul>
 <p style="text-align: center;">Ceiling_Simple_1_Rad_2</p>	<p><b>Description:</b> this block is used for modelling a ceiling that divides the upper zone (1, described by the <i>simple model</i>) to the lower zone (2, in which the <i>radiative model</i> is used).</p> <p><b>Parameters:</b></p> <ul style="list-style-type: none"> <li>• Wall stratigraphy;</li> <li>• Surface properties;</li> <li>• Slope of the element;</li> <li>• Total area of internal surface of the lower zone.</li> </ul>

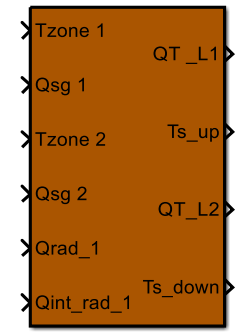
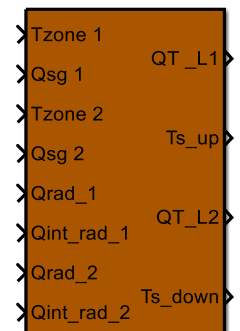
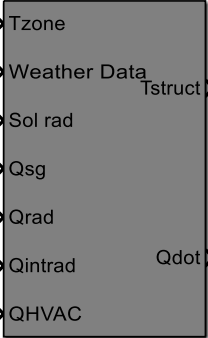
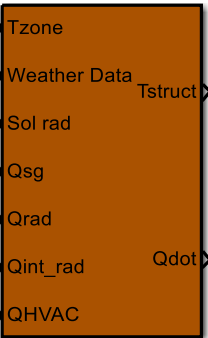
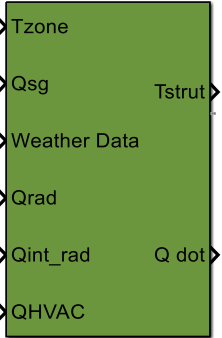
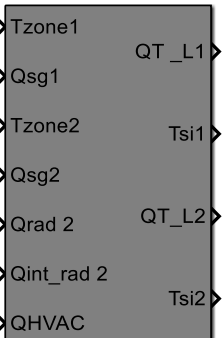
 <p>Ceiling_Rad_1_Simple_2</p>	<p><b>Input:</b></p> <ul style="list-style-type: none"> <li>• Temperature zone bus of the upper zone (labelled 1);</li> <li>• Solar gains from the upper zone (labelled 1);</li> <li>• Temperature zone bus of the lower zone (labelled 2);</li> <li>• Solar gains from the lower zone (labelled 2);</li> <li>• Radiative heat flux involving the internal surface of the element, facing zone 1;</li> <li>• Radiative component of internal gains of zone 1.</li> </ul>
<p><b>Description:</b> this block is used for modelling a ceiling that divides the upper zone (1, described by the <i>radiative model</i>) from the lower zone (2, in which the <i>simple model</i> is used).</p> <p><b>Parameters:</b></p> <ul style="list-style-type: none"> <li>• Wall stratigraphy;</li> <li>• Surface properties;</li> <li>• Slope of the element;</li> <li>• Total area of internal surface of the upper zone.</li> </ul>	<p><b>Output:</b></p> <ul style="list-style-type: none"> <li>• Power bus to zone 1;</li> <li>• Temperature of the surface facing the upper zone;</li> <li>• Power bus to the lower zone;</li> <li>• Temperature of the surface facing the lower zone 2.</li> </ul>
 <p>Ceiling_Rad_1_Rad_2</p>	<p><b>Input:</b></p> <ul style="list-style-type: none"> <li>• Temperature zone bus of upper zone;</li> <li>• Solar gains from the upper zone;</li> <li>• Temperature zone bus of lower zone;</li> <li>• Solar gains from the lower zone;</li> <li>• Radiative heat flux involving the ceiling internal surface, facing zone 1;</li> <li>• Radiative component of internal gains of zone 1;</li> <li>• Radiative heat flux involving the ceiling internal surface, facing zone 2;</li> <li>• Radiative component of internal gains of zone 2.</li> </ul>
<p><b>Description:</b> this block is used for modelling a ceiling that divides two thermal zone, both described by the <i>radiative model</i>.</p> <p><b>Parameters:</b></p> <ul style="list-style-type: none"> <li>• Wall stratigraphy;</li> <li>• Surface properties;</li> <li>• Slope of the element;</li> <li>• Total area of internal surface of both the zone.</li> </ul>	<p><b>Output:</b></p> <ul style="list-style-type: none"> <li>• Power bus to zone 1;</li> <li>• Temperature of the surface facing the upper zone (1);</li> <li>• Power bus to the lower zone (2);</li> <li>• Temperature of the surface facing the lower zone 2.</li> </ul>

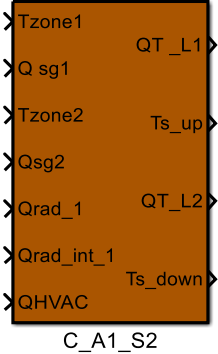
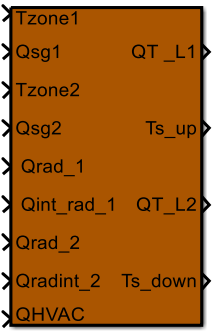


Table C- 4. List of Active Building Massive Element blocks.

	<p><b>Input:</b></p> <ul style="list-style-type: none"> <li>• Temperature zone bus;</li> <li>• Weather Data bus;</li> <li>• Solar radiation bus, accounting the incident radiation on external surface;</li> <li>• Internal Solar gains;</li> <li>• Radiative heat flux involving the internal surface of the element;</li> <li>• Radiative component of internal gains;</li> <li>• Power released by the fluid flowing across the element.</li> </ul>
<p><b>Description:</b> this block is used for the simulation of an external active wall. An additional node is added to the 3R4C network for accounting the active layer.</p> <p><b>Parameters:</b></p> <ul style="list-style-type: none"> <li>• Wall stratigraphy and position of the active layer;</li> <li>• Surface properties (area, solar absorbance and infrared emissivity of each side of the wall).</li> <li>• Total area of internal surface of the zone.</li> </ul>	<p><b>Output:</b></p> <ul style="list-style-type: none"> <li>• Superficial temperature bus;</li> <li>• Power bus of the building element.</li> </ul>
	<p><b>Input:</b></p> <ul style="list-style-type: none"> <li>• Temperature zone bus;</li> <li>• Weather Data bus;</li> <li>• Solar radiation bus, accounting the incident radiation on external surface;</li> <li>• Internal Solar gains;</li> <li>• Radiative heat flux involving the internal surface of the element;</li> <li>• Radiative component of internal gains;</li> <li>• Power released by the fluid flowing across the element.</li> </ul>
<p><b>Description:</b> this block is used for the modelling of an active roof or non-vertical external massive elements. An additional node is added for the modelling of the active layer.</p> <p><b>Parameters:</b></p> <ul style="list-style-type: none"> <li>• Wall stratigraphy and position of the active layer;</li> <li>• Surface properties;</li> <li>• Slope of the element;</li> <li>• Total area of internal surface of the zone.</li> </ul>	<p><b>Output:</b></p> <ul style="list-style-type: none"> <li>• Superficial temperature bus;</li> <li>• Power bus of the building element.</li> </ul>

 <p>Act No Elements</p>	<p><b>Input:</b></p> <ul style="list-style-type: none"> <li>• Temperature zone bus;</li> <li>• Internal Solar gains;</li> <li>• Weather Data bus;</li> <li>• Radiative heat flux involving the internal surface of the element;</li> <li>• Radiative component of internal gains;</li> <li>• Power released by the fluid flowing across the element.</li> </ul>
<p><b>Description:</b> this block is used for the modelling of an active slab-on-grade floor. An additional node is added for the modelling of the active layer.</p> <p><b>Parameters:</b></p> <ul style="list-style-type: none"> <li>• Floor stratigraphy and position of the active layer;</li> <li>• Ground data (EN 13370);</li> <li>• Additional floor data (EN 13370);</li> <li>• Surface properties;</li> <li>• Total area of internal surface of the zone.</li> </ul>	<p><b>Output:</b></p> <ul style="list-style-type: none"> <li>• Superficial temperature bus;</li> <li>• Power bus of the building element.</li> </ul>
 <p>Simple_1_Active_2</p>	<p><b>Input:</b></p> <ul style="list-style-type: none"> <li>• Temperature zone bus of zone 1;</li> <li>• Solar gains from zone 1;</li> <li>• Temperature zone bus of zone 2;</li> <li>• Solar gains from zone 2.</li> <li>• Radiative heat flux involving the internal wall surface (to zone 2);</li> <li>• Radiative component of internal gains of zone 2.</li> <li>• Power released by the fluid flowing across the element.</li> </ul>
<p><b>Description:</b> this block is used for the modelling of an active internal wall dividing a zone (1) in which the <i>simple model</i> is adopted to a zone (2) described by the <i>radiative model</i>.</p> <p><b>Parameters:</b></p> <ul style="list-style-type: none"> <li>• Wall stratigraphy and position of the active layer;</li> <li>• Surface properties (area, solar absorbance and infrared emissivity of each side of the wall).</li> <li>• Total area of internal surface of the zone 2.</li> </ul>	<p><b>Output:</b></p> <ul style="list-style-type: none"> <li>• Power bus to zone 1;</li> <li>• Temperature of the surface facing zone 1;</li> <li>• Power bus to zone 2;</li> <li>• Temperature of the surface facing zone 2.</li> </ul>

	<p><b>Input:</b></p> <ul style="list-style-type: none"> <li>• Temperature zone bus of zone 1;</li> <li>• Solar gains from zone 1;</li> <li>• Temperature zone bus of zone 2;</li> <li>• Solar gains from zone 2.</li> <li>• Radiative heat flux involving the internal wall surface (to zone 1);</li> <li>• Radiative heat flux involving the internal wall surface (to zone 2);</li> <li>• Radiative component of internal gains of zone 1;</li> <li>• Radiative component of internal gains of zone 2.</li> <li>• Power released by the fluid flowing across the element.</li> </ul>
<p><b>Description:</b> this block is used for the modelling of an active internal wall dividing a two thermal zones in which the <i>radiative model</i> is adopted.</p> <p><b>Parameters:</b></p> <ul style="list-style-type: none"> <li>• Wall stratigraphy and position of the active layer;</li> <li>• Surface properties (area, solar absorbance and infrared emissivity of each side of the wall).</li> <li>• Total area of internal surface of both the zones.</li> </ul>	<p><b>Output:</b></p> <ul style="list-style-type: none"> <li>• Power bus to zone 1;</li> <li>• Temperature of the surface facing zone 1;</li> <li>• Power bus to zone 2;</li> <li>• Temperature of the surface facing zone 2.</li> </ul>
	<p><b>Input:</b></p> <ul style="list-style-type: none"> <li>• Temperature zone bus of upper zone;</li> <li>• Solar gains from the upper zone;</li> <li>• Temperature zone bus of lower zone;</li> <li>• Solar gains from the lower zone;</li> <li>• Radiative heat flux involving the ceiling internal surface, facing zone 2;</li> <li>• Radiative component of internal gains of zone 2;</li> <li>• Power released by the fluid flowing across the element.</li> </ul>
<p><b>Description:</b> this block is used for the simulation of an active ceiling dividing the upper zone (1) described by the <i>simple model</i> to the lower zone (2) in which the <i>radiative model</i> is adopted. Thus, the active surface is facing the upper zone (radiant ceiling).</p> <p><b>Parameters:</b></p> <ul style="list-style-type: none"> <li>• Wall stratigraphy and active layer position;</li> <li>• Surface properties;</li> <li>• Total area of internal surface of the lower zone.</li> </ul>	<p><b>Output:</b></p> <ul style="list-style-type: none"> <li>• Power bus to zone 1;</li> <li>• Temperature of the surface facing the upper zone;</li> <li>• Power bus to the lower zone;</li> <li>• Temperature of the surface facing the lower zone 2.</li> </ul>

 <p style="text-align: center;">C_A1_S2</p>	<p><b>Input:</b></p> <ul style="list-style-type: none"> <li>• Temperature zone bus of upper zone;</li> <li>• Solar gains from the upper zone;</li> <li>• Temperature zone bus of lower zone;</li> <li>• Solar gains from the lower zone;</li> <li>• Radiative heat flux involving the ceiling internal surface, facing zone 1;</li> <li>• Radiative component of internal gains of zone 1;</li> <li>• Power released by the fluid flowing across the element.</li> </ul>
<p><b>Description:</b> this block is used for the simulation of an active ceiling dividing the upper zone (1) described by the <i>radiative model</i> to the lower zone (2) in which the <i>simple model</i> is adopted. Thus, the active surface is facing the upper zone (radiant floor).</p> <p><b>Parameters:</b></p> <ul style="list-style-type: none"> <li>• Wall stratigraphy and position of the active layer;</li> <li>• Surface properties;</li> <li>• Slope of the element;</li> <li>• Total area of internal surface of the upper zone.</li> </ul>	<p><b>Output:</b></p> <ul style="list-style-type: none"> <li>• Power bus to zone 1;</li> <li>• Temperature of the surface facing the upper zone;</li> <li>• Power bus to the lower zone;</li> <li>• Temperature of the surface facing the lower zone 2.</li> </ul>
 <p style="text-align: center;">C_R1_A2</p>	<p><b>Input:</b></p> <ul style="list-style-type: none"> <li>• Temperature zone bus of upper zone;</li> <li>• Solar gains from the upper zone;</li> <li>• Temperature zone bus of lower zone;</li> <li>• Solar gains from the lower zone;</li> <li>• Radiative heat flux involving the ceiling internal surface, facing zone 1;</li> <li>• Radiative component of internal gains of zone 1;</li> <li>• Radiative heat flux involving the ceiling internal surface, facing zone 2;</li> <li>• Radiative component of internal gains of zone 2;</li> <li>• Power released by the fluid flowing across the element.</li> </ul>
<p><b>Description:</b> this block is used for the simulation of an active ceiling dividing the two thermal zone described by the <i>radiative model</i>. The active surface is facing the lower zone (radiant ceiling).</p> <p><b>Parameters:</b></p> <ul style="list-style-type: none"> <li>• Wall stratigraphy and active layer position;</li> <li>• Surface properties;</li> <li>• Slope of the element;</li> <li>• Total area of internal surface of both the zones.</li> </ul>	<p><b>Output:</b></p> <ul style="list-style-type: none"> <li>• Power bus to zone 1;</li> <li>• Temperature of the surface facing the upper zone;</li> <li>• Power bus to the lower zone;</li> <li>• Temperature of the surface facing the lower zone 2.</li> </ul>

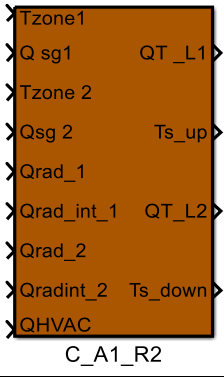
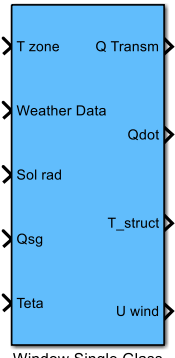
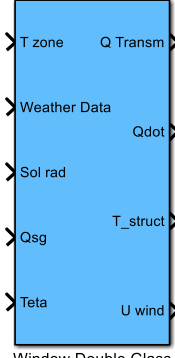
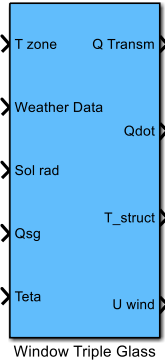
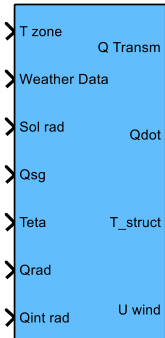
	<p><b>Input:</b></p> <ul style="list-style-type: none"> <li>• Temperature zone bus of upper zone;</li> <li>• Solar gains from the upper zone;</li> <li>• Temperature zone bus of lower zone;</li> <li>• Solar gains from the lower zone;</li> <li>• Radiative heat flux involving the ceiling internal surface, facing zone 1;</li> <li>• Radiative component of internal gains of zone 1;</li> <li>• Radiative heat flux involving the ceiling internal surface, facing zone 2;</li> <li>• Radiative component of internal gains of zone 2;</li> <li>• Power released by the fluid flowing across the element.</li> </ul>
<p><b>Description:</b> this block is used for the simulation of an active ceiling dividing the two thermal zone described by the <i>radiative model</i>. The active surface is facing the upper zone (radiant floor).</p> <p><b>Parameters:</b></p> <ul style="list-style-type: none"> <li>• Wall stratigraphy and active layer position;</li> <li>• Surface properties;</li> <li>• Slope of the element;</li> <li>• Total area of internal surface of both the zones.</li> </ul>	<p><b>Output:</b></p> <ul style="list-style-type: none"> <li>• Power bus to zone 1;</li> <li>• Temperature of the surface facing the upper zone;</li> <li>• Power bus to the lower zone;</li> <li>• Temperature of the surface facing the lower zone 2.</li> </ul>

Table C- 5. List of blocks composing the Building Clear Component subsystem.

 <p style="text-align: center;">Window Single Glass</p>	<p><b>Input:</b></p> <ul style="list-style-type: none"> <li>• Temperature zone bus;</li> <li>• Weather Data bus;</li> <li>• Solar radiation bus accounting the incident solar radiation on external surface of the window;</li> <li>• Internal solar gain;</li> <li>• Angle of incidence of beam solar radiation.</li> </ul>
<p><b>Description:</b> this block is used for simulating the dynamic behaviour of a single glass window, if the two-star model is adopted for the thermal balance of the zone</p> <p><b>Parameters:</b></p> <ul style="list-style-type: none"> <li>• Window area;</li> <li>• Frame properties (frame factor, emissivity...)</li> <li>• Glass optical properties;</li> <li>• Shading devices properties;</li> <li>• Shutter properties</li> </ul>	<p><b>Output:</b></p> <ul style="list-style-type: none"> <li>• Direct and diffuse solar radiation transmitted by the window;</li> <li>• Power bus of the building element;</li> <li>• Superficial temperature bus;</li> <li>• Thermal transmittance of the window.</li> </ul>
 <p style="text-align: center;">Window Double Glass</p>	<p><b>Input:</b></p> <ul style="list-style-type: none"> <li>• Temperature zone bus;</li> <li>• Weather Data bus;</li> <li>• Solar radiation bus accounting the incident solar radiation on external surface of the window;</li> <li>• Internal solar gain;</li> <li>• Angle of incidence of beam solar radiation</li> </ul>
<p><b>Description:</b> this block is used for simulating the dynamic behaviour of a double glass window, if the two-star model is adopted for the thermal balance of the zone</p> <p><b>Parameters:</b></p> <ul style="list-style-type: none"> <li>• Window area;</li> <li>• Frame properties (frame factor, emissivity...)</li> <li>• Glass optical properties;</li> <li>• Gas gap properties;</li> <li>• Shading devices properties;</li> <li>• Shutter properties.</li> </ul>	<p><b>Output:</b></p> <ul style="list-style-type: none"> <li>• Direct and diffuse solar radiation transmitted by the window;</li> <li>• Power bus of the building element;</li> <li>• Superficial temperature bus;</li> <li>• Thermal transmittance of the window.</li> </ul>

 <p style="text-align: center;">Window Triple Glass</p>	<p><b>Input:</b></p> <ul style="list-style-type: none"> <li>• Temperature zone bus;</li> <li>• Weather Data bus;</li> <li>• Solar radiation bus accounting the incident solar radiation on external surface of the window;</li> <li>• Internal solar gain;</li> <li>• Angle of incidence of beam solar radiation.</li> </ul>
<p><b>Description:</b> this block is used for simulating the dynamic behaviour of a triple glass window, if the two-star model is adopted for the thermal balance of the zone.</p> <p><b>Parameters:</b></p> <ul style="list-style-type: none"> <li>• Window area;</li> <li>• Frame properties (frame factor, emissivity...)</li> <li>• Glass optical properties;</li> <li>• Gas gap properties;</li> <li>• Shading devices properties;</li> <li>• Shutter properties.</li> </ul>	<p><b>Output:</b></p> <ul style="list-style-type: none"> <li>• Direct and diffuse solar radiation transmitted by the window;</li> <li>• Power bus of the building element;</li> <li>• Superficial temperature bus of the element;</li> <li>• Thermal transmittance of the window.</li> </ul>
 <p style="text-align: center;">Window Single Glass Rad</p>	<p><b>Input:</b></p> <ul style="list-style-type: none"> <li>• Temperature zone bus;</li> <li>• Weather Data bus;</li> <li>• Solar radiation bus accounting the incident solar radiation on external surface of the window;</li> <li>• Internal solar gain;</li> <li>• Angle of incidence of beam solar radiation.</li> <li>• Radiative heat transfer of the internal surface of the window with the surroundings;</li> <li>• Window fraction of the radiative component of the internal heat gains.</li> </ul>
<p><b>Description:</b> this block is used for simulating the dynamic behaviour of a single glass window, if the detailed radiative model is adopted for the thermal balance of the zone.</p> <p><b>Parameters:</b></p> <ul style="list-style-type: none"> <li>• Window area;</li> <li>• Frame properties (frame factor, emissivity...)</li> <li>• Glass optical properties;</li> <li>• Shading devices properties;</li> <li>• Shutter properties.</li> </ul>	<p><b>Output:</b></p> <ul style="list-style-type: none"> <li>• Direct and diffuse solar radiation transmitted by the window;</li> <li>• Power bus of the building element;</li> <li>• Superficial temperature bus;</li> <li>• Thermal transmittance of the window.</li> </ul>

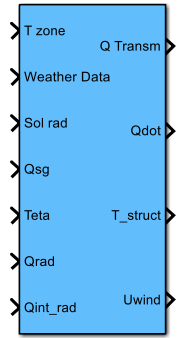
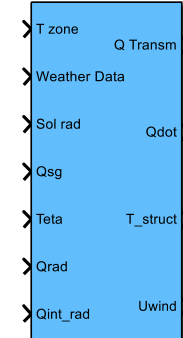
 <p style="text-align: center;">Window Double Glass Rad</p>	<p><b>Input:</b></p> <ul style="list-style-type: none"> <li>• Temperature zone bus;</li> <li>• Weather Data bus;</li> <li>• Solar radiation bus accounting the incident solar radiation on external surface of the window;</li> <li>• Internal solar gain;</li> <li>• Angle of incidence of beam solar radiation.</li> <li>• Radiative heat transfer of the internal surface of the window with the surroundings;</li> <li>• Window fraction of the radiative component of the internal heat gains.</li> </ul>
<p><b>Description:</b> this block is used for simulating the dynamic behaviour of a double glass window, if the detailed radiative model is adopted for the thermal balance of the zone.</p> <p><b>Parameters:</b></p> <ul style="list-style-type: none"> <li>• Window area;</li> <li>• Frame properties;</li> <li>• Glass optical properties;</li> <li>• Gas gap properties;</li> <li>• Shading devices properties;</li> <li>• Shutter properties.</li> </ul>	<p><b>Output:</b></p> <ul style="list-style-type: none"> <li>• Direct and diffuse solar radiation transmitted by the window;</li> <li>• Power bus of the building element;</li> <li>• Superficial temperature bus;</li> <li>• Thermal transmittance of the window.</li> </ul>
 <p style="text-align: center;">Window Triple Glass Rad</p>	<p><b>Input:</b></p> <ul style="list-style-type: none"> <li>• Temperature zone bus;</li> <li>• Weather Data bus;</li> <li>• Solar radiation bus accounting the incident solar radiation on external surface of the window;</li> <li>• Internal solar gain;</li> <li>• Angle of incidence of beam solar radiation.</li> <li>• Radiative heat transfer of the internal surface of the window with the surroundings;</li> <li>• Window fraction of the radiative component of the internal heat gains.</li> </ul>
<p><b>Description:</b> this block is used for simulating the dynamic behaviour of a triple glass window, if the detailed radiative model is adopted for the thermal balance of the zone.</p> <p><b>Parameters:</b></p> <ul style="list-style-type: none"> <li>• Window area;</li> <li>• Frame properties;</li> <li>• Glass optical properties;</li> <li>• Gas gap properties;</li> <li>• Shading devices properties;</li> <li>• Shutter properties.</li> </ul>	<p><b>Output:</b></p> <ul style="list-style-type: none"> <li>• Direct and diffuse solar radiation transmitted by the window;</li> <li>• Power bus of the building element;</li> <li>• Superficial temperature bus;</li> <li>• Thermal transmittance of the window.</li> </ul>



Table C- 6. List of Building Thermal Balance blocks, for both temperature and ideal power evaluations.

<p style="text-align: center;">Temp Eval</p>	<p><b>Input:</b></p> <ul style="list-style-type: none"> <li>• Total power bus related to external walls;</li> <li>• Total power bus related to zone roofs;</li> <li>• Power bus related to floor;</li> <li>• Total power bus related to zone windows;</li> <li>• Total power bus related to zone intersections (ceilings and internal walls);</li> <li>• Total power bus related to zone partitions;</li> <li>• Ventilation bus;</li> <li>• Thermal bridges power bus;</li> <li>• Power bus related to internal gains;</li> <li>• Power bus related to HVAC emitters.</li> </ul> <p><b>Output:</b></p> <ul style="list-style-type: none"> <li>• Temperature zone bus;</li> <li>• Total power bus of the zone;</li> <li>• Total ventilation bus of the zone.</li> </ul>
<p style="text-align: center;">Ideal Power</p>	<p><b>Input:</b></p> <ul style="list-style-type: none"> <li>• Total power bus related to external walls;</li> <li>• Total power bus related to zone roofs;</li> <li>• Power bus related to floor;</li> <li>• Total power bus related to zone windows;</li> <li>• Total power bus related to zone intersections (ceilings and internal walls);</li> <li>• Total power bus related to zone partitions;</li> <li>• Ventilation bus;</li> <li>• Thermal bridges power bus;</li> <li>• Power bus related to internal gains;</li> <li>• Air set-point temperature.</li> </ul> <p><b>Output:</b></p> <ul style="list-style-type: none"> <li>• Temperature zone bus;</li> <li>• Total power bus of the zone;</li> <li>• Total ventilation bus of the zone.</li> </ul>

<p style="text-align: center;">Temp Eval Rad</p>	<p><b>Input:</b></p> <ul style="list-style-type: none"> <li>• Total power bus related to external walls;</li> <li>• Total power bus related to zone roofs;</li> <li>• Power bus related to floor;</li> <li>• Total power bus related to zone windows;</li> <li>• Total power bus related to zone intersections (ceilings and internal walls);</li> <li>• Total power bus related to zone partitions;</li> <li>• Ventilation bus;</li> <li>• Thermal bridges power bus;</li> <li>• Power bus related to internal gains;</li> <li>• Power bus related to HVAC emitters;</li> <li>• Vector composed by the internal surface temperature of the elements.</li> </ul>
<p><b>Description:</b> this block is used for the evaluation of the air and mean radiant temperature of the thermal zone, according to the <i>radiative model</i>. The mean air temperature is evaluated from internal surface temperature of the envelope elements collected in the <i>Tsi vect</i>. These temperatures have to be listed in the same order used in the geometrical description of the thermal zone.</p> <p><b>Parameters:</b></p> <ul style="list-style-type: none"> <li>• Initial air and radiative temperature;</li> <li>• Net volume of the zone;</li> <li>• View factor (between internal surface and temperature sensor) matrix.</li> </ul>	<p><b>Output:</b></p> <ul style="list-style-type: none"> <li>• Temperature zone bus;</li> <li>• Total power bus of the zone;</li> <li>• Total ventilation bus of the zone.</li> </ul>
<p style="text-align: center;">Ideal Power Rad</p>	<p><b>Input:</b></p> <ul style="list-style-type: none"> <li>• Total power bus related to external walls;</li> <li>• Total power bus related to zone roofs;</li> <li>• Power bus related to floor;</li> <li>• Total power bus related to zone windows;</li> <li>• Total power bus related to zone intersections (ceilings and internal walls);</li> <li>• Total power bus related to zone partitions;</li> <li>• Ventilation bus;</li> <li>• Thermal bridges power bus;</li> <li>• Power bus related to internal gains;</li> <li>• Air temperature set-point;</li> <li>• Vector composed by the internal surface temperature of the elements.</li> </ul>
<p><b>Description:</b> this block is used for the evaluation of the ideal convective power required by the thermal zone for maintaining the air temperature equal to set point value. Convective power is estimated by adopting the simple model, whilst mean radiative temperature is calculated using the <i>radiative model</i>.</p> <p><b>Parameters:</b></p> <ul style="list-style-type: none"> <li>• Initial mean radiative temperature;</li> <li>• Net volume of the zone;</li> <li>• View factor (between internal surface and temperature sensor) matrix.</li> </ul>	<p><b>Output:</b></p> <ul style="list-style-type: none"> <li>• Temperature zone bus;</li> <li>• Total power bus of the zone;</li> <li>• Total ventilation bus of the zone.</li> </ul>

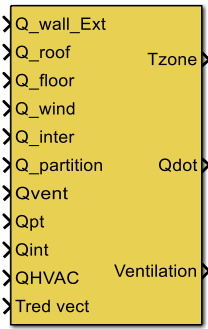
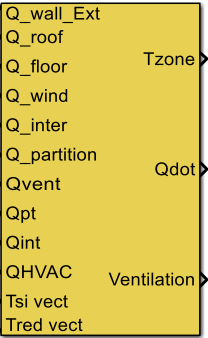
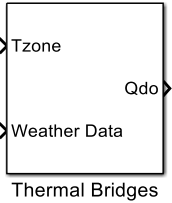
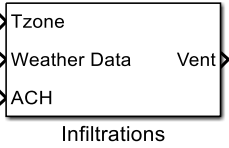

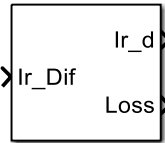
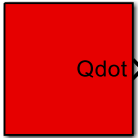
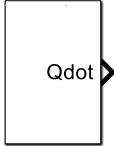
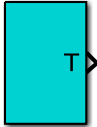
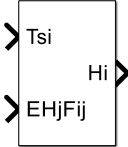
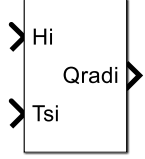
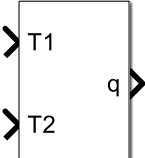
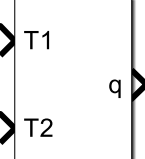
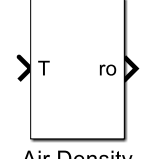
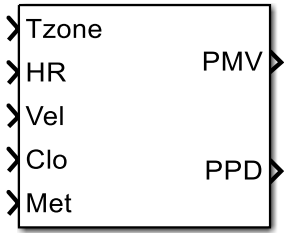
 <p>BTB convective model</p>	<p><b>Input:</b></p> <ul style="list-style-type: none"> <li>• Total power bus related to external walls;</li> <li>• Total power bus related to zone roofs;</li> <li>• Power bus related to floor;</li> <li>• Total power bus related to zone windows;</li> <li>• Total power bus related to zone intersections (ceilings and internal walls);</li> <li>• Total power bus related to zone partitions;</li> <li>• Ventilation bus;</li> <li>• Thermal bridges power bus;</li> <li>• Power bus related to internal gains;</li> <li>• Power bus related to HVAC emitters;</li> <li>• Vector composed by the reduced air temperature of thermal zone cells.</li> </ul>
<p><b>Description:</b> in this block the thermal balance of the zone is solved according to the <i>convective model</i>. The mean indoor air temperature is evaluated by the reduced temperature of each air cell in which the zone is split. The mean radiant temperature is estimated by the one-star network.</p> <p><b>Parameters:</b></p> <ul style="list-style-type: none"> <li>• Initial mean radiative temperature;</li> <li>• Net volume of the zone.</li> </ul>	<p><b>Output:</b></p> <ul style="list-style-type: none"> <li>• Temperature zone bus;</li> <li>• Total power bus of the zone;</li> <li>• Total ventilation bus of the zone.</li> </ul>
 <p>BTB fully detailed</p>	<p><b>Input:</b></p> <ul style="list-style-type: none"> <li>• Total power bus related to external walls;</li> <li>• Total power bus related to zone roofs;</li> <li>• Power bus related to floor;</li> <li>• Total power bus related to zone windows;</li> <li>• Total power bus related to zone intersections (ceilings and internal walls);</li> <li>• Total power bus related to zone partitions;</li> <li>• Ventilation bus;</li> <li>• Thermal bridges power bus;</li> <li>• Power bus related to internal gains;</li> <li>• Power bus related to HVAC emitters;</li> <li>• Vector composed by the internal surface temperature of the elements;</li> <li>• Vector composed by the reduced air temperature of thermal zone cells.</li> </ul>
<p><b>Description:</b> in this block the thermal balance of the zone is solved according to the <i>fully detailed model</i>. Convective and radiative models are coupled, therefore mean indoor air temperature is evaluated by the reduced temperature of each air cell in which the zone is split; whilst the mean radiant temperature is estimated by the internal surface temperature of the envelope elements, by knowing the view factor among temperature sensor and envelope elements.</p> <p><b>Parameters:</b></p> <ul style="list-style-type: none"> <li>• Initial mean radiative temperature;</li> <li>• Net volume of the zone;</li> <li>• View factor (between internal surface and temperature sensor) matrix.</li> </ul>	<p><b>Output:</b></p> <ul style="list-style-type: none"> <li>• Temperature zone bus;</li> <li>• Total power bus of the zone;</li> <li>• Total ventilation bus of the zone.</li> </ul>

Table C- 7. Additional blocks used for the description of a thermal zone.

	<p><b>Input:</b></p> <ul style="list-style-type: none"> <li>• Temperature zone bus;</li> <li>• Weather data bus.</li> </ul> <p><b>Output:</b> Power bus.</p>
<p><b>Description:</b> this block is used for the evaluation of the heat transfer across the thermal bridges. A simplified model is adopted, consisting in the evaluation of the total heat losses coefficient; heat losses are equally split in convective and radiative thermal loads.</p>	<p><b>Parameters:</b></p> <ul style="list-style-type: none"> <li>• Total heat losses coefficient;</li> <li>• Total thermal bridge length;</li> <li>• Mean thermal capacity of walls in the zone.</li> </ul>
	<p><b>Input:</b></p> <ul style="list-style-type: none"> <li>• Temperature zone bus;</li> <li>• Weather data bus;</li> <li>• Air change rate.</li> </ul> <p><b>Output:</b> Ventilation bus.</p>
<p><b>Description:</b> this block is used for the evaluation of thermal loads due to air infiltrations.</p>	<p><b>Parameters:</b> Net volume of the thermal zone.</p>
	<p><b>Input:</b> Solar radiation bus composed by the transmitted incident solar radiation.</p> <p><b>Output:</b></p> <ul style="list-style-type: none"> <li>• Beam solar gain for each envelope element of the thermal zone;</li> <li>• Sum of diffuse solar radiation transmitted by the window and of the reflected fraction of the transmitted beam solar radiation not absorbed by the envelope element.</li> </ul>
<p><b>Description:</b> <i>Direct Distribution</i> block (see 2.7.2), this block is used for the calculation of distribution, among the internal surface of the envelope elements composing the thermal zone in which the specific window linked to this block is inserted, of the beam component of the incident solar radiation transmitted by the window.</p>	<p><b>Parameters:</b></p> <ul style="list-style-type: none"> <li>• Name of the thermal zone in which the window is inserted;</li> <li>• Row index of the geometry matrix defining the position of the window in the thermal zone.</li> </ul>

 <p style="text-align: center;">Diffuse Distribution</p> <p><b>Description:</b> <i>Diffuse Distribution</i> block (see 2.7.2), this block is used for the calculation of the diffuse component of the solar gain due to the solar radiation transmitted by the window.</p>	<p><b>Input:</b> Sum of diffuse solar radiation transmitted by the window and of the reflected fraction of the transmitted</p> <p><b>Output:</b></p> <ul style="list-style-type: none"> <li>• Diffuse solar gain for each envelope element of the thermal zone in which the window is inserted;</li> <li>• Solar radiation transmitted back to the external environment.</li> </ul> <p><b>Parameters:</b> Name of the thermal zone in which the window is inserted.</p>
 <p style="text-align: center;">Internal Gains</p> <p><b>Description:</b> this block is used for the definition of the internal gain profile for a specific thermal zone.</p>	<p><b>Input:</b> None</p> <p><b>Output:</b> Power bus.</p> <p><b>Parameters:</b></p> <ul style="list-style-type: none"> <li>• Convective internal gain schedule for weekdays;</li> <li>• Radiative internal gain schedule for weekdays;</li> <li>• Convective internal gain schedule for weekend;</li> <li>• Radiative internal gain schedule for weekend.</li> </ul>
 <p style="text-align: center;">Qdot</p> <p><b>Description:</b> this block is used for defining a constant power bus.</p>	<p><b>Input:</b> None</p> <p><b>Output:</b> Power bus.</p> <p><b>Parameters:</b> Signals of the Power bus.</p>
 <p style="text-align: center;">Constant T</p> <p><b>Description:</b> this block is used for the definition of a constant air temperature bus.</p>	<p><b>Input:</b> None.</p> <p><b>Output:</b> Temperature zone bus.</p> <p><b>Parameters:</b></p> <ul style="list-style-type: none"> <li>• Air temperature;</li> <li>• Mean radiant temperature.</li> </ul>
 <p style="text-align: center;">Radiosity Calc</p> <p><b>Description:</b> <i>Radiosity Calculation</i> block, used for the calculation of the radiosity of a surface, by means of equation (4.1).</p>	<p><b>Input:</b></p> <ul style="list-style-type: none"> <li>• Temperature of the surface;</li> <li>• Incident infrared radiation.</li> </ul> <p><b>Output:</b> Radiosity of the surface.</p> <p><b>Parameters:</b> Infrared emissivity of the surface.</p>

 <p style="text-align: center;">Radiative Calc</p>	<p><b>Input:</b></p> <ul style="list-style-type: none"> <li>• Radiosity of the surface;</li> <li>• Temperature of the surface.</li> </ul> <p><b>Output:</b> Net radiative heat flux of the surface.</p>
<p><b>Description:</b> <i>Radiative calculation</i> block, used for the evaluation of the net radiative heat flux of a surface.</p>	<p><b>Parameters:</b></p> <ul style="list-style-type: none"> <li>• Infrared emissivity of the surface;</li> <li>• Area of the surface.</li> </ul>
 <p style="text-align: center;">Vertical Layer</p>	<p><b>Input:</b></p> <ul style="list-style-type: none"> <li>• Temperature of the air cell 1;</li> <li>• Temperature of the air cell 2.</li> </ul> <p><b>Output:</b> Heat flux across the layer.</p>
<p><b>Description:</b> this block is used for the evaluation of the heat transfer due to the mass transfer across a vertical layer, that separates two adjacent air cells, according to the <i>convective model</i>.</p>	<p><b>Parameters:</b></p> <ul style="list-style-type: none"> <li>• Air pressure;</li> <li>• Layer length;</li> <li>• Layer height;</li> <li>• Discharge factor.</li> </ul>
 <p style="text-align: center;">Horizontal Layer</p>	<p><b>Input:</b></p> <ul style="list-style-type: none"> <li>• Temperature of the upper air cell;</li> <li>• Temperature of the lower air cell.</li> </ul> <p><b>Output:</b> Heat flux across the layer.</p>
<p><b>Description:</b> this block is used for the evaluation of the heat transfer due to the mass transfer across a horizontal layer, that separates two adjacent air cells, according the <i>convective model</i>. Label 1 refers to the upper air cell.</p>	<p><b>Parameters:</b></p> <ul style="list-style-type: none"> <li>• Air pressure;</li> <li>• Layer length;</li> <li>• Height of the upper cell;</li> <li>• Height of the lower cell;</li> <li>• Discharge factor.</li> </ul>
 <p style="text-align: center;">Air Density</p>	<p><b>Input:</b> Air temperature of the cell.</p> <p><b>Output:</b> Air density.</p>
<p><b>Description:</b> this block is used for the evaluation of the air density, adopting the perfect gas law.</p>	<p><b>Parameters:</b> Pressure of the air cell.</p>

 <p style="text-align: center;">Comfort</p>	<p><b>Input:</b></p> <ul style="list-style-type: none"><li>• Temperature zone bus;</li><li>• Indoor humidity ratio;</li><li>• Air velocity;</li><li>• Clothing (clo);</li><li>• Metabolic rate (met).</li></ul> <p><b>Output:</b></p> <ul style="list-style-type: none"><li>• Predicted Mean Vote (PMV);</li><li>• Percentage of Person Dissatisfied (PPD).</li></ul> <p><b>Parameters:</b> None</p>
<p><b>Description:</b> this block is used for the evaluation of the comfort indexes PMV and PPD evaluated according to EN 7730.</p>	









In this Appendix the reader can find an example of ALMABuild script for the introduction of a BME block for external walls in the Simulink desktop. The script manages via From/Goto blocks the input/output signals among the blocks and the calling of the parameters from the Matlab structures originated with specific GUIs.

Specific commands are used for the creation of links (add\_line) and to add blocks (add\_block) in the Simulink desktop.

```
% Creo i sottosistemi relativi alle pareti esterne.
if par>0
    val=char('+'*ones(1,par));

    % Inserisco il blocco GOTO per le potenze liminari del muro
add_block('simulink/Signal Routing/Goto',[Prog '/' Nome_Loc
        '/Qwall_ext'],...
        'Position',[x y dx dy], ...
        'GotoTag','Q_wall_ext')
    % inserisco il blocco somma per i flussi di tutti i blocchi
if par>1
    add_block('simulink/Math Operations/Add',
        [Prog '/' Nome_Loc '/Sum_wall'],...
        'Position',[x y dx dy],...
        'Inputs',val)
add_block('ALMADIN/ALMABuild/Building Component/Sum ETF ',...
        [Prog '/' Nome_Loc '/Vector_wall'],...
        'Position',[x y dx dy])
    add_line([Prog '/' Nome_Loc],'Sum_wall/1','Vector_wall/1')
    add_line([Prog '/' Nome_Loc],'Vector_wall/1','Qwa_ext/1')
end
for p_ext = 1 : par

Name=cell2mat(Strutture(Ausilio.(Nome_Loc).Par_Ext.Indice(p_ext,1
),2));
    Name2=Name;
    Space=isspace(Name);
    for k = 1 : size(Space,2)
        if Space(k)==1;
            Name2(k)='_';
        end
    end
end
add_block('ALMADIN/ALMABuild/Building Component/Building
```

```

        Massive Element/External_Wall', ...
[Prog '/' Nome_Loc '/' Name '_' num2str(p_ext)],...
'Position',[x y dx dy],...
'Assorb',['Building_Data.Ext_Walls.' Name2 '.Alfa'],
'Emis',['Building_Data.Ext_Walls.' Name2 '.Emis'],
'L',['Building_Data.Ext_Walls.' Name2
        '.Stratigraphy(:,1)'], ...
'lambda',['Building_Data.Ext_Walls.' Name2
        '.Stratigraphy(:,2)'], ...
'ro',['Building_Data.Ext_Walls.' Name2
        '.Stratigraphy(:,3)'], ...
'cp',['Building_Data.Ext_Walls.' Name2
        '.Stratigraphy(:,4)'],...
'Area',['cell2mat('Building_Data.Ext_Walls.' Nome_Loc
'.Structures(' num2str(Par_Ext.Indice(p_ext,1)) ',3))')]

% collego i sottosistemi con il From relativo ai Dati Climatici
if p_ext==1
    add_block('simulink/Signal Routing/From', ...
        [Prog '/' Nome_Loc '/Dati_Clima'], ...
        'Position',[x y dx dy], ...
        'ForegroundColor','green', ...
        'GotoTag','Dati_clima')
    add_line([Prog '/' Nome_Loc],'Dati_Clima/1', ...
        [Name '_' num2str(p_ext) '/2'])

    % From Temperature nel locale
    add_block('simulink/Signal Routing/From',[Prog '/'
        Nome_Loc '/Tloc'], ...
        'Position',[x y dx dy],
        'ForegroundColor','red',...
        'GotoTag',['T_' Nome_Loc])
    add_line([Prog '/' Nome_Loc],'Tloc/1',
        [Name '_' num2str(p_ext) '/1'])
else
    add_line([Prog '/' Nome_Loc],...
        'Dati_Clima/1',[Name '_' num2str(p_ext) '/2'],...
        'autorouting','on')

    % Temperatura del Locale
    add_line([Prog '/' Nome_Loc],...
        'Tloc/1',[Name '_' num2str(p_ext) '/1'],...
        'autorouting','on')
end
% From Irraggiamento solare

nn_Exp=cell2mat(Dati_Edificio.Thermal_Zones.(Nome_Loc).Structures
(Ausilio.(Nome_Loc).Par_Ext.Indice(p_ext,1),4));
    add_block('simulink/Signal Routing/From',...
        [Prog '/' Nome_Loc '/Irr_' nn_Exp '_'
num2str(p_ext)], ...
        'Position',[x y dx dy],...
        'ForegroundColor','blue',...
        'GotoTag',['Irr_' nn_Exp])

```

```

add_line([Prog '/' Nome_Loc],...
        ['Irr_' nn_Exp '_' num2str(p_ext) '/1'],...
        [Name '_' num2str(p_ext) '/4'],...
        'autorouting','on')
% From Irraggiamento solare dalle finestre
add_block('simulink/Signal Routing/From',...
        [Prog '/' Nome_Loc '/F_P_Ext_' num2str(p_ext)], ...
        'Position',[x y dx dy],...
        'GotoTag',['Irr_Wind_Sun_' Nome_Loc '_'
num2str(Ausilio.(Nome_Loc).Par_Ext.Indice(p_ext,1))]);
add_line([Prog '/' Nome_Loc],
        ['F_P_Ext_' num2str(p_ext) '/1'],...
        [Name '_' num2str(p_ext) '/5'],'autorouting','on');
% Collego alla somma delle potenze o direttamente ai goto
if par>1
    add_line([Prog '/' Nome_Loc],...
            [Name '_' num2str(p_ext) '/2'],
            ['Sum_wall/' num2str(p_ext)],'autorouting','on')
else
    add_line([Prog '/' Nome_Loc],...
            [Name '_' num2str(p_ext)
            '/2'],'Qwall_ext/1','autorouting','on')
end
% inserisco un terminator per bloccare il segnale di
% temperature superficiali del muro
add_block('simulink/Sinks/Terminator',...
        [Prog '/' Nome_Loc '/end_' num2str(p_ext)],...
        'Position',[x y dx dy])
add_line([Prog '/' Nome_Loc], ...
        [Name '_' num2str(p_ext) '/1'],...
        ['end_' num2str(p_ext) '/1'], 'autorouting','on')

end
else
    add_block('ALMADIN/ALMABuild/Building Component/Constant
Fluxes/Qdot',...
        [Prog '/' Nome_Loc '/Wall_Ext'], ...
        'Position',[120 100 200 300],...
        'BackgroundColor','gray',...
        'Qce','0', ...
        'Qre','0',...
        'Qextra','0',...
        'Qsolop','0',...
        'Qci','0',...
        'Qri','0',...
        'Qsolincfin','0',...
        'Qground','0')
    add_block('simulink/Signal Routing/Goto',...
        [Prog '/' Nome_Loc '/Qwall_EXT'],...
        'Position',[220 190 280 210],...
        'GotoTag','Q_wall_ext')
    add_line([Prog '/' Nome_Loc],'Wall_Ext/1','Qwall_EXT/1'...
            , 'autorouting','on')
end

```